HAL
open science

Fonctions métaboliques de Sirtuine 1 dans le muscle strié squelettique : contribution à l'étude de la régulation de l'expression de SREBP-1c et rôle potentiel lors d'un jeûne chez des myotubes C2C12

Aurélia Defour

▶ **To cite this version:**

Aurélia Defour. Fonctions métaboliques de Sirtuine 1 dans le muscle strié squelettique : contribution à l'étude de la régulation de l'expression de SREBP-1c et rôle potentiel lors d'un jeûne chez des myotubes C2C12. Médecine humaine et pathologie. Université Jean Monnet - Saint-Etienne, 2010. Français. NNT : 2010STET011T . tel-00677025

HAL Id: tel-00677025

https://theses.hal.science/tel-00677025

Submitted on 7 Mar 2012

HAL is a multi-disciplinary open access archive for the deposit and dissemination of scientific research documents, whether they are published or not. The documents may come from teaching and research institutions in France or abroad, or from public or private research centers.

L'archive ouverte pluridisciplinaire **HAL**, est destinée au dépôt et à la diffusion de documents scientifiques de niveau recherche, publiés ou non, émanant des établissements d'enseignement et de recherche français ou étrangers, des laboratoires publics ou privés.

Université Jean Monnet – Saint Etienne
Faculté de Médecine Jacques Lisfranc

Thèse de Doctorat d'Université

Ecole Doctorale EDSIS n°488 : Sciences, Ingénierie, Santé
Spécialité : Biologie, Médecine et Santé
Option : Motricité Humaine et Handicap

FONCTIONS METABOLIQUES DE SIRTUINE 1 DANS LE MUSCLE STRIE SQUELETTIQUE :
- CONTRIBUTION A L'ETUDE DE LA REGULATION DE L'EXPRESSION DE SREBP-1C
- ROLE POTENTIEL LORS D'UN JEUNE CHEZ DES MYOTUBES C2C12

Aurélia DEFOUR

Présentée et soutenue publiquement le 15 octobre 2010
devant le jury composé de :

Membres du Jury

M. Gérard CABELLO, UMR 866, INRA, Montpellier	Rapporteur
Mlle Lydie COMBARET, UMR 1019, INRA, Clermont Ferrand	Rapporteur
Mme Dominique DESPLANCHES, UMR 5123, CNRS, Lyon	Rapporteur
M. Damien ROUSSEL, UMR 5123, CNRS, Lyon	Examinateur
M. Daniel BECHET, UMR 1019, INRA, Clermont Ferrand	Co-directeur de thèse
M. Damien FREYSSENET, EA 4338, Saint Etienne	Directeur de thèse

Remerciements

Voici venu le moment des remerciements, et ils sont nombreux. Afin de n'oublier personne, je tiens à remercier toutes les personnes qui de près ou de loin ont permis de rendre possible ce travail de thèse.

Je tiens donc à remercier tous les membres de mon jury, Mesdames Lydie COMBARET et Dominique DESPLANCHES et Monsieur Gérard CABELLO qui ont accepté d'être rapporteurs de ce manuscrit et Monsieur Damien ROUSSEL qui m'a fait l'honneur de juger mon travail.

Plus particulièrement, mes remerciements vont à mon directeur de thèse Damien FREYSSENET pour tout ce qu'il m'a appris toutes ces années, pour sa confiance, sa disponibilité et ses encouragements. Je n'oublierais pas tout ce que je lui dois. Je tiens également à remercier mon co-directeur de thèse Daniel BECHET pour sa gentillesse et sa générosité, me permettant ainsi de finir ma thèse dans de meilleures conditions.

Merci à la Caisse d'Epargne Rhone Alpes qui a permis de financer cette thèse. J'en profite pour remercier tous les membres de la fondation Rhône-Alpes Futur et plus particulièrement Philippe COURPRON pour son aide et son appui pour l'obtention de cette bourse.

Merci à tous les membres du Laboratoire de Physiologie de l'Exercice pour tout ce qu'ils m'ont appris, ainsi que pour m'avoir intégrée à tous les niveaux dans le laboratoire.

Un énorme merci à Josiane CASTELLS pour sa gentillesse, sa bonne humeur et pour son aide tout au long de ce travail de thèse.

Merci aussi à tous les doctorants du Laboratoire de Physiologie de l'Exercice qui m'ont apporté leur aide et leur soutien au cours de cette thèse, les anciens Vanessa, Adel et François et les nouveaux, Olivier et Yann.

Je remercie aussi toutes les équipes qui m'ont acceuillie en dehors de Saint Etienne pour peaufiner mon apprentissage. Merci donc à André Peinnequin, Thomas Poyot, Pascal Pugnières et Vanessa Euthine.

Un immense merci à Etienne Lefai pour sa gentillesse, son enthousiasme et sa générosité.

Je remercie aussi tous mes collègues élus au conseil de l'école doctorale EDSIS de Saint Etienne, sans qui ces conseils auraient été moins agréables (Typhaine, Aurélien et Loïc).

Merci à mes amis et notamment Melek et Nelly qui me supportent depuis déjà plusieurs années.

Un très grand merci à mes parents Nicole et Jean Pierre, qui me soutiennent et m'encouragent depuis toute petite et sans qui cette thèse n'aurait pas été possible. Cette thèse est d'ailleurs un peu la leur. Un très grand merci aussi à mes frères, Damien et Gaël, qui me protègent depuis toujours, à ma belle sœur, Marlène, et mes deux petits rayons de soleil, Emma et Antoine.

Enfin, merci à mon chéri, Rémi, qui aura toujours été là pour moi. Merci de m'avoir écoutée, soutenue, encouragée et conseillée.

SOMMAIRE

ABREVIATIONS **9**

AVANT-PROPOS **15**

REVUE BIBLIOGRAPHIQUE **19**

SIRTUINE 1 : GENE, PROTEINE ET REGULATION 21
I. INTRODUCTION *21*
1. Généralités 21
2. Histones acétyltransférases 22
3. Histones déacétylases 23
II. SIRTUINES *23*
1. Sirtuines chez la levure 23
2. Sirtuines chez les mammifères 24
a. Généralités 24
b. Réactions de déacétylation et d'ADP-ribosylation 25
c. Fonctions des sirtuines chez les mammifères 26
III. SIRTUINE 1 : DU GENE A LA PROTEINE *27*
1. Gène sirt1 27
a. Localisation du gène 27
b. Organisation génomique 28
2. Protéine 30
IV. REGULATIONS DE L'EXPRESSION ET DE L'ACTIVITE DE SIRT1 ..... *32*
1. Régulation du niveau d'expression de Sirt1 32
2. Régulation transcriptionnelle de l'expression de Sirt1 32
a. Foxo3a : activateur transcriptionnel de l'expression de Sirt1 32
b. E2F1 : activateur transcriptionnel de l'expression de Sirt1 33
c. HIC1 : inhibiteur transcriptionnel de l'expression de Sirt1 33
3. Régulation de l'activité de Sirt1 34
a. AROS : activateur de l'activité de Sirt1 34
b. DBC1 : inhibiteur de l'activité de Sirt1 35
c. SENP1 : inhibiteur de l'activité de Sirt1 36
4. Régulation pharmacologique de l'activité de Sirt1 36
a. Activateurs 36
b. Inhibiteurs 39
FONCTIONS REGULATRICES DE SIRT1 41
I. INTRODUCTION *41*
II. FONCTIONS DE SIRT1 DANS LE TISSU ADIPEUX *43*
III. FONCTION DE SIRT1 DANS LE PANCREAS *45*
IV. FONCTIONS DE SIRT1 DANS LE FOIE *47*
1. Régulation de la néoglucogenèse 47
2. Régulation du métabolisme lipidique et du cholestérol 50
V. FONCTIONS DE SIRT1 DANS LE MUSCLE STRIE SQUELETTIQUE *52*
1. Régulation de la différenciation myogénique 52
2. Régulation du métabolisme oxydatif du muscle strié squelettique 54
a. Régulation de PGC-1α 54
b. Rôle de l'AMPK 57

OBJECTIFS **63**

MATERIELS ET METHODES **67**

RECUPERATION DE PLASMIDE SUR PAPIER WHATMAN 69
TRANSFORMATION DE BACTERIES COMPETENTES 71
PREPARATION DE STABS 73
NUCLEOSPIN QUICK PURE D'ADN PLASMIDIQUE 75
GIGAPREPARATION D'ADN PLASMIDIQUE 77
VERIFICATION DES ADN PLASMIDIQUES PAR DES ENZYMES DE RESTRICTION ET ELECTROPHORESE EN GEL D'AGAROSE 79
TRANSFERT DE GENES *IN VIVO* 81
PRELEVEMENT TISSULAIRE ET CONDITIONNEMENT DES ECHANTILLONS 83
EXTRACTION PROTEIQUE SUR TISSU MUSCULAIRE CONGELE POUR ACTIVITES BIOLUMINESCENTES 85
DOSAGE DE PROTEINES 87
DOSAGE CHEMILUMINESCENT DE L'ACTIVITE ß-GALACTOSIDASE 89

DOSAGE FIREFLY LUCIFERASE 91
EXTRACTION PROTEIQUE AVEC TAMPON COMPLET SUR TISSU MUSCULAIRE/CELLULES .. 93
ELECTROPHORESE SDS PAGE/WESTERN BLOT 95
LUMINEX 101
CITRATE SYNTHETASE 103
3-HYDROXYL ACYL-COENZYME A DESHYDROGENASE 105
HEXOKINASE 107
LACTATE DESHYDROGENASE 109
CHYMOTRYPSINE-LIKE 111
TRYPSINE-LIKE 113
CATHEPSINE (B + L) 115
EXTRACTION MUSCULAIRE POUR DOSAGES DE METABOLITES 117
PHOSPHOCREATINE – ATP - GLUCOSE-6-PHOSPHATE 119
GLYCOGENE 121
PYRUVATE MUSCULAIRE 123

RESULTATS 125

MANUSCRIT 1 127
MANUSCRIT 2 165

DISCUSSION 195

CONCLUSION ET PERSPECTIVES 205

REFERENCES 209

ANNEXES 225

I. ARTICLES DANS DES REVUES INTERNATIONALES 227
II. COMMUNICATIONS AFFICHEES LORS DE CONGRES NATIONAUX ET INTERNATIONAUX ... 265

ABREVIATIONS

Liste des abréviations utilisées

°C	degré celsius
2’-OAADPr	2’-O-acétyl-ADP-ribose
4E-BP1	eukaryotic initiation factor 4E-binding protein
aa	acide aminé
ABCA1	ATP-binding cassette transporter 1
Ac	groupement acétyl
AceCS	acétyl-CoA synthétase
ADN	acide déoxyribonucléique
ADP	adénosine diphosphate
AICAR	5-aminoimidazole-4-carboxyamide-1-β-D-ribofuranide
AMP	adénosine monophosphate
AMPK	AMP kinase
AP1	activator-protein 1
AR	androgen receptor
ARN	acide ribonucléique
ARNm	ARN messager
ARNsh	small hairpin ARN
ARNsi	small interfering ARN
AROS	active regulator of Sirt1
atg	autophagy-related protein
ATP	adénosine triphosphate
C/EBP-α/δ	CCAAT/enhancer-binding protein α ou δ
CBP	CREB binding protein
CBS1	C/EBP-α binding site 1
CK	créatine kinase
COX IV	cytochrome c oxidase subunit IV
CPT-1a/b	carnitine palmitoyltransférase 1 a ou b
CRTC2	CREB regulated transcription coactivator 2
CS	citrate synthétase
DBC1	deleted in breast cancer 1
DO	densité optique
eNOS	endothelial nitric oxide synthase

ERR-α	estrogen-related receptor α
FoxO 1/3a	forkhead box O 1 ou 3a
g, mg, µg	gramme, milligramme, microgramme
G6P	glucose-6-phosphate
G-6-Pase	glucose-6-phosphatase
G6PDH	glucose-6-phosphate déshydrogénase
GK	glucokinase
GLUT4	glucose transporter type 4
H	histone
H_2O	eau
HAD	3-hydroxy-acyl-coenzymeA déshydrogénase
HAT	histone acétyltransférase
HDAC	histone déacétylase
HIC1	hypermethylated in cancer 1
HK	hexokinase
HNF-4α	hepatic nuclear factor 4α
kb	kilobase
kDa	kilodalton
KO	knock-out
L, mL, µL	litre, millilitre, microlitre
LDH	lactate déshydrogénase
LXR-α	liver X receptor α
M, mM, µM	molaire, millimolaire, micromolaire
mA	milliampère
mar	mating-type regulator
MCAD	medium chain acyl-CoA dehydrogenase
MDH	malate déshydrogénase
MEF	mouse embryonic fibroblast
MEF2C/D	myocyte-specific enhancer factor 2 C ou D
MR	milieu réactionnel
ms, µs	milliseconde, microseconde
mTOR	mammalian target of rapamycin
NAD^+/NADH	nicotinamide adénine dinucléotide
NAM	nicotinamide

Nampt	nicotinamide phosphoribosyltransférase
NCoR	nuclear receptor co-repressor
NF-κB	nuclear factor-κ-light-chain-enhancer of activated B cells
nm	nanomètre
Nmnat	nicotinamide/acide nicotinique mononucléotide adénylyltransférase
Npt	acide nicotinique phosphoribosyltransférase
NRF1	nuclear respiratory factor 1
pb	paire de bases
pCAF	p300-CBP associated factor
PEP-CK	phosphoénol-pyruvate carboxykinase
PGC-1α/β	peroxisome proliferator-activated receptor γ coactivator 1 α ou β
PK	pyruvate kinase
PPAR-γ	peroxisome proliferator-activated receptor γ
PPi	pyrophosphate inorganique
PRPP	5-phosphoribosyl-1-pyrophosphate
PTP1B	protein tyrosine phosphatase 1B
RBP1	retinol binding protein 1
RXR	retinoid X receptor
S6	ribosomal protein S6
S6K	ribosomal protein S6 kinase
SENP1	sentrin-specific protease 1
Sir	silent information regulator
Sirt	sirtuine
Smad	smothers against decapentaplegic homolog
SREBP-1c	sterol regulatory element binding protein 1c
SUMO	small ubiquitin-related modifier
TFAM	facteur de transcription mitochondrial A
TLE1	transducin like enhancer of splin 1
TR	thyroid hormone receptors
U	unité
Ub	ubiquitine
UCP2/3	uncoupling protein 2 ou 3
V	volt
λ	longueur d’onde

AVANT-PROPOS

Sirtuine 1 (Sirt1) est une protéine histone déacétylase dépendante du NAD^+ qui est impliquée dans de nombreux phénomènes biologiques : inflammation, survie cellulaire, prolifération cellulaire ou métabolisme cellulaire. Plus particulièrement, il a été observé que Sirt1 intervenait dans la régulation du métabolisme du glucose en activant la néoglucogenèse et en inhibant la glycolyse dans le foie. Par ailleurs, il a été exposé que Sirt1 induisait aussi l'oxydation des acides gras dans le muscle strié squelettique et le tissu adipeux. De plus, Sirt1 est impliquée dans la régulation de la sécrétion d'insuline par le pancréas. Enfin, des souris, soumises à un régime gras et à un traitement à base d'activateurs potentiels de Sirt1, deviennent résistantes à l'obésité et au développement de l'insulino-résistance. Cependant, le rôle que pourrait exercer Sirt1 dans la régulation du métabolisme du glucose dans le muscle strié squelettique n'est pas encore connu. Ce rôle, s'il existe, pourrait être particulièrement important compte tenu que, de part sa masse (40 % du poids corporel) et ses fonctions physiologiques consommatrices d'énergie (maitien postural, mouvement volontaire ou thermorégulation), le muscle strié squelettique est le principal consommateur de glucose. Le travail de thèse présenté ici s'intéresse au rôle propre de Sirt1 dans la régulation du métabolisme de glucose dans le muscle strié squelettique.

La première partie de ce mémoire consiste en une revue de la littérature sur Sirt1 constituée de deux chapitres : le premier chapitre présente les données générales de la protéine Sirt1, et le second chapitre expose les différentes fonctions de Sirt1 dans le tissu adipeux, pancréas, foie et muscle strié squelettique.

La seconde partie de ce mémoire consiste en la présentation de l'ensemble des résultats acquis lors de ma thèse. Ce travail a conduit à l'écriture de deux manuscrits : le premier manuscrit traite de l'implication et du mécanisme d'action de Sirt1 dans la régulation de l'expression des gènes régulant le métabolisme du glucose dans le muscle strié squelettique ; et le second expose les effets d'un jeûne sur la régulation des voies Akt/mTOR, autophagie/lysosome et ubiquitine/protéasome chez des myotubes C2C12.

Enfin, l'ensemble des résultats sera discuté et analysé dans une dernière partie, et finalement mis en perspective.

REVUE BIBLIOGRAPHIQUE

SIRTUINE 1 : GENE, PROTEINE ET REGULATION

I. INTRODUCTION

1. Généralités

La transcription cellulaire, dont celle du muscle strié squelettique, est influencée par le niveau de compactage de l'ADN. L'organisation et le compactage de l'ADN sont dus à des protéines histones qui créent deux niveaux de condensation de l'ADN. Le premier niveau de condensation, le nucléosome, est réalisé par les histones H2A, H2B, H3 et H4 créant des octamères globulaires autour desquels 146 paires de bases (pb) d'ADN s'enroulent. Le deuxième niveau de condensation est réalisé par les histones H1 qui permettent la compaction des nucléosomes (1-4) (Figure 1).

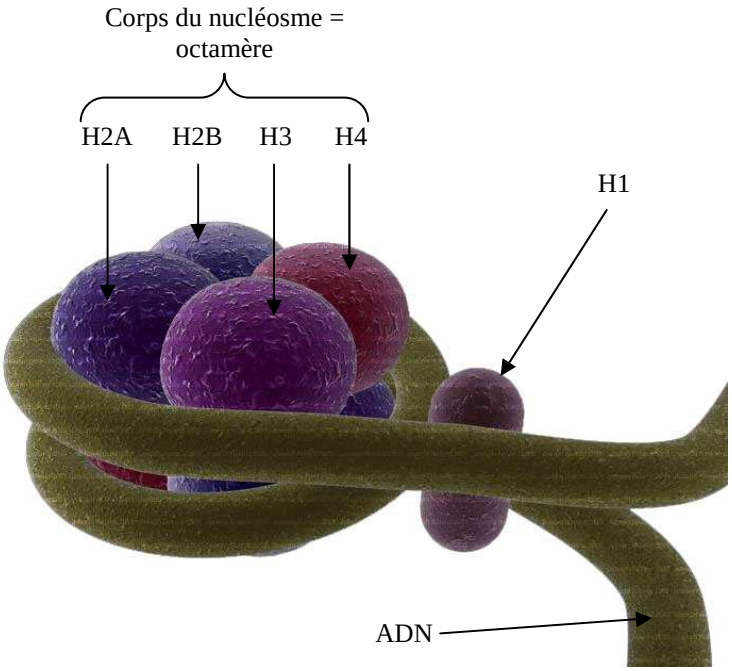

Figure 1. Condensation de l'ADN (modifiée d'après http://www.thomasenielsen.org/histone.jpg ; ADN : acide déoxyribonucléique ; H : histone).

La condensation de l'ADN peut être régulée par des modifications des extrémités N-terminales des histones, telles que phosphorylation, méthylation, ubiquitination, sumoylation ou encore acétylation. L'état d'acétylation des histones dépend d'une balance entre l'activité des histones acétyltransférases (HAT) et des histones déacétylases (HDAC). L'acétylation par les HAT au niveau des résidus lysines diminue l'interaction inter-nucléosome et entraîne le relâchement de la chromatine, ce qui facilite ainsi la fixation des facteurs de transcription. Les HDAC ont l'effet inverse. Ainsi, en général, une augmentation du niveau d'acétylation des histones par les HAT (hyper-acétylation) se traduit par une augmentation de l'activité transcriptionnelle, alors qu'une déacétylation par les HDAC (hypo-acétylation) est associée à une répression de la transcription des gènes (2, 4-6) (Figure 2). Bien qu'à l'origine, il ait été montré que les HAT et les HDAC avaient pour substrat les histones, de nombreux travaux ont depuis décrit que les HAT et les HDAC pouvaient avoir d'autres substrats.

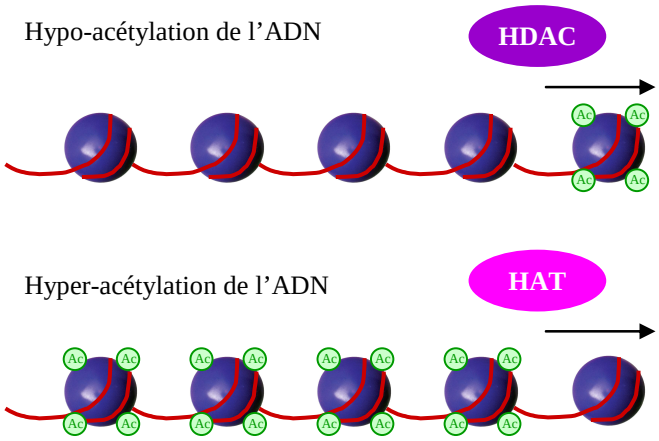

Figure 2. Régulation du niveau d'acétylation de l'ADN par les HDAC et HAT (modifiée d'après (4) ; Ac : groupement acétyl ; ADN : acide déoxyribonucléique ; HAT : histone acétyltransférase ; HDAC : histone déacétylase).

2. Histones acétyltransférases

Les HAT sont regroupées en plusieurs familles basées sur la conservation de la séquence du domaine catalytique (7, 8). Chez les mammifères, les principales familles sont :

- la famille GCN5/pCAF, nommée d'après le membre originel de levure yGcn5 et son orthologue humain pCAF (p300-CBP associated factor),
- la famille MYST, nommée d'après les membres MOZ humain, Ybf2/Sas3 de levure, Sas2 de levure et Tip60 humain,

- la famille CBP/p300 regroupant les homologues humains CBP (CREB binding protein) et p300.

3. Histones déacétylases

Les HDAC chez les mammifères sont classées en 3 familles (4, 9, 10) :

- la famille classique des HDAC divisée en 2 classes, les HDAC de classe 1 et les HDAC de classe 2 qui ont une forte homologie de séquence du domaine déacétylase, mais qui diffèrent par leur séquence N-terminale. Les HDAC de classe 1 regroupant les HDAC 1, 2, 3 et 8, ayant une homologie avec l'HDAC de levure y*Rpd*3, d'une taille moyenne de 50 kDa, sont exprimées ubiquitairement et situées principalement dans le noyau. Les HDAC de classe 2 regroupant les HDAC 4, 5, 6, 7, 9 et 10 ayant une homologie avec l'HDAC de levure y*Hda*1, d'une taille moyenne comprise entre 120 et 150 kDa, sont exprimées de façon tissu spécifique et situées dans le noyau et le cytoplasme. Le passage dans le noyau est un moyen de régulation de leur activité.
- la famille des sirtuines ou HDAC de classe 3, ayant une homologie avec l'HDAC de levure y*Sir2*.
- l'HDAC 11, récemment identifiée, possédant quelques similitudes avec les HDAC de classe 1 et 2, constitue l'HDAC de classe 4 (11).

II. SIRTUINES

1. Sirtuines chez la levure

Les sirtuines doivent leur nom aux protéines Sir (silent information regulator), comprenant 4 Sir (Sir1 à 4) (12), identifiées en 1979 chez la levure comme des répresseurs de l'activité transcriptionnelle et anciennement nommées Mar (mating-type regulator) (13, 14). Sir2, l'homologue le plus proche des sirtuines de mammifères (15), est une HDAC dépendante du NAD^+ (16-18) qui contrôle la durée de vie dans de nombreux organismes, tels que levure, ver et drosophile. Chez la levure, une délétion du gène ysir2 réduit de 50 % la durée de vie réplicative (nombre de divisions cellulaires générées à partir de la cellule mère),

alors qu'une surexpression de ysir2 l'augmente de 30 % (19). Il en est de même chez le ver chez qui une augmentation de l'expression du gène sir2.1, homologue de ysir2, allonge la durée de vie (20, 21), et chez la drosophile chez qui l'augmentation de l'expression de dsir2, homologue de ysir2, prolonge la durée de vie. Le fait que Sir2 semble étroitement lié à la régulation de la durée de vie, et le fait qu'une restriction calorique prolonge la durée de vie (22), suggèrent que le contrôle de la durée de vie par Sir2 est associé à l'état métabolique. En effet, chez la levure, l'activation de ySir2 par le NAD^+ est nécessaire à l'augmentation de la durée de vie induite par restriction calorique (23). De même, chez la drosophile, dSir2 est nécessaire à l'augmentation de la longévité induite par restriction calorique (21).

2. Sirtuines chez les mammifères

a. Généralités

Chez les mammifères, il a été identifié 7 sirtuines nommées de Sirt1 à 7 (15, 24) ayant des localisations et des activités enzymatiques différentes. Les sirtuines 1, 6 et 7 sont nucléaires avec une localisation dans les régions euchromatiques pour Sirt1, dans les régions hétérochromatiques pour Sirt6 et dans le nucléole pour Sirt7. Les sirtuines 3, 4 et 5 sont mitochondriales et Sirt2 est cytoplasmique (25). Toutes les sirtuines possèdent une séquence identique de 275 acides aminés, composant le domaine catalytique dépendant du NAD^+. Les sirtuines 1, 2, 3 et 5 possèdent un domaine déacétylase dépendant du NAD^+ et les sirtuines 4 et 6 ont un domaine ADP-ribosyl-transférase dépendant du NAD^+ (26) (Tableau 1).

Sirtuines	Activité du domaine catalytique	Localisation	Poids moléculaire (kDa)
Sirt1	Déacétylation	Noyau	81,7
Sirt2	Déacétylation	Cytoplasme	43,2
Sirt3	Déacétylation	Mitochondrie	43,6
Sirt4	ADP-ribosylation	Mitochondrie	35,2
Sirt5	Déacétylation	Mitochondrie	33,9
Sirt6	ADP-ribosylation	Noyau	39,1
Sirt7	?	Noyau	44,9

Tableau 1. Les différentes sirtuines chez les mammifères (ADP : adénosine diphosphate ; kDa : kilodaltons ; Sirt : sirtuine).

b. Réactions de déacétylation et d'ADP-ribosylation

La réaction de déacétylation, catalysée par Sirt1, 2, 3 et 5, consiste tout d'abord au clivage de la liaison glycosidique entre la base nicotinamide et le ribose du NAD^+, puis à la libération du nicotinamide, et au transfert du radical acétyl d'une protéine acétylée sur l'ADP ribose avec production de 2'-O-acétyl-ADP-ribose (2'-OAADPr) et de protéine déacétylée (27-29)(Figure 3).

$$\text{Protéine acétylée} + NAD^+ \xrightarrow{\text{déacétylase}} \text{nicotinamide} + \text{2'-OAADPr} + \text{protéine}$$

La réaction d'ADP-ribosylation, catalysée par Sirt4 et 6, consiste au clivage de la liaison glycosidique entre la base nicotinamide et le ribose du NAD^+, puis à la libération du nicotinamide et au transfert du radical ADP-ribosyl sur une protéine (Figure 3).

$$\text{Protéine} + NAD^+ \xrightarrow{\text{ADP-ribosyl-transférase}} \text{nicotinamide} + \text{protéine ADP-ribosylée}$$

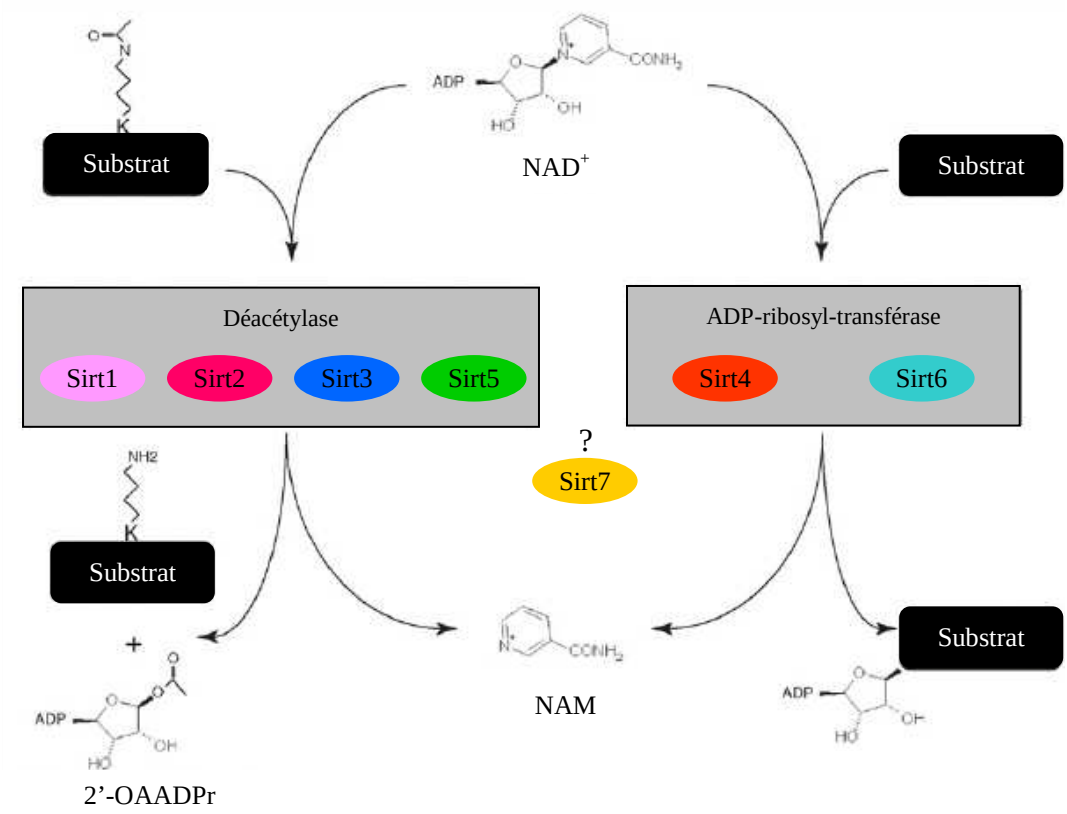

Figure 3. Activités de déacétylation des Sirt1, 2, 3 et 5 et d'ADP-ribosylation des Sirt4 et 6 (modifiée d'après (30) ; 2'-OAADPr : 2'-O-acétyl-ADP-ribose ; ADP : adénosine diphosphate ; NAD : nicotinamide adénine dinucléotide ; NAM : nicotinamide ; Sirt : sirtuine).

c. Fonctions des sirtuines chez les mammifères

Pour étudier les rôles des différentes sirtuines, plusieurs modèles de souris KO ont été créés (31). La figure ci-dessous regroupe les fonctions connues des sirtuines à partir des modèles KO de souris (Figure 4).

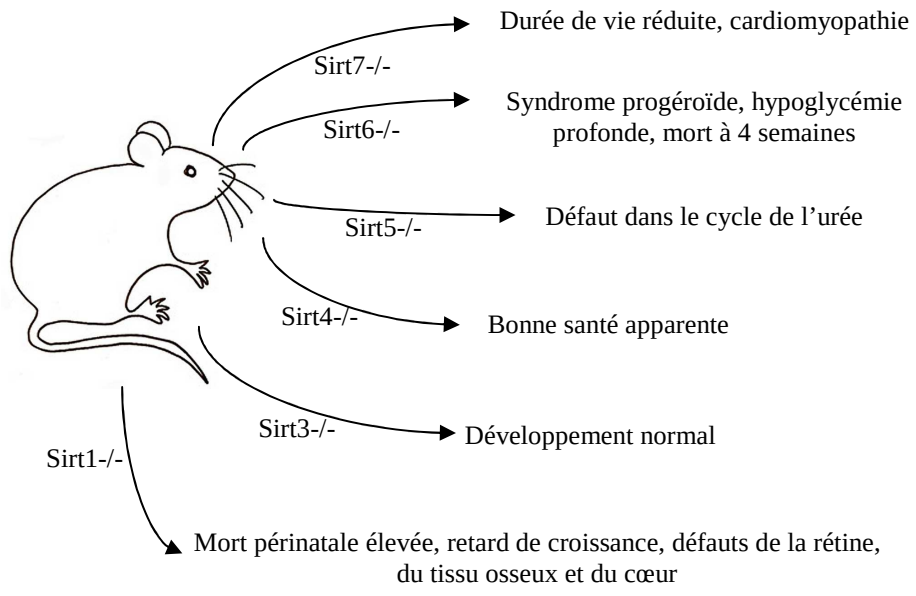

Figure 4. Modèles de souris KO sirtuines (modifiée d'après (32) ; Sirt : sirtuine).

L'invalidation des gènes sirt1, 6 et 7 se traduit par une croissance réduite des souris, et de nombreuses atteintes physiologiques importantes conduisant à une durée de vie limitée. Au contraire, en ce qui concerne l'invalidation des gènes Sirt3, 4 et 5, aucun effet sur la durée de vie n'est détecté (32).

III. SIRTUINE 1 : DU GENE A LA PROTEINE

1. Gène sirt1

a. Localisation du gène

Sirt1 est la sirtuine des mammifères qui possède le plus d'homologie de séquence avec Sir2 (24). Le gène sirt1 humain se situe sur le bras long du chromosome 10 au niveau du locus 21.3 (Figure 5).

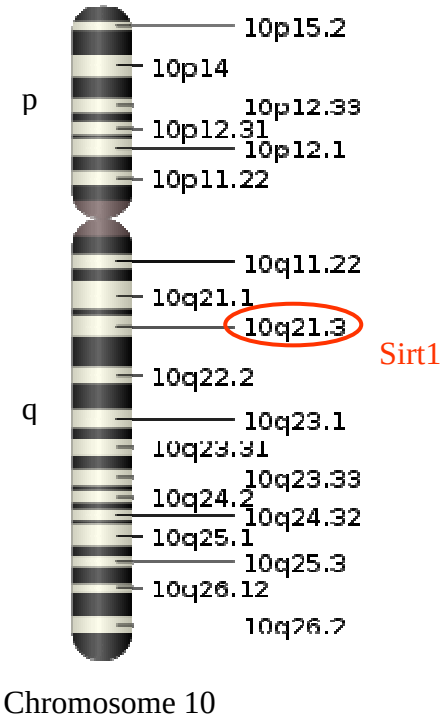

Figure 5. Localisation chromosomale du gène Sirt1 humain (modifiée d'après (33) ; Sirt1 : sirtuine 1).

b. Organisation génomique

Le gène sirt1 est composé d'une région de 33,7 kb environ comprenant 9 exons d'une taille allant de 80 pb pour l'exon 6 à 2120 pb pour l'exon 9 (Figure 6 et Tableau 2). Le domaine catalytique hautement conservé entre les différentes espèces se situe entre les exons 3 et 8 (Figures 6 et 7). L'ARNm de Sirt1 humain d'une taille de 4107 pb code pour une protéine composée de 747 acides aminés.

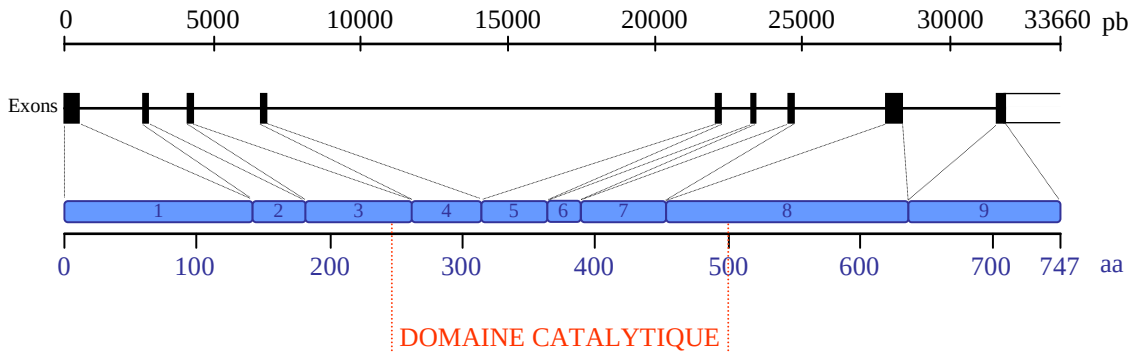

Figure 6. Organisation génomique du gène sirt1 (modifiée d'après (33) ; aa : acides aminés ; pb : paire de bases).

Exons	**Taille exons (pb)**	**Introns**	**Taille introns (pb)**
1	483	1	2265
2	117	2	1348
3	242	3	2278
4	153	4	15234
5	148	5	1108
6	80	6	1130
7	187	7	3031
8	558	8	3233
9	2126		

Tableau 2. Taille des exons et des introns du gène sirt1 humain (modifié d'après (33) ; pb : paire de bases).

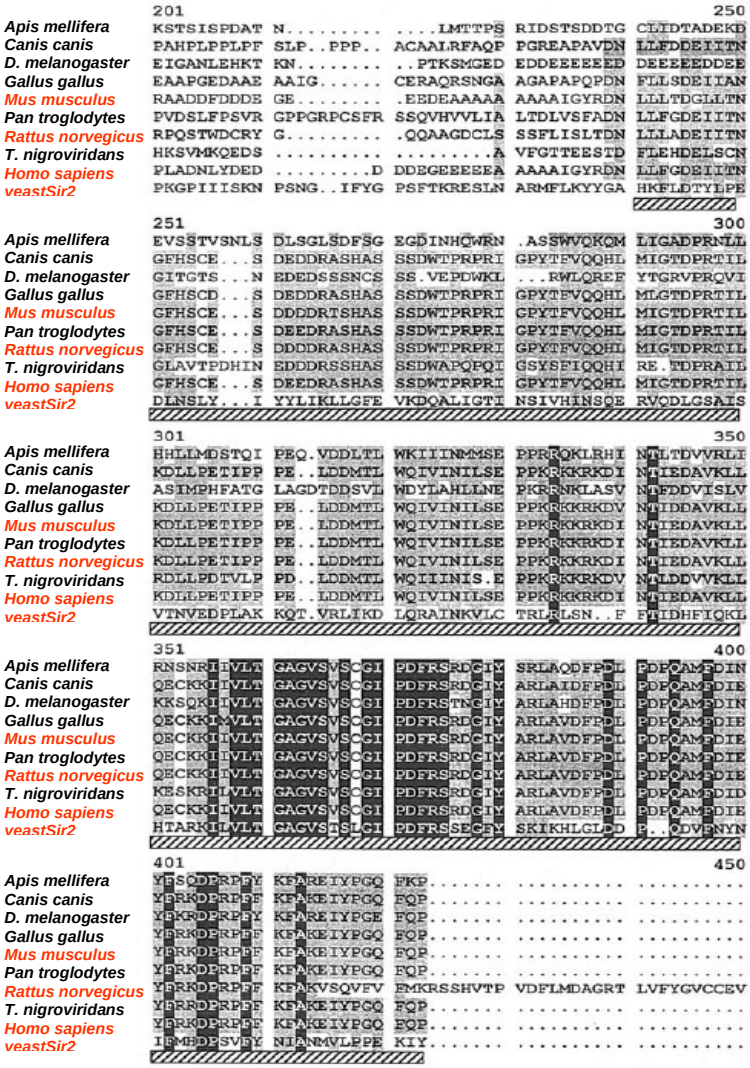

Figure 7. Alignement de la séquence en acides aminés du domaine catalytique (en rayé) de Sirt1 chez différentes espèces (logiciel clustalW) (modifiée d'après (33) ; Noir : > 75 % d'homologie dans la colonne ; gris : > 50 % d'homologie dans la colonne).

2. Protéine

La protéine Sirt1 humaine, composée de 747 acides aminés pour un poids moléculaire de 81,7 kDa, comporte 4 régions (Figure 8) :

- la région N-terminale regroupant les acides aminés de 1 à 180 (exons 1 et 2),
- le site allostérique allant de l'acide aminé 181 à 243 (exons 2 et 3),
- le site catalytique regroupant les acides aminés de 244 à 498 (exons 3, 4, 5, 6, 7 et 8),
- la région C-terminale allant de l'acide aminé 499 à 747 (exons 8 et 9).

La structure tridimensionnelle de la protéine Sirt1 apparaît désordonnée avec de longues régions flexibles C et N-terminales. Le site catalytique, commun aux différentes

sirtuines humaines, possède deux domaines particuliers, le pli Rossman, et un petit sous-domaine où se localise un atome de zinc (34). A l'interface de ces deux domaines, se trouve le site de liaison pour le NAD^+ : la molécule de NAD^+ s'insère dans une poche spécifique constituée d'une partie hydrophobe du petit sous-domaine et d'une partie hydrophile du pli Rossman. La boucle flexible permet un réarrangement structural durant la fixation du NAD^+, essentiel pour la catalyse (35). L'ion zinc est coordonné de façon tétraédrique par les groupements thiols de 4 cystéines (371, 374, 395 et 398) plissées dans une structure unique. Ce domaine de liaison au zinc joue un rôle important lors de la liaison spécifique de Sirt1 au substrat. Le site allostérique, composé de quatre hélices α, se situe entre la région N-terminale et le corps catalytique. Ainsi, il peut contrôler l'activité catalytique par changements conformationnels (36).

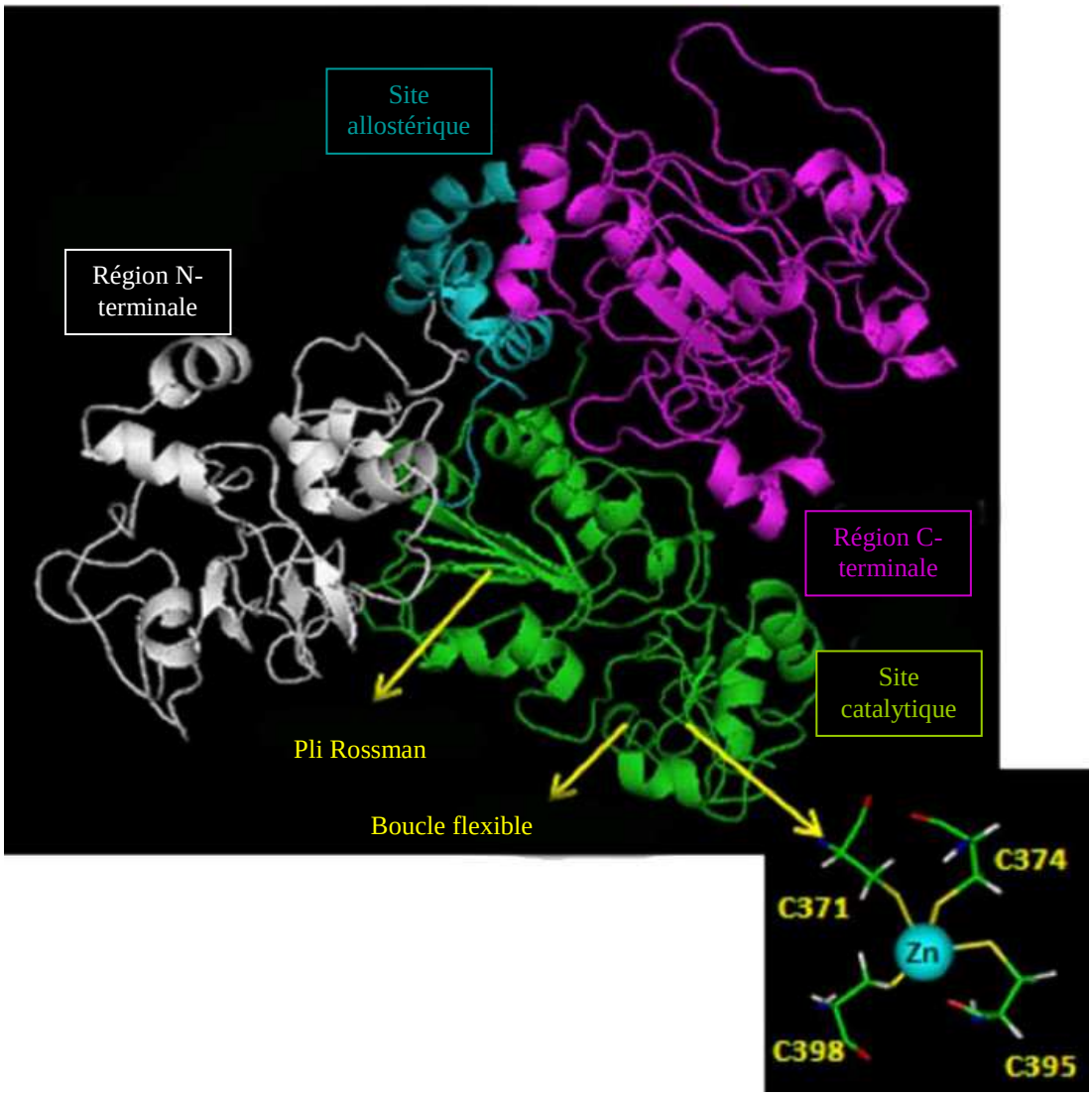

Figure 8. Structure tridimensionnelle de la protéine Sirt1 humaine (modifiée d'après (36)).

IV. REGULATIONS DE L'EXPRESSION ET DE L'ACTIVITE DE SIRT1

1. Régulation du niveau d'expression de Sirt1

Bien que Sirt1 soit ubiquitaire, son niveau d'expression varie d'un tissu à l'autre (24, 25) et en fonction de nombreuses conditions physiologiques ((37) pour revue). La restriction calorique, chez les rongeurs ou les humains, stimule l'expression de Sirt1 aussi bien dans le muscle, le cœur ou le tissu adipeux, alors qu'un régime gras tend à diminuer son expression (38-44). Cependant, l'expression de Sirt1 semble être régulée de manière différente dans le foie puisque l'expression de Sirt1 est réduite en cas de restriction calorique et augmentée par un régime gras (45). Lors du vieillissement, l'expression de Sirt1 diminue dans le cœur ou le thymus mais augmente en cas de maladie comme le cancer ou la neurodégénération (46-49), mais le rôle exact de Sirt1 dans ces processus reste encore à élucider. L'expression de Sirt1 peut également augmenter dans le muscle strié squelettique chez des rats soumis à un exercice à l'endurance ou à un entrainement musculaire (50). Enfin, l'expression protéique de Sirt1 est stimulée en cas d'hypoxie (51, 52).

2. Régulation transcriptionnelle de l'expression de Sirt1

a. FoxO 3a : activateur transcriptionnel de l'expression de Sirt1

La transcription du promoteur Sirt1 peut être contrôlée par le facteur de transcription FoxO (forkhead box O) 3a (53). En effet, il a été montré, chez des cellules cancéreuses neuronales PC12 soumises à un jeûne, que le facteur de transcription FoxO3a était transloqué dans le noyau où il se liait aux éléments de réponse du facteur de transcription p53 du promoteur Sirt1. Cette liaison supprime ainsi l'interaction de p53 au promoteur Sirt1. Etant donné que p53 réprime l'expression du gène sirt1, son recrutement par FoxO3a active la transcription de Sirt1. Cette notion est confirmée dans des modèles de souris KO p53 où une augmentation de l'ARNm de Sirt1 est observée (37, 53) (Figure 9).

b. E2F1 : activateur transcriptionnel de l'expression de Sirt1

L'expression de Sirt1 est aussi sous le contrôle du facteur de transcription E2F1 (54). E2F1 est un facteur transcriptionnel intervenant dans la régulation du cycle cellulaire (55) qui induit l'apoptose en cas d'augmentation de la prolifération (56). Il a été montré qu'E2F1 induisait l'expression de Sirt1 en réponse à un stress génotoxique (54). Effectivement, une transfection d'E2F1 chez des cellules cancéreuses H1299 aboutit à la fois à l'augmentation du niveau d'expression de la protéine Sirt1 et de son ARNm, mais aussi à l'activation du promoteur Sirt1. De plus, une infection par le virus Ad-7 induit une augmentation de l'expression de Sirt1 chez des fibroblastes embryonaires de souris (MEF) mais pas chez des MEF $E2F1^{-/-}$ (54) (Figure 9).

c. HIC1 : inhibiteur transcriptionnel de l'expression de Sirt1

Un autre régulateur de Sirt1 au niveau transcriptionnel est le supresseur de tumeur HIC (hypermethylated in cancer) 1 (57). HIC1 est un répresseur transcriptionnel coopérant avec p53 pour supprimer le développement de cancers liés au vieillissement (58, 59). Il a été montré, chez des cellules cancéreuses, que la présence d'HIC1 réprimait la transcription de Sirt1. Cette répression aboutit à l'acétylation et l'activation de p53, responsable d'un arrêt de la croissance et d'une stimulation de l'apoptose. Au contraire, en cas de perte d'expression d'HIC1, Sirt1 est surexprimée induisant la déacétylation et l'inactivation de p53, aboutissant ainsi à une augmentation du risque de développement tumoral (57). Sirt1 possède donc des fonctions anti-apoptotiques et pro-oncogéniques induites en cas d'inactivation de HIC1 (37) (Figure 9).

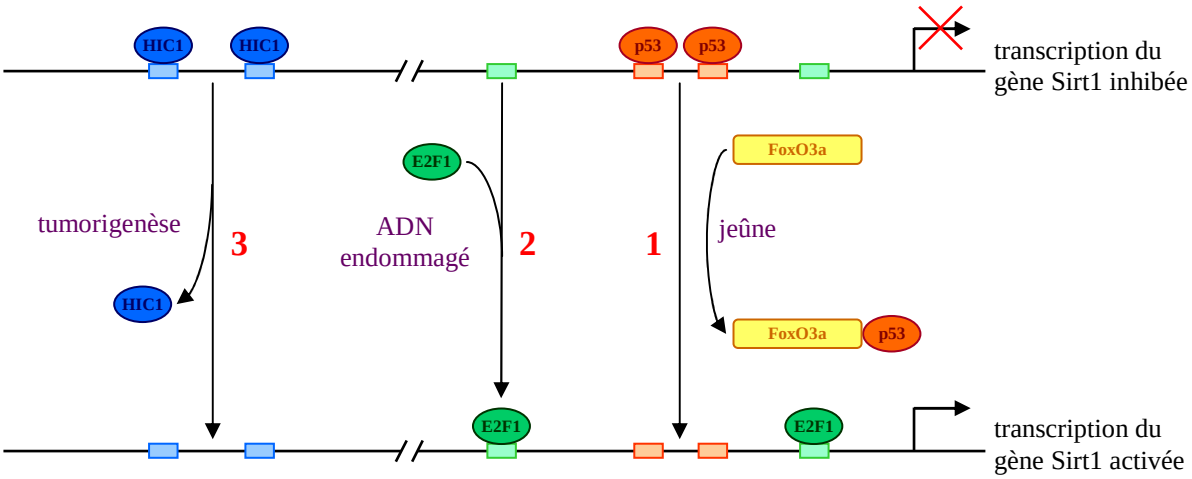

Figure 9. Régulation transcriptionnelle de Sirt1 (modifiée d'après (37)). **1** : la liaison du facteur de transcription p53 sur le promoteur de Sirt1 réprime sa transcription. Cependant, durant un jeûne, Foxo3a s'associe à p53 et lève la fonction d'inhibition de p53, activant ainsi la transcription de Sirt1. **2** : en cas de stress génotoxique, E2F1 est surégulé et va se fixer sur le promoteur de Sirt1 permettant ainsi sa transcription. **3** : en conditions normales, HIC1 se fixe sur le promoteur de Sirt1 empêchant sa transcription ; cependant lors d'un développement tumoral, l'expression d'HIC1 diminue induisant ainsi la transcription de Sirt1 (HIC 1 : hypermethylated in cancer 1 ; FoxO3a : forkhead box O 3a ; Sirt1 : sirtuine 1).

3. Régulation de l'activité de Sirt1

Trois protéines majeures sont capables de réguler l'activité de Sirt1 par une liaison directe protéine-protéine.

a. AROS : activateur de l'activité de Sirt1

AROS (active regulator of Sirt1) agit comme un régulateur positif de Sirt1. En effet, il a été montré qu'AROS augmentait la déacétylation de p53 dépendante de Sirt1, inhibant ainsi l'activité transcriptionnelle de p53 (60). La protéine AROS se lie à un domaine contenu dans la région N-terminale de Sirt1, qui augmente la capacité de Sirt1 à déacétyler p53. Cette interaction entre AROS et Sirt1 induirait un changement de conformation de la structure de Sirt1 qui augmenterait l'efficacité enzymatique du site catalytique de Sirt1 (60) (Figure 10).

b. DBC1 : inhibiteur de l'activité de Sirt1

Une seconde protéine peut réguler l'activité de Sirt1 : DBC (deleted in breast cancer) 1. DBC1 a été identifiée à l'origine comme un gène récessif délété dans les cancers du sein. DBC1 code une protéine impliquée dans les processus apoptotiques. Il a été montré que DBC1 pouvait former un complexe stable avec Sirt1 *in vivo* et *in vitro* et réguler négativement son activité (61, 62). DBC1 interagit directement avec le domaine catalytique de Sirt1 au moyen d'un motif leucine zipper (61, 63). Cette interaction entre DBC1 et Sirt1 empêche probablement l'accès des substrats de Sirt1 à son site catalytique, puisqu'il a été montré qu'une surexpression de DBC1 diminuait la liaison et la déacétylation de substrats de Sirt1, tels que p53 ou FoxO3a (Figure 10). Ainsi, dans le cas du cancer du poumon, la régulation négative de Sirt1 par DBC1 pourrait retarder la tumorigenèse (64).

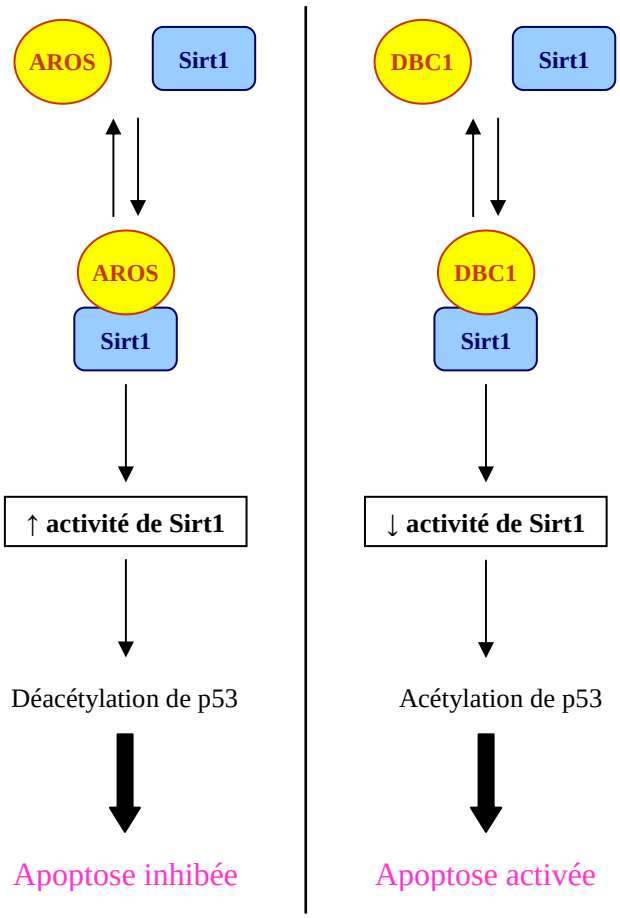

Figure 10. Représentation schématique de l'action d'AROS et de DBC1 sur Sirt1. AROS stimule l'activité de Sirt1 et conduit à une hypo-acétylation de p53 induisant ainsi une inhibition de son activité pro-apoptotique. Au contraire, DBC1 inhibe l'activité de Sirt1 et aboutit à une hyper-acétylation de p53 induisant son activité pro-apoptotique (AROS : active regulator of Sirt1 ; DBC1 : deleted in breast cancer 1 ; Sirt1 : sirtuine 1).

c. SENP1 : inhibiteur de l'activité de Sirt1

L'activité de Sirt1 peut également être modulée au moyen d'une sumoylation. La sumoylation est une modification post-transcriptionnelle dans laquelle des protéines SUMO (small ubiquitin-related modifier) sont fixées sur des résidus lysine de protéines cibles. Comme l'ubiquitination, la sumoylation est catalysée en trois étapes impliquant une enzyme activatrice E1, une enzyme de conjugaison E2 et une ligase E3. La réaction inverse de désumoylation est effectuée au moyen des SENP (sentrin-specific protease) désumoylases (65). En 2007, Yang *et al*. ont montré, chez des cellules DU145, que la sumoylation de la lysine 734 de Sirt1 entraînait une augmentation de son activité. Inversement, une mutation de cette lysine en arginine, ainsi qu'une désumoylation de Sirt1 par une désumoylase nucléaire, SENP1, aboutissaient à une inhibition de l'activité de Sirt1 (66) (Figure 11).

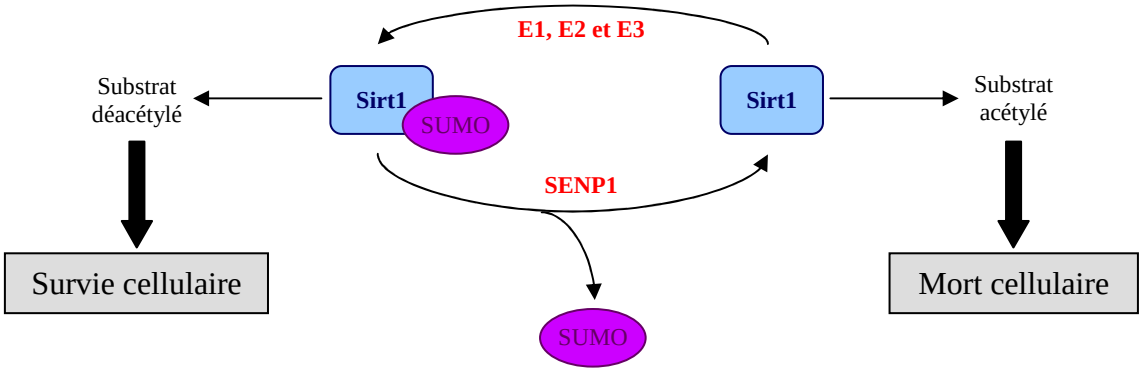

Figure 11. Représentation schématique de l'action de SENP1 sur Sirt1 (modifiée d'après (66)). En conditions normales, Sirt1 est sumoylée et active. Sirt1 déacétyle et supprime l'activité des substrats apoptotiques favorisant ainsi la survie cellulaire. En réponse à un stress génotoxique, SENP1 s'associe avec Sirt1 qui devient désumoylée et moins active. Ainsi les substrats pro-apoptotiques inhibés par Sirt1 deviennent actifs et causent la mort cellulaire (SENP1 : sentrin-specific protease 1 ; Sirt1 : sirtuine 1 ; SUMO : small ubiquitin-related modifier).

4. Régulation pharmacologique de l'activité de Sirt1

De nombreuses molécules sont capables d'influencer l'activité catalytique de Sirt1 par modification de l'affinité de Sirt1 pour ses substrats.

a. Activateurs

Le NAD^+ est un activateur naturel de Sirt1 (17, 18). Une enzyme, la nicotinamide phosphoribosyltransférase (Nampt), essentielle dans la régulation de la synthèse du NAD^+

(Figure 12), intervient dans cette régulation. En effet, une augmentation de la concentration de la Nampt stimule l'activité de Sirt1, *via* une augmentation du NAD^+ (67).

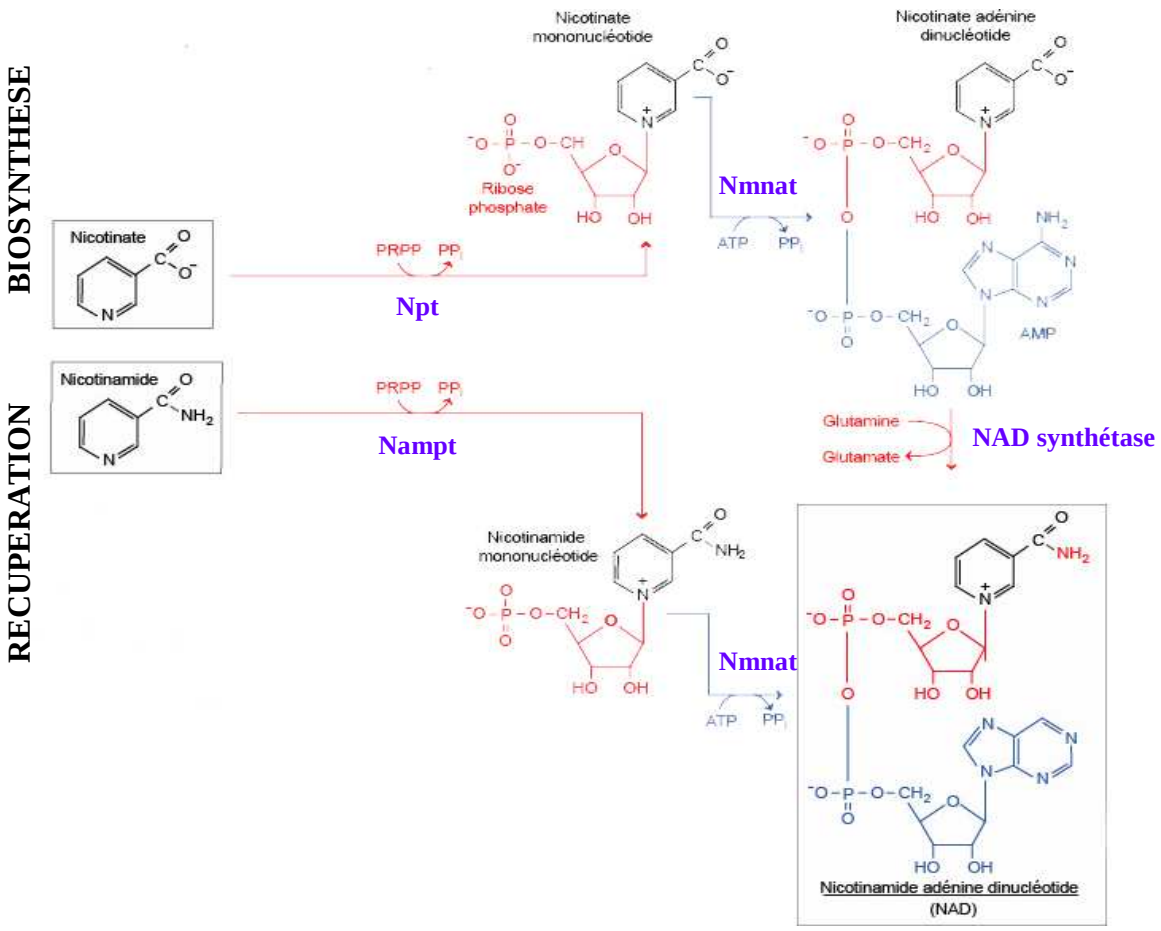

Figure 12. Voie de biosynthèse du NAD^+ à partir du nicotinate et voie de récupération du NAD^+ à partir du nicotinamide (modifiée d'après http://hermendis.perso.sfr.fr). **Biosynthèse** : chez les mammifères, le nicotinate est converti en NAD par ajouts successifs d'un groupement ribose phosphate par la Npt, d'un groupement AMP par la Nmnat et d'un groupement amine par la NAD synthétase, groupements fournis respectivement par le PRPP, l'ATP et la glutamine. **Récupération** : chez les mammifères, le nicotinamide est converti en nicotinamide mononucléotide par la Nampt, puis en NAD par la Nmnat par ajouts successifs d'un groupement ribose phosphate et d'un groupement AMP, fournis respectivement par le PRPP et l'ATP (AMP : adénosine monophosphate ; ATP : adénosine triphosphate ; NAD : nicotinamide adénine dinucléotide ; Nampt : nicotinamide phosphoribosyltransférase ; Nmnat : nicotinamide/acide nicotinique mononucléotide adénylyltransférase ; Npt : acide nicotinique phosphoribosyltransférase ; PPi : pyrophosphate inorganique ; PRPP : 5-phosphoribosyl-1-pyrophosphate).

D'autres activateurs chimiques de Sirt1 sont connus. Tous les activateurs décrits ci-dessous apparaissent réguler l'activité de Sirt1 par diminution de la constante michaelienne des substrats acétylés, permettant ainsi une meilleure affinité de Sirt1 pour son substrat (68). Parmi ces activateurs, les polyphénols, issus des plantes, sont caractérisés par la présence d'un ou de plusieurs groupements phénoliques. Ils appartiennent principalement à trois catégories :

les chalcones (comme la butéine), les flavones (telle que la quercétine) et les stilbènes (resveratrol) (Tableau 3) (68, 69).

Nom commun	Nom chimique	Structure du composé	Stimulation de Sirt1
Resveratrol	3,5,4'-trihydroxy-*trans*-stilbène		x 13,4
Butéine	3,4,2',4'-tétrahydroxychalcone		x 8,5
Quercétine	3,5,7,3',4'-pentahydroxyflavone		x 4,6

Tableau 3. Activateurs naturels de Sirt1 : les polyphénols (modifié d'après (69)). La stimulation de Sirt1 correspond à l'activité de Sirt1 avec le composé (100 µM) divisée par l'activité de Sirt1 avec le véhicule chez des cellules HeLa (Sirt1 : sirtuine 1 ; µM : micromolaire).

Le resveratrol permet d'augmenter la durée de vie de nombreuses espèces, telles que la levure et le ver (69-74) et d'améliorer l'état de santé général, chez les mammifères, de façon dépendante à Sirt1 (75-80). Cependant, il a été montré que le resveratrol n'était pas un activateur direct de Sirt1 et qu'il pouvait aussi agir sur d'autres protéines (81-83). L'AMPK (AMP-activated protein kinase), enzyme métabolique qui régule la transcription de l'enzyme Nampt, en est un exemple (84-86). Ainsi, le resveratrol activerait l'AMPK qui elle-même activerait à son tour Sirt1 *via* une augmentation de la synthèse de NAD^+ (cf chapitre V.2.b de la seconde partie).

Dans le but de trouver des activateurs spécifiques de Sirt1, de nouvelles molécules ont été décrites : SRT1720, SRT1460 et SRT2183 (87). Ces molécules, qui possèdent des structures différentes des composés naturels précédents (Figure 13), sont jusqu'à 1000 fois plus puissantes que le resveratrol (Figure 14) (87). La spécificité de ces molécules est aussi controversée (cf chapitre V.2.b de la seconde partie).

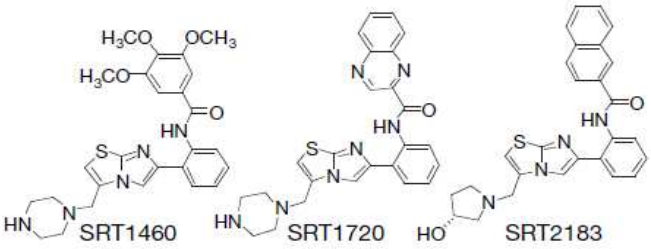

Figure 13. Structure chimique des activateurs de Sirt1 (modifiée d'après (87)).

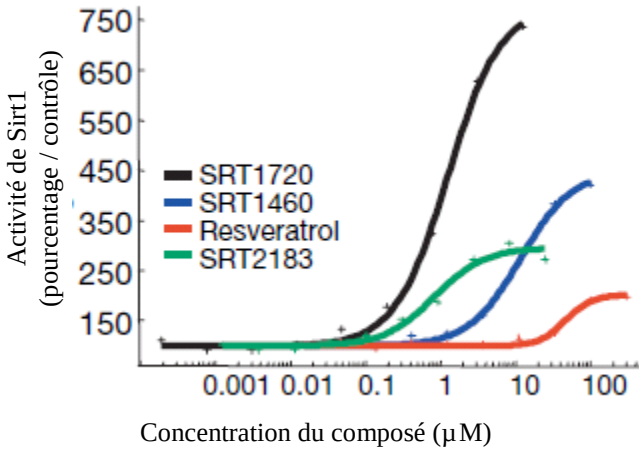

Figure 14. Comparaison de l'efficacité du resveratrol, du SRT1460, SRT1720 et SRT2183 sur l'activité de Sirt1 mesurée avec le substrat Fluor de Lys (modifiée d'après (87) ; Sirt1 : sirtuine 1 ; µM : micromolaire).

b. Inhibiteurs

Les inhibiteurs de Sirt1 les plus anciens sont le sirtinol (88) et la splitomicine (89, 90) (Figure 15). Depuis, de nombreux inhibiteurs de Sirt1 ont été mis en évidence : le phloroglucinol (91), l'indol (92) ou les dérivés de suramine (93). Cependant, la majorité des composés mentionnés ci-dessus peuvent aussi bien inhiber Sirt1 que Sirt2 (68). Le nicotinamide, produit issu de la réaction de déacétylation de Sirt1, est également un inhibiteur naturel de Sirt1 (Figure 15) (94). De façon analogue au NAD^+, activateur de Sirt1, le NADH peut, lui, inhiber l'activité de Sirt1. Enfin, pour compléter cette liste, les composés, tels que le dihydrocoumarine, le HR73, l'EX527 ou encore l'AGK2 appartiennent également à la famille des inhibiteurs de Sirt1 (95).

Sirtinol

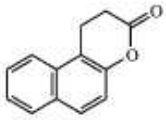

Splitomicine

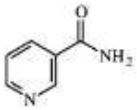

Nicotinamide

Figure 15. Structure chimique de quelques inhibiteurs de Sirt1 (d'après (90)).

FONCTIONS REGULATRICES DE SIRT1

I. INTRODUCTION

Du fait de l'importance de Sir2 dans la régulation de la durée de vie et de son rôle lors d'une restriction calorique, de nombreuses études se sont intéressées au rôle de Sirt1 dans la régulation de plusieurs fonctions métaboliques chez les mammifères. Le tableau ci-dessous (Tableau 4) regroupe les nombreuses cibles de Sirt1 et par conséquent les fonctions régulées par Sirt1 *via* ces cibles.

Substrat	Tissu / Cellules	Activation/inhibtion	Effets biologiques	Références
AceCS1	Cos-7	Activation	↑ lipogenèse	(96)
AP1	JB6	Activation	↑ activité transcriptionnelle	(97)
AR	LnCaP	Inhibition	↓ activité transcriptionnelle	(98, 99)
Atg5, 7 et 8	HeLa	Activation	↑ autophagie	(100)
cJun	HEK293	Inhibition	↓ activité transcriptionnelle	(101)
CLOCK **BMAL1**	Foie, NIH3T3 et JEG3	Activation	↑ transcription des gènes circadiens	(102, 103)
cortactin	MEF	Activation	↑ mobilité cellulaire	(104)
E2F1	U2OS et H1299S	Inhibition	↓ apoptose	(54)
eNOS	Cellules endothéliales de veine et d'aorte	Activation	↑ homéostasie vasculaire	(105)
FoxO1	HepG2 et HEK293	Activation	↑ activité transcriptionnelle	(106)
	Sv40	Activation	↑ néoglucogénèse	(78)
		Inhibition	↓ stress oxydatif	
	HEK293 et 3T3	Activation	↓ activité transcriptionnelle	(107)
	HEK293	Activation	↑ activité du promoteur IGFBP	(108)
FoxO3	293T et fibroblastes	Inhibition	↓ apoptose	(109)
FoxO3a	HEK293T et HeLa	Inhibition	↓ apoptose ↓ activité transcriptionnelle	(110)
FoxO4		Activation	↑ résistance au stress	(111)
	HEK293T	Activation	↑ activité transcriptionnelle	(112)
H1	293F	Activation	↑ formation hétérochromatine	(113)
HES1 **HEY2**	293T	Activation	↓ activité transcriptionnelle	(114)
HNF4-α	HepG2	Inhibition	↓ activité transcriptionnelle	(115)
Ku70	Q293A	Activation	↑ activité réparatrice de l'ADN	(116)
	293T	Activation	↓ apoptose	(38)
LKB1	HepG2, HEK293T et HeLa	Activation	↓ accumulation lipidique hépatique	(117, 118)
LXR	HEK293T	Activation	↑ fuite cholestérol ↑ lipogénèse	(119)

MEF2D	93T et C2C12	Inhibition	↓ myogénèse	(62)
MyoD **pCAF**	293T et C2C12	Inhibition	↓ myogénèse	(120, 121)
NF-κB	NCI-H460 Cellules neuronales primaires corticales	Inhibition Inhibition	↓ activité transcriptionnelle ↑ apoptose ↑ inflammation ↑ neuroprotection	(122) (76)
p300	Cellules HEK293	Inhibition	↓ activité transcriptionnelle	(123)
p53	H1299 MEF SV40 MEF MEF ES	Inhibition Inhibition Activation Inhibition Inhibition Inhibition	↓ apoptose ↑ apoptose ↓ apoptose ↓ activité transcriptionnelle ↓ sénescence cellulaire ↓ apoptose ↓ apoptose	(124) (125) (126) (127) (128) (129)
p73	HEK293 et HeLa	Inhibition	↓ activité transcriptionnelle	(130)
PGC-1α	PC12 Foie et hépatocytes Muscle et C2C12 Muscle et C2C12 Tissu adipeux	Activation Activation Activation Activation Activation	 ↑ néoglucogénèse ↑ fonctions mitochondriales ↑ fonctions mitochondriales ↑ oxydation des acides gras ↑ fonctions mitochondriales ↑ thermogénèse	(131) (132, 133) (80, 134, 135) (136) (80, 134)
PPAR-γ	3T3-L1	Inhibition	↓ adipogénèse ↑ lipolyse	(75)
PTP1B	C2C12	Inhibition	↑ sensibilité à l'insuline	(43)
RBP1	H1299 et HeLa	Inhibition	↓ sénescence cellulaire	(137)
Smad7	Cos-7	Inhibition	↓ apoptose	(138)
Sox9	293	Activation	↑ activité transcriptionnelle	(139)
Tat	HEK293 et HeLa	Activation	↑ transactivation HIV	(140)
TLE1	HeLa	Activation	↓ activité transcriptionnelle	(141)
UCP2 **UCP3**	INS-1 et MIN6 Muscle et C2C12	Inhibition Inhibition	↑ sécrétion insuline	(142, 143) (144)
WRN	HEK293	Activation	↑ stabilité du génome	(145)

Tableau 4. Gènes dont l'expression est directement régulée par Sirt1 et fonctions métaboliques associées. (modifié d'après (146) ; AceCS1 : acetyl-CoA synthetase 1 ; AP1 : activator-protein 1 ; AR : androgen receptor ; atg : autophagy-related protein ; CLOCK/BMAL1 : circadian clock genes ; eNOS : endothelial nitric oxide synthase ; FoxO : forkhead box O ; H1 : histone 1 ; HES1/HEY2 : bHLH repressor proteins ; HNF4-α : hepatic nuclear factor 4α ; LKB1 : serine/threonine kinase ; LXR : liver X receptor ; MEF2D : myocyte-specific enhancer factor 2D ; NF-κB : nuclear factor-κ-light-chain-enhancer of activated B cells ; pCAF : p300/CBP-associated factor ; PGC-1α : peroxisome proliferator-activated receptor γ coactivator 1α ; PPAR-γ : peroxisome proliferator-activated receptor γ ; PTP1B : protein tyrosine phosphatase 1B ; RBP1 : retinol binding protein 1 ; Smad7 : mothers against decapentaplegic homolog 7 ; Tat : human immunodeficiency virus protein ; TLE1 : transducin like enhancer of splin 1 ; UCP : uncoupling protein ; WRN : Werner syndrome protein).

Par la suite, on s'intéressera aux fonctions de Sirt1 dans :

- le tissu adipeux,
- le pancréas,
- le foie,
- le muscle strié squelettique.

Ces fonctions principales sont résumées dans la figure 16.

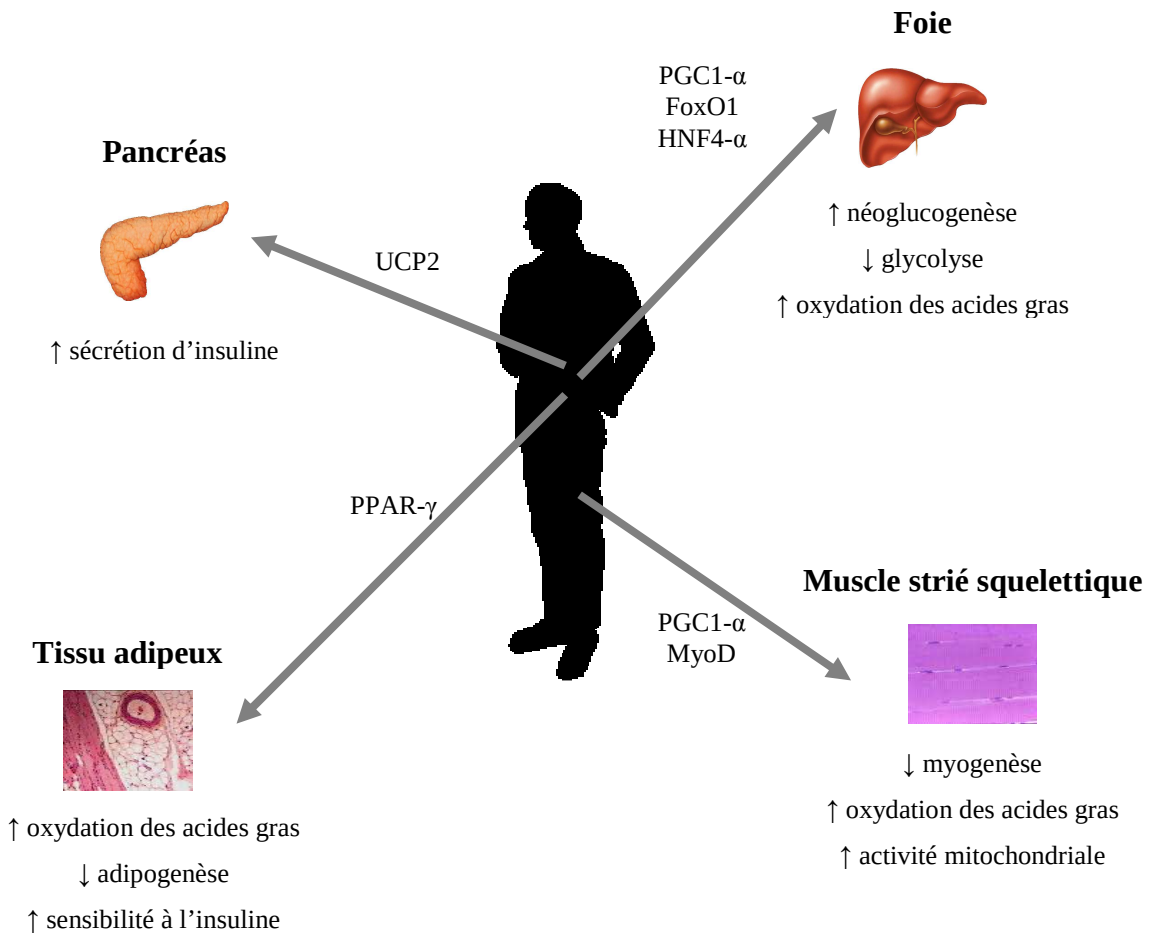

Figure 16. Fonctions principales de Sirt1 dans différents tissus (FoxO1 : forkhead box O 1 ; HNF-4α : hepatic nuclear factor 4α ; PGC-1α : peroxisome proliferator-activated receptor γ coactivator 1α ; PPAR-γ : peroxisome proliferator-activated receptor γ ; UCP2 : uncoupling protein 2).

II. FONCTIONS DE SIRT1 DANS LE TISSU ADIPEUX

Le récepteur nucléaire peroxisome proliferator-activated receptor (PPAR)-γ est un régulateur transcriptionnel clé du métabolisme du tissu adipeux. Il intervient dans la régulation de l'adipogenèse et du stockage des acides gras dans le tissu adipeux blanc (147). La perte d'activité de PPAR-γ chez des souris KO PPAR-γ entraine une perte de tissu adipeux (148). Il a été montré que Sirt1 pouvait à la fois réguler le programme de différenciation des adipocytes, mais aussi l'oxydation des acides gras chez des adipocytes différenciés, en se liant à PPAR-γ (Tableau 5). En effet, chez des préadipocytes 3T3-L1, le blocage de Sirt1 au moyen d'un ARNsi induit l'adipogenèse avec une augmentation du niveau d'expression en ARNm et en protéine de PPAR-γ et de ses gènes cibles, tels que les facteurs de transcription

CCAAT/enhancer-binding protein (C/EBP)-α et –δ impliqués dans la différenciation adipocytaire (75, 149). Chez des cellules 3T3-L1 différenciées, cette invalidation aboutit à l'accumulation de triglycérides (75). Au contraire, une surexpression de Sirt1 exerce des effets inverses, c'est-à-dire, un retard de l'adipogenèse avec une diminution du niveau d'expression de PPAR-γ et C/EBP-α et –δ, et une stimulation de l'oxydation des acides gras chez des adipocytes différenciés. Cette inhibition de PPAR-γ par Sirt1 est induite par la liaison de Sirt1 au corépresseur NCoR (nuclear receptor co-repressor) de PPAR-γ (75). Il a été montré, plus récemment, que par un rétrocontrôle négatif de C/EBP-α sur Sirt1, C/EBP-α pouvait réduire sa propre expression et donc inhiber l'adipogenèse en activant l'expression de Sirt1 (150) (Figure 17). Ainsi, chez des préadipocytes, une surexpression de C/EBP-α induit une augmentation du niveau d'expression endogène en ARNm et en protéine Sirt1. Plus spécifiquement, C/EBP-α se lie directement à l'élément de réponse CBS (C/EBP-α binding site) 1, situé en position -567 à -550 du promoteur Sirt1 afin de réguler la transcription de Sirt1 (150).

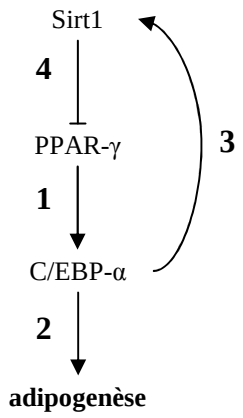

Figure 17. Régulation transcriptionnelle de l'adipogenèse par Sirt1. **1** : PPAR-γ stimule la transcription de C/EBP-α ; **2** : l'activation de C/EBP-α a pour but d'induire l'adipogenèse ; **3** : l'expression de C/EBP-α va activer par rétrocontrôle la transcription de Sirt1 ; **4** : Sirt1 va inhiber la transcription de PPAR-γ (C/EBP-α : CCAAT/enhancer-binding protein ; PPAR-γ : peroxisome proliferator-activated receptor γ ; Sirt1 : sirtuine 1).

Sirt1 semble aussi avoir un rôle dans la régulation de la sécrétion de l'adiponectine, protéine sécrétée par le tissu adipeux pour sensibiliser le foie et le muscle à l'action de l'insuline. Des souris surexprimant Sirt1 soumises à un régime gras possèdent une sécrétion d'adiponectine augmentée, ainsi qu'une meilleure sensibilité à l'insuline comparativement à des souris sauvages (151). De façon contradictoire, une autre étude montre qu'une

transfection d'un ARNsi Sirt1 chez des adipocytes différenciés induit une augmentation de la sécrétion d'adiponectine (152).

Comme Sirt1 semble favoriser la sensibilité à l'insuline, cette dernière pourrait être une cible pharmacologique intéressante chez des patients atteints de diabète de type II et/ou d'obésité. Il a été montré que le traitement de souris par du resveratrol ou du SRT1720 rend les animaux résistants à l'obésité induite par un régime gras, et les protègent contre le développement de l'insulino-résistance (43, 79, 80, 87, 134) (Tableau 5). Ceci pourrait en partie s'expliquer par une stimulation du métabolisme oxydatif et une diminution de la taille des adipocytes avec activation des gènes contrôlant les dépenses énergétiques, tels que PPAR-α et γ et TR (thyroid hormone receptors) (134).

Techniques utilisées	Fonctions inhibées ou stimulées	Références
ARNsi de Sirt1	↑ accumulation des triglycérides ↑ adipogenèse	(75, 149)
Surexpression de Sirt1	↑ oxydation des acides gras ↓ adipogenèse	(75)
Resveratrol	↑ sensibilité à l'insuline ↑ nombre et taille des mitochondries	(43, 79, 80, 87)
SRT1720	↑ sensibilité à l'insuline ↑ nombre et taille des mitochondries ↓ taille des adipocytes	(134)

Tableau 5. Modulations expérimentales de Sirt1 et effets physiologiques associés dans le tissu adipeux (ARNsi : acide ribonucléique small intefering ; Sirt1 : sirtuine 1).

III. FONCTION DE SIRT1 DANS LE PANCREAS

En plus de réguler la sensibilité à l'insuline, Sirt1 peut également intervenir dans la régulation de la sécrétion de cette dernière (Tableau 6). Il a tout d'abord été observé que Sirt1 était spécifiquement exprimée dans les cellules β-pancréatiques (142, 143), suggèrant que Sirt1 interviendrait dans la fonction endocrine du pancréas. En effet, chez des souris surexprimant Sirt1 spécifiquement dans les cellules β-pancréatiques (BESTO), il y a une augmentation de leur capacité à sécréter de l'insuline en réponse au glucose (143). Cette régulation de la sécrétion d'insuline passe par la régulation de l'expression d'UCP (mitochondrial uncoupling protein) 2, protéine régulant négativement la sécrétion d'insuline.

Quand UCP2 diminue dans les cellules β-pancréatiques, le couplage entre la respiration et la synthèse d'ATP augmente, d'où une augmentation de la production mitochondriale d'ATP qui facilite la sécrétion d'insuline (153). Dans les cellules BESTO, une diminution du niveau en ARNm et en protéine UCP2, ainsi qu'une augmentation de la production d'ATP, ont été observées (143). De plus, une surexpression de Sirt1 chez des cellules pancréatiques MIN6 s'accompagne d'une diminution du niveau en ARNm UCP2, alors qu'une invalidation du gène Sirt1 par ARNsi chez les cellules MIN6 ou INS-1 induit une augmentation de l'ARNm UCP2 (142, 143). De manière similaire, il a été montré, chez des cellules MIN6 ou INS-1, qu'une inhibition de l'activité de Sirt1 par du nicotinamide, aboutissait à une augmentation du niveau en ARNm et en protéine UCP2, ainsi qu'à un blocage de la sécrétion d'insuline (142). Plus spécifiquement, Sirt1 réprime la transcription d'UCP2 par liaison directe avec son promoteur (142). Cependant, la stimulation de la sécrétion d'insuline en réponse au glucose chez les souris BESTO est abolie avec l'âge (154). Chez ces souris âgées, on n'observe aucune diminution de l'expression d'UCP2. Il semblerait que l'abolition de la sécrétion d'insuline en réponse au glucose soit liée à une diminution de la synthèse du NAD^+, puisque le nicotinamide mononucléotide, composé intermédiaire synthétisé à partir du nicotinamide dans la voie de biosynthèse du NAD^+ (Figure 12), est diminué chez les souris BESTO âgées (154). De plus, chez ces dernières, une injection de nicotinamide mononucléotide restaure l'effet bénéfique de Sirt1 sur la sécrétion d'insuline stimulée par du glucose. Ainsi, au cours du vieillissement, la synthèse du NAD^+ et l'activité de Sirt1 diminuent aboutissant à l'inhibition de l'effet positif de Sirt1 sur la sécrétion d'insuline chez les souris BESTO.

Techniques utilisées	**Fonctions inhibées ou stimulées**	**Références**
Surexpression de Sirt1	↑ sécrétion d'insuline	(143)
ARNsi de Sirt1 Nicotinamide	↓ sécrétion d'insuline	(142)

Tableau 6. Modulations expérimentales de Sirt1 et effets physiologiques associés dans le pancréas (ARNsi : acide ribonucléique small intefering ; Sirt1 : sirtuine 1).

IV. FONCTIONS DE SIRT1 DANS LE FOIE

1. Régulation de la néoglucogenèse

PGC (peroxisome proliferator-activated receptor γ coactivator)-1α est un coactivateur transcriptionnel, découvert dans les cellules de tissu adipeux brun (155) intervenant dans la régulation de nombreuses fonctions physiologiques. Ce dernier est notamment un régulateur clé de la production de glucose dans le foie chez les souris diabétiques ou soumises à un jeûne par sa régulation de la néoglucogenèse (156-160). Or, puisqu'il a été mis en évidence que, chez des souris soumises à un régime gras et à un traitement au resveratrol, il y avait une augmentation du nombre de mitochondries dans le foie et une augmentation de la déacétylation de PGC-1α, il est possible que Sirt1 puisse intervenir dans la régulation du métabolisme hépatique (79) (Tableau 7). Effectivement, chez des souris soumises à un jeûne, il y a une augmentation conjointe du niveau d'expression protéique de Sirt1 et de PGC-1α dans le foie (132). A l'inverse, une inhibition de l'activité de Sirt1 par du nicotinamide dans des cellules 293T favorise l'acétylation de PGC-1α (132). De plus, il a été montré que Sirt1, en coactivant et déacétylant PGC-1α de façon dépendante au NAD^+, pouvait favoriser l'expression génique d'enzymes de la voie néoglucogénique et inhiber l'expression génique d'enzymes de la voie glycolytique dans le foie en réponse à un jeûne (132). De plus, chez des hépatocytes surexprimant PGC-1α et cultivés en présence de pyruvate (augmentant le ratio NAD^+/NADH), il y a une stimulation de l'expression des gènes de la néoglucogenèse, tels que les gènes de la phosphoénol-pyruvate carboxykinase (PEP-CK) et glucose-6-phosphatase (G-6-Pase) et une inhibition de l'expression des gènes de la glucokinase (GK) et la pyruvate kinase (PK) de la glycolyse (132). De façon contraire, la transfection d'un ARNsi Sirt1 dans ces hépatocytes aboutit à la répression de l'expression de PEP-CK et de G-6-Pase et à l'activation de l'expression de GK et de PK (132). Plus spécifiquement, il a été montré que Sirt1 formait un complexe protéique avec PGC-1α et HNF (hepatic nuclear factor)-4α (132), facteur transcriptionnel essentiel à l'induction de l'expression génique des gènes de la néoglucogenèse par PGC-1α (159) (Figure 18 et Tableau 7).

Une étude plus récente (161) montre également que FoxO1 et HNF-4α sont impliqués dans la régulation de l'expression génique de la GK chez des hépatocytes soumis à un traitement au resveratrol. FoxO1 est un facteur transcriptionnel essentiel à la régulation de la production hépatique de glucose (158, 162, 163). Dans l'étude de Ganjam *et al.*, suite au

traitement de souris avec du resveratrol, il y a une augmentation du niveau en ARNm de PEP-CK, mais une diminution en ARNm et en protéine de la GK (161). De façon plus spécifique, il a été montré, chez des hépatocytes, que FoxO1 était déacétylé en présence de resveratrol, et qu'il était requis pour la diminution de l'expression de la GK induite par le resveratrol. Cette diminution de l'expression de la GK résulte de l'action de FoxO1 avec HNF-4α : le resveratrol augmente leur interaction dans les hépatocytes, ce qui supprime le recrutement de HNF-4α sur son site de liaison situé sur le promoteur GK et ainsi diminue la transcription de la GK (161) (Figure 18 et Tableau 7).

Une autre étude montre également l'importance de Sirt1 dans la régulation de la néoglucogenèse par la déacétylation de FoxO1 (78). La déacétylation de FoxO1 par Sirt1, suite à un traitement des cellules H4IIE par du resveratrol, favorise l'accumulation de FoxO1 dans le noyau, augmentant ainsi la transcription de gènes néoglucogéniques dépendante de FoxO1, comme la G-6-Pase (78) (Figure 18). D'après l'étude de Puigserver *et al.* (158), FoxO1 et PGC-1α interagissent ensemble dans le programme néoglucogénique. En effet, PGC-1α se lie et coactive FoxO1 dans le but d'induire la néoglucogenèse (158). D'après les études précédentes, on peut ainsi dire que l'action de Sirt1 sur la régulation de la néoglucogenèse pourrait être dépendante de la coactivation de FoxO1 par PGC-1α (Figure 18 et Tableau 7).

Chez des rats diabétiques, dont les niveaux en ARNm et en protéine Sirt1 sont diminués de 75 % grâce à un oligonucléotide anti-sens Sirt1, on observe une diminution des niveaux en ARNm et en protéine PEP-CK et du niveau en ARNm de la G-6-Pase (164). Ces diminutions sont probablement le résultat d'une diminution de l'activité transcriptionnelle du facteur FoxO1 et du coactivateur PGC-1α puisqu'en présence d'oligonucléotide anti-sens Sirt1, leurs niveaux d'acétylation est fortement augmenté (164) (Figure 18 et Tableau 7).

Une autre étude de Rodgers *et al.* (165) utilisant des souris invalidées pour Sirt1 hépatique par ARNsh renforce les observations ci-dessus. En effet, l'invalidation du gène Sirt1 hépatique en condition de jeûne chez ces souris diminue l'expression des gènes de la néoglucogénèse, tels que PEP-CK et G-6-Pase et favorise l'expression de ceux de la glycolyse. Comme précédemment, ces effets sont étroitement liés à l'activité transcriptionnelle de FoxO1 et PGC-1α, puisque l'invalidation hépatique de Sirt1 s'accompagne d'une augmentation du niveau d'acétylation de ces deux protéines (165). De plus, une surexpression de Sirt1 chez ces souris rétablit tous les changements créés par l'invalidation du gène Sirt1 hépatique et cela de façon dépendante de PGC-1α (165) (Figure 18 et Tableau 7).

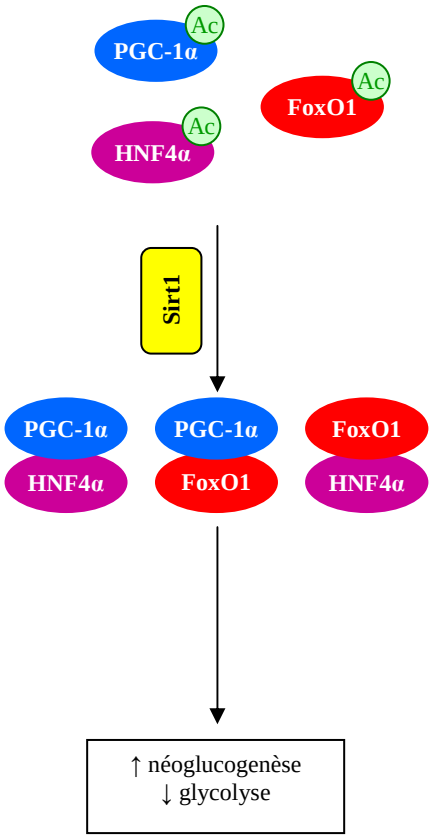

Figure 18. Régulation transcriptionnelle de la néoglucogenèse et de la glycolyse par Sirt1. En cas de stimulation de l'expression de Sirt1, Sirt1 va déacétyler PGC-1α, FoxO1 et HNF-4α et favoriser leur interaction dans le but de stimuler la néoglucogenèse et inhiber la glycolyse (PGC-1α/HNF-4α : (132) ; PGC-1α/FoxO1 : (158) ; FoxO1/HNF-4α : (161) ; Ac : groupement acétyl ; FoxO1 : forkhead box O 1 ; HNF-4α : hepatic nuclear factor 4α ; PGC-1α : peroxisome proliferator-activated receptor γ coactivator 1α ; Sirt1 : sirtuine 1).

L'effet stimulateur de Sirt1 sur la néoglucogenèse décrit dans les études ci-dessus est cependant soumis à controverse (115, 166) (Tableau 7). En effet, chez des hépatocytes soumis à un jeûne, l'addition de SRT1720 ou de resveratrol aboutit à la déacétylation et à l'inhibition de CRTC (CREB regulated transcription coactivator) 2, stimulateur de l'expression des gènes de la néoglucogenèse (166). De plus, l'ajout d'isonicotinamide ou de resveratrol, activateurs de Sirt1, chez des hépatocytes HepG2 conduit à une diminution de l'ARNm de PEP-CK (115). Le promoteur PEP-CK possède un site de liaison à HNF4-α situé en position -272 à -252. Ainsi, une fois activée par l'isonicotinamide, Sirt1 déacétyle HNF4-α diminuant ainsi l'affinité de liaison d'HNF4-α pour son site de liaison au promoteur PEP-CK, ce qui inhibe la transcription du gène PEP-CK (115).

Pour résumer, les études montrant une stimulation de la néoglucogenèse par Sirt1 utilisent des techniques qui régulent directement l'expression de Sirt1 (ARNsi, ARNsh,

surexpression…), alors que les deux études contradictoires utilisent quant à elles des molécules activatrices de l'activité de Sirt1 dont la spécificité est controversée (cf chapitre V.2.b). Ainsi, même si dans ces études il y a une inhibition de la néoglucogenèse en cas d'activation de Sirt1, il est à envisager que les molécules utilisées pour réguler l'activité de Sirt1 ne sont peut être pas spécifiques de cette dernière et qu'elles jouent également un rôle dans la régulation d'autres protéines, comme pour le resveratrol qui active également l'AMPK (cf chapitre V.2.b).

2. Régulation du métabolisme lipidique et du cholestérol

Comme décrit précédemment, de nombreuses études ont montré que Sirt1 était essentielle à la régulation de la néoglucogenèse et de la glycolyse. Cependant, il semblerait que Sirt1 intervienne également dans la régulation du métabolisme lipidique, ainsi que dans celui du cholestérol (165). En effet, l'invalidation *in vivo* du gène Sirt1 hépatique diminue l'expression des gènes de l'oxydation des acides gras, tels que MCAD (medium chain acyl-CoA deshydrogenase) ou CPT (carnitine palmitoyltransferase)-1a. De plus, Sirt1 régule l'expression de LXR (liver X receptor)-α et PGC-1β, qui sont eux-mêmes impliqués dans la régulation de l'expression des gènes du transport du cholestérol (167-170). En effet, leurs expressions géniques sont diminuées en présence d'ARNsh Sirt1. De plus, une seconde étude a également montré que chez des souris Sirt1-/-, les niveaux en ARNm de cibles de LXR-α comme SREBP (sterol regulatory element binding protein)-1c (165) ou ABCA (ATP-binding cassette transporter) 1, régulateurs majeurs de l'homéostasie lipidique et du cholestérol (171, 172), étaient diminués dans le foie (119).

Regardons de plus près le mécanisme par lequel Sirt1 régule LXR-α et donc celui de ces gènes cibles. LXR-α, fortement exprimé dans le foie, est un récepteur nucléaire activé par les oxystérols ayant un rôle central dans le contrôle transcriptionnel du métabolisme lipidique (169). LXR-α fonctionne en formant un hétérodimère avec le récepteur RXR (retinoid X receptor) et en se liant aux éléments de réponse LXRE spécifiques localisés dans le promoteur des gènes cibles (167, 173-175). Il a été montré chez des cellules HEK293T que Sirt1 déacétylait la lysine K432 de LXR-α du complexe LXR/RXR (119). Cependant, il a curieusement été observé une corrélation inverse entre le niveau d'activité de LXR-α et son niveau protéique chez des MEF Sirt1-/- (119). Ceci peut s'expliquer par le fait que l'acétylation de LXR-α bloque son ubiquitination et sa dégradation. En effet, comme décrit

dans la Figure 19, après fixation du complexe LXR/RXR sur les éléments de réponse LXR du promoteur des gènes cibles et induction de la transcription des gènes cibles, Sirt1 déacétyle LXR permettant ainsi à la molécule LXR d'être ubiquitinylée et dégradée par le protéasome. Cette dégradation aboutit au recrutement d'une nouvelle molécule LXR pour un second cycle de transcription du gène cible. Ce turnover ainsi stimulé par Sirt1 permet donc l'augmentation de la transcription des gènes cibles de LXR (119) (Figure 19).

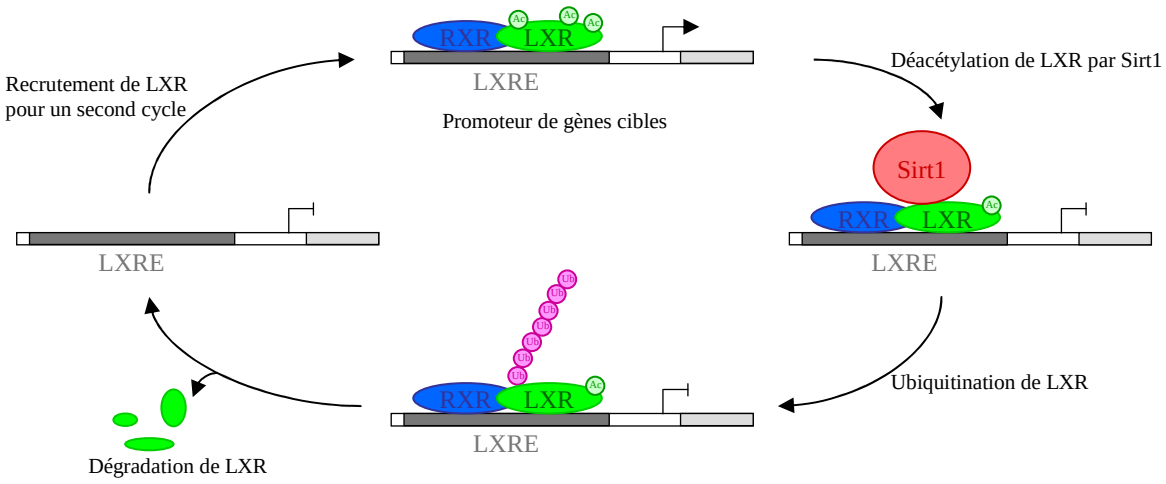

Figure 19. Modèle du rôle de Sirt1 dans la régulation de la transactivation des promoteurs des gènes cibles de LXR (modifiée d'après (119) ; Ac : groupement acétyl ; LXR : liver X receptor ; LXRE : éléments de réponse LXR ; RXR : retinoid X receptor ; Sirt1 : sirtuine 1 ; Ub : ubiquitine).

Techniques utilisées	Fonctions inhibées ou stimulées	Références
ARNsi de Sirt1	↓ néoglucogenèse ↑ glycolyse	(165)
Resveratrol	↓ glycolyse	(161)
Resveratrol	↑ néoglucogenèse	(78)
Oligonucléotide antisens de Sirt1	↓ néoglucogenèse	(164)
ARNsh Sirt1 hépatique	↓ production de glucose ↓ néoglucogenèse ↑ glycolyse ↑ synthèse lipidique ↑ métabolisme du cholestérol	(165)
Resveratrol Isonicotinamide	↓ néoglucogenèse	(115) (166)

Tableau 7. Modulations expérimentales de Sirt1 et effets physiologiques associés dans le foie (ARNsi : acide ribonucléique small intefering ; ARNsh : acide ribonucléique small hairpin ; Sirt1 : sirtuine 1).

V. FONCTIONS DE SIRT1 DANS LE MUSCLE STRIE SQUELETTIQUE

1. Régulation de la différenciation myogénique

Il y a une quinzaine d'années, alors que Sirt1 n'était pas connue, beaucoup d'études se sont intéressées au rôle des HDAC et HAT dans la différenciation myogénique chez les mammifères (Figure 20). Il a été montré que les HAT favorisaient la myogenèse. La famille des protéines CBP/p300 intervient dans le programme de différenciation terminale des cellules musculaires (176-178) pour coactiver le facteur myogénique MyoD. p300 va ainsi s'associer et acétyler MyoD permettant la stimulation de la transcription des gènes dépendante de MyoD (178-180). De plus, CBP/p300 peut également favoriser la myogenèse en stimulant la transactivation médiée par un autre facteur myogénique MEF (myocyte enhancer factor) 2 (181). La famille GCN5/pCAF, en formant de la même manière un complexe avec MyoD, permet aussi de stimuler la formation des myotubes (182). Les HDAC vont quant à elles inhiber la myogenèse. En effet, les HDAC, en s'associant et en déacétylant MyoD ou MEF2, vont empêcher la différenciation musculaire (183, 184). Les HDAC de classe 2, telles que HDAC 4, 5 et 7 possèdent un domaine de liaison leur permettant de s'associer avec MEF2 et d'inhiber la transcription dépendante de MEF2 (185, 186-189). Plus particulièrement, l'HDAC 4 peut inhiber l'activité transcriptionnelle de MEF2 par déacétylation (62). Quant à HDAC 1 de classe 1, elle s'associe directement avec MyoD et le déacétyle, inhibant ainsi son activité transcriptionnelle (190).

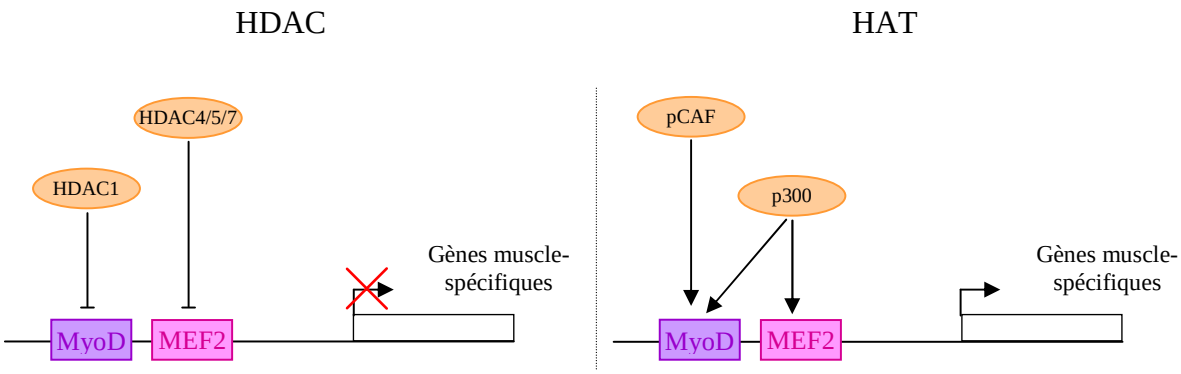

Figure 20. Rôles des HAT et HDAC dans le contrôle de l'expression génique musculaire (modifiée d'après (183) ; HAT : histone acétyltransférase ; HDAC : histone déacétylase ; MEF2 : myocyte-specific enhancer factor 2 ; pCAF : p300-CBP associated factor).

Puisque l'expression des gènes musculaires est régulée par les activités concertées et opposées des HDAC et HAT, des études se sont penchées sur le rôle de Sirt1 dans la régulation de la myogenèse chez les mammifères. La première, en 2003 (120), montre que, comme HDAC1, Sirt1 inhibe le facteur myogénique MyoD et la différenciation myogénique (Tableau 8). Une surexpression de Sirt1, chez des myoblastes C2C12, aboutit à la formation d'un complexe protéique ternaire composé de Sirt1, pCAF et MyoD. Ce complexe s'accompagne d'une diminution du niveau d'acétylation de MyoD et de pCAF et d'une diminution du niveau d'expression des gènes musculaires dont la transcription est dépendante de MyoD, tels que myogénine ou MEF2C, et d'une inhibition de la différenciation (120). Au contraire, l'addition de nicotinamide permet d'augmenter le niveau d'acétylation de pCAF et de MyoD, et l'invalidation de Sirt1 au moyen d'un ARNsh induit la différenciation avec une augmentation de l'expression des gènes musculaires, comme myogénine et MEF2C (120). Il est également possible que Sirt1 régule négativement la myogenèse en inhibant MEF2D, puisqu'il a été montré que Sirt1 pouvait fonctionner comme une déacétylase de MEF2D chez des cellules 293T (62).

On a vu précemment que l'activité déacétylase de Sirt1 était sensible aux variations du ratio NAD^+/NADH (120). Si le ratio NAD^+/NADH est augmenté chez des myoblastes C2C12 (addition de pyruvate), l'expression des gènes myogéniques est diminuée. Cependant, si l'expression du gène Sirt1 est invalidée au moyen d'un ARNsh, la réponse des myoblastes au pyruvate est largement diminuée (120). De plus, Sirt1 peut aussi réguler la myogenèse en réponse à des modifications de la concentration en glucose (191). Ainsi, des myoblastes C2C12 cultivés en présence d'une faible quantité de glucose (augmentant le ratio NAD^+/NADH), possèdent un retard de la myogenèse avec une accumulation de Sirt1 dans les

noyaux, alors qu'en présence d'une forte concentration de glucose (diminuant le ratio NAD^+/NADH), l'induction de la myogenèse est normale avec une diminution de l'accumulation de Sirt1 dans les noyaux (191).

2. Régulation du métabolisme oxydatif du muscle strié squelettique

a. Régulation de PGC-1α

Dans le muscle strié squelettique, PGC-1α est considéré comme le régulateur maître de la biogénèse mitochondriale et du métabolisme oxydatif. Etant donné qu'il a été montré que Sirt1 déacétylait PGC-1α dans le foie (132), et dans les cellules PC12 (131), il est à envisager que Sirt1 puisse réguler le métabolisme oxydatif dans le muscle strié squelettique au moyen d'une déacétylation de PGC-1α (Tableau 8). La première équipe à avoir envisager ce rôle est celle de Lagouge *et al.* (80). Dans cette étude, des souris soumises à un régime gras et à un traitement au resveratrol, présentaient une augmentation de la capacité aérobie avec une augmentation du nombre et de la taille des mitochondries dans le muscle strié squelettique (80). Cette amélioration proviendrait d'une diminution du niveau d'acétylation de PGC-1α et donc d'une augmentation de son activité, qui est associée à une induction des gènes stimulant la biogenèse mitochondriale comme NRF (nuclear respiratory factor)-1, ERR (estrogen-related receptor)-α ou TFAM (facteur de transcription mitochondrial A). Ces effets seraient dépendants de Sirt1 puisque chez des myotubes C2C12 surexprimant PGC-1α, l'inactivation de Sirt1 au moyen d'un ARNsh bloque la stimulation de l'expression d'ERR-α induite par PGC-1α (80). Cependant, comme l'efficacité du resveratrol en tant qu'activateur spécifique de Sirt1 est soumise à controverse (cf chapitre V.2.b) et qu'aucune preuve directe de l'implication n'ait été fournie, l'étude précédente (80) laisse en suspens la question de l'implication directe de Sirt1 dans la régulation du métabolisme oxydatif dans le muscle strié squelettique. Dans une seconde étude, chez des souris soumises à un régime gras (134), le SRT1720, un activateur de Sirt1, semble avoir une action limitée sur la régulation du métabolisme oxydatif mitochondrial, mais stimule le programme d'oxydation des acides gras (134). En effet, aucune augmentation de l'expression en ARNm des gènes, tels que PGC-1α, cytochrome c ou citrate synthétase n'est observée chez ces souris, alors que l'expression des gènes de l'oxydation des acides gras, tels que CPT-1b ou MCAD, est stimulée (134) (Tableau 8).

Toutefois, une étude plus probante de Gerhart-Hines *et al.* en 2007 (135) apporte des éléments de réponse à la question évoquée ci-dessus. Premièrement, Sirt1 régule l'expression des gènes du métabolisme mitochondrial et de l'oxydation des acides gras, puisque l'inhibition de l'expression de Sirt1 au moyen d'un ARNsh chez des myotubes primaires ou l'invalidation de Sirt1 chez des MEF Sirt1-/- diminue le niveau en ARNm de gènes codant des protéines mitochondriales, tels que cytochrome c, MCAD et CPT-1b (135). Deuxièmement, ils montrent que Sirt1 est nécessaire à la régulation du métabolisme mitochondrial et à l'oxydation des acides gras, de façon dépendante de PGC-1α. En effet, chez des myotubes C2C12 surexprimant PGC-1α, l'inhibition du gène Sirt1 au moyen d'un ARNsh diminue la stimulation de l'expression de gènes, tels que cytochrome c, MCAD ou CPT-1b induite par la surexpression de PGC-1α (135). Cet effet serait médié par la déacétylation de PGC-1α puisque chez des MEF Sirt1-/-, le niveau d'acétylation de PGC-1α est augmenté (135). Enfin, chez des MEF Sirt1-/-, en réponse à une restriction en glucose qui conduit à une augmentation du ratio NAD^+/NADH et à une déacétylation de PGC-1α, aucune stimulation de l'expression des gènes de l'oxydation des acides gras n'a été observée, contrairement aux MEF Sirt1+/+ (135) (Figure 21 et Tableau 8).

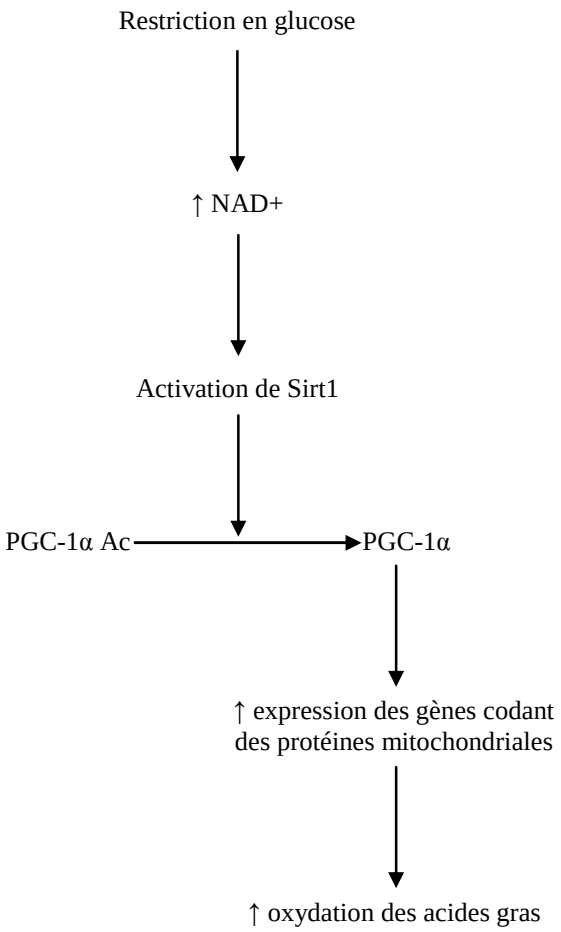

Figure 21. Modèle du contrôle de l'oxydation des acides gras *via* la voie Sirt1/PGC-1α (modifiée d'après (135) ; Ac : groupement acétyl ; NAD^+ : nicotinamide adénine dinucléotide ; PGC-1α : peroxisome proliferator-activated receptor γ coactivator 1α ; Sirt1 : sirtuine 1).

Par ailleurs, il a été montré que Sirt1 régulait l'activité du promoteur PGC-1α *via* MyoD (136). En effet, Sirt1 déacétyle PGC-1α dans le but de permettre à ce dernier d'augmenter son activité transcriptionnelle par liaison directe avec MyoD (136) (Figure 22).

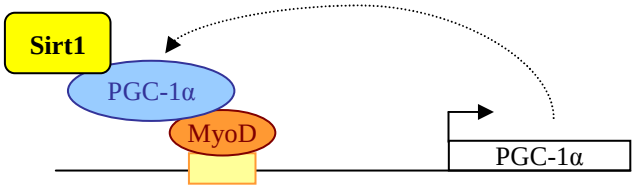

Figure 22. Représentation schématique du mécanisme de régulation de la transcription du gène PGC-1α par Sirt1 (modifiée d'après (136) ; PGC-1α : peroxisome proliferator-activated receptor γ coactivator 1α ; Sirt1 : sirtuine 1).

Le rôle stimulateur de Sirt1 sur la biogenèse mitochondriale est cependant soumis à controverse (192). Gurd *et al*. (192) ont montré que l'activité déacétylase de Sirt1 n'était pas

associée à la capacité oxydative du muscle strié squelettique. Plus précisément, il existe même une corrélation inverse entre le niveau d'expression de Sirt1 et de PGC-1α dans le *gastrocnemius* blanc, le *gastrocnemius* rouge, le *tibialis anterior* blanc et le *tibialis anterior* rouge (192). Lors d'une stimulation de la biogenèse mitochondriale par stimulation électrique chronique basse fréquence ou par administration d'AICAR (5-aminoimidazole-4-carboxyamide-1-β-D-ribofuranoside), il y a une augmentation du niveau d'expression de PGC-1α, COX (cytochrome c oxidase subunit) IV et une diminution de celle de Sirt1 (192). Enfin, une surexpression de Sirt1 dans le muscle conduit à une diminution en protéine PGC-1α et COXIV (192) (Tableau 8). Des conclusions similaires ont été faites par Chabi *et al.* (193) : lors d'une stimulation de la biogenèse mitochondriale chez des rats, soit par un exercice, soit par une stimulation électrique chronique basse fréquence, on observe une augmentation du niveau protéique de PGC-1α et du cytochrome c, mais aucune modification de celui de Sirt1 (193).

Techniques utilisées	**Fonctions inhibées ou stimulées**	**Références**
Surexpression de Sirt1	↓ myogenèse	(120)
ARNsh Sirt1	↑ myogenèse	(120)
Resveratrol	↑ biogenèse mitochondriale	(80)
SRT1720	↑ oxydation des acides gras	(134)
ARNsh Sirt1 MEF Sirt1-/-	↓ oxydation des acides gras ↓ gènes codant des protéines mitochondriales	(135)
Surexpression de Sirt1	↓ biogenèse mitochondriale	(192)

Tableau 8. Modulations expérimentales de Sirt1 et effets physiologiques associés dans le muscle strié squelettique (ARNsh : acide ribonucléique small hairpin ; MEF : mouse embryonic fibroblast ; Sirt1 : sirtuine 1).

b. Rôle de l'AMPK

Dans les études précédentes, de nombreuses molécules connues comme activatrices de Sirt1 ont été utilisées dans le but de stimuler son activité. Cependant, si on regarde de plus près le mécanisme d'action de ces molécules, il semblerait que leurs effets sur Sirt1 ne soient pas aussi efficaces et spécifiques qu'initialement souhaités. Par exemple, il a été montré que le resveratrol et le SRT1720 n'activaient Sirt1 que lorsqu'elle était dosée avec un subsstrat commercial comportant un fluorochrome (Fluor-de-Lys) (194, 195). De plus, le resveratrol peut stimuler l'activité de Sirt1 indirectement *via* l'activité de l'AMPK. En effet, il a été

observé que le resveratrol stimulait l'activité de l'AMPK dans des cellules neuro2a et des neurones primaires (196), ainsi que dans des cellules CHO et dans le foie de souris (79). De plus, chez des myotubes L6, l'inhibition de l'activité de l'AMPK abolit la stimulation de la prise de glucose induite par du resveratrol (197).

L'AMPK est une enzyme fonctionnant comme un capteur de l'énergie cellulaire qui est activée par une augmentation du ratio AMP/ATP (198). L'AMPK peut donc être activée par des stimuli inhibant la production d'ATP comme l'hypoxie, le stress oxydatif, la restriction en glucose, ou par des stimuli accélérant la consommation d'ATP, tels que l'exercice musculaire (86). La première étude décrivant l'implication de l'AMPK dans la régulation de Sirt1 est celle de Fulco *et al.* (121) où il est question de l'importance de la Nampt dans le mécanisme d'inhibition de la myogenèse par Sirt1 en cas de restriction en glucose (121). La Nampt est une enzyme essentielle à la production du NAD^+ à partir du nicotinamide (Figure 12). L'AMPK est nécessaire à l'inhibition de la myogenèse par Sirt1, puisqu'en cas de mutation de la sous-unité α-2-catalytique de l'AMPK (K45R), des myoblastes soumis à une restriction en glucose (induisant une augmentation du ratio AMP/ATP), peuvent se différencier (121). La Nampt, dont l'expression est stimulée par l'AMPK, serait essentielle dans ce mécanisme puisqu'une inhibition de la Nampt au moyen d'un ARNsh permet la différenciation des myoblastes en myotubes (121). Ainsi, en cas de restriction en glucose, il y a une activation de l'AMPK qui induit une augmentation de la transcription de la Nampt, aboutissant à une augmentation du ratio NAD^+/NADH et à une activation de Sirt1, ceci aboutit à l'inhibition de la myogenèse (121) (Figure 23).

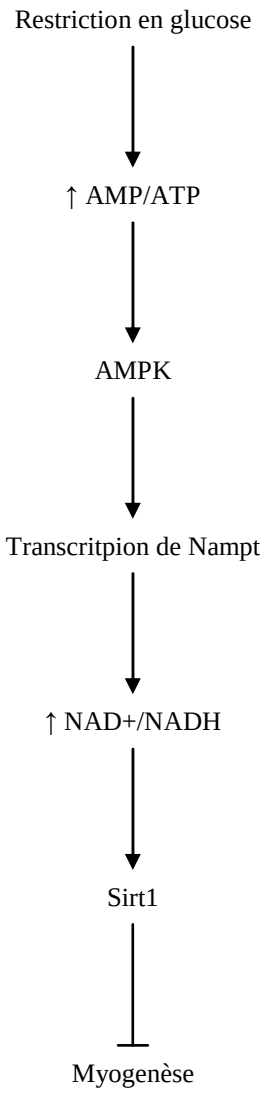

Figure 23. Illustration de l'inhibition de la myogenèse par la voie AMPK/Nampt/Sirt1 (modifiée d'après (121) ; AMP : adénosine monophosphate ; AMPK : AMP kinase ; ATP : adénosine triphosphate ; NAD^+/NADH : nicotinamide adénine dinucléotide ; Nampt : nicotinamide phosphoribosyltransférase ; Sirt1 : sirtuine 1).

Cependant, l'AMPK pourrait aussi réguler l'activité de PGC-1α, en modulant l'activité de Sirt1 par une augmentation du ratio NAD^+/NADH, mais de façon indépendante à une augmentation de l'expression de Nampt (85) (Figure 24). Tout d'abord, l'ajout d'AICAR, un activateur de l'AMPK, dans le milieu de myoblastes C2C12 permet d'augmenter la déacétylation et l'activité de PGC-1α, et cela de façon dépendante à Sirt1 (85). De plus, chez des myotubes C2C12, l'invalidation du gène Sirt1, au moyen d'un ARNsh, diminue l'augmentation de l'expression des gènes cibles de PGC-1α comme CPT-1b et cytochrome c, induite par l'AICAR. Cette régulation de Sirt1 par l'AMPK est dépendante du ratio NAD^+/NADH, puisque l'ajout d'AICAR chez des myotubes C2C12 ou chez des souris

aboutit à l'augmentation de ce ratio (85). Cependant, au contraire de l'étude précédente, l'action de l'AMPK sur l'activité de Sirt1 serait indépendante de Nampt, puisque l'inhibition de l'activité de Nampt ne prévient pas la déacétylation de PGC-1α (85). L'augmentation du ratio NAD^+/NADH serait, dans ce cas, due à la stimulation du métabolisme d'oxydation des lipides (85). En cas de stress énergétique (restriction de la concentration en glucose chez des myotubes C2C12), ces mêmes auteurs observent les évènements suivants : augmentation de l'activité de l'AMPK (18-24h), puis augmentation de la concentration en NAD^+ et de l'activité Sirt1 avec augmentation de la déacétylation de PGC-1α (30-36h) (84). Ils ont également montré que l'AMPK était la molécule clé à l'origine des adaptations métaboliques dépendantes de Sirt1. Des myotubes C2C12 surexprimant une forme dominante négative de la sous-unité α-1-catalytique de l'AMPK, ou des souris KO AMPK-γ-3 ne présentent pas de modification de la concentration de NAD^+, ni de déacétylation de PGC-1α, ni d'augmentation d'expression des gènes mitochondriaux lors d'une restriction calorique (84). L'activation de Sirt1 pourrait ainsi être une conséquence indirecte des adaptations métaboliques et transcriptionnelles induites par l'activation de l'AMPK.

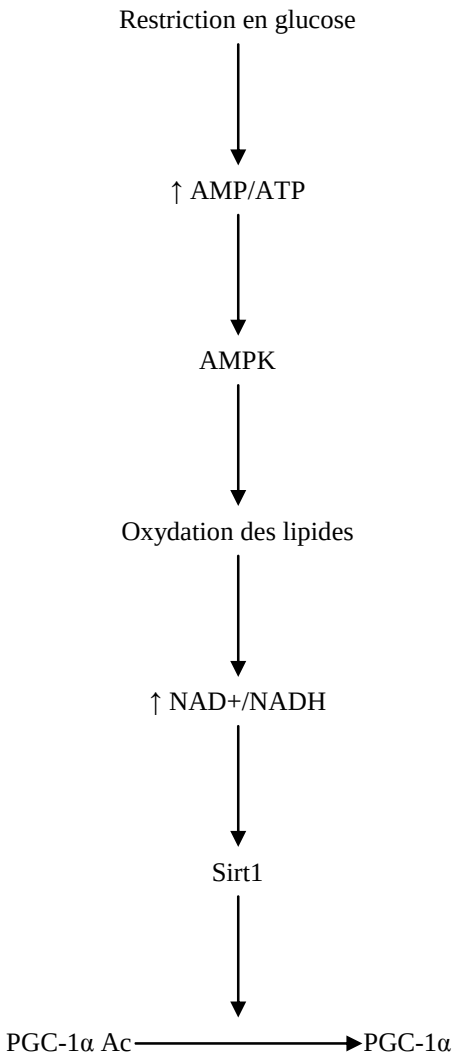

Figure 24. Activation de PGC-1α par la voie AMPK/Sirt1 (modifiée d'après (85) ; Ac : groupement acétyl ; AMP : adénosine monophosphate ; AMPK : AMP kinase ; ATP : adénosine triphosphate ; NAD^+/NADH : nicotinamide adénine dinucléotide ; PGC-1α : peroxisome proliferator-activated receptor γ coactivator 1α ; Sirt1 : sirtuine 1).

Enfin, une dernière étude plus récente de Um *et al.* montre que l'AMPK est la cible clé des effets métaboliques du resveratrol (199). En effet, le resveratrol induit une augmentation du niveau d'expression de PGC-1α et de cytochrome c, ainsi qu'une augmentation du ratio NAD^+/NADH et une déacétylation de PGC-1α chez des souris sauvages, alors que des souris KO AMPK sont insensibles à l'action du resveratrol (199).

Les drogues utilisées jusqu'à aujourd'hui, connues comme activatrices de Sirt1 semblent donc avoir un spectre d'action plus large que l'activation de Sirt1 (194, 195). Il faut donc utiliser et analyser avec précaution les résultats obtenus dans ces conditions là. Les effets bénéfiques de ces drogues semblent indirectement liés à l'activité de Sirt1 et directement liés à celle de l'AMPK. Les deux protéines AMPK et Sirt1 semblent donc

fonctionner de façon coordonnée pour adapter les réponses cellulaires aux modifications environnementales. Il est donc à envisager un axe AMPK/Sirt1 qui contrôlerait de nombreuses fonctions physiologiques dans le muscle strié squelettique (86, 200, 201).

OBJECTIFS

D'après l'étude bibliographique présentée ci-dessus, il est clairement établi que Sirt1 est une protéine clé de la régulation du métabolisme du glucose. Sirt1 facilite tout d'abord l'action de l'insuline en augmentant sa sécrétion par le pancréas et en augmentant sa sensibilité au niveau de différents tissus (muscle, tissu adipeux). De plus, dans le foie, Sirt1 stimule la néoglucogenèse et inhibe la glycolyse. Enfin, au niveau du muscle strié squelettique ou du tissu adipeux, Sirt1 favorise l'oxydation des acides gras. Toutefois, l'action directe de Sirt1 sur la régulation du métabolisme du glucose dans le muscle strié squelettique n'est pas encore connue. C'est pourquoi, nous avons émis l'hypothèse que Sirt1 serait impliquée dans la régulation du métabolisme du glucose dans le muscle strié squelettique.

Dans ce contexte, le travail de thèse présenté ici tentera d'apporter de nouveaux éléments de compréhension sur la régulation de ce métabolisme par Sirt1 dans le muscle strié squelettique. Pour cela, nos objectifs étaient :

- de déterminer *in vivo* si Sirt1 était impliquée dans la régulation de l'expression des gènes régulant le métabolisme du glucose,
- de déterminer *in vivo* quel était le mécanisme d'action de Sirt1 sur cette régulation de l'expression des gènes régulant le métabolisme du glucose,
- de caractériser *in vitro* les adaptations métaboliques de myotubes C2C12 lors d'un jeûne.

MATERIELS ET METHODES

RECUPERATION DE PLASMIDE SUR PAPIER WHATMAN

Références

- Tris trizma base (Sigma-Aldrich T1503)

Principe

Certains des plasmides utilisés au cours de ce travail ont été généreusement fournis pas d'autres équipes de recherche. Pour cela, une quantité d'ADN plasmidique nu avait été déposé sur un morceau de papier whatman dans une zone délimitée. Il s'agit donc de récupérer cet ADN afin de l'utiliser pour transformer des bactéries compétentes.

Solutions

tris	10 mM

Protocole

1. Découper délicatement autour du cercle.
2. Disposer le morceau de papier au fond d'un tube eppendrof 2 mL.
3. Déposer 50 µL de Tris 10 mM.
4. Agiter pendant 5 secondes puis attendre 5 secondes sans agiter.
5. Renouveler pendant 5 minutes.
6. Disposer le morceau de papier dans un filtre adapté au tube eppendorf.
7. Centrifuger 5 secondes à faible vitesse.
8. Récupérer le tampon contenant l'ADN plasmidique.

TRANSFORMATION DE BACTERIES COMPETENTES

Références

- JM109 competents cells (Qiagen L1001)
- LB Luria Bernati broth (Sigma-Aldrich L3152)
- Agar (Fluka 5039)
- Ampicilline (Sigma-Aldrich A9518)
- Kanamycine (Sigma-Aldrich K1876)

Principe

La compétence d'une bactérie est un état temporaire qui lui permet d'absorber des molécules d'ADN exogènes. Des bactéries JM109 d'*Echerichia Coli* compétentes sont transformées avec le plasmide recombinant qui ne s'intègre pas au génome et se réplique simultanément à la bactérie de façon autonome. La transformation permet une amplification exponentielle rapide et sans modification de la séquence du plasmide. Le plasmide est porteur d'un gène de résistance à un antibiotique (ampicilline ou kanamycine) permettant la sélection des bactéries transformées.

Solutions

- *antibiotiques*

ampicilline	50 mg/mL
kanamycine	150 mg/mL

- *milieux de culture* pH = 7,5

Solide : 15 g d'agar et 25 g de LB dans 1 L d'eau (autoclave)
Liquide : 25 g de LB dans 1 L d'eau (autoclave)

Protocole

1. Décongeler, à température ambiante, 100 µL de bactéries compétentes. Ajouter 1 µL d'ADN plasmidique.
2. Laisser dans la glace pendant 1 heure.
3. Incuber à 42°C pendant 2 minutes dans un bloc chauffant ou un bain-marie.
4. Ajouter 1 mL de milieu LB, puis mélanger délicatement. Incuber 1 heure à 37°C au bain-marie.
5. Centrifuger à 3500g pendant 3 minutes à température ambiante.
6. Eliminer 1 mL de surnageant. Reprendre délicatement le culot avec les 100 µL restants.
7. Inoculer une boîte de culture contenant l'antibiotique approprié. Laisser incuber à 37°C pendant 15 minutes à l'endroit, puis laisser pousser la boîte à l'envers pendant 12-16 heures.

Puis, le second jour, sélectionner une demie colonie et inoculer 10 mL de milieu LB contenant l'antibiotique approprié.

PREPARATION DE STABS

Références

- Glycérol (Fisher Scientific G/P450/08)

Principe

Les stabs bactériens permettent de conserver des bactéries compétentes transformées avec de l'ADN plasmidique plusieurs mois au -80°C.

Solutions

- *glycérol à 80 %*

80 mL de glycérol + 20 mL d'eau. Autoclaver.

Protocole

1. Suivre la DO_{600nm} du LB contant les bactéries.
2. Lorsque la DO_{600nm} se situe entre 0,3 et 0,4, mélanger 400 µL de culture bactérienne à 1 mL de glycérol 80 % stérile. Homogénéiser.
3. Stocker à – 80°C.

Pour décongeler un stab, prélever à l'aide d'une œse une petite portion du stab congelé et inoculer une boite de culture contenant l'antibiotique approprié.

NUCLEOSPIN QUICK PURE D'ADN PLASMIDIQUE

Références

- Ampicilline (Sigma-Aldrich A9518)
- Kanamycine (Sigma-Aldrich K1876)
- LB Luria Bernati broth (Sigma-Aldrich L3152)
- NucleoSpin Plasmid Quickpure (Machinery Nagel 740 615.50)
- Ethanol (Riedel de Haën 34935)

Principe

Cette technique permet d'obtenir très rapidement de l'ADN plasmidique et d'en vérifier sa composition. Après lyse de la paroi bactérienne, digestion enzymatique des ARNs, précipitation puis séparation de l'ADN génomique, l'ADN plasmidique est fixé sur une colonne de chromatographie échangeuse d'anions. Une série de lavages permet d'éliminer une grande partie des protéines. L'ADN est ensuite élué de la colonne par ajout d'une solution de plus grande force ionique.

Solutions

- *antibiotiques*

ampicilline	50 mg/mL
kanamycine	150 mg/mL

- *ajouter la RNAse dans le tube A1*

- *ajouter 8 mL d'éthanol à la solution AQ*

- *milieu de culture LB* à pH = 7,5

Liquide : 25 g de LB dans 1 L d'eau (autoclave)

Protocole

- *Jour 1*

1. Inoculer 5 mL de LB contenant l'antibiotique approprié (5 µL pour l'ampicilline à 50 mg/mL et 1,66 µL pour la kanamycine à 150 mg/mL) avec une colonie isolée.
2. Incuber pendant toute la nuit à 37°C sous agitation.

- *Jour 2*

1. Centrifuger 2 mL de culture bactérienne dans un tube eppendorf 2 mL à 11000 g pendant 30 secondes à température ambiante.
2. Jeter le surnageant et resuspendre le culot bactérien avec 250 µL de tampon A1 contenant la RNAse en vortexant.
3. Ajouter 250 µL de tampon A2. Mélanger par 6-8 retournements. Incuber à température ambiante pendant 5 minutes.
4. Ajouter 300 µL de tampon A3. Mélanger immédiatement par 6-8 retournements.
5. Centrifuger à 11000 g pendant 5 minutes à température ambiante.
6. Pendant la centrifugation, placer une colonne NucleoSpin Plasmid Quickpure dans le tube collecteur 2 mL. En fin de centrifugation, charger le surnageant dans la colonne.
7. Centrifuger l'ensemble à 11000 g pendant 1 minute à température ambiante. Jeter le filtrat.
8. Remettre la colonne dans le tube collecteur et ajouter 450 µL de tampon AQ contenant l'éthanol.
9. Centrifuger l'ensemble à 11000 g pendant 3 minutes à température ambiante.
10. Jeter le filtrat. Puis éluer l'ADN dans un eppendorf 1,5 mL avec 50 µL de tampon AE.
11. Incuber 1 minute à température ambiante.
12. Centrifuger à 11000 g pendant 1 minute à température ambiante.
13. Garder le filtrat.

GIGAPREPARATION D'ADN PLASMIDIQUE

Références

- Ampicilline (Sigma-Aldrich A9518)
- Kanamycine (Sigma-Aldrich K1876)
- LB Luria Bernati broth (Sigma-Aldrich L3152)
- Endofree plasmid giga kit (Qiagen 12391)
- Isopropanol (Sigma-Aldrich 19516)
- Ethanol (Riedel de Haën 34935)
- NaCl sodium chloride (Sigma-Aldrich S8776)

Solutions

- *éthanol à 70 %*

70 mL d'éthanol + 30 mL d'eau

- *antibiotiques*

ampicilline	50 mg/mL
kanamycine	150 mg/mL

- *ajouter la RNAse dans le tampon P1*

- *milieu de culture* pH = 7,5

Liquide : 25 g de LB dans 1 L d'eau (autoclave)

Protocole

- *Jour 1*

1. Inoculer 5 mL de LB contenant l'antibiotique approprié (5 µL pour l'ampicilline à 50 mg/mL et 1,66 µL pour la kanamycine à 150 mg/mL) avec une colonie isolée.
2. Incuber pendant toute la nuit à 37°C sous agitation.

- *Jour 2*

1. Mettre 2,5 mL de préculture dans 2,5 L de LB contenant l'antibiotique approprié (2,5 mL pour l'ampicilline à 50 mg/mL et 833 µL pour la kanamycine à 150 mg/mL).
2. Incuber jusqu'au jour 3 à 37°C sous agitation.

- *Jour 3*

1. Collecter les bactéries par centrifugation à 6000 g pendant 15 minutes à 4°C.
2. Resuspendre le culot bactérien dans 125 mL de tampon P1 contenant la RNAse. Cette étape permet la resuspension des bactéries et apporte l'enzyme nécessaire à la digestion des ARN.
3. Ajouter 125 mL de tampon P2. Mélanger par 4-6 retournements. Incuber 5 minutes à température ambiante. Préparer la Qiafilter fournie en la vissant sur une bouteille de 500 mL (DURAN). Connecter la cartouche au vide. Cette étape permet une lyse de la paroi bactérienne et la libération de leur contenu dans le lysat.
4. Ajouter 125 mL de tampon P3 au lysat. Mélanger immédiatement par 4-6 retournements. Cette étape permet de stopper la réaction de lyse et de faire précipiter l'ADN génomique de la bactérie.
5. Verser le lysat dans la colonne. Incuber 10 minutes à température ambiante dans la Qiafilter.
6. Enclencher le vide. Laisser la cartouche en place en fin de filtration. Les débris bactériens et l'ADN génomique restent dans la Qiafilter, l'ADN plasmidique et les protéines sont filtrés et constituent le lysat.
7. Ajouter 50 mL de tampon FWB pour rincer la Qiafilter. Décoller délicatement le précipité avec une spatule stérile pour faciliter la filtration. Enclencher le vide jusqu'à ce que tout le liquide soit filtré.
8. Ajouter 30 mL de tampon ER au lysat dans la bouteille. Mélanger par une dizaine de retournements. Incuber 30 minutes sur la glace. Cette étape permet d'éliminer les endotoxines bactériennes (procédé propre au fabricant).
9. Pendant la réaction, équilibrer un TIP 10000 avec 75 mL de tampon QBT.
10. Charger le lysat.
11. Laver la colonne avec 600 mL de tampon QC. L'ADN plasmidique reste accroché sur la colonne, le reste est éliminé.
12. Eluer avec 75 mL de tampon QN.
13. Répartir l'éluât dans 4 tubes falcon de 50 mL. Précipiter l'ADN avec 13 mL d'isopropanol à température ambiante par tube. Centrifuger à 18500 g pendant 30 minutes à 4°C.

14. Laver chaque culot avec 2,5 mL d'éthanol 70 % à température ambiante. Centrifuger à 18500 g à 4°C pendant 10 minutes.

15. Transvaser les culots dans un tube falcon de 15 mL. Laisser sécher à l'air pendant 15 minutes. Reprendre avec un volume approprié de NaCl.

16. Vérifier la concentration en ADN (DO_{260nm}) et le contenu en protéines (DO_{280nm}). Calculer le rapport DO_{260nm}/ DO_{280nm} qui doit être compris entre 1,8 et 2. Si ce rapport est inférieur à 1,8 alors le contenu en protéines est trop important.

VERIFICATION DES ADN PLASMIDIQUES PAR DES ENZYMES DE RESTRICTION ET ELECTROPHORESE EN GEL D'AGAROSE

Références

- Tris trizma base (Sigma-Aldrich T1503)
- EDTA acide éthylène diamine tétracyclique (Sigma-Aldrich EDS)
- Bleu bromophénol sodium (Sigma-Aldrich B5525)
- Xylène cyanol (Sigma-Aldrich X4126)
- Glycérol (Fisher Scientific Bioblock G/P450/08)
- Agarose (Sigma-Aldrich A9539)
- BET bromure d'éthidium (Sigma-Aldrich E1510)
- Lambda DNA Bste II digest (Sigma-Aldrich D9793)
- Acide acétique glacial (Sigma-Aldrich A6283)

Principe

Le but de la manipulation est l'identification et la purification de fragments d'ADN. Pour cela, des sites de restrictions spécifiques ont été déterminés grâce à la carte de restriction des plasmides recombinants utilisés après analyse à l'aide du logiciel DNA strider® ou ApE®. Le nombre et la taille des fragments d'ADN issus de la digestion enzymatique sont vérifiés par migration en électrophorèse d'agarose 1 % contenant du bromure d'éthidium pouvant s'intercaler entre les bases nucléiques de la double hélice d'ADN. Ainsi, les molécules d'ADN sont fluorescentes lors d'un éclairage aux rayons ultraviolets. La migration en électrophorèse va dépendre de l'intensité de courant appliqué, de la concentration en agarose, de la force ionique du tampon et de la densité des enroulements de la super hélice.

Solutions

- TAE (Tris, Acétate, EDTA) 50X

tris	2 M
EDTA	50 mM

Ajuster à pH = 7,2 avec de l'acide acétique glacial (environ 57 mL) et autoclaver.

- tampon de charge 5X

bromophénol blue	0,25 %
xylène cyanol blue	0,25 %
glycérol	30 %

- agarose 1 %

Préparer une solution d'agarose à 1 % avec du TAE 1X puis dissoudre au micro-onde.

Protocole

- préparation de l'ADN

Le volume final doit être de 20 µL.

1. Diluer environ 1 µL d'ADN issu de la nucléospin® dans de l'eau.
2. Ajouter le tampon de réaction spécifique de l'enzyme (concentré 10 fois soit 1,6 µL) puis l'enzyme de réaction appropriée (2 µL).
3. Incuber les tubes 2-3 heures à 37°C.
4. Après avoir laissé incuber pendant un temps raisonnable, ajouter le tampon de charge (4 µL pour 16 µL).
5. Réaliser un choc thermique afin d'inactiver l'activité enzymatique à 65°C pendant 2 minutes.
6. Refroidir dans la glace rapidement pendant quelques secondes.
7. Centrifuger 3-4 secondes.
8. Préparer le marqueur de poids moléculaire en y ajoutant le tampon de charge (ce tube ne subit ni l'incubation à 37°C ni le choc thermique).

- préparation du gel

1. Mettre en place la chambre de coulage.
2. Préparer le gel d'électrophorèse : pour 50 mL d'agarose, ajouter 2,5 µL de la solution de bromure d'éthidium.
3. Couler dans la chambre de coulage et laisser solidifier.

4. Puis enlever le peigne et mettre en place le gel dans la cuve d'électrophorèse.
5. Verser le tampon d'électrophorèse TAE 1X dans la cuve.

- migration
1. Charger les échantillons.
2. Laisser migrer à 80 V en suivant le parcours des marqueurs : le bleu de bromophénol a une migration identique à celle d'un fragment de 300 paires de bases et le xylène cyanol à celle d'un fragment d'ADN de 400 paires de base dans un gel d'agarose à 1 %.
3. En fin de migration, sortir le gel et le disposer sur une table munie d'un éclairage ultraviolet et le photographier.

Nom usuel du plasmide	Enzymes de restriction	Nombre de fragments	Taille des fragments (pb)
pCMV-β-Gal	EcoR I Pst I	1 2	7200 4500/2700
p3.1 Zéo	EcoR I EcoR I + Sal I	1 3	5000 2100/1900/1000
pGL3-SREBP-1c pGL3-SREBP-1c LXR-/-	Xba I Xba I + Sal I	1 2	5700 5300/400
pBabe-Sirt1	Xho I Xho I + Pvu I	1 2	7400 5300/2100
pCMV-LXR	Bgl II Pvu I + Bgl II	1 3	6000 3500/1400/1100

TRANSFERT DE GENES *IN VIVO*

Références

- GET 42 générateur de courant (Electronique et Informatique du Pilat)
- Xylamine 2 % (Bayer)
- Kétamine 50 mg/mL (Panpharma)

Principe

Le transfert de gène consiste à introduire du matériel génétique (ADN) dans le tissu musculaire pour que celui-ci soit exprimé. Pour faciliter la pénétration de l'ADN dans les cellules musculaires, un courant électrique est appliqué grâce au générateur GET 42.

Protocole

1. Anesthésier les animaux par injection intrapéritonéale d'un mélange de Xylamine et Kétamine.
2. Raser la surface cutanée du muscle *Tibialis Anterior*.
3. Injecter l'ADN dans la portion centrale pour les rats et dans le muscle entier pour les souris de façon la plus reproductible possible (6 abords pour les rats : 3 en supérieur et 3 en inférieur plus profondément et 4 pour les souris : 2 en supérieur et 2 en inférieur plus profondément).
4. Stimuler le muscle au moyen des électrodes du GET 42 (4 * 2 pulses d'intensité de 50 mA et de durée de 100 µs pour les rats et 3 * 2 pulses de 50 mA et 20 ms pour les souris).

PRELEVEMENT TISSULAIRE ET CONDITIONNEMENT DES ECHANTILLONS

Références

- Xylamine 2 % (Bayer)
- Kétamine 50 mg/mL (Panpharma)

Principe

Après 7 jours suite à l'électrotransfert de gène, les muscles sont prélevés. Les muscles sont prélevés sur l'animal vivant profondément anesthésié par un mélange de Xylamine et Kétamine, et les muscles sont systématiquement pesés entiers avant leur conditionnement. A la suite du prélèvement, l'animal est sacrifié par une overdose de produit anesthésique.

Protocole

Le muscle en entier (souris) ou la portion centrale du muscle (rat) est plongé dans de l'azote liquide jusqu'à congélation complète de l'échantillon. Pour réaliser une extraction protéique, l'échantillon est préalablement réduit en poudre sous azote liquide à l'aide d'un pilon.

EXTRACTION PROTEIQUE SUR TISSU MUSCULAIRE CONGELE POUR ACTIVITES BIOLUMINESCENTES

Références

- RLB Reporter Lysis Buffer 5X (Promega E3971)

Principe

L'extraction permet une lecture avec un bioluminomètre.

Solutions

- solution

RLB 1/5 dans de l'eau

Protocole

1. Refroidir un tube Eppendorf 2 mL à fond rond.
2. Ajouter 200 µL de tampon d'extraction à 4°C. Tarer.
3. Déposer le morceau de muscle dans le tube. Peser.
4. Replacer l'ensemble rapidement dans la glace.
5. Ajuster le volume final pour avoir une dilution finale de 1/10 (poids/volume).
6. Homogénéiser le tissu à l'aide de l'ultrathurrax à 4°C (2 broyages de 3-5 secondes à 13500 rpm).
7. Réaliser 3 cycles de congélation (azote liquide) - décongélation (37°C). Vortexer vigoureusement pendant 15 secondes entre chaque cycle.
8. Centrifuger à 15000 g pendant 10 minutes à 4°C afin d'éliminer les débris cellulaires non dissous.
9. Récupérer le surnageant dans un tube préalablement refroidi à 4°C.

DOSAGE DE PROTEINES

Références

- BSA bovine serum albumine (PAA K41-001)
- Protein assay reagent A (BioRad 500-0113)
- Protein assay reagent B (BioRad 500-0114)

Principe

Le kit Bio-Rad permet la mesure de la concentration en protéine (réaction similaire à celle du Lowry) d'extraits par colorimétrie.

Solutions

BSA 2 mg/mL

Protocole

- courbe étalon

µg protéines	0	10	20	30	40	50
Δ H_2O, µL	195	190	185	180	175	170
Tampon extraction, µL	5					
BSA 2 mg/mL, µL	0	5	10	15	20	25
Solution A, µL	100					
Solution B, µL	800					

1. Ajouter les différentes solutions dans l'ordre décrit. Afin d'obtenir une coloration homogène, l'addition de la solution B doit se faire tout en vortexant. Faire les mesures en double.
2. Incuber 15 minutes à température ambiante à l'abri de la lumière.
3. Lire l'absorbance au spectrophotomètre à 750 nm.

- mode opératoire

1. Faire les dosages en double ou en triple.
2. Mettre 195 µL d'eau.
3. Ajouter 5 µL d'extrait.
4. Ajouter 100 µL de la solution A.
5. Ajouter 800 µL de la solution B en vortexant.
6. Incuber 15 minutes à température ambiante à l'abri de la lumière.
7. Lire l'absorbance au spectrophotomètre à 750 nm.

DOSAGE CHEMILUMINESCENT DE L'ACTIVITE ß-GALACTOSIDASE

Références

- RLB Reporter Lysis Buffer 5X (Promega E3971)
- β-gal reporter gene assay, chemiluminescent® (Roche 1758 241)

Principe

Pour mesurer l'efficacité de transfection, le cotransfectant β-galactosidase, enzyme non présente naturellement dans le muscle, est utilisé.

L'essai chemiluminescent est réalisé à partir du kit commercial β-gal reporter gene assay, chemiluminescent® et selon les recommandations du fournisseur. Dans la première étape de la réaction, le substrat du kit β-gal reporter gene assay, chemiluminescent® est déglycosylé grâce à l'action de l'enzyme β-galactosidase. Cette étape est réalisée à pH 7,8 où l'activité enzymatique de la β-galactosidase bactérienne est optimale. A ce pH, le dioxetane clivé est protoné et ne produit aucun signal lumineux. Cet intermédiaire stable s'accumule dans le milieu. La réaction lumineuse est déclenchée après un saut de pH pour des valeurs supérieures à 12. L'intermédiaire accumulé devient déprotoné et sa décomposition s'accompagne d'une émission de lumière à 475 nm. Dans ces conditions le signal lumineux atteint son maximum au bout d'une seconde avec une demi-vie approximative de 10 minutes. Le domaine de détection se situe entre 20 fg et 20 ng de β-galactosidase. Le kit est mis au point spécifiquement pour la β-galactosidase bactérienne. En cas de présence de β-galactosidase endogène il est conseillé de faire une inactivation thermique de la β-galactosidase.

Solutions

- *substrat reagent*

1 volume de substrat β-galactosidase
99 volumes de tampon d'essai

β-gal substrat, µL	Assay buffer, mL	Nombre d'essais
25	2,475	25
40	3,96	40
50	4,95	50
100	9,90	100
250	24,75	250
500	49,50	500

- *initiation reagent*

1 volume d'enhancer (bouteille 3)
5 volumes de solution d'initiation (bouteille 4)
6 volumes d'eau

Enhancer, µL	Initiation solution, mL	ΔH_2O, mL	Nombre d'essais
312,5	1,5625	1,875	25
500	2,5	3	40
625	3,125	3,75	50
1250	6,25	7,5	100
3125	15,625	18,75	250
6250	31,25	37,5	500
8000	40	48	640

- *reporter lysis buffer*

1 volume de reporter lysis buffer
4 volumes d'eau

Protocole

Toutes les solutions doivent être à température ambiante avant utilisation. L'essai est généralement réalisé avec 5-10 µg de protéines sous un volume d'environ 10 µL.

1. Préparer une dilution au 1/10 des extraits protéiques avec du lysis reagent.
2. Prélever x µL d'extrait dilué de façon à avoir 5-10 µg de protéine.
3. Compléter à 50 µL avec du lysis reagent.
4. Ajouter 100 µL du substrat reagent à l'aide d'un dispenser.
5. Incuber 20 minutes à température ambiante sous une légère agitation (~70 rpm Minitron).
6. Charger les tubes dans le bioluminomètre. Sélectionner le *Mode Pulse* pour l'agitation et fixer le *Delay Time* à 5 secondes et l'*Integration Time* à 10 secondes.
7. Déclencher la réaction en ajoutant 150 µL d'initiation reagent à l'aide d'un dispenser.
8. Relever les valeurs *Integration* et *Peak* (la valeur peak se stabilise 50 secondes environ après injection de l'initiation buffer).

DOSAGE FIREFLY LUCIFERASE

Références

- DTT dithiothréitol (Sigma-Aldrich D9163)
- EDTA acide éthylène diamine tétracyclique (Sigma-Aldrich EDS)
- $MgSO_4$ magnésium sulphate (Prolabo 25164265)
- ATP adenosine triphosphate (Sigma-Aldrich A8937)
- Glycylglycine (Sigma-Aldrich G1002)
- Beetle D-luciferin (Promega E160)
- Coenzyme A (Sigma-Aldrich C3019)
- RLB Reporter Lysis Buffer 5X (Promega E3971)

Principe

La protéine luciférase est une protéine reportrice qui, comme la β-galactosidase, est largement utilisée pour l'étude de l'expression génique.

Solutions

- solutions

EDTA	125 mM pH = 8,0
DTT	500 mM
$MgSO_4$	500 mM
ATP	50 mM
coenzymeA	16 mM

- luciferin stock solution (LSS)

	Concentration finale	Pour 2,5 mL	Pour 5 mL
Glycylglycine, mg	31,25 mM	10,3	20,6
EDTA 125 mM, µL	625 µM	12,5	25
DTT 500 mM, µL	2,5 mM	12,5	25
$MgSO_4$ 500 mM, µL	12,5 mM	62,5	125

Ajuster à pH = 7,8.
Préparer une solution de Beetle D-luciferin à 13,13 mM avec cette solution LSS.

- luciferase assay reagent (LAR)

	Concentration finale	Pour 25 mL	Pour 50mL
Glycylglycine, g	31,25 mM	103,2	206,4
EDTA 125 mM, µL	625 µM	125	250
DTT 500 mM, µL	2,5 mM	125	250
$MgSO_4$ 500 mM, µL	12,5 mM	625	1250
ATP 50 mM, µL	656 µM	328	656
Coenzyme A 16 mM, µL	355 µM	555	1110

Ajuster à pH = 7,8.

- luciferase assay buffer (LAB)
Ajouter 250 µL de LSS contenant la luciférine à 5 mL de LAR.

	Concentration finale
Glycylglycine	3125 mM pH=7,8
EDTA	625 µM
DTT	2,5 mM
$MgSO_4$	12,5 mM
ATP	625 µM
Coenzyme A	338 µM
D-Luciferin	625 µM

- *reporter lysis buffer*
  1 volume de reporter lysis buffer
  4 volumes d'eau

Protocole

1. Prélever x µL d'extrait de façon à avoir entre 5 et 10 µg de protéines.
2. Compléter à 60 µL avec du reporter lysis buffer.
3. Charger le tube dans le bioluminomètre réglé sous mode *Integration time* 10 secondes et *Delay time* 5 secondes en mode *continu*.
4. Déclencher la réaction en ajoutant 240 µL de LAB l'aide d'un dispenser.
5. Relever la valeur *Integrale* et *Peak* (la valeur peak se stabilise environ 45 secondes après l'injection d'initiation reagent).

EXTRACTION PROTEIQUE AVEC TAMPON COMPLET SUR TISSU MUSCULAIRE/CELLULES

Références

- Tris HCl tris hydrochloride (Sigma-Aldrich T3253)
- NaCl sodium chloride (Sigma-Aldrich S5886)
- β-glycérophosphate (Sigma-Aldrich G6251)
- Sodium fluorure (Sigma-Aldrich S7920)
- Triton X-100 (Sigma-Aldrich T8532)
- EDTA acide éthylène diamine tétracyclique (Sigma-Aldrich EDS)
- EGTA acide éthylène glycol-bisβaminoéthyéther tétraacétique (Sigma-Aldrich E4378)
- Na_3VO_4 sodium orthovanadate (Sigma-Aldrich S6508)
- Acide okaïdique (Sigma-Aldrich 07760)
- Benzamidine (Sigma-Aldrich B6506)
- PMSF phenylméthanesulfomyl fluoride (Sigma-Aldrich P7626)
- Aprotinine (Sigma-Aldrich A1153)
- Leupeptine (Sigma-Aldrich L8511)
- DPBS (PAA H15-002)

Solutions

- solutions

EDTA	200 mM	pH = 8,0
EGTA	200 mM	
Na_3VO_4	100 mM	
acide okaïdique	605 µM	
benzamidine	300 mM	
PMSF	100 mM	
aprotinine	1 µg/µL	
leupeptine	1 µg/µL	

Protocole

- préparation du tampon complet

Concentration solution finale	solution mère	Volume solution finale, mL					
		5	10	20	30	40	50
Tris HCl 50 mM, mg		39,4	78,8	157,6	236,4	315,2	394
NaCl 100 mM, mg		29,2	58,4	116,9	175,3	233,8	292,2
EDTA 2 mM, µL	200 mM	50	100	200	300	400	500
EGTA 2 mM, µL	200 mM	50	100	200	300	400	500
ß-glycérophosphate 50 mM, mg		54	108	216	324	432	540
sodium fluorure 50 mM, mg		10.5	21	42	63	84	105
Na_3VO_4 1 mM, µL	100 mM	50	100	200	300	400	500
acide okaïdique 120 nM, µL	605 µM	1	2	4	6	8	10
benzamidine 3 mM, µL	300 mM	50	100	200	300	400	500
PMSF 1 mM, µL	100 mM	50	100	200	300	400	500
aprotinine 10 µg/mL, µL	1 µg/µL	50	100	200	300	400	500
leupeptine 10 µg/mL, µL	1 µg/µL	50	100	200	300	400	500
Triton X-100 1 %, µL		100	200	400	600	800	1000

Combiner les différents réactifs. Ajuster le pH à 7,4. Ajuster le volume final dans une éprouvette graduée.

- *mode opératoire pour tissu musculaire*

1. Peser environ 20-25 mg de tissu dans un tube eppendorf refroidi.
2. Ajouter le tampon complet de façon à réaliser une dilution finale 1/20 (poids/volume).
3. Homogénéiser le tissu 2 fois pendant 10 secondes dans la glace à l'Ultrathurax.
4. Centrifuger à 12000 g pendant 20 minutes à 4°c.
5. Récupérer le surnageant.

- *mode opératoire pour cellules*

1. Rincer 2 fois chaque boite ou puits avec du DPBS contenant du calcium.
2. Ajouter 250 µL de tampon complet pour une boite de 10 cm.
3. Racler avec une spatule.
4. Récupérer le tampon dans un tube eppendorf préalablement refroidi dans la glace.
5. Répéter les étapes 2, 3 et 4.
6. Vortexer vigoureusement.
7. Réaliser 3 cycles de congélation (azote liquide) - décongélation (température ambiante). Entre chaque cycle, soniquer 10 secondes.
8. Centrifuger à 10000 g pendant 10 minutes à 4°C.
9. Récupérer le surnageant.

ELECTROPHORESE SDS PAGE/WESTERN BLOT

Références

- APS Ammonium persulfate (Sigma-Aldrich A9164)
- Glycérol (Fisher Scientific Bioblock G/P450/08)
- SDS sodium dodécyl sulfate (Fisher Scientific Bioblock S/5200/53)
- Acrylamide (Sigma-Aldrich A7802)
- Temed tétraméthyléthyléthylènediamine (Sigma-Aldrich T7024)
- β-mercaptoéthanol (Sigma-Aldrich M7154)
- Tris trizma base (Sigma-Aldrich T1503)
- Glycine (Sigma-Aldrich G8898)
- Méthanol (Fisher Scientific Bioblock M/4058/17)
- Acide acétique glacial (Sigma-Aldrich A6283)
- Bleu bromophénol sodium (Sigma-Aldrich B5525)
- Brilliant blue G (Sigma-Aldrich B0770)
- Butanol (Prolabo 20810.298)
- NaCl sodium chloride (Sigma-Aldrich S5886)
- Tween (Sigma-Aldrich P9416)
- Ponseau (Fluka 81462)
- Whatman gel blot papier (Sigma-Aldrich Z613908)
- Whatman protran nitrocellulose membrane (Sigma-Aldrich Z613665)
- Fixater (Sigma-Aldrich P7167)
- Developer (Sigma-Aldrich P7042)
- Western blotting detection reagents (GE Healthcare RPN2109)
- Hyperfilm ECL (GE Healthcare 28906835)

Principe

Cette technique regroupe deux étapes : une électrophorèse suivie d'un Western Blot. L'électrophorèse permet de séparer les protéines, préalablement dénaturées, selon leur poids moléculaire. Le Western Blot permet le transfert de ces protéines sur une membrane où elles seront exposées à un anticorps primaire spécifique de la protéine d'intérêt. Avec un anticorps secondaire fluorescent spécifique de l'anticorps primaire, il est possible de détecter la présence et la concentration de la protéine d'intérêt.

Solutions

- solutions

APS	10 %
Glycérol	50 %
SDS	10 %

Protocole

- préparation de la solution du gel de séparation

Le pourcentage en acrylamide du gel de séparation est déterminé en fonction de la taille des protéines d'intérêt.

% en acrylamide	taille des protéines
15 %	15 à 45 kDa
12,5 %	15 à 60 kDa
10 %	18 à 75 kDa
7 %	30 à 120 kDa
gradient progressif	60 à 212 kDa

Solution, concentration finale	% en acrylamide				
	Gel 4 %	Gel 7 %	Gel 10 %	Gel 12,5 %	Gel 15 %
Acrylamide, mL	5	8,75	12,5	15,63	18,75
Tris, 0,375 M	2,27 g				
SDS, 0,2 %	1 mL SDS 10 %				
Glycérol, 10 %	10 mL glycérol 50 %				

Compléter à 45 mL avec ΔH_2O. Ajuster le pH à 8,8. Compléter le volume final à 50 mL avec ΔH_2O.

- *préparation de la solution du gel de concentration 3 %*

tris 0,125 M	757 mg
acrylamide 3 %	3,75 mL
SDS 0,2 %	1 mL de SDS 10 %
glycérol 3 %	3 mL de glycérol 50 %

Compléter à 45 mL avec ΔH_2O. Ajuster le pH à 6,8. Compléter le volume final à 50 mL avec ΔH_2O. Ajouter une spatule de bleu de bromophénol.

- *préparation des tampons*

Tampon d'électrophorèse :

tris 25 mM	3 g
glycine 192 mM	14,41 g
SDS 0,2 %	20 mL de SDS 10 %

Compléter à 950 mL avec ΔH_2O. Ajuster le pH entre 8,1 et 8,4. Compléter le volume final à 1000 mL avec ΔH_2O.

Tampon de transfert :

tris 25 mM	3 g
glycine 192 mM	14,41 g
méthanol 20 %	200 mL

Compléter à 950 mL avec ΔH_2O. Ajuster le pH entre 8,1 et 8,4. Compléter le volume final à 1000 mL avec ΔH_2O. Le méthanol améliore l'absorption sur une membrane de nitrocellulose, mais diminue l'efficacité du transfert. L'ajout de SDS 0,1 % (soit 1 g) dans le tampon de transfert augmente l'efficacité du transfert mais diminue la capacité de la membrane à retenir certaines protéines.

Tampon d'échantillon 4X :

tris 250 mM	1,51 g
glycerol 20 %	20 mL de glycérol 50 %
SDS 4 %	20 mL de SDS 10 %

Compléter à 40 mL avec ΔH_2O. Ajuster le pH à 6,8. Compléter le volume final à 45 mL avec ΔH_2O. Ajouter une spatule de bleu de bromophérol. (Le jour de l'expérimentation ajouter 10 % (volume/volume) de β-mercaptoéthanol).

- *préparation des solutions d'incubation*

Solution de coloration au bleu de Coomassie :

brilliant blue G	1 g
méthanol	450 mL
H_2O	450 mL
acide acétique glacial	100 mL

Agiter toute la nuit et filtrer pour enlever les particules du colorant non dissoutes.

Solution de décoloration :

méthanol	100 mL
acide acétique glacial	100 mL
H_2O	800 mL

Solutions de rinçage :

* TBS tris buffered saline 10X

tris 100 mM	12,11 g
NaCl 1,5 M	87,66 g

Compléter à 950 mL avec ΔH_2O. Ajuster le pH à 7,5. Compléter le volume final à 1000 mL avec ΔH_2O.
Diluer au 1/10 pour utilisation (100 mL de TBS 10X + 900 mL ΔH_2O).

* TBS tris buffered saline 1X-Tween 0,05 %

tris 10 mM	1,21 g
NaCl 150 mM	8,76 g
Tween	500 µL (préalablement chauffé à 40°C)

Compléter à 950 mL avec ΔH_2O. Ajuster le pH à 7,5. Compléter le volume final à 1000 mL avec ΔH_2O.

- *préparation du gel*

Mise en place des plaques d'électrophorèse

Nettoyer les plaques au micro 90 en vérifiant l'absence d'impuretés à leurs surfaces. Rincer abondamment avec ΔH_2O. Nettoyer ensuite les plaques avec de l'alcool à 95°. Les mettre en place en suivant les indications du fournisseur (BioRad). Vérifier l'ajustement des plaques et des spacers afin d'éviter les fuites lors du coulage.

Préparation et coulage du gel de séparation

La polymérisation de l'acrylamide est initiée par l'addition d'APS au 1/100 et d'un accélérateur, le Temed, au 1/666. Attendre que les réactifs soient à température ambiante, puis préparer le gel comme indiqué ci-dessous :

Solutions	1 mini-gel	2 mini-gels
Solution gel de concentration, mL	2,5	5
Temed, µL	3,75	7,5
APS, µL	25	50

Verser le gel de concentration avec une pipette, puis mettre le peigne en position. Laisser polymériser au moins 30 minutes.

Mise en place des plaques d'électrophorèse dans la cuve

Dégager le cadre de coulage. Avec une feuille de papier enlever les débris polymérisés au bas du gel. Mettre en place les plaques avec leurs supports dans la cuve d'électrophorèse. Verser le tampon d'électrophorèse de façon à égaliser les niveaux de part et d'autre des plaques. Enlever délicatement les peignes, puis nettoyer les puits à l'aide d'une seringue de façon à enlever les débris de gel qui pourraient affecter la migration.

- *préparation des échantillons*

Préparation

Dans un tube Eppendrof 0,5 mL combiner 3 volumes d'échantillon protéique à 1 volume de tampon d'échantillon 4X contenant du β-mercaptoéthanol 10 % (volume/volume). Le choix du volume d'extrait protéique dépend de sa concentration. En général 30 µg par puits sont largement suffisants.

Chauffer à 100°C pendant 3 minutes.

Centrifuger brièvement (3 secondes) dans une centrifugeuse pour récupérer le volume.

Chargement

Charger délicatement l'échantillon dans le puits. Faire attention à ne pas introduire de bulles d'air. Prévoir un puits pour le marqueur de poids moléculaire.

Migration

Fixer les électrodes. Des bulles d'air doivent se former lorsque le courant passe. Le front de migration est indiqué par le bleu de bromophénol contenu dans le tampon d'échantillon 4X.

Faire migrer à 80 V pendant 15 minutes puis augmenter la tension (90 V) et laisser plusieurs heures (à adapter suivant la protéine d'intérêt) à 4°C.

Couper l'alimentation. Enlever les plaques délicatement.

- *transfert liquide sur membrane des protéines*

Préparation de la membrane de transfert

Découper 4 morceaux de papier Whatman légèrement supérieurs à la taille du gel soit 8,5 * 6 cm. Découper un morceau de membrane de nitrocellulose de la taille des papiers. Faire un repère pour orienter la membrane en coupant un coin de la membrane.

Tremper progressivement la membrane dans le tampon de transfert. Laisser à 4°C pendant 15 minutes. Cette étape est importante car elle permet d'éviter la formation de micro-bulles qui pourraient affecter le transfert.

Transfert

Enlever le gel de concentration. Faire un repère afin d'orienter le gel en coupant le coin supérieur gauche. Tremper le gel pendant 15 minutes dans le tampon de transfert à 4°C afin d'éliminer l'excès de SDS.

Faire tremper les feuilles de papier Whatman dans le tampon de transfert. Tremper un pad mousse dans le tampon de transfert. Le disposer sur la face négative noire du sandwich, proche du côté avec les charnières. Prendre une feuille de papier Whatman et la disposer sur le pad mousse. Chasser les bulles en roulant une pipette sur le papier de transfert. Déposer délicatement le gel en mettant le coin coupé en haut à droite.

Disposer la membrane de transfert sur le gel en faisant correspondre les entailles. Ne pas enfermer de bulles entre le gel et la membrane.

Prendre une feuille de papier whatman et la disposer sur la membrane. Chasser les bulles en roulant une pipette sur le papier whatman sans trop appuyer pour ne pas dilater le gel. Tremper un pad mousse dans le tampon de transfert. Le disposer sur le sandwich. Fermer délicatement le sandwich. Le mettre en place dans son support, noir contre noir et blanc contre blanc.

Mettre en place le support dans la cuve de transfert, puis verser du tampon de transfert jusqu'à ce que le gel soit complètement immergé. Positionner ensuite le système réfrigérant contenant de la glace.

Transférer à ampérage constant à 4°C pendant plusieurs heures (selon la masse des protéines d'intérêt). Au terme du transfert, prélever délicatement le gel et la membrane pour les mettre à colorer dans 2 solutions : rouge Ponseau pour la membrane et bleu de Coomassie pour le gel.

<u>Colorations</u>

* Membrane au rouge Ponseau

Cette étape est facultative. Elle permet cependant de vérifier que le transfert des protéines du gel sur la membrane a correctement fonctionné.

Tremper pendant 5 minutes la membrane dans la solution de rouge Ponseau sous agitation. Sauver la solution de Ponseau et rincer la membrane avec du TBS 1X, et observer les bandes de protéines colorées en rouge.

Laver deux fois la membrane avec du TBS 1X pendant 5 minutes de façon à décolorer complètement la membrane. Les bandes rouges ont alors complètement disparues.

* Gel au bleu de Coomassie

Le processus de coloration/décoloration permet de visualiser les bandes protéiques du gel. Après coloration, tout transfert sera impossible car les protéines ont été fixées par le colorant.

Laisser incuber le gel pendant 1 heure dans le bleu de Coomassie sous agitation. Sauver la solution de bleu de Coomassie et ajouter la solution de décoloration. Mettre une feuille de papier absorbant ce qui permettra de piéger le colorant qui est libéré. Réaliser un autre bain lorsque la solution de décoloration est saturée par le colorant. Répéter l'opération jusqu'à ce que le gel soit complètement décoloré (ou laisser sous agitation toute la nuit en recouvrant de papier d'alu pour emprisonner l'odeur). Sauver les derniers bains de décoloration pour une réutilisation.

- *blocage de la membrane*

Cette étape permet de bloquer les sites de fixation potentiels non spécifiques des anticorps sur la membrane en la saturant avec des protéines du lait (caséine). Il en résultera une diminution du bruit de fond lors de la révélation.

Préparer une solution 5 % Régilait dans du TBS 1X (5 g de Régilait pour 100 mL de TBS 1X). Agiter pendant 5 minutes pour dissoudre le Régilait. Faire tremper la membrane pendant au moins une heure sous agitation à température ambiante dans la solution TBS 1X-Régilait 5 %.

Laver la membrane avec du TBS 1X pendant 10 minutes.

- *marquage de la membrane avec les anticorps*

<u>Anticorps primaire</u>

Préparer une solution 5 % Régilait dans du TBS 1X ou une solution 5 % BSA dans du TBS 1X selon la fiche technique de l'anticorps.

Recouvrir une plaque en verre avec du parafilm. La disposer dans un plateau.

Préparer l'anticorps primaire à la dilution appropriée dans du TBS 1X-Régilait 5 %. Les anticorps primaires sont généralement préparés pour être utilisées à des dilutions s'étendant de 1/250 à 1/1000. Compter environ 2 mL de TBS 1X-Régilait 1 % pour une membrane entière.

Déposer la solution contenant l'anticorps sur le parafilm, puis disposer la membrane de telle sorte que la face avant protéique soit au contact du parafilm. Eviter la formation de bulles qui pourraient prévenir la fixation de l'anticorps. Recouvrir le plateau avec de l'aluminium.

Laisser incuber une heure à température ambiante ou toute la nuit à 4°C.

Laver ensuite 2 fois la membrane avec TBS 1X-Tween 0,05 % pendant 5 minutes. Laver la membrane avec TBS 1X pendant 10 minutes.

Anticorps secondaire

Recouvrir une plaque en verre avec du parafilm.

Préparer l'anticorps secondaire à la dilution appropriée dans TBS 1X-Régilait 5 % préparé lors du marquage avec l'anticorps primaire. Les anticorps secondaires sont généralement préparés à des dilutions s'étendant de 1/2500 à 1/5000 (en fonction du système de révélation). Vérifier la compatibilité de l'anticorps secondaire avec l'hôte dans lequel a été produit l'anticorps primaire.

Déposer la membrane de telle sorte que la face arrière non protéique soit au contact du parafilm. Déposer ensuite 2 mL de TBS 1X-Régilait 5 % avec l'anticorps sur la face protéique de la membrane. S'assurer que la totalité de la membrane est recouverte. Recouvrir l'ensemble.

Laisser incuber une heure à température ambiante ou toute la nuit à 4°C.

Laver ensuite 2 fois la membrane avec TBS-Tween 0,05 % pendant 5 minutes. Laver la membrane avec TBS pendant 10 minutes.

- *révélation*

Préparation des réactifs de développement et de révélation

Développeur : 50 mL de développeur + 200 mL ΔH_2O. Conserver à l'abri de la lumière dans un flacon bouché recouvert de papier aluminium.

Fixateur : 50 mL de fixateur + 200 mL ΔH_2O. Conserver à l'abri de la lumière dans un flacon bouché recouvert de papier aluminium.

Réaction de révélation (en chambre noire)

Préparer la solution de révélation en ajoutant un volume de solution A et un volume de solution B. Compter environ 1 mL au total par mini-gel.

Enlever l'excès de la dernière solution de rinçage. Déposer la membrane face protéique en avant sur une plaque de verre. Recouvrir complètement la membrane avec la solution de révélation. Laisser incuber une minute à l'abri de la lumière. La technique de révélation est basée sur la réaction chimioluminescente catalysée par HorseRadish Peroxidase en présence du substrat luminol.

Enlever rapidement l'excès de solution de révélation, puis recouvrir la membrane avec un transparent type rétroprojecteur en évitant la formation de bulles. Ne pas sécher complètement la membrane qui doit toujours rester humide. Placer la membrane et son support dans la cassette, face protéique en avant. Placer le film directement contre la membrane recouverte du transparent. Noter les contours de la membrane sur le film. Fermer la cassette. **Attention ne pas exposer les films à la lumière blanche.**

Les temps d'exposition sont variables et dépendent de l'abondance de la protéine d'intérêt, de l'activité HRP et de la sensibilité du système de révelation. Généralement, se fixer un temps d'exposition de 3 à 5 minutes, puis l'ajuster en fonction de l'intensité du signal.

Développement du film (en chambre noire)

Placer en série 3 bacs d'incubation contenant dans l'ordre le développeur, de l'eau du robinet et le fixateur.

Prendre le film de la cassette. Le tremper entièrement pendant 1 minute dans le développeur. Rincer ensuite le film dans le bac contenant de l'eau du robinet. Tremper ensuite entièrement le film dans la solution de fixation pendant 3 minutes. Rincer abondamment le film à l'eau du robinet. Laisser sécher.

Vérifier que le signal n'est pas surexposé. Sinon recommencer l'exposition avec un temps plus court, ou attendre une dizaine de minutes avant de remettre le film au contact de la membrane.

LUMINEX

Principe

Ce sytème multi-analytique est constitué d'un cytomètre en flux à deux lasers. La puissance de ce système réside dans le fait qu'il est possible d'analyser simultanément jusqu'à 100 types de microsphères par puits. Les applications sont nombreuses. Les deux plus grands domaines concernés sont la génétique grâce à la réaction d'hybridation moléculaire, et l'immunologie, grâce à la réaction antigène-anticorps. C'est cette dernière qu'on utilisera pour la révélation de protéines d'intérêt.

- les microsphères :

Il s'agit de billes de 5,6 µm de diamètre marquées par incubation dans des bains renfermant un mélange de deux solutions fluorescentes. La solution fluorescente est piégée à l'intérieur de la microsphère. En variant la proportion des deux fluorochromes, on obtient une gamme de 100 microsphères, avec pour chacune un ratio unique selon l'intensité de la fluorescence émise par les deux fluorochromes dans leur spectre d'émission respectif : fluorescence rouge (675 nm) et infra-rouge (> 712 nm).

- le cytomètre :

Il comporte un laser rouge à diode (633 nm) excitant les fluorochromes à l'intérieur des microsphères, permettant ainsi l'identification précise de la microsphère et ainsi de la protéine d'intérêt, et un laser vert (532 nm) qui excite le fluorochrome reporter (phycoérythrine PE) lié à la biotine, permettant dans ce cas de quantifier la protéine d'intérêt.

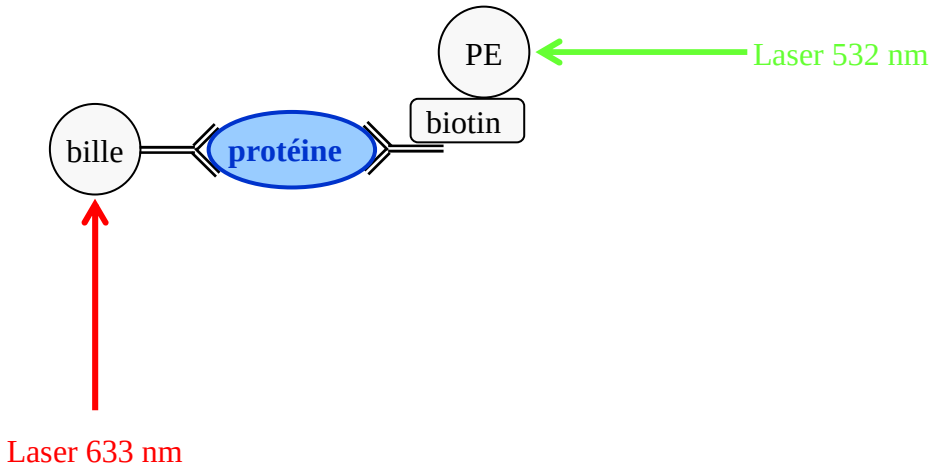

Solutions

- Dilution des anticorps et fluorochromes :

Billes	1/40
Biotine	1/40
PE	1/50

Protocole

1. Imbiber les puits de la plaque 96 puits avec de l'assay buffer. Aspirer.
2. Charger les billes. Aspirer.
3. Laver avec 50 µL d'assay buffer avec aspiration 2 fois.
4. Charger les extraits.
5. Incuber toute la nuit à 4°C sous agitation (30 secondes à forte puissance puis plus doucement). Aspirer.
6. Laver avec 50 µL d'assay buffer avec aspiration 2 fois.
7. Charger la biotine.
8. Incuber 1 heure à température ambiante sous agitation (30 secondes à forte puissance puis plus doucement). Aspirer.
9. Laver avec 50 µL d'assay buffer avec aspiration 2 fois.
10. Charger la PE.
11. Incuber 15 minutes à température ambiante sous agitation (30 secondes à forte puissance puis plus doucement).
12. Ajouter l'amplificateur.

13. Incuber 15 minutes à température ambiante sous agitation (30 secondes à forte puissance puis plus doucement). Aspirer.
14. Laver avec 50 µL d'assay buffer avec aspiration 2 fois.
15. Resuspendre les puits avec 150 µL d'assay buffer par puits.
16. Lire au luminex.

CITRATE SYNTHETASE

Références

- Tris trizma base (Sigma-Aldrich T1503)
- Acétyl-CoA (Sigma-Aldrich A2056)
- EDTA acide éthylène diamine tétracyclique (Sigma-Aldrich EDS)
- Malate (Sigma-Aldrich M9138)
- NAD nicotinamide adénine dinucléotide (Roche 127 965)
- Triton X-100 (Sigma-Aldrich T8532)
- NADH,H^+ nicotinamide adénine dinucléotide (Roche 107 735)
- MDH malate déshydrogénase (Roche 127 256)

Principe

En présence de NAD^+ et de malate, la malate déshydrogénase va produire de l'oxaloacétate et du NADH,H^+. Les conditions expérimentales permettent d'obtenir rapidement une situation d'équilibre. La modification de l'équilibre réactionnel est rendue possible par la consommation d'oxaloacétate due à la citrate synthétase (CS) en présence d'acétyl-CoA. Il en résulte que la production de NADH,H^+ et d'oxaloacétate par la malate déshydrogénase est proportionnelle à l'activité de la citrate synthétase.

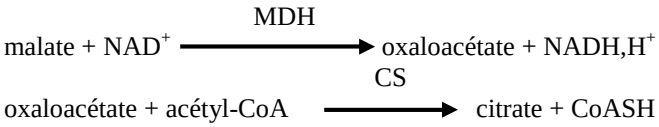

Solutions

-solutions

tris	1 M	pH = 8,0
acétyl-CoA	5 mM	
EDTA	200 mM	
malate	250 mM	
NAD^+	50 mM	
NADH,H^+	1 mM	
triton X-100	10 %	
MDH	6000 U/mL	

Protocole

- préparation du milieu réactionnel MR

tris 1M pH = 8,0	5 mL
EDTA 200 mM	500 µL
malate 250 mM	250 µL
NAD^+ 50 mM	250 µL
MDH 6000 U/mL	48,5 µL

Ajuster le volume final à 48,5 mL avec de l'eau.

- étalonnage du fluorimètre

$\lambda_{excitation}$ = 340 nm ; $\lambda_{émission}$ = 450 nm

Faire le point haut à 150 sur 10 nmoles de NADH,H^+ et le 0 sur 0 nmoles de NADH,H^+.

- courbe étalon

nmoles $NADH,H^+$	0	2	4	6	8	10
Milieu réactionnel, µL	970					
$NADH,H^+$ 1 mM, µL	0	2	4	6	8	10
ΔH_2O, µL	30	28	26	24	22	20

-mode opératoires

1. Mettre 970 µL de MR.
2. Ajouter 10 µL de Triton X-100 10 %.
3. Ajouter 10 µL d'extrait.
4. Incuber 5 minutes à température ambiante afin de permettre au Triton de solubiliser les membranes mitochondriales.
5. Déclencher la réaction en ajoutant 10 µL d'acétyl-CoA 5 mM.
6. Incuber 5 minutes à température ambiante.
7. Suivre la réaction pendant 10 minutes.

3-HYDROXYL ACYL-COENZYME A DESHYDROGENASE

Références

- Tris trizma base (Sigma-Aldrich T1503)
- NADH,H^+ nicotinamide adénine dinucléotide (Sigma-Aldrich N6005)
- Triton X-100 (Sigma-Aldrich T8532)
- Acéto-acétyl-CoA (Sigma-Aldrich A1625)
- EDTA acide éthylène diamine tétracyclique (Sigma-Aldrich EDS)

Principe

L'oxydation de NADH,H^+ par la 3-hydroxyl acyl-coenzyme A déshydrogénase (HAD) s'accompagne d'une diminution de l'émission de fluorescence à 450 nm.

$$\text{Acéto-acétyl CoA} + \text{NADH,H}^+ \xrightarrow{\text{HAD}} \text{Hydroxyl acylCoA} + \text{NAD}^+$$

Solutions

- solutions

tris	1 M	pH = 7,0
EDTA	200 mM	
NADH,H^+	5 mM	
triton X-100	10 %	
acéto-acétyl-CoA	5 mM	

Protocole

- préparation du milieu réactionnel MR

tris 1M pH = 7,0	2,5 mL
EDTA 200 mM	500 µL
NADH,H^+ 5 mM	500 µL

Ajuster le volume final à 48 mL avec de l'eau.

- étalonnage du fluorimètre

$\lambda_{excitation}$ = 340 nm ; $\lambda_{émission}$ = 450 nm

Faire le point haut à 150 sur 50 nmoles de NADH,H^+ et le 0 sur 0 nmoles de G6P.

- courbe étalon

Milieu d'étalonnage :

750 µL de Tris 1M pH = 7,0
150 µL d'EDTA 200 mM

Ajuster le volume final à 15 mL avec de l'eau.

nmoles NADH,H^+	0	10	20	30	40	50
Milieu étalonnage, µL	970					
NADH,H^+ 5 mM, µL	0	2	4	6	8	10
ΔH_2O, µL	30	28	26	24	22	20

- mode opératoire

1. Mettre 965 µL de MR.
2. Ajouter 10 µL de Triton 10 %.
3. Ajouter 10 µL d'extrait.
4. Attendre 5 minutes à température ambiante.
5. Déclencher la réaction en ajoutant 15 µL d'acéto-acétyl-CoA 5 mM.
6. Attendre 5 minutes à température ambiante.
7. Suivre la réaction pendant 15 minutes.

HEXOKINASE

Références

- Tris trizma base (Sigma-Aldrich T1503)
- $MgCl_2$ magnésium chlorure (Prolabo 25 108.295)
- NADP nicotinamide adénine dinucléotide phosphate (Roche 128 058)
- Glucose (Prolabo 24 370.294)
- DTT dithiothreitol (Sigma-Aldrich D9163)
- ATP adénosine triphosphate (Roche 519 979)
- G6P glucose-6-phosphate (Roche 127 027)
- G6PDH glucose-6-phosphate-déshydrogénase (Roche 127 655)

Principe

En présence de glucose et d'ATP, l'hexokinase (HK) va produire du glucose-6-phosphate et de l'ADP. Les conditions expérimentales permettent d'obtenir rapidement une situation d'équilibre. La modification de l'équilibre réactionnel est rendue possible par la consommation du glucose-6-phosphate par la glucose-6-phosphate déshydrogénase. Il en résulte une production de $NADH,H^+$ et de gluconolactone-6-phosphate par la glucose-6-phosphate déshydrogénase qui est directement proportionnelle à l'activité de l'hexokinase.

$$\text{Glucose} + \text{ATP} \xrightarrow{\text{HK}} \text{G6P} + \text{ADP}$$

$$\text{G6P} + \text{NADP} \xrightarrow{\text{G6PDH}} \text{Gluconolactone-6-Phosphate} + \text{NADPH}$$

Solutions

- solutions

tris	1 M	pH = 8,0
$MgCl_2$	400 mM	
glucose	100 mM	
NADP	100 mM	
ATP	200 mM	
DTT	10 %	
G6P	10 mM	
G6PDH 117 U/mL		

Protocole

- préparation du milieu réactionnel MR

tris 1M pH = 8,0	5 mL
$MgCl_2$ 400 mM	500 µL
NADP 100 mM	75 µL
glucose 100 mM	2 mL
DTT 10 %	100 µL

Ajuster le volume final à 100 mL avec de l'eau.

- étalonnage du fluorimètre

$\lambda_{excitation}$ = 340 nm ; $\lambda_{émission}$ = 450 nm

Faire le point haut à 150 sur 10 nmoles de G6P et le 0 sur 0 nmoles de G6P.

- courbe étalon

Faire une dilution du G6P à 10 mM au 1/20 pour avoir une solution finale de G6P à 0,5 mM.

nmoles G6P	0	2,5	5	7,5	10
Milieu réactionnel, mL	1				
G6P 0,5 mM, µL	0	5	10	15	20
ΔH_2O, µL	50	45	40	35	30
G6PDH, µL	10				

Incuber 20 minutes dans l'obscurité à température ambiante.

- *mode opératoire*

1. Mettre 1 mL de MR.
2. Ajouter 10 µL de G6PDH.
3. Ajouter 30 µL d'extrait.
4. Attendre 4 minutes à température ambiante.
5. Déclencher la réaction en ajoutant 10 µL d'ATP 200 mM.
6. Suivre la réaction pendant 15 minutes.

LACTATE DESHYDROGENASE

Références

- Tris trizma base (Sigma-Aldrich T1503)
- $NADH,H^+$ nicotinamide adénine dinucléotide (Roche 107 735)
- EDTA acide éthylène diamine tétracyclique (Sigma-Aldrich EDS)
- Pyruvate (Sigma-Aldrich P2256)

Principe

L'oxydation du $NADH,H^+$ par la lactate déshydrogénase (LDH) s'accompagne d'une diminution de l'émission de fluorescence à 450 nm. La baisse de fluorescence au cours du temps due à la consommation de $NADH,H^+$ est détectée au fluorimètre.

$$\text{Pyruvate} + NADH,H^+ \xrightarrow{\text{LDH}} \text{Lactate} + NAD^+$$

Solutions

- solutions

tris	1 M	pH = 7,6
EDTA	200 mM	
$NADH,H^+$	5 mM	
pyruvate	100 mM	

Protocole

- préparation du milieu réactionnel MR

tris 1M pH = 7,6	2,5 mL
EDTA 200 mM	500 µL
$NADH,H^+$ 5 mM	500 µL

Ajuster le volume final à 49 mL avec de l'eau.

- étalonnage du fluorimètre

$\lambda_{excitation}$ = 340 nm ; $\lambda_{émission}$ = 450 nm

Faire le point haut à 150 sur 50 nmoles de $NADH,H^+$ et le 0 sur 0 nmoles de $NADH,H^+$.

- courbe étalon

Milieu d'étalonnage :

500 µL de tris 1M pH = 7,6 + 100 µL d'EDTA 200 mM

Ajuster le volume final à 10 mL avec de l'eau.

nmoles $NADH,H^+$	0	10	20	30	40	50
Milieu étalonnage, µL	970					
$NADH,H^+$ 5 mM, µL	0	2	4	6	8	10
ΔH_2O, µL	30	28	26	24	22	20

- mode opératoire

1. Mettre 980 µL de MR.
2. Ajouter 10 µL d'extrait.
3. Déclencher la réaction en ajoutant 10 µL de pyruvate 100 mM.
4. Suivre la réaction pendant 15 minutes.

CHYMOTRYPSINE-LIKE

Références

- Imidazole (Sigma-Aldrich I0125)
- AMC 7-amino-4-méthyl-coumarin (Sigma-Aldrich A9891)
- Suc-Leu-Leu-Val-Tyr-AMC = Suc-LLVY-AMC (Bachem I-1395)
- DMSO diméthyl sulfoxide (Sigma-Aldrich D5879)

Principe

La protéolyse ubiquitine ATP dépendante joue un rôle majeur dans la dégradation des protéines musculaires. La dégradation est assurée par un complexe protéolytique comprenant le protéasome 26S, lui-même constitué du protéasome 20S, le coeur de la machinerie protéolytique, et de 2 complexes de régulation 19S. Le protéasome présente 5 activités enzymatiques différentes dont trois principales : l'activité chymotrypsine-like (la principale), l'activité trypsine-like et l'activité caspase-like.

Pour mesurer l'activité chymotrypsine-like, le peptide Suc-Leu-Leu-Val-Tyr-AMC est ici utilisé comme substrat fluorogénique. La reconnaissance du substrat par le site actif de l'enzyme détermine la coupure de la liaison entre l'AMC et le tétrapeptide. La fluorescence de la molécule d'AMC, qui est alors libérée, peut être suivie au fluorimètre à 460 nm. La spécificité de la réaction peut être vérifiée à l'aide d'un inhibiteur spécifique du complexe 20S, le peptide Z-Ile-Glu(OtBu)-Ala-Leu-CHO.

Solutions

- solutions

AMC	4 mM dans du DMSO
Z-LLVY-AMC	10 mM dans du DMSO

Protocole

- préparation du milieu réactionnel MR

imidazole	60 mM pH = 7,4

- étalonnage du fluorimètre

$\lambda_{excitation}$ = 380 nm ; $\lambda_{émission}$ = 460 nm

Faire le point haut à 150 sur 200 pmoles d'AMC et le 0 sur le milieu réactionnel seul.

- courbe étalon

Faire une dilution de l'AMC à 4 mM au 1/400 pour avoir une solution finale d'AMC à 10 µM.

pmoles AMC	0	40	80	120	160	200
AMC 10 µM, µL	0	4	8	12	16	20
Milieu réactionnel, µL	1000	996	992	988	984	980

- mode opératoire

1. Mettre 985 µL de MR.
2. Ajouter 5 µL d'extrait.
3. Déclencher la réaction en ajoutant 10 µL de Z-LLVY-AMC 10 mM.
4. Suivre la réaction pendant 20 minutes.

TRYPSINE-LIKE

Références

- Tris HCl tris hydrochloride (Sigma-Aldrich T3253)
- $MgCl_2$ magnésium chlorure (Prolabo 25 108.295)
- DTT dithiothreitol (Sigma-Aldrich D9163)
- AMC 7-amino-4-méthyl-coumarin (Sigma-Aldrich A9891)
- Boc-Leu-Ser-Thr-Arg-AMC = Boc-LSTR -AMC (Bachem I-1940)
- DMSO diméthyl sulfoxide (Sigma-Aldrich D5879)

Principe

La protéolyse ubiquitine ATP dépendante joue un rôle majeur dans la dégradation des protéines musculaires. La dégradation est assurée par un complexe protéolytique comprenant le protéasome 26S, lui-même constitué du protéasome 20S, le coeur de la machinerie protéolytique, et de 2 complexes de régulation 19S. Le protéasome présente 5 activités enzymatiques différentes dont trois principales : l'activité chymotrypsine-like (la principale), l'activité trypsine-like et l'activité caspase-like.

Pour mesurer l'activité trypsine-like, le peptide Boc-Leu-Ser-Thr-Arg-AMC est ici utilisé comme substrat fluorogénique. La reconnaissance du substrat par le site actif de l'enzyme détermine la coupure de la liaison entre l'AMC et le tétrapeptide. La fluorescence de la molécule d'AMC, qui est alors libérée, peut être suivie au fluorimètre à 460 nm. La spécificité de la réaction peut être vérifiée à l'aide d'un inhibiteur spécifique la leupeptine.

Solutions

- *solutions*

AMC	4 mM dans du DMSO
Boc-LSTR-AMC	2 mM dans du DMSO

Protocole

- *préparation du milieu réactionnel MR*

tris HCl	1,97 g
$MgCl_2$	508,25 mg
DTT	38,55 mg

Ajuster le pH à 8,0 et le volume final à 250 mL avec de l'eau.

- *étalonnage du fluorimètre*

$\lambda_{excitation}$ = 380 nm ; $\lambda_{émission}$ = 460 nm

Faire le point haut à 150 sur 200 pmoles d'AMC et le 0 sur le milieu réactionnel seul.

- *courbe étalon*

Faire une dilution de l'AMC à 4 mM au 1/400 pour avoir une solution finale d'AMC à 10 µM.

pmoles AMC	0	40	80	120	160	200
AMC 10 µM, µL	0	4	8	12	16	20
Milieu réactionnel, µL	1000	996	992	988	984	980

- *mode opératoire*

1. Mettre 960 µL de MR.
2. Ajouter 5 µL d'extrait.
3. Déclencher la réaction en ajoutant 35 µL de Boc-LSTR-AMC 2 mM.
4. Suivre la réaction pendant 60 minutes (lire toutes les 15 minutes).

CATHEPSINE (B + L)

Références

- CH_3COONa acétate de sodium (Sigma-Aldrich S2889)
- EDTA acide éthylène diamine tétracyclique (Sigma-Aldrich EDS)
- AMC 7-amino-4-méthyl-coumarin (Sigma-Aldrich A9891)
- Z-Phe-Arg-AMC (Bachem I-1160)
- DMSO diméthyl sulfoxide (Sigma-Aldrich D5879)

Principe

Le peptide fluorogénique Z-Phe-Arg-AMC est ici utilisé comme substrat pour les cathepsines. La reconnaissance du substrat par le site actif de l'enzyme détermine la coupure de la liaison entre l'AMC et le dipeptide. La fluorescence de la molécule d'AMC alors libérée peut être suivie au fluorimètre à 460 nm. La spécificité de la réaction peut être vérifiée à l'aide d'un inhibiteur, la molécule E-64.

Solutions

- *solutions*

AMC	4 mM dans du DMSO
Z-Phe-Arg-AMC	10 mM dans du DMSO

Protocole

- *préparation du milieu réactionnel MR*

acétate de sodium	100 mM
EDTA	1 mM

Ajuster le pH à 6,0.

- *étalonnage du fluorimètre*

$\lambda_{excitation}$ = 380 nm ; $\lambda_{émission}$ = 460 nm

Faire le point haut à 150 sur 100 pmoles d'AMC et le 0 sur le milieu réactionnel seul.

- *courbe étalon*

Faire une dilution de l'AMC à 4 mM au 1/400 pour avoir une solution finale d'AMC à 10 µM.

pmoles AMC	0	20	40	60	80	100
AMC 10 µM, µL	0	2	4	6	8	10
Milieu réactionnel, µL	1000	998	996	994	992	990

- *mode opératoire*

1. Mettre 970 µL de MR.
2. Ajouter 20 µL d'extrait.
3. Déclencher la réaction en ajoutant 10 µL de Z-Phe-Arg-AMC 10 mM.
4. Suivre la réaction pendant 15 minutes.

EXTRACTION MUSCULAIRE POUR DOSAGES DE METABOLITES

Références

- $HClO_4$ acide perchlorique (Sigma-Aldrich 244252)
- KOH potassium hydroxyde (Prolabo 26 668.263)
- KCl potassium chlorure (Prolabo 26 764.298)
- TEA triéthanolamine (Sigma-Aldrich T1377)

Principe

L'extraction se réalise en deux étapes. Une extraction acide est réalisée au moyen d'acide perchlorique et est suivie d'une neutralisation.

Solutions

- *solutions*

$HClO_4$ 0,65 M

soit 56 mL de $HClO_4$ à 70 % (soit à peu près 11,6 N) dans 944 mL d'eau.

- *solution pour la neutralisation*

KOH 2N dans 0,4 M de TEA et 0,4 M de KCl

soit 5,61 g de KOH + 1,50 g KCl + 3 g TEA dans 50 mL d'eau.

On mesure la quantité de KOH 2N nécessaire pour neutraliser 1 mL d'acide perchlorique 0,65 M et obtenir un pH entre 7,2 et 7,4 (environ 330 µL de KOH).

Protocole

1. Mettre 4 mg de tissu sec (ou à peu près 16 mg de tissu frais) dans 1 mL de $HClO_4$ 0,65 M refroidi à 4°C.
2. Laisser agir 15 minutes à 4°C.
3. Centrifuger pendant 10 minutes à 4°C à 5000 g.
4. Prélever ensuite une quantité déterminée du surnageant acide.
5. Réaliser la neutralisation :

- pour 1 mL de surnageant acide, ajouter la quantité nécessaire de KOH 2 N.
- centrifuger pendant 10 minutes à 4°C à 10000 g.
- obtention d'un surnageant neutralisé.

PHOSPHOCREATINE – ATP - GLUCOSE-6-PHOSPHATE

Références

- Tris HCl tris hydrochloride (Sigma-Aldrich T3253)
- $MgCl_2$ magnésium chlorure (Prolabo 25 108.295)
- DTT dithiothreitol (Sigma-Aldrich D9163)
- NADP nicotinamide adénine dinucléotide phosphate (Roche 128 058)
- BSA bovine serum albumine (PAA K41-001)
- Glucose (Prolabo 24 370.294)
- ADP adénosine diphosphate (Roche 127 507)
- $NADH,H^+$ nicotinamide adénine dinucléotide (Roche 107 735)
- P^1P^5diadénosine pentaphosphate (Sigma-Aldrich D4022)
- KOH potassium hydroxyde (Prolabo 26 668.263)
- KCl potassium chlorure (Prolabo 26 764.298)
- TEA triéthanolamine (Sigma-Aldrich T1377)
- $HClO_4$ acide perchlorique (Sigma-Aldrich 244252)
- G6PDH glucose-6-phosphate-déshydrogénase (Roche 127 655)
- HK hexokinase (Roche 426 362)
- CK créatine kinase (Roche 127 566)
- ATP adénosine triphosphate (Sigma-Aldrich A8937)
- PCr créatine phosphate (Roche 621 714)
- G6P glucose-6-phosphate (Roche 127 027)

Principe

$$\text{PCr} + \text{ADP} \xrightarrow{\text{CK}} \text{Créatine} + \text{ATP}$$

$$\text{ATP} + \text{Glucose} \xrightarrow{\text{HK}} \text{G6P} + \text{ADP}$$

$$\text{G6P} + H_2O + NADP^+ \xrightarrow{\text{G6PDH}} \text{6PGluconolactone} + NADPH,H^+$$

Solutions

- *solutions*

tris HCl	1 M	pH = 8,0
$MgCl_2$	400 mM	
DTT	400 mM	
NADP	100 mM	
BSA	10 %	
glucose	100 mM	
ADP	10 mM	
$NADH,H^+$	1 mM	
P^1P^5	100 mM	
G6PDH	1750 U/mL	
HK	1500 U/mL	
CK	1400 U/mL	

- *solution pour la neutralisation*

KOH 2N : 5,61 g de KOH + 1,50 g KCl + 3 g TEA dans 50 mL d'eau.

- *solution N*

Trouver la quantité adéquate de KOH 2N pour neutraliser la solution $HCLO_4$ 0,65 M. (voir extractions pour les métabolites). Centrifuger à 10000 g pendant 10 secondes. Prélever le surnageant.

Protocole

- *préparation des solutions étalons*

Solution mère :
Peser dans 20 mL d'eau :

- 13,6 mg PCr soit 2,08 mM
- 6,2 mg ATP soit 512 µM

- 1,6 mg G6P soit 263 µM

- *courbe étalon*

Attention : les concentrations des différents étalons diffèrent suivant les pesées et la quantité de KOH 2N nécessaire à la neutralisation de $HClO_4$.

$$= \frac{\text{Molarité de l'étalon * volume de la solution mère à diluer}}{\text{Vol. total (1mL } HClO_4 \text{ + vol. KOH 2N + vol. de la solution mère à diluer)}} * 30\ \mu L$$

Solution mère, µL	50	100	150	200
$HClO_4$ 0,65M, µL	1000 15 secondes d'incubation à 4°C			
KOH 2N, µL	330 10 secondes de centrifugation à 4°C à 10000 g			
PCr nmoles/30µL	2,26	4,36	6,32	8,16
ATP nmoles/30µL	0,56	1,07	1,56	2,01
G6P nmoles/30µL	0,29	0,55	0,8	1,03

- *préparation du milieu réactionnel MR*

tris HCl 1M pH = 8,0	2,5 mL
$MgCl_2$ 400 mM	250 µL
DTT 400 mM	100 µL
NADP 100 mM	32 µL
BSA 10 %	200 µL
P^1P^5 100 mM	10 µL

Ajuster le volume final à 100 mL avec de l'eau.

- *étalonnage du fluorimètre*

$\lambda_{excitation}$ = 340 nm ; $\lambda_{émission}$ = 450 nm

Faire le point haut à 150 sur 1 mL MR + 15 nmoles de $NADH,H^+$ (soit 15 µL d'une solution mère de 1 mM) et le 0 sur MR seul.

- *mode opératoire*

	Blanc	Etalon	Essai
MR, µL	1000 30 µL solution N	30 µL étalon	30µL d'extrait
T° ambiante	Lecture 1		
G6PDH, µL	10		
3 minutes à T° ambiante	Lecture 2		
Glucose, µL HK, µL	10 10		
8 minutes à T° ambiante	Lecture 3		
ADP, µL CK, µL	10 10		
30 minutes à T° ambiante	Lecture 4		

- *résultats*

L2 - L1 correspond à la consommation de G6P
L3 - L2 correspond à la consommation d'ATP
L4 - L3 correspond à la consommation de PCr

GLYCOGENE

Références

- Tris HCl tris hydrochloride (Sigma-Aldrich T3253)
- $MgCl_2$ magnésium chlorure (Prolabo 25 108.295)
- DTT dithiothreitol (Sigma-Aldrich D9163)
- BSA bovine serum albumine (PAA K41-001)
- NADP nicotinamide adénine dinucléotide phosphate (Roche 107 058)
- ATP adénosine triphosphate (Roche 519 979)
- G6PDH glucose-6-phosphate-déshydrogénase (Roche 127 655)
- HK hexokinase (Roche 426 362)
- NaOH sodium hydroxyde (Prolabo 28 244.295)
- Glycogène (Sigma-Aldrich G0885)
- Glucose (Prolabo 24 370.294)
- HCl acide chlorhydrique (Riedel de Haën 07115)

Principe

$$\text{Glycogène} \xrightarrow{\text{hydrolyse acide}} \text{n-D-Glucose}$$

$$\text{D-Glucose + ATP} \xrightarrow{\text{HK}} \text{D-Glucose-6-P + ADP}$$

$$\text{Glucose-6-P + NADP} \xrightarrow{\text{G6PDH}} \text{6-P-gluconolactone + NADPH,H}^+$$

Solutions

- solutions

tris HCl	1 M	pH = 8,0
BSA	10 %	
NADP	100 mM	
DTT	10 %	
ATP	0,5 M	
$MgCl_2$	100 mM	
G6PDH	1750 U/mL	
HK	100 U/mL	
NaOH	1N	
glucose	13 mM	

Protocole

- préparation de la solution étalon de glycogène à 0,25 %

Hydrolyse : 80 µL solution de glycogène à 0,25 % + 2 mL HCl 1N.
Laisser agir 2 heures à 100°C.

- hydrolyse des extraits musculaires

Dans un tube en verre à bouchon vissé : mettre 1 mg de tissu sec ou le culot de centrifugation des métabolites + 1 mL HCl 1N.
Laisser agir 2 heures à 100°C.

- préparation du milieu réactionnel MR

tris HCl 1 M pH = 8,0	5 mL
BSA 10 %	200 µL
NADP 100 mM	200 µL
DTT 10 %	50 µl
ATP 0,5 M	100 µL
$MgCl_2$ 400 mM	250 µL
G6PDH 17500 U/mL	20 µL

Ajuster le volume final à 100 mL avec de l'eau.

- *étalonnage du fluorimètre*

$\lambda_{excitation}$ = 340 nm ; $\lambda_{émission}$ = 450 nm

Faire le point haut à 150 sur 50 nmoles de glucose et le 0 sur le milieu sans glucose.

- *courbe étalon*

Réaliser une dilution du glucose à 13 mM de façon à avoir une solution à 0,5 mM (80 µL de solution à 13 mM + 2 mL HCl 1 N ou d'eau).

nmoles glucose	0	10	20	30	40	50
Milieu réactionnel, µL	1000					
Glucose 0,5 mM, µL	0	20	40	60	80	100
NaOH 1N, µL	0	20	40	60	80	100
ΔH_2O, µL	200	160	120	80	40	0
HK 100 U/mL, µL	10					

Incuber 20 minutes à température ambiante.

- *mode opératoire*

1. Mettre 1000 µL de MR.
2. Ajouter 20 µL de NaOH 1N.
3. Ajouter 20 µL d'extrait hydrolysé.
4. Incuber 10 minutes à température ambiante.
5. Faire la lecture L1 correspondant à la quantité de glucose-6-phosphate endogène.
6. Ajouter 10 µL d'HK à 100 U/mL.
7. Incuber 20 minutes à température ambiante.
8. Réaliser la lecture L2.

- *résultats*

L2-L1 correspond à la quantité de glycogène

PYRUVATE MUSCULAIRE

Références

- Pyruvate (Sigma-Aldrich P2256)
- Tris trizma base (Sigma-Aldrich T1503)
- Tris HCl tris hydrochloride (Sigma-Aldrich T3253)
- LDH lactate déshydrogenase (Roche 127 230)
- NADH,H^+ nicotinamide adénine dinucléotide (Roche 107 735)

Principe

$$\text{Pyruvate} + \text{NADH,H}^+ \xrightarrow{\text{LDH}} \text{Lactate} + \text{NAD}^+$$

Solutions

-solutions

tris	1 M	pH = 8,0
pyruvate1,	25 mM	
NADH,H^+	10 mM	
LDH	110 U/mL	

- utilisation des échantillons extraits en solution acide puis neutralisés

Protocole

- préparation du milieu réactionnel MR

tris 1 M pH = 8,0	5 mL
NADH 10 mM	10 µL

Ajuster le volume final à 100 mL avec de l'eau.

- étalonnage du fluorimètre

$\lambda_{excitation}$ = 340 nm ; $\lambda_{émission}$ = 450 nm

Faire le point haut à 150 sur 2 nmoles de NADH,H^+ et le 0 sur de l'eau.

- courbe étalon

Faire une dilution au 1/250 du pyruvate pour obtenir une solution à 5 µM.

nmoles pyruvate	0	0,1	0,25	0,4	0,5
Milieu réactionnel, µL	1000				
5 minutes à T° ambiante	Lecture L1				
Pyruvate 5 µM, µL	0	20	50	80	100
LDH 110 U/mL, µL	10				
10 minutes à T° ambiante	Lecture L2				

- mode opératoire

1. Mettre 1000 µL de MR.
2. Incuber 5 minutes à température ambiante et faire la lecture L1.
3. Ajouter 100 µL d'extrait.
4. Ajouter 10 µL de LDH 110 U/mL.
5. Incuber 10 minutes à température ambiante et faire la lecture L2.

- résultats

L2 – L1 correspond à la quantité de pyruvate musculaire

RESULTATS

MANUSCRIT 1

Sirtuin 1 regulates SREBP-1c and hexokinase II gene expression in skeletal muscle

Sirtuine 1 (SIRT1) est une protéine histone déacétylase dépendante du NAD^+ qui exerce un rôle métabolique important en limitant l'accumulation de graisses et en augmentant la sensibilité à l'insuline chez des souris soumises à un régime gras. De récentes études indiquent que ces effets métaboliques sont en partie médiés par l'induction d'un programme de transcription de l'oxydation des acides gras, mais la possibilité que SIRT1 puisse également participer au contrôle du métabolisme du glucose dans le muscle strié squelettique n'a jamais été étudié. Nous montrons, ici, que des souris déficientes pour le gène SIRT1 présentaient une altération significative de la glycolyse, se traduisant par une augmentation du contenu intramusculaire en glycogène, glucose-6-phosphate et pyruvate et une diminution marquée de l'expression de l'hexokinase II. L'expression de SREBP-1c, un puissant activateur de l'expression génique de l'hexokinase, et l'expression de LXR-β, un puissant activateur de l'expression génique de SREBP-1c, étaient significativement diminuées chez les souris déficientes pour le gène SIRT1. Les expériences d'électrotransfert de gènes ont montré que SIRT1 régulait le promoteur de SREBP-1c de façon LXR-dépendante. Enfin, l'inhibition de SIRT1 par l'EX527 permettait de réduire la consommation de glucose de myotubes C2C12 de façon dose dépendante. Nos données montrent que SIRT1 régule l'expression de SREBP-1c de façon LXR-dépendante, ce mécanisme pouvant contribuer à la régulation de l'expression de l'hexokinase II. Cette voie pourrait contribuer à la régulation du métabolisme du glucose dans le muscle strié squelettique.

Sirtuin 1 regulates SREBP-1c and hexokinase II gene expression in skeletal muscle

Defour Aurélia[1], Lefai Etienne[2], Poyot Thomas[3], Castro Perez Andréa[1], Castells Josiane[1], Durand Christine[2], Euthine Vanessa[2], Béchet Daniel[4], Gu Yansong[5], Peinnequin André[3], Freyssenet Damien[1]

[1]Université de Lyon, Université Jean Monnet, Laboratoire de Physiologie de l'Exercice EA 4338, Saint Etienne, France
[2]Université de Lyon, Université Claude Bernard Lyon 1, INSERM U870, Régulations Métaboliques Nutrition et Diabètes, Oullins, France
[3]Pôle de Génomique, Institut de Recherche Biomédicale des Armées, Centre de Recherche du Service de Santé des Armées, La Tronche, France
[4]INRA UMR 1019, Unité Nutrition Humaine, St Genès Champanelle, France
[5]Obenomics, Inc., Bellevue, WA, USA

Corresponding author: Damien Freyssenet
Laboratoire de Physiologie de l'Exercice
Faculté de Médecine, 15 rue Ambroise Paré
42023 Saint-Etienne Cedex 2, France
Tel: 033 4 77 42 14 77
Fax: 033 4 77 42 14 78
E-mail: damien.freyssenet@univ-st-etienne.fr

Short running title: SIRT1, hexokinase and SREBP-1c in skeletal muscle

Sirtuin 1 (SIRT1) is a NAD^+-dependent protein deacetylase that exerts a prominent metabolic function by limiting fat accumulation and increasing insulin sensitivity of mice fed with a high-fat diet. Current studies indicate that these metabolic effects are partly mediated by the induction of a metabolic transcription program of mitochondrial fatty acid oxidation, but the possibility that SIRT1 can also directly participate to the control of glucose metabolism in skeletal muscle has never been investigated. Here, we show that SIRT1 gene deficiency significantly altered skeletal muscle glycolysis in mice, as evidenced by an increased intramuscular content of glycogen, glucose-6-phosphate and pyruvate, together with a marked decrease in hexokinase II expression. Expression of SREBP-1c, a strong activator of hexokinase II gene expression, and LXR-ß, a strong activator of SREBP-1c gene expression, were both significantly decreased in response to SIRT1 gene deficiency. Gene electrotransfer experiments further showed that SIRT1 regulated SREBP-1c promoter in a LXR-dependent manner. Finally, SIRT1 inhibition by EX527 was sufficient to dose-dependently decrease glucose consumption of C2C12 myotubes. Our data support the mechanism by which SIRT1 regulates hexokinase II expression in skeletal muscle by modulating SREBP-1c promoter transactivation in a LXR-dependent manner. This mechanism probably contributes to the regulation of glucose metabolism by skeletal muscle.

INTRODUCTION

Mammalian Sirtuin 1 (SIRT1) is a member of the sirtuin family of nicotinamide adenine dinucleotide (NAD^+)-dependent protein deacetylases of class III (1). SIRT1, the mammalian ortholog of the yeast Sir2 (2), has a wide range of substrates and cellular functions. SIRT1 can induce chromatin silencing by deacetylating histones (3), as well as by regulating histone and DNA methylation (4; 5). SIRT1 can also modulate the activity of transcription factors, such as p53 (6; 7), NF-κB (8), forkhead box O (FoxO) family of transcription factors (9-11), and peroxisome proliferator-activated receptor γ (PPAR-γ) (12), as well as transcriptional coregulators such as p300 (13) and PPAR-γ coactivator 1-α (PGC-1α) (14). Altogether, these data involves SIRT1 in a broad range of biological processes, such as inflammation, cell survival, cell proliferation, and cell metabolism.

The deacetylase activity of SIRT1 is controlled by the NAD^+/NADH ratio (15). SIRT1 is therefore considered to act as a sensor of the metabolic status of the cell that can mediate adaptative changes in gene expression to regulate energy metabolism (16). SIRT1 has thus been reported to deacetylate and activate PGC-1α to increase the transcription of gluconeogenic genes, such as phosphoenolpyruvate carboxykinase and glucose-6-phosphatase in liver (14). SIRT1 also deacetylates and activates FoxO1 to induce gluconeogenesis and glucose release from hepatocytes (9). Moreover, knockdown of SIRT1 in liver abrogates the fasting-induced expression of gluconeogenic genes, whereas SIRT1 overexpression has the opposite effects (17). In skeletal muscle, SIRT1 also deacetylates and activates PGC-1α to induce a metabolic transcription program of mitochondrial fatty oxidation (18). Furthermore, treatment of mice submitted to a high-fat diet with non-specific SIRT1 activators (resveratrol, SRT1720) increases PGC-1α deacetylation and transcription of genes encoding mitochondrial proteins (19).

SIRT1 also contributes to the regulation of glucose homeostasis. Mice fed with a high-fat diet that either received resveratrol or SRT1720 are resistant to the development of obesity and insulin resistance. They also display improved response to intraperitoneal glucose tolerance test (19; 20). Similarly, SIRT1 gain of function has been shown to improve glucose tolerance in mice (21). The ability of SIRT1 to regulate whole body glucose homeostasis can be partly explained by the previously described stimulatory effect of SIRT1 on fatty acid oxidation in skeletal muscle (18) and insulin secretion by pancreatic ß cells (22; 23), but the possibility that SIRT1 can also regulate glucose metabolism in skeletal muscle must be considered. Indeed, skeletal muscle represents 40% of total body weight and plays a crucial role in the regulation of glucose metabolism (24). Therefore, any adaptative changes triggered by SIRT1 that can improve glucose metabolism in skeletal muscle may contribute to whole body regulation of glucose homeostasis by SIRT1. Currently, however, there is no direct evidence that SIRT1 participates to the control of glucose metabolism in skeletal muscle.

Because SIRT1 interacts with and deacetylates target proteins to regulate gene expression, we hypothesized that SIRT1 could participate to the regulation of glucose metabolism in skeletal muscle by modulating the expression of critical glucose-related genes. We report that SIRT1 gene deficiency led to an altered glycolysis and a strong decrease in hexokinase II expression in mouse skeletal muscle. Expression of SREBP-1c, a transcriptional activator of hexokinase II gene expression, and LXR-ß was also decreased. We further showed that SIRT1 regulated SREBP-1c promoter in a LXR-dependent manner. Finally, inhibition of SIRT1 by EX527 decreased glucose consumption in a dose dependent manner. The control of SREBP1c gene expression by SIRT1 may be an important element in the regulatory mechanisms that links SIRT1 to the control of glucose metabolism.

RESEARCH DESIGN AND METHODS

Animals. SIRT1$^{\Delta ex4/\Delta ex4}$ mice (16.43 ± 1.80 months; n = 4) and SIRT1$^{+/\Delta ex4}$ mice (14.80 ± 2.00 months; n = 4) were previously described (25). SIRT1$^{\Delta ex4/\Delta ex4}$ mice lack exon 4, which encodes 51 amino acids of the conserved SIRT1 catalytic domain (25). SIRT1$^{\Delta ex4/\Delta ex4}$ mice thus expressed a SIRT1 mutant inactive protein and are phenotypically identical to SIRT1 null mice (25). SIRT1$^{+/\Delta ex4}$ mice were used as controls (25; 26). Morphological characteristics of SIRT1$^{\Delta ex4/\Delta ex4}$ and SIRT1$^{+/\Delta ex4}$ mice are reported in Table 1. Mice were housed in a special-pathogen free facility. All procedures were approved by the University of Washington Animal Care and Use Committee.

Eight week-old male OFI mice (32.9 ± 1.2 g; n = 24) were used for gene electrotransfer experiments. Mice were maintained in the Animalerie Centrale de la Faculté de Médecine (Université Jean Monnet, Saint-Etienne) under a constant 12:12h light-dark cycle with food and water *ad libitum*. The study was approved by the Comité d'Ethique Animale de la Plate-Forme d'Expérimentation Animale de la Faculté de Médecine (Université Jean Monnet, Saint-Etienne).

Determination of intramuscular content of glycogen, glucose-6-phosphate and pyruvate. Samples of freeze clamped *gastrocnemius* muscles were homogenized in 0.65 M perchloric acid (1:30 dilution wt/vol) and incubated for 15 min at 4°C. Muscle homogenates were centrifuged at 5,000 g for 10 min at 4°C. Resulting pellets resuspended with 1 N HCl and neutralized by 2 N KOH were used for the fluorometric measurement of glycogen content by coupled enzyme assays (27). Acid supernatants were neutralized with 2 N KOH in 0.4 M TEA/KCl and used for the fluorometric determination of pyruvate and glucose-6-phosphate contents by coupled enzyme assays (27).

mRNA isolation and reverse transcription reaction. *Gastrocnemius* and *tibialis anterior* muscle samples from Sirt1$^{\Delta ex4/\Delta ex4}$ and Sirt1$^{+/\Delta ex4}$ mice were conditioned in RNALater

(Qiagen). The samples were homogenized with a Mixer Mill MM300 (Eppendorf) in 300 µL Trizol (Invitrogen) following the manufacturer's instructions [30 Hz, 2 min; 2 tungsten 2 mm carbide beads (Qiagen)]. A double chloroform extraction (400 µl followed by 15 min centrifugation, then 150 µl chloroform followed by 5 min centrifugation) was performed to obtain a clean aqueous phase. The extraction of mRNA was carried out on the Qiacube automate by loading the whole aqueous phase (Rneasy protocol). A 50 µl final volume of mRNA was eluted for each sample. RT was immediately performed using the Reverse Transcription Core Kit (Eurogentec). The reaction was carried out from 200 ng of mRNA with 50 µM Oligo d(T) primer, 2 IU Rnase inhibitor and 6.25 U reverse transcriptase according to the manufacturer's instructions. The cDNA was stored at −80°C until used.

Primer design. The primer design and its optimization regarding the primer dimer, the self-priming formation and the primer melting temperature were done with MacVector software (Accelrys). The specificities of the PCR amplification were documented with the LightCycler melting curve analysis as previously described (28). The melting peaks obtained from the RT-product and the specific recombinant DNA were identical. The oligonucleotide primers were synthesized by Eurogentec. The selected forward (FW) and reverse (RW) primer sequences are listed in Table 2.

Real time quantitative PCR. The PCR was carried out with the Light Cycler Fast Start DNA Master SYBR Green kit (Roche Applied Science) in a 20 µl final volume, 4 mM $MgCl_2$ and optimized concentration of each primer (final concentration). Quantitative PCR was performed using LightCycler (Roche Applied Science) for 50 cycles of 95°C for 20 s (denaturation), 54–60°C for 5 s (annealing temperatures are presented in Table 2) and a final step of 8 s at 72°C (elongation). The amplification specificity was checked using the melting curve, following the manufacturer's instructions. The Cycle of quantification (C_q) values were calculated from the Light Cycler Software v.3.5 (Roche Applied Science) using the second

derivative maximum method. The quantification was achieved using a pool of cDNA samples as calibrator (28), according to the comparative threshold cycle method (29) improved for multiple reference genes use (30). The normalization was performed by geometric averaging of three internal control genes [cyclophylin A (CycA), hypoxanthine guanine phosphorybosyl transferase (HPRT) and acidic ribosomal phosphoprotein (ARBP)] after validation using geNorm software (31).

Protein extraction. Proteins were extracted from *gastrocnemius* and *tibialis anterior* muscles as described previously (32). Protein concentration was spectrophotometrically determined at 750 nm (BioRad).

Enzyme assays. Hexokinase, lactate dehydrogenase, 3-hydroxy-acyl-Coenzyme A dehydrogenase and citrate synthase enzyme activities were fluorometrically determined as previously described (33; 34).

Immunoblot analysis. Protein concentration was spectrophotometrically determined at 750 nm (BioRad). Muscle samples were homogenized (1:20 dilution, wt/vol) at 4°C [50 mM Tris-HCl (pH = 7.4), 100 mM NaCl, 2 mM EDTA, 2 mM EGTA, 50 mM ß-glycerophosphate, 50 mM sodium fluoride, 1 mM $NaVO_4$, 120 nM okadaic acid, 1% Triton X-100]. Homogenates were centrifuged at 12,000 g for 20 min at 4°C. Proteins (20 to 50 µg) were subjected to SDS-PAGE and transferred to nitrocellulose membranes. Gel loading was systematically checked by Coomassie and Ponceau staining (data not shown). Blots were incubated overnight at 4°C with antibodies against 20D6 (1:40,000 dilution wt/vol), Core2 (1:20,000 dilution wt/vol), 13.4 (1:4,000 dilution wt/vol), SIRT1 (1:1,000 dilution wt/vol, Upstate 05707) and nuclear SREBP-1c (1:400 dilution wt/vol, Santa Cruz Biotechnology sc-8984). Corresponding horseradish peroxidase-conjugated rabbit anti-mouse (1:3,000 dilution wt/vol, Dako) and goat anti-rabbit (1:3,000 dilution wt/vol, Dako) antibodies were used for chemiluminescent detection of proteins (ECL, GE Health Care). The films were scanned and quantified using

N.I.H. image 1.63.

Plasmids. pBabe-SIRT1, the full length murine SIRT1 cDNA into pBabepuro expression vector, was a gift from Dr J Luo (Institute of Cancer Genetics and Department of Pathology College of Physicians & Surgeons, Columbia University, New York, USA) (7). pCMV-LXR-α (Source BioScience/Geneservice, Cambridge, UK) is the full length murine LXR-α cDNA into a pCMV-Sport vector. Human SREBP-1c promoter (-571/+90 bp) reporter gene (pSREBP-1c-Luc) and human SREBP-1c promoter (-571/+90 bp) reporter gene with two deleted mutations in LXR-response elements located at -311/-296 bp and -260/-245 bp (pSREBP-1c-Luc m1/2) were previously described (35) (Fig. 5*A*). pCMV-ß-galactosidase was from Clontech. pcDNA3.1-Zeo (Clontech) is a null empty vector used to maintain constant the amount of DNA injected.

In vivo gene electrotransfer. Mice were anesthetized (*i.p.* injection of 90 mg/kg ketamine and 10 mg/kg xylazine) and *tibialis anterior* muscles were injected with 125 µl of DNA mixtures in 0.9 % NaCl endotoxin free containing : *i)* 30 µg of pSREBP-1c-Luc, 30 µg of pCMV-ß-galactosidase, and 20 µg of pcDNA3.1-Zeo (n = 8), *ii)* 30 µg of SREBP-1c-Luc, 20 µg of pBabe-SIRT1 and 30 µg of pCMV-ß-galactosidase (n = 8), and *iii)* 30 µg of pSREBP-1c-Luc, 20 µg of pCMV-LXR-α and 30 µg of pCMV-ß-galactosidase (n = 8). Corresponding contralateral muscles were injected with the same DNA mixture except that pSREBP-1c-Luc was omitted and replaced by 30 µg of pSREBP-1c-Luc m1/2. Thirty seconds after injection, 6 pulses (20 ms, 50 mA) were delivered by using GET42 electroporator as previously described (36; 37). Seven days after gene electrotransfer, animals were anesthetized and the *tibialis anterior* muscles were removed, weighted, and stored at –80°C.

Firefly luciferase and ß-galactosidase assays. Proteins isolation and measurement of firefly luciferase activity were performed as described previously (36). Protein concentration was spectrophotometrically determined at 750 nm (BioRad). To correct for interindividual

variations in transfection efficiency, luciferase activity was normalized to β-galactosidase activity (36).

Cell culture and glucose assay. C2C12 muscle cells (ATCC CRL-1772) were cultured in Dulbecco's modified Eagle's medium (DMEM) supplemented with 20% fetal bovine serum and 1% penicillin-streptomycin (P/S) at 37°C and 5% CO_2 in air in 6-well plates. At 80% confluence, cells were allowed to differentiate in DMEM supplemented with 2% horse serum and 1% penicillin-streptomycin. Glucose concentration in the culture medium was determined over 48 hours from day 5 of differentiation by using an electrochemical analyser YSI 2300 STAT PLUS (Yellow Springs Instruments, Ohio, USA) (38). Calibration was done by using a 5 mM standard glucose solution.

Statistics. Data are means ± SE. Statistical comparisons were performed using unpaired t-test, two-way and one-way analysis of variance when appropriate (StatView^{TM}SE+^{Graphics}, Abacus Concept, Inc). The 0.05 level of confidence was accepted for statistical significance.

RESULTS

Loss of SIRT1 leads to an intramuscular accumulation of glycogen, glucose-6-phosphate and pyruvate. Glycogen content was moderately but significantly increased by about 25% in the *gastrocnemius* muscle of SIRT1$^{\Delta ex4/\Delta ex4}$ mice (Fig. 1*A*). We next assessed whether increased glycogen content could result from diminished glycolytic capacity. In agreement with this hypothesis, glucose-6-phosphate and pyruvate accumulated in the *gastrocnemius* muscles of SIRT1$^{\Delta ex4/\Delta ex4}$ ($P < 0.05$) (Fig. 1*B* and *C*). Furthermore, hexokinase II mRNA level, hexokinase activity and lactate dehydrogenase activity were all significantly reduced by about 50% in the *gastrocnemius* muscles of SIRT1$^{\Delta ex4/\Delta ex4}$ mice (Fig. 2), whereas skeletal muscle oxidative capacity remained unchanged (Fig. 3).

Expression of SREBP-1c and LXR-ß is down-regulated in the *gastrocnemius* muscle of SIRT1$^{\Delta ex4/\Delta ex4}$ mice. The marked decrease in hexokinase II mRNA and hexokinase activity prompted us to determine whether SIRT1 could regulate hexokinase expression. SREBP-1c is a transcription factor that has been shown to strongly regulate hexokinase II gene expression in muscle cells (39; 40). We show here that both SREBP-1c mRNA level and nuclear SREBP-1c protein level were significantly decreased in the *gastrocnemius* muscle of SIRT1$^{\Delta ex4/\Delta ex4}$ mice (Fig. 4*A*). Similar results were also observed in the *tibialis anterior* muscle (data not shown). There are two functional LXR-response elements in SREBP-1c promoter that have been described to strongly activate SREBP-1c gene expression in muscle cells (35). In the present study, mRNA level of LXR-β was significantly reduced by about 25% in the *gastrocnemius* muscle of SIRT1$^{\Delta ex4/\Delta ex4}$ mice, whereas LXR-α mRNA level remained unchanged (Fig. 4*B*).

SIRT1 regulates SREBP-1c expression in a LXR-dependent manner. Next, we determined whether SIRT1 regulates SREBP-1c gene expression in a LXR-dependent manner. Mouse *tibialis anterior* muscle was electrotransfected with a SIRT1 expression

vector together with a SREBP-1c reporter gene construct that exhibits or not deleted mutations of two LXR-response elements located at -311/-296 bp and -260/-245 bp (35) (Fig. 5*A*). Gene electrotransfer of a SIRT1 expression vector in mouse *tibialis anterior* muscle effectively led to an increase in SIRT1 protein level (Fig. 5*B*). As a positive control of SREBP-1c promoter transactivation, we co-electrotransfected a LXR-α expression vector. As expected, this strongly transactivated SREBP-1c promoter (Fig. 5*C*), whereas SREBP-1c promoter transactivation was completely abolished when the two LXR-response elements were deleted, illustrating the functionality and dependency of SREBP-1c promoter transactivation towards LXR transcription factors. Importantly, SIRT1 overexpression increased SREBP-1c promoter transactivation by about 2-fold ($P < 0.05$) (Fig. 5*C*). By contrast, mutations of the two LXR-response elements completely abolished SREBP-1c promoter transactivation by SIRT1 ($P < 0.001$), demonstrating that functional LXR-response elements are involved in the stimulatory effect of SIRT1 on SREBP-1c promoter transactivation in mouse skeletal muscle.

SIRT1 inhibition lowers glucose consumption in C2C12 myotubes. To functionally assess the relevance of SIRT1 on glucose metabolism, we next determined whether modulating SIRT1 activity would effect glucose consumption. SIRT1 enzymatic activity was inhibited in C2C12 myotubes by EX527. EX527 is a small, selective inhibitor of SIRT1 that does not inhibit histone deacetylases and is specific for Sirt1 over other sirtuin family members (20; 41-43). Exposure of C2C12 myotubes for 48 hours led to a dose-dependent decrease in glucose consumption (Fig. 6). At the highest concentration (2 µM), EX527 decreased glucose consumption by about 20% ($P < 0.001$). Similar results were obtained following 24 hours of exposure (data not shown).

DISCUSSION

SIRT1 gene deficiency led to an accumulation of glycogen, glucose-6-phosphate, and pyruvate in *gastrocnemius* muscle, strongly suggesting an impairment in glycolysis. This is further supported by the observation that hexokinase and lactate dehydrogenase activity were decreased, whereas mitochondrial oxidative potential remained unchanged. This latter observation may be surprising since SIRT1 has been shown to promote PGC-1α deacetylation and the expression of selected mitochondrial genes (18; 19; 44). However, other studies have shown that SIRT1 and PGC-1α are independently regulated and that variations in SIRT1 expression are not correlated with variations in mitochondrial content in skeletal muscle (45; 46). To reconcile these data, possibilities would be that SIRT1 expression is more closely related to the rate of mitochondrial biogenesis rather than the steady-state content of mitochondria (45) and/or that SIRT1 stimulates mitochondrial biogenesis only under conditions where skeletal muscle is metabolically challenged (19; 44). Finally, it also possible that the expression of mitochondrial genes is already altered in skeletal muscle of $SIRT1^{-/\Delta ex4}$ mice, which were used as control mice in the present study (see below).

Previous data indicate that hexokinase II expression is strongly activated by SREBP-1c (39; 40) and that SREBP-1c gene expression is regulated by LXR (35) in muscle cells. In the present study, the down-regulation of hexokinase II, SREBP-1c and LXR-β expression in $SIRT1^{\Delta ex4/\Delta ex4}$ mice, together with our observation that SIRT1 regulates SREBP-1c promoter in a LXR-dependent manner, support the mechanism whereby SIRT1 regulates hexokinase II expression in skeletal muscle in a SREBP-1c/LXR-dependent manner. The way by which SIRT1 could regulate LXR transcriptional activity has not been explored in the present study. However, a previous report by Li *et al.* in HEK 293 cells (47) showed that SIRT1 interacted with LXR and promoted its deacetylation and subsequent ubiquitination. Furthermore, they also showed that loss of SIRT1 reduced expression of a variety of LXR target genes *in vivo*.

They propose that LXR deacetylation by SIRT1 would be necessary to facilitate its degradation, thus allowing the recruitment of new LXR at transcriptional active sites of target genes, ultimately leading to an increase in transcriptional activity (47). Whether such a mechanism is functional in skeletal muscle needs to be determined.

The two LXR subtypes, LXR-α and -β, probably do not play identical roles, as judged by the phenotype of LXR knockout mice. LXR-α knockout mice massively accumulate cholesterol on cholesterol feeding (48), increase their fat content, but remain insulin sensitive in response to a high-fat diet (49). By contrast, absence of LXR-β induces protection against high fat diet-induced obesity, but induces insulin resistance (49), suggesting that LXR-β would be a regulator of glucose homeostasis. In agreement with this observation, of the two isoforms, only the expression of LXR-β was significantly reduced in the *gastrocnemius* muscle of $SIRT1^{\Delta ex4/\Delta ex4}$ mice, suggesting that LXR-β could be involved in the regulation of SREBP-1c promoter transactivation.

SIRT1 has been well described to deacetylate and activate PGC-1α (18; 19; 44; 50). One may therefore reasonably ask whether SIRT1-dependent deacetylation of PGC-1α could also contribute to the regulation of SREBP-1c gene expression in skeletal muscle. However, current studies suggest that PGC-1β, rather than PGC-1α, could be a target of SIRT1 to regulate SREBP-1c gene expression. Indeed, previous reports indicate that PGC-1β coactivates SREBP transcription factor family in liver (51). Furthermore, it has also been reported that SIRT1 mRNA expression was significantly correlated with PGC-1β expression (52). Altogether, these data suggest that SIRT1 could also regulate SREBP-1c gene expression by modulating PGC-1β activity.

Our observations that SIRT1 inhibition significantly lowers glucose consumption of C2C12 myotubes clearly illustrate the functional relevance of SIRT1 in the regulation of glucose metabolism. We propose that the regulation of hexokinase II expression by SIRT1

may contribute to this effect. Of course, we cannot exclude the possibility that the regulatory influence of SIRT1 may be also exerted on the expression of glucose transporter and other glycolytic enzymes, as we showed for lactate dehydrogenase. One should also note that EX527 reduces glucose consumption by about 20%, clearly indicating that the regulation of glucose metabolism by SIRT1 under non-stimulatory condition is therefore just one contributory mechanism to the overall response. Taken together, our data are in line with other observations showing that SIRT1 activity may contribute to the regulation of whole-body energy balance [(52-54), see (1; 55; 56) for reviews], and further support that activating SIRT1 could be a valuable strategy for the treatment and prevention of insulin resistance.

One limitation of our analysis of the SIRT1 gene deficiency in mouse is the potential for metabolic effects in SIRT1$^{+/\Delta ex4}$ mice. Heterozygous littermates of SIRT1$^{\Delta ex4/\Delta ex4}$ mice were used in order to avoid variations in the genetic background. However, we cannot exclude the possibility that the reported alteration in gene expression was already partially compromised in SIRT1$^{+/\Delta ex4}$ mice. For instance, it was previously reported that the regulation of lipolysis in adipocytes upon fasting was altered in SIRT1$^{+/\Delta ex4}$ mice when compared to wild type mice (12). However, if gene expression was already compromised in SIRT1$^{+/\Delta ex4}$ mice, this would rather mitigate the extent of variations when compared to SIRT1$^{\Delta ex4/\Delta ex4}$ mice. The generation of muscle specific SIRT1 transgenic and knockout mouse models will be necessary to further delineate the physiological roles of muscle SIRT1 in metabolism.

In summary, we demonstrated that SIRT1 gene deficiency altered glycolysis and decreased hexokinase II expression in mouse skeletal muscle. This is likely to reflect the decreased expression of SREBP-1c and LXR-ß in SIRT1$^{\Delta ex4/\Delta ex4}$ mice. This could be partly explained by the LXR-dependent transactivating effect of SIRT1 on SREBP-1c promoter. This may ultimately contribute to the regulation of glucose consumption.

ACKNOWLEDGMENTS

Aurélia Defour was financially supported by a grant from the Caisse d'Epargne Rhone-Alpes. Catherine Godinot is acknowledged for the kind provision of respiratory chain complex III and ATP synthase antibodies. Li Hongzhe (University of Washington, Seattle, USA) is acknowledged for tissue collection. The authors are grateful to Henri Benoit, Laboratoire de Physiologie de l'Exercice (Université Jean Monnet), for helpful discussions. Philippe Courpron, Caisse d'Epargne Rhone-Alpes, is also gratefully acknowledged for his constant support.

TABLE 1
Morphometric characteristics of SIRT1$^{\Delta ex4/\Delta ex4}$ mice.

Characteristics	SIRT1$^{+/\Delta ex4}$	SIRT1$^{\Delta ex4/\Delta ex4}$
Body weight (g)	33.78 ± 1.86	22.80 ± 1.15 **
Body mass index	30.92 ± 1.52	27.03 ± 1.52
Gastrocnemius weight (mg)	137.00 ± 12.00	92.00 ± 8.00 *
Tibialis anterior weight (mg)	50.00 ± 5.00	35.00 ± 3.00 *
Extensor digitorum longus weight (mg)	10.40 ± 0.12	7.93 ± 0.62 *
Soleus weight (mg)	5.89 ± 0.67	4.20 ± 0.45 $^{p = 0.08}$
Gastrocnemius (mg/g of body weight)	4.06 ± 0.33	4.01 ± 0.24
Tibialis anterior (mg/g of body weight)	1.49 ± 0.15	1.52 ± 0.12
Extensor digitorum longus (mg/g of body weight)	0.29 ± 0.02	0.31 ± 0.03
Soleus (mg/g of body weight)	0.18 ± 0.02	0.19 ± 0.01

Data are means ± SE. *$P < 0.05$ and **$P < 0.01$ versus SIRT1$^{+/\Delta ex4}$ mice.

TABLE 2
Primers sequences and annealing temperatures of genes used for RT-PCR analysis

Gene	GenBank Accession no.	5'-3' sequence of forward (FW) and reverse (RW) primers	Annealing temperature (°C)
ARBP	NM_007475	FW GAAAATCTCCAGAGGCACCATTG RW TCCCACCTTGTCTCCAGTCTTTATC	54
CYCA	NM_008907	FW GGCAAATGCTGGACCAAACAC RW CTTCCCAAAGACCACATGCTTG	54
HK II	NM_013820	FW CAACCCTGGCAAACAGAGGTT RW AGCCCCCGCTTTGTGAAAT	56
HPRT	NM_013556	FW CTCATGGACTGATTATGGACAGGAC RW GCAGGTCAGCAAAGAACTTATAGCC	60
LXR-α	NM_013839	FW TCCAAGTAGAGAGGCTGCAACAC RW TTAGCATCCGTGGGAACATCAG	57
LXR-β	NM_009473	FW GAAGGCGTCCACCATTGAGAT RW AGTCGTCCTTGCTGTAGGTGAAGT	56
MCAD	NM_007382	FW GAGTACCCTGTGGAGAAGCTGATG RW TTTTCAATGTGCTCACGAGCTATG	56
SREBP-1c	NM_011480	FW CGGGATGCGGCTGTTGTCT RW GCAGCAAGATGTCCTCCTGTGTACT	56

ARBP: acidic ribosomal phosphoprotein; CYCA: cyclophilin A; HK II: hexokinase II; HPRT: hypoxanthine guanine phosphoribosyl transferase; LXR: liver X receptor; MCAD: medium chain acyl-Coenzyme A dehydrogenase; SREBP-1c: sterol regulatory element binding protein 1c.

REFERENCES

1. Finkel T, Deng CX, Mostoslavsky R: Recent progress in the biology and physiology of sirtuins. *Nature* 460:587-591, 2009
2. Frye RA: Phylogenetic classification of prokaryotic and eukaryotic Sir2-like proteins. *Biochem Biophys Res Commun* 273:793-798, 2000
3. Vaquero A, Scher M, Lee D, Erdjument-Bromage H, Tempst P, Reinberg D: Human SirT1 interacts with histone H1 and promotes formation of facultative heterochromatin. *Mol Cell* 16:93-105, 2004
4. Vaquero A, Scher M, Erdjument-Bromage H, Tempst P, Serrano L, Reinberg D: SIRT1 regulates the histone methyl-transferase SUV39H1 during heterochromatin formation. *Nature* 450:440-444, 2007
5. O'Hagan HM, Mohammad HP, Baylin SB: Double strand breaks can initiate gene silencing and SIRT1-dependent onset of DNA methylation in an exogenous promoter CpG island. *PLoS Genet* 4:e1000155, 2008
6. Vaziri H, Dessain SK, Ng Eaton E, Imai SI, Frye RA, Pandita TK, Guarente L, Weinberg RA: hSIR2(SIRT1) functions as an NAD-dependent p53 deacetylase. *Cell* 107:149-159, 2001
7. Luo J, Nikolaev AY, Imai S, Chen D, Su F, Shiloh A, Guarente L, Gu W: Negative control of p53 by Sir2alpha promotes cell survival under stress. *Cell* 107:137-148, 2001
8. Yeung F, Hoberg JE, Ramsey CS, Keller MD, Jones DR, Frye RA, Mayo MW: Modulation of NF-kappaB-dependent transcription and cell survival by the SIRT1 deacetylase. *Embo J* 23:2369-2380, 2004
9. Frescas D, Valenti L, Accili D: Nuclear trapping of the forkhead transcription factor FoxO1 via Sirt-dependent deacetylation promotes expression of glucogenetic genes. *J Biol Chem* 280:20589-20595, 2005
10. Motta MC, Divecha N, Lemieux M, Kamel C, Chen D, Gu W, Bultsma Y, McBurney M, Guarente L: Mammalian SIRT1 represses forkhead transcription factors. *Cell* 116:551-563, 2004
11. Brunet A, Sweeney LB, Sturgill JF, Chua KF, Greer PL, Lin Y, Tran H, Ross SE, Mostoslavsky R, Cohen HY, Hu LS, Cheng HL, Jedrychowski MP, Gygi SP, Sinclair DA, Alt FW, Greenberg ME: Stress-dependent regulation of FOXO transcription factors by the SIRT1 deacetylase. *Science* 303:2011-2015, 2004
12. Picard F, Kurtev M, Chung N, Topark-Ngarm A, Senawong T, Machado De Oliveira R, Leid M, McBurney MW, Guarente L: Sirt1 promotes fat mobilization in white adipocytes by repressing PPAR-gamma. *Nature* 429:771-776, 2004
13. Bouras T, Fu M, Sauve AA, Wang F, Quong AA, Perkins ND, Hay RT, Gu W, Pestell RG: SIRT1 deacetylation and repression of p300 involves lysine residues 1020/1024 within the cell cycle regulatory domain 1. *J Biol Chem* 280:10264-10276, 2005
14. Rodgers JT, Lerin C, Haas W, Gygi SP, Spiegelman BM, Puigserver P: Nutrient control of glucose homeostasis through a complex of PGC-1alpha and SIRT1. *Nature* 434:113-118, 2005
15. Imai S, Armstrong CM, Kaeberlein M, Guarente L: Transcriptional silencing and longevity protein Sir2 is an NAD-dependent histone deacetylase. *Nature* 403:795-800, 2000
16. Freyssenet D: Energy sensing and regulation of gene expression in skeletal muscle. *J Appl Physiol* 102:529-540, 2007
17. Rodgers JT, Puigserver P: Fasting-dependent glucose and lipid metabolic response through hepatic sirtuin 1. *Proc Natl Acad Sci U S A* 104:12861-12866, 2007

18. Gerhart-Hines Z, Rodgers JT, Bare O, Lerin C, Kim SH, Mostoslavsky R, Alt FW, Wu Z, Puigserver P: Metabolic control of muscle mitochondrial function and fatty acid oxidation through SIRT1/PGC-1alpha. *Embo J*, 2007
19. Feige JN, Lagouge M, Canto C, Strehle A, Houten SM, Milne JC, Lambert PD, Mataki C, Elliott PJ, Auwerx J: Specific SIRT1 Activation Mimics Low Energy Levels and Protects against Diet-Induced Metabolic Disorders by Enhancing Fat Oxidation. *Cell Metab* 8:347-358, 2008
20. Milne JC, Lambert PD, Schenk S, Carney DP, Smith JJ, Gagne DJ, Jin L, Boss O, Perni RB, Vu CB, Bemis JE, Xie R, Disch JS, Ng PY, Nunes JJ, Lynch AV, Yang H, Galonek H, Israelian K, Choy W, Iffland A, Lavu S, Medvedik O, Sinclair DA, Olefsky JM, Jirousek MR, Elliott PJ, Westphal CH: Small molecule activators of SIRT1 as therapeutics for the treatment of type 2 diabetes. *Nature* 450:712-716, 2007
21. Banks AS, Kon N, Knight C, Matsumoto M, Gutierrez-Juarez R, Rossetti L, Gu W, Accili D: SirT1 gain of function increases energy efficiency and prevents diabetes in mice. *Cell Metab* 8:333-341, 2008
22. Moynihan KA, Grimm AA, Plueger MM, Bernal-Mizrachi E, Ford E, Cras-Meneur C, Permutt MA, Imai S: Increased dosage of mammalian Sir2 in pancreatic beta cells enhances glucose-stimulated insulin secretion in mice. *Cell Metab* 2:105-117, 2005
23. Bordone L, Motta MC, Picard F, Robinson A, Jhala US, Apfeld J, McDonagh T, Lemieux M, McBurney M, Szilvasi A, Easlon EJ, Lin SJ, Guarente L: Sirt1 regulates insulin secretion by repressing UCP2 in pancreatic beta cells. *PLoS Biol* 4:e31, 2006
24. Baron AD, Brechtel G, Wallace P, Edelman SV: Rates and tissue sites of non-insulin- and insulin-mediated glucose uptake in humans. *Am J Physiol* 255:E769-774, 1988
25. Cheng HL, Mostoslavsky R, Saito S, Manis JP, Gu Y, Patel P, Bronson R, Appella E, Alt FW, Chua KF: Developmental defects and p53 hyperacetylation in Sir2 homolog (SIRT1)-deficient mice. *Proc Natl Acad Sci U S A* 100:10794-10799, 2003
26. Li H, Rajendran GK, Liu N, Ware C, Rubin BP, Gu Y: SirT1 modulates the estrogen-IGF-1 signaling for postnatal development of mammary gland in mice. *Breast Cancer Res* 9:R1, 2007
27. Lowry P: *A flexible system of enzymatic analysis*, 1972
28. Peinnequin A, Mouret C, Birot O, Alonso A, Mathieu J, Clarencon D, Agay D, Chancerelle Y, Multon E: Rat pro-inflammatory cytokine and cytokine related mRNA quantification by real-time polymerase chain reaction using SYBR green. *BMC Immunol* 5:3, 2004
29. Livak KJ, Schmittgen TD: Analysis of relative gene expression data using real-time quantitative PCR and the 2(-Delta Delta C(T)) Method. *Methods* 25:402-408, 2001
30. Hellemans J, Mortier G, De Paepe A, Speleman F, Vandesompele J: qBase relative quantification framework and software for management and automated analysis of real-time quantitative PCR data. *Genome Biol* 8:R19, 2007
31. Vandesompele J, De Preter K, Pattyn F, Poppe B, Van Roy N, De Paepe A, Speleman F: Accurate normalization of real-time quantitative RT-PCR data by geometric averaging of multiple internal control genes. *Genome Biol* 3:RESEARCH0034, 2002
32. Freyssenet D, Connor MK, Takahashi M, Hood DA: Cytochrome c transcriptional activation and mRNA stability during contractile activity in skeletal muscle. *Am J Physiol* 277:E26-32, 1999
33. Duguez S, Feasson L, Denis C, Freyssenet D: Mitochondrial biogenesis during skeletal muscle regeneration. *Am J Physiol Endocrinol Metab* 282:E802-809, 2002
34. Freyssenet D, Berthon P, Barthelemy JC, Busso T, Geyssant A, Denis C: Energetic status and mitochondrial oxidative capacity of rat skeletal muscle in response to creatine analogue ingestion. *Biochim Biophys Acta* 1228:211-215, 1995

35. Dif N, Euthine V, Gonnet E, Laville M, Vidal H, Lefai E: Insulin activates human sterol-regulatory-element-binding protein-1c (SREBP-1c) promoter through SRE motifs. *Biochem J* 400:179-188, 2006
36. Durieux AC, Bonnefoy R, Manissolle C, Freyssenet D: High-efficiency gene electrotransfer into skeletal muscle: description and physiological applicability of a new pulse generator. *Biochem Biophys Res Commun* 296:443-450, 2002
37. Durieux AC, Bonnefoy R, Busso T, Freyssenet D: In vivo gene electrotransfer into skeletal muscle: effects of plasmid DNA on the occurrence and extent of muscle damage. *J Gene Med* 6:809-816, 2004
38. Jahnke VE, Sabido O, Defour A, Castells J, Lefai E, Roussel D, Freyssenet D: Evidence for mitochondrial respiratory deficiency in rat rhabdomyosarcoma cells. *PLoS One* 5:e8637, 2010
39. Gosmain Y, Lefai E, Ryser S, Roques M, Vidal H: Sterol regulatory element-binding protein-1 mediates the effect of insulin on hexokinase II gene expression in human muscle cells. *Diabetes* 53:321-329, 2004
40. Gosmain Y, Dif N, Berbe V, Loizon E, Rieusset J, Vidal H, Lefai E: Regulation of SREBP-1 expression and transcriptional action on HKII and FAS genes during fasting and refeeding in rat tissues. *J Lipid Res* 46:697-705, 2005
41. Napper AD, Hixon J, McDonagh T, Keavey K, Pons JF, Barker J, Yau WT, Amouzegh P, Flegg A, Hamelin E, Thomas RJ, Kates M, Jones S, Navia MA, Saunders JO, DiStefano PS, Curtis R: Discovery of indoles as potent and selective inhibitors of the deacetylase SIRT1. *J Med Chem* 48:8045-8054, 2005
42. Solomon JM, Pasupuleti R, Xu L, McDonagh T, Curtis R, DiStefano PS, Huber LJ: Inhibition of SIRT1 catalytic activity increases p53 acetylation but does not alter cell survival following DNA damage. *Mol Cell Biol* 26:28-38, 2006
43. Pacholec M, Bleasdale JE, Chrunyk B, Cunningham D, Flynn D, Garofalo RS, Griffith D, Griffor M, Loulakis P, Pabst B, Qiu X, Stockman B, Thanabal V, Varghese A, Ward J, Withka J, Ahn K: SRT1720, SRT2183, SRT1460, and resveratrol are not direct activators of SIRT1. *J Biol Chem* 285:8340-8351, 2010
44. Canto C, Gerhart-Hines Z, Feige JN, Lagouge M, Noriega L, Milne JC, Elliott PJ, Puigserver P, Auwerx J: AMPK regulates energy expenditure by modulating NAD+ metabolism and SIRT1 activity. *Nature* 458:1056-1060, 2009
45. Chabi B, Adhihetty PJ, O'Leary MF, Menzies KJ, Hood DA: Relationship between Sirt1 expression and mitochondrial proteins during conditions of chronic muscle use and disuse. *J Appl Physiol* 107:1730-1735, 2009
46. Gurd BJ, Yoshida Y, Lally J, Holloway GP, Bonen A: The deacetylase enzyme SIRT1 is not associated with oxidative capacity in rat heart and skeletal muscle and its overexpression reduces mitochondrial biogenesis. *J Physiol* 587:1817-1828, 2009
47. Li X, Zhang S, Blander G, Tse JG, Krieger M, Guarente L: SIRT1 Deacetylates and Positively Regulates the Nuclear Receptor LXR. *Mol Cell* 28:91-106, 2007
48. Peet DJ, Turley SD, Ma W, Janowski BA, Lobaccaro JM, Hammer RE, Mangelsdorf DJ: Cholesterol and bile acid metabolism are impaired in mice lacking the nuclear oxysterol receptor LXR alpha. *Cell* 93:693-704, 1998
49. Korach-Andre M, Parini P, Larsson L, Arner A, Steffensen KR, Gustafsson JA: Separate and overlapping metabolic functions of LXR{alpha} and LXR{beta} in C57Bl/6 female mice. *Am J Physiol Endocrinol Metab* 298:E167-178, 2010
50. Canto C, Jiang LQ, Deshmukh AS, Mataki C, Coste A, Lagouge M, Zierath JR, Auwerx J: Interdependence of AMPK and SIRT1 for Metabolic Adaptation to Fasting and Exercise in Skeletal Muscle. *Cell Metab* 11:213-219, 2010

51. Lin J, Yang R, Tarr PT, Wu PH, Handschin C, Li S, Yang W, Pei L, Uldry M, Tontonoz P, Newgard CB, Spiegelman BM: Hyperlipidemic effects of dietary saturated fats mediated through PGC-1beta coactivation of SREBP. *Cell* 120:261-273, 2005
52. Rutanen J, Yaluri N, Modi S, Pihlajamaki J, Vanttinen M, Itkonen P, Kainulainen S, Yamamoto H, Lagouge M, Sinclair DA, Elliott P, Westphal C, Auwerx J, Laakso M: SIRT1 mRNA Expression May Be Associated With Energy Expenditure and Insulin Sensitivity. *Diabetes* 59:829-835, 2010
53. de Kreutzenberg SV, Ceolotto G, Papparella I, Bortoluzzi A, Semplicini A, Man CD, Cobelli C, Fadini GP, Avogaro A: Downregulation of the longevity-associated protein sirtuin 1 in insulin resistance and metabolic syndrome: potential biochemical mechanisms. *Diabetes* 59:1006-1015, 2010
54. Zillikens MC, van Meurs JB, Rivadeneira F, Hofman A, Oostra BA, Sijbrands EJ, Witteman JC, Pols HA, van Duijn CM, Uitterlinden AG: Interactions between dietary vitamin E intake and SIRT1 genetic variation influence body mass index. *Am J Clin Nutr*, 2010
55. Liang F, Kume S, Koya D: SIRT1 and insulin resistance. *Nat Rev Endocrinol* 5:367-373, 2009
56. Feige JN, Auwerx J: Transcriptional coregulators in the control of energy homeostasis. *Trends Cell Biol* 17:292-301, 2007

FIGURE LEGENDS

FIG. 1. Intramuscular content of glycogen, glucose-6-phosphate and pyruvate in the *gastrocnemius* muscle of $SIRT1^{+/\Delta ex4}$ mice (■) and $SIRT1^{\Delta ex4/\Delta ex4}$ mice (□). *A*: Glycogen content. *B*: Glucose-6-phosphate content. *C*: Pyruvate content. Data are means ± SE. * $P < 0.05$: significantly different from $SIRT1^{+/\Delta ex4}$ mice.

FIG. 2. Hexokinase (HK) II mRNA level, HK activity and lactate dehydrogenase (LDH) activity in the *gastrocnemius* muscle of $SIRT1^{+/\Delta ex4}$ mice (■) and $SIRT1^{\Delta ex4/\Delta ex4}$ mice (□). *A*: HK II mRNA level (left panel) and HK activity (right panel). *B*: LDH activity. Data are means ± SE. * $P < 0.05$, ** $P < 0.01$ and *** $P < 0.001$: significantly different from $SIRT1^{+/\Delta ex4}$ mice.

FIG. 3. Expression of nuclear genes encoding mitochondrial proteins in skeletal muscle of $SIRT1^{+/\Delta ex4}$ mice (■) and $SIRT1^{\Delta ex4/\Delta ex4}$ mice (□). *A*: 3-hydroxy-acyl-Coenzyme A dehydrogenase (HAD) activity, medium-chain acyl-Coenzyme A dehydrogenase (MCAD) mRNA level and citrate synthase (CS) activity in the *gastrocnemius* muscle. *B*: HAD activity, MCAD mRNA level and CS activity in the *tibialis anterior* muscle. *C*: Representative immunoblot (left panel) and densitometric analysis (right panel) of mitochondrial respiratory chain proteins of complex III (Core II, 13.4) and complex V (20D6) in the *gastrocnemius* (▩) and *tibialis anterior* (▨) muscles.

FIG. 4. Expression of sterol regulatory element binding protein (SREBP)-1c and liver X receptor (LXR)-α and -β in the *gastrocnemius* muscle of $SIRT1^{+/\Delta ex4}$ mice (■) and $SIRT1^{\Delta ex4/\Delta ex4}$ mice (□). *A*: SREBP-1c mRNA level (left panel) and protein level (right panel). *B*: LXR-α and LXR-β mRNA level. Data are means ± SE. * $P < 0.05$: significantly different from $SIRT1^{+/\Delta ex4}$ mice.

FIG. 5. SIRT1 regulates SREBP-1c promoter transactivation through a LXR-dependent mechanism. *A*: Human SREBP-1c promoter (-571/+90 bp) reporter gene (pSREBP-1c-Luc) and human SREBP-1c promoter (-571/+90 bp) reporter gene with two deleted mutations in LXR-response elements (LXRE) located at -311/-296 bp and -260/-245 bp (pSREBP-1c-Luc m1/2) (35). *B*: Gene electrotransfer of SIRT1 expression vector increases SIRT1 protein level in mouse *tibialis anterior* muscle. Muscles were electrotransfected with either a control vector (pcDNA3.1Zeo, ■) or a SIRT1 expression vector (pBabe-SIRT1, ■). Seven days after gene electrotransfer, muscles were removed and analyzed by western blot. SIRT1 protein was detected as a 85-90 kDa band. Data are means ± SE. ** $P < 0.01$: significantly different from pcDNA3.1-Zeo *C*: Mutations of LXR-response elements in SREBP-1c promoter abolished SIRT1-induced SREBP-1c promoter transactivation. Gene electrotransfer of pSREBP-1c-Luc (■, n = 8), pSREBP-1c-Luc and pBabe-SIRT1 (■, n = 8), or pSREBP-1c-Luc and pCMV-LXR-α (□, n = 8) was performed. Contralateral *tibialis anterior* muscle was injected with the same DNA mixture except that pSREBP-1c-Luc was omitted and replaced by pSREBP-1c-Luc m1/2. In order to correct for variations in transfection efficiency, luciferase activity was normalized to β-galactosidase activity. RLU, relative light unit. Data are means ± SE. * $P < 0.05$ and *** $P < 0.001$: significantly different from pSREBP-1c-Luc alone; †† $P < 0.01$ and ††† $P < 0.001$: significantly different from corresponding gene electrotransfer with pSREBP-1c-Luc.

FIG. 6. EX527 lowers glucose consumption of C2C12 myotubes. C2C12 myoblasts were differentiated into myotubes for 5 days and treated with EX527 for an additional 48 hours. Glucose concentration in the culture medium was determined before and after 48 hours EX527 exposure. Data are means ± SE from 8 independent experiments * $P < 0.05$ and *** $P < 0.001$: significantly different from control myotubes (0 µM).

Figure 1.

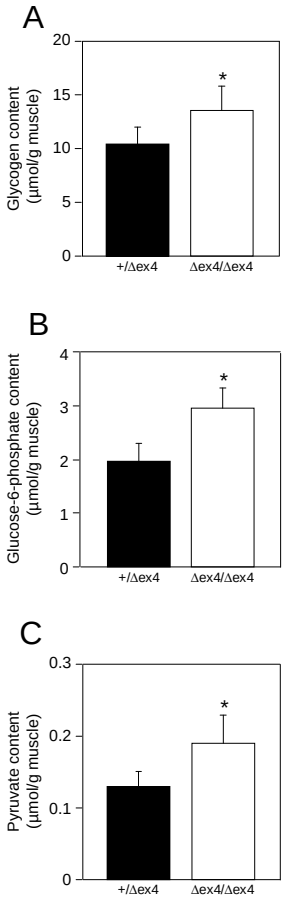
A
Glycogen content
(µmol/g muscle)
20
15
10
5
0
*
+/Δex4
Δex4/Δex4
B
Glucose-6-phosphate content
(µmol/g muscle)
4
3
2
1
0
*
+/Δex4
Δex4/Δex4
C
Pyruvate content
(µmol/g muscle)
0.3
0.2
0.1
0
*
+/Δex4
Δex4/Δex4

Figure 2.

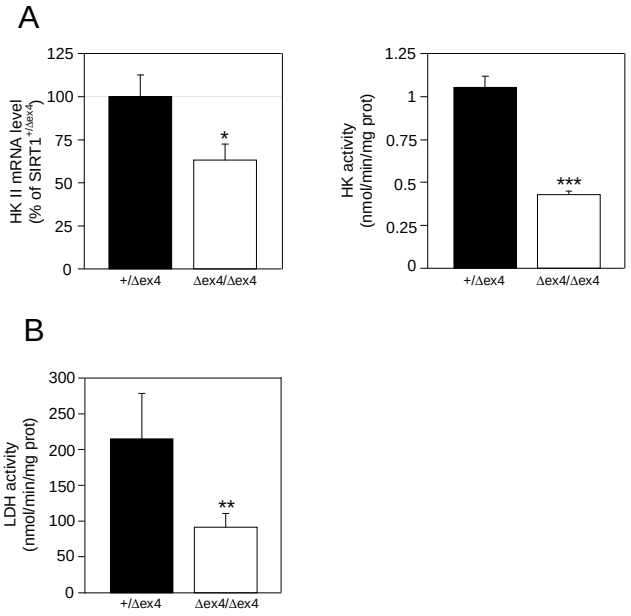
A
HK II mRNA level
(% of SIRT1+/Δex4)
125
100
75
50
25
0
*
+/Δex4
Δex4/Δex4
HK activity
(nmol/min/mg prot)
1.25
1
0.75
0.5
0.25
0
***
+/Δex4
Δex4/Δex4
B
LDH activity
(nmol/min/mg prot)
300
250
200
150
100
50
0
**
+/Δex4
Δex4/Δex4

Figure 3.

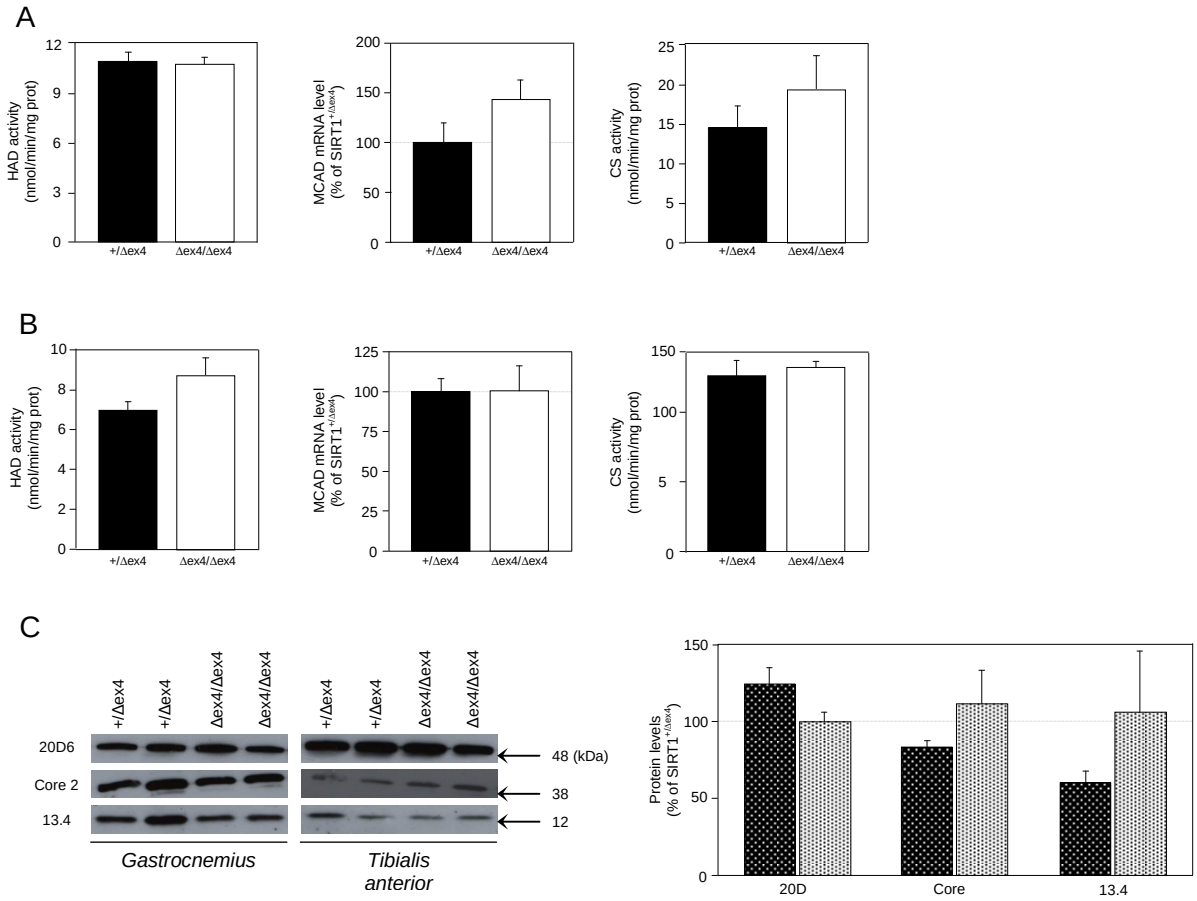
A
HAD activity (nmol/min/mg prot)
MCAD mRNA level (% of SIRT1+/Δex4)
CS activity (nmol/min/mg prot)
+/Δex4
Δex4/Δex4
B
HAD activity (nmol/min/mg prot)
MCAD mRNA level (% of SIRT1+/Δex4)
CS activity (nmol/min/mg prot)
+/Δex4
Δex4/Δex4
C
+/Δex4
+/Δex4
Δex4/Δex4
Δex4/Δex4
20D6
Core 2
13.4
48 (kDa)
38
12
Gastrocnemius
Tibialis anterior
Protein levels (% of SIRT1+/Δex4)
20D
Core
13.4

Figure 4.

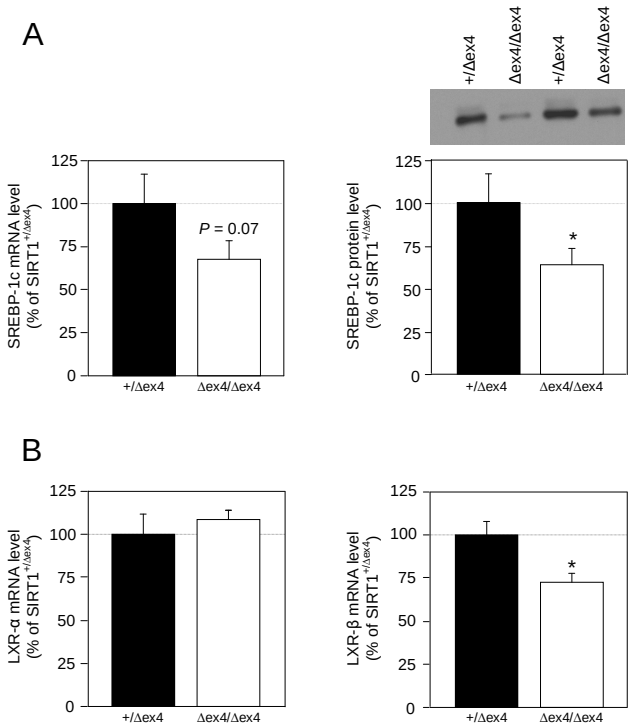
A
+/Δex4
Δex4/Δex4
+/Δex4
Δex4/Δex4
SREBP-1c mRNA level
(% of SIRT1+/Δex4)
P = 0.07
SREBP-1c protein level
(% of SIRT1+/Δex4)
*
B
LXR-α mRNA level
(% of SIRT1+/Δex4)
LXR-β mRNA level
(% of SIRT1+/Δex4)
*
125
100
75
50
25
0
+/Δex4
Δex4/Δex4

Figure 5.

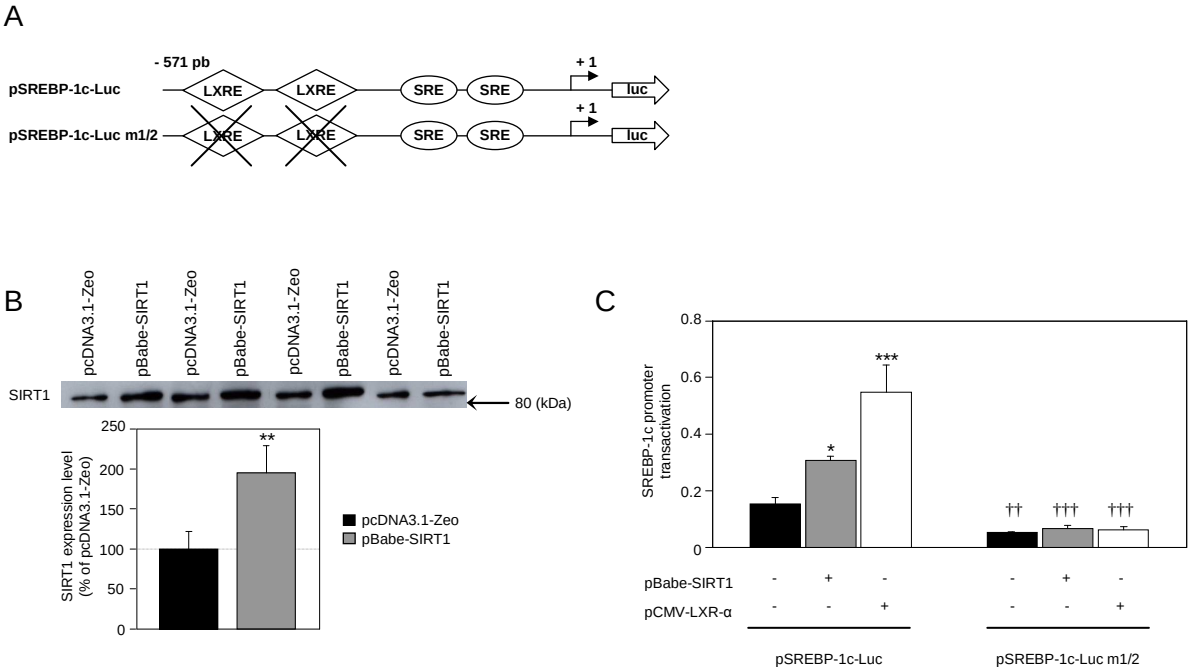
A
- 571 pb
pSREBP-1c-Luc
LXRE
LXRE
SRE
SRE
+ 1
luc
pSREBP-1c-Luc m1/2
LXRE
LXRE
SRE
SRE
+ 1
luc
B
pcDNA3.1-Zeo
pBabe-SIRT1
pcDNA3.1-Zeo
pBabe-SIRT1
pcDNA3.1-Zeo
pBabe-SIRT1
pcDNA3.1-Zeo
pBabe-SIRT1
SIRT1
80 (kDa)
SIRT1 expression level
(% of pcDNA3.1-Zeo)
250
200
150
100
50
0
**
pcDNA3.1-Zeo
pBabe-SIRT1
C
SREBP-1c promoter
transactivation
0.8
0.6
0.4
0.2
0
***
*
††
†††
†††
pBabe-SIRT1
pCMV-LXR-α
pSREBP-1c-Luc
pSREBP-1c-Luc m1/2

Figure 6.

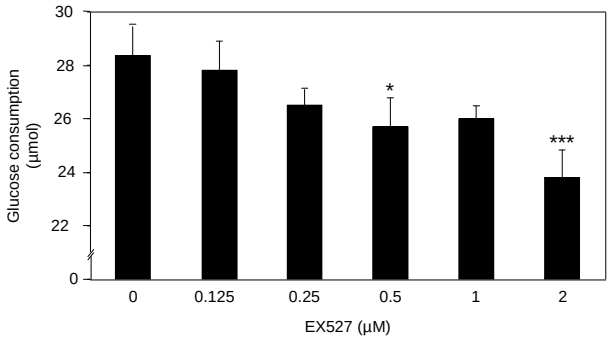
30
28
26
24
22
0
Glucose consumption (µmol)
*
***
0
0.125
0.25
0.5
1
2
EX527 (µM)

MANUSCRIT 2

Regulation of Akt/mTOR pathway, ubiquitin proteasome pathway and autophagy in response to fasting/refeeding in C2C12 myotubes

L'amyotrophie résulte d'un déséquilibre de la balance entre la synthèse et la dégradation des protéines. On peut observer cette perte de masse musculaire dans plusieurs conditions comme lors du vieillissement, lors d'un alitement prolongé ou lors d'un jeûne. Le but de l'étude suivante a été de déterminer la régulation de la balance entre la synthèse et la dégradation des protéines se produisant lors d'un jeûne chez des myotubes C2C12. Ainsi, nous montrons, que chez des myotubes C2C12, un jeûne de 4 heures induisait une déphosphorylation précoce (30 minutes à 1 heure) d'Akt^{S473}, GSK3$^{S21/S9}$, p70S6K^{T412} et S6$^{S235/S236}$ précédant une amyotrophie de 15 % des myotubes observée à 2 heures de jeûne. Cette déphosphorylation s'accompagnait d'une augmentation très rapide de l'activité cathepsine B + L, alors qu'aucune modification de la voie du protéasome n'était observée. La renutrition s'accompagnait d'un retour à la normale de ces différents paramètres à l'exception de l'activité cathepsine B + L qui restait elevée. Ainsi, ces données préliminaires suggèrent que le jeûne et la renutrition aboutissent à une régulation de la voie Akt, régulatrice de la masse musculaire et de la voie autophagie/lysosome impliquée dans la dégradation des protéines chez des myotubes C2C12. D'autres marqueurs des voies de dégradation ubiquitine/protéasome et autophagie/lysosome seront à envisager. Enfin, étant donné que la protéine Sirt1 est impliquée dans la restriction calorique, son rôle lors du jeûne et de la renutrition sera également à étudier.

Regulation of Akt/mTOR pathway, ubiquitin proteasome pathway and autophagy in response to fasting/refeeding in C2C12 myotubes

[1]Defour Aurélia, [2]Pugnière Pascal, [1]Castells Josiane, [3]Béchet Daniel, [2]Peinnequin André, and [1]Freyssenet Damien

[1]Université de Lyon, Université Jean Monnet, Laboratoire de Physiologie de l'Exercice EA 4338, Saint Etienne, France
[2]Pôle de Génomique, Institut de Recherche Biomédicale des Armées, Centre de Recherche du Service de Santé des Armées, La Tronche, France
[3]INRA UMR 1019, Unité Nutrition Humaine, St Genès Champanelle, France

Corresponding author: Damien Freyssenet

Laboratoire de Physiologie de l'Exercice

Faculté de Médecine, 15 rue Ambroise Paré

42023 Saint-Etienne Cedex 2, France

Tel: 033 4 77 42 14 77

Fax: 033 4 77 42 14 78

E-mail: damien.freyssenet@univ-st-etienne.fr

Amyotrophy results from an imbalance between protein synthesis and degradation. Muscle mass loss is observed in several conditions such as aging, prolonged immobilization or fasting. The purpose of this study was to determine the regulation between protein synthesis and degradation during fasting in C2C12 myotubes. We showed that in C2C12 myotubes, a 4 hours fasting induced an early dephosphorylation (30 minutes to 1 hour) of Akt^{S473}, $GSK3^{S21/S9}$, $p70S6K^{T412}$ and $S6^{S235/S236}$, that preceded a 15% decrease in myotubes area (2 hours of fasting). This dephosphorylation was accompanied by a rapid increase in cathepsin B + L activity, while no change in proteasome activity was observed. Refeeding was accompanied by a return to normal values, with the exception of cathepsin B + L activity which remained elevated. Thus, these preliminary data suggest that fasting and refeeding lead to a regulation of the Akt pathway, which may both regulate protein synthesis and autophagy/lysosome pathway, and ultimately myotubes area. Other markers of degradation of ubiquitin/proteasome and autophagy/lysosome pathways will be determined. Finally, given that the protein Sirt1 is involved in caloric restriction, its role in the regulation of these processes during fasting and refeeding needs to be studied.

INTRODUCTION

The loss of muscle protein is a widespread phenomenon known as muscle atrophy or wasting that leads to rapid alterations in muscle structure and functions. Skeletal muscle atrophy occurs systematically with prolonged inactivity, denervation, normal aging, fasting and with many diseases, including cancer, diabetes, sepsis, renal failure and chronic obstructive pulmonary disease. During these catabolic conditions, skeletal muscle is subjected to a major metabolic challenge, which particularly triggers an increased reliance on protein catabolism to provide amino acids for the maintenance of vital functions of critical organs such as the heart, brain, liver and kidney.

Accelerated breakdown of proteins have been largely attributed to activation of ubiquitine-proteasome pathway. Expression of several subunits of the proteasome, as well as that of atrophy-specific-ubiquitin ligases, atrogin1/muscle atrophy F-box (MAFbx) and muscle ring finger-1 (MuRF-1), has been consistently observed in numerous conditions leading to muscle mass loss (2, 13, 22). Furthermore, the role of autophagy-lysosomal pathway, which has long been largely ignored despites consistent evidence that it stimulates protein degradation in skeletal muscle (8, 26), is now becoming increasingly important. Indeed, recent studies have shown that expression of certain components of the autophagy-lysosomal pathway is upregulated in various models of atrophy (13, 15, 22, 27). Particularly, expression of autophagy-related genes, such as LC3, Gabarapl1, Bnip3 and Bnip3l, is strongly induced in skeletal muscle during fasting (15, 27).

Genetic and pharmacological studies have shown that both ubiquitine-proteasome and autophagy-lysosomal pathways are under the control of Akt/Foxo pathway. In cultured myotubes undergoing atrophy, Akt activity decreases, leading to activation of Foxo transcription factors and atrogin-1 expression, whereas IGF-1 treatment or Akt overexpression inhibits Foxo transcriptional activity and atrogin-1 expression (23-25).

Similarly, acute activation of Akt inhibits autophagosome formation and lysosomal-dependent protein degradation during fasting both *in vitro* and *in vivo* (15, 27). Furthermore, it has been clearly shown that the overexpression of a constitutionally active form of FoxO3 induced autophagy, whereas Akt activation blocked FoxO3-induced autophagy (15, 27). This effect is mediated by a FoxO-dependent transcription of autophagy genes such as Atg12, Bnip, Gabarapl and LC3b (15, 27). The Akt-dependent regulation of FoxO transcription factors thus allows a coordinate regulation of ubiquitine-proteasome and autophagy-lysosomal pathways in skeletal muscle.

The aim of the study was to characterize the kinetic response of signaling pathways associated with muscle atrophy. We specifically investigated the kinetic response of Akt/mTOR, ubiquitin-proteasome and autophagy-lysosome during fasting and refeeding in C2C12 myotubes.

MATERIALS AND METHODS

Cell culture. C2C12 muscle cells (ATCC CRL-1772) were cultured in Dulbecco's modified Eagle's medium (DMEM) supplemented with 20% fetal bovine serum and 1% penicillin-streptomycin (P/S) at 37°C and 5% CO_2 in air in 10 mm plate dishes or 6-well plates. At 80% confluence, cells were allowed to differentiate for 6 days in DMEM supplemented with 2% horse serum (HS) and 1% P/S. Myotubes were then submitted to a metabolic challenge consisting in 4 hours of complete fasting followed by 4 hours of refeeding. Fasting was realized by substituting the differentiation medium by Dulbecco's Phosphate Buffered Saline (DPBS) supplemented with 2% HS and 1% P/S. Four hours later, myotubes were refed with the differentiation medium.

Videomicroscopy. C2C12 myotubes cultured in 6-well cell culture plate at 37°C and 5% CO_2 in air were filmed during fasting and refeeding (Zeiss, Cell Observer Z1, IFR143). Myotube area was quantified from 6 different fields (x 10) by using Axion Vision 4.7.

Glucose and lactate concentrations. Lactate and glucose concentrations in the culture medium were determined at the indicated time points during 24 hours following fasting by using an electrochemical analyser YSI 2300 STAT PLUS (Yellow Springs Instruments, Yellow Springs , Ohio, USA) (11). Calibration was done by using a 1.25 mM standard lactate solution and a 5 mM standard glucose solution.

Protein extraction. At the indicated time points, cells were harvested and the proteins were extracted at 4°C with a buffer consisting of 50 mM Tris-HCl (pH = 7.4), 100 mM NaCl, 2 mM EDTA, 2 mM EGTA, 50 mM ß-glycerophosphate, 50 mM sodium fluoride, 1 mM $NaVO_4$, 120 nM okadaic acid, and 1% Triton X-100. Homogenates were centrifuged at 12,000 g for 20 min at 4°C. Protein concentration was spectrophotometrically determined at 750 nm using a protein assay (BioRad).

Enzyme assays. Chymotrypsin-like and trypsin-like activities of 20S proteasome, as well as cathepsin B+L activities were fluorometrically measured as previously described (1, 4).

Luminex and western blot analyses. Protein extracts were transferred into 96-well dishes and diluted with 25 µl buffered solution. Fluorescent capturing beads coupled to antibodies directed against the phosphorylated forms of glycogen synthase kinase (GSK)-3 (Ser9/21) (Biorad, cat. no.171V23318), phospho-ribosomal protein S6 (Ser235/236) (Biorad, cat. no.171V25374), phospho-ribosomal protein S6 kinase (p70S6K) (Thr412) (Millipore, cat. no. 46-629), phospho-Akt Ser473) (Millipore, cat. no. 46-677) were used. Antibodies directed against phosphorylated and non-phosphorylated forms of p70S6K (Millipore, cat. no. 46-630) and Akt (Millipore, cat. no. 46-677) were also used. The antibody-conjugated beads were added into each well and incubated overnight. The plates were washed and incubated with biotinylated antibodies to fix each target protein. Streptavidin–phycoerythrin solution was then added. The analysis consisted of a double-laser fluorescence detection, which allowed simultaneous identification of the target protein through the red fluorescence emission signal of the bead and quantification of the target protein through the fluorescence intensity of phycoerythrin. A positive control, consisting of a standard protein extract from control cell line, was added to each series. Results were recorded as mean fluorescence intensities. The phosphorylation level of ribosomal S6 protein was also determined by western blot. Fifty µg of proteins were separated on SDS-PAGE and transferred to nitrocellulose membranes. Blots were incubated overnight at 4°C with antibody against the phosphorylayed form of ribosomal S6 protein (Ser235/236) (1:1,000 dilution wt/vol, Cell Signaling Technologies, cat. no.4856). Horseradish peroxidase-conjugated goat anti-rabbit (1:2,000 dilution wt/vol, Dako) antibody was used for the chemiluminescent detection of proteins (ECL, GE Health Care). The films were scanned and quantified using N.I.H. image 1.63.

Statistics. Data are means ± SE from 6/8 independent culture dishes/wells. Statistical comparisons were performed using one way analysis of variance (StatView^{TM}SE+^{Graphics}, Abacus Concept, Inc). The 0.05 level of confidence was accepted for statistical significance.

RESULTS

Fasting triggers atrophy of C2C12 myotubes. We first aimed to characterize the morphological response of C2C12 myotubes in response to fasting/refeeding by videomicroscopy. A quantitative analysis indicated that fasting induced a progressive atrophy of myotubes that reached statistical significance after 2 hours (Figure 1). By the end of the fasting period, myotube area was reduced by 15% ($P < 0.001$). Importantly, the size of the myotubes was entirely restored to control values following 1 hour of refeeding and was even further increased by 10-15% 3 and 4 hours following fasting ($P < 0.05$).

Fasting profoundly alters glucose consumption and lactate production during refeeding. To get insights into the metabolic response of atrophic myotubes to refeeding, glucose consumption and lactate production were determined. Glucose consumption of fasted C2C12 myotubes was significantly higher when compared to the control values during the first hour following fasting, and then progressively returned to control level (Figure 2A). Lactate production, which was strongly reduced by fasting, then progressively increased to stabilize around control values by 4 hours of refeeding (Figure 2B).

Fasting markedly inhibits the Akt/mTOR pathway. The maintenance of skeletal muscle mass mainly results from the balance between protein synthesis and protein degradation (5). We first determined whether fasting inhibits the Akt/mTOR pathway that controls protein synthesis. Fasting-induced C2C12 myotube atrophy was associated with a significant decrease in the phosphorylation of Akt on Ser473 (-50%), GSK-3 on S29/S21 (-45%), p70S6K on Thr412 (-70%) and S6 on Ser235/S236 (-80%), while at the same time Akt and p70S6k total protein level remained unchanged (Figure 3 A-E). With the exception of S6 whose phosphorylation was decreased after 60 minutes, Akt, GSK-3 and p70S6k phosphorylation was significantly decreased as soon as 30 minutes of fasting. Overall, these data clearly indicate that the Akt/mTOR pathway is rapidly and strongly inhibited by fasting

in C2C12 myotubes. Phosphorylation of Akt, GSK-3, p70S6k and S6 was rapidly induced within 15 minutes after the cessation of fasting (Figure 3). The response was even more pronounced for Akt and p70S6k, whose the phosphorylation level was increased by about 5-fold. However, this increase was transitory as the phosphorylation level of Akt and p70S6k almost returned to control level after 4 hours of refeeding.

Fasting does not alter the ubiquitine-proteasome pathway, but strongly activates lysosomal cathepsin B+L enzyme activities. The main proteolytic pathways involved in the regulation of skeletal muscle mass are the ubiquitine-proteasome and autophagy pathways. The chymotrypsin-like and trypsin-like activities of 20S proteasome remained unchanged over the entire experimental period (Figure 4), suggesting that the ubiquitine-proteasome pathway remained insensitive to the fasting of C2C12 myotubes. By contrast, the lysosomal enzyme activity of cathepsine B+L increased significantly during fasting in a time-dependant manner to reach a level that was about 3-fold higher at the end of the fasting period ($P < 0.001$) (Figure 5). Importantly cathepsin B+L enzyme activity remained elevated and only slightly decreased during the refeeding period. These data suggest that fasting strongly activates the autophagy pathway in fasted C2C12 myotubes.

DISCUSSION

Among potential signaling pathways that can regulate fasting-induced skeletal muscle atrophy, the Akt/mTOR pathway appears to be a good candidate by its capacity to coordinately and inversely regulate protein synthesis and proteolysis. In the present study, the effect of fasting on the down-regulation of Akt/mTOR pathway and up-regulation of cathepsin B+L enzyme activity is consistent this hypothesis. Although protein synthesis has not been measured, the marked decrease in the phosphorylation level of Akt, GSK3, p70S6K and S6 suggests that a reduction in protein synthesis had occurred in fasted myotubes. In agreement with previous studies, we also showed that the autophagy-lysosome pathway is strongly activated during fasting. Importantly both time course responses (the down-regulation of Akt/mTOR pathway and the activation of autophagy-lysosome pathway) preceded the atrophy of myotubes, suggesting that they mainly contribute to induction of myotube atrophy.

These data raise a number of questions. One may first question which mechanisms trigger the down-regulation of Akt/mTOR pathway? It should be noted that the serum concentration was maintained to 2% during fasting, therefore excluding the possibility that a decrease in IGF-1 concentration would be responsible for the down-regulation of Akt. By contrast, C2C12 myotubes were completely deprived of amino acids and particularly of leucine, whose stimulatory action on Akt/mTOR pathway has been largely documented (see (6, 12) for example). Furthermore, leucine limitation has been also shown to stimulate lysosomal proteolysis (16). Leucine deprivation may therefore both contribute to the down-regulation of Akt/mTOR pathway and the stimulation of lysosomal proteolysis. The restriction in glucose, which is know to increase the amount of NAD^+ inside the cell (7), may also trigger the activation of sirtuin1 (SIRT1) and contribute to the regulation of Akt/mTOR pathway. Indeed, it was recently shown SIRT1 negatively regulated mTOR phosphorylation in Hela cells (9). In

support of this observation, we conversely observed that the phosphorylation level of Akt S473 and S6 S235/236 was increased the skeletal muscle of SIRT1 deficient mice (Defour, unpublished observations).

Second, what is the functional relationship between the down-regulation of Akt/mTOR pathway and the regulation of autophagy? In skeletal muscle, acute activation of Akt has been shown to inhibit autophagosome formation and lysosomal-dependent protein degradation during fasting both *in vivo* and *in vitro* (15, 27). Furthermore, overexpression of a constitutionally active form of FoxO3 induced autophagy by mediating the expression of autophagy genes such as Atg12, Bnip, Gabarapl and LC3b, whereas Akt activation blocked FoxO3-induced autophagy (15, 27). Although the phosphorylation status of FoxO3a has not been measured in the present study, the simultaneous and opposite regulation of Akt/mTOR pathway and cathepsinB+L activity support the above mechanism. The expression of autophagy genes is currently under investigation.

SIRT1 could also contribute to the regulation of autophagy in our experimental model. SIRT1 is a protein deacetylase that catalyzes the NAD^+ dependent deacetylation of specific ε-amino-acetylated lysine residues from its protein substrates. Hepatic SIRT1 expression has been shown to be activated by fasting and caloric restriction *in vivo* (3, 18, 20) and decreased by glucose addition *in vitro* (21). Importantly, SIRT1 expression would be also stimulated in skeletal muscle during fasting (10). Furthermore, knockdown of FoxO3a in PC12 cells inhibits the fasting-induced increase in Sirt1 expression (19), suggesting that the regulation of SIRT1 expression may be linked to the regulation of Akt/FoxO pathway. Finally, recent evidences also suggest that SIRT1 is an important regulator of autophagy. Indeed, SIRT1 is able to form molecular complex with several essential components of the autophagy machinery, such as autophagy genes (Atg)5, Atg7 and Atg8, and $SIRT1^{-/-}$ mice partially resembles Atg5-/- mice, including the accumulation of damaged organelles (14). Furthermore,

SIRT1 overexpression promotes the autophagic flux in human cancer cells, and this effect can be prevented by the pharmacological SIRT1 inhibitor EX527 (17). Altogether, these data provide a functional link between Akt/FoxO pathway, autophagy, SIRT1 and the overall cellular response to altered nutrient availability. It will be therefore important to define the role of SIRT1 in the regulation of autophagy during fasting in skeletal muscle. The *in vitro* model of muscle atrophy used in the present study could be useful to identify the downstream events triggered by SIRT1 that are important for the regulation of autophagy and the development of muscle atrophy during fasting.

The observation that the ubiquitine-proteasome pathway remained insensitive to the fasting protocol despites that Akt/mTOR pathway is strongly inhibited may be surprising since a decrease in Akt activity has been shown to activate Foxo transcription factors and the subsequent expression of atrogenes (23-25). Our data rather suggest that the regulation of ubiquitine-proteasome pathway is more complex and that other signaling influences contribute to the regulation of ubiquitine-proteasome pathway.

In summary, our data provide a descriptive analysis of the regulation of Akt/mTOR pathway, ubiquitine-proteasome pathway and autophagy lysosomal pathway during fasting and refeeding of C2C12 myotubes. This preliminary study will be extended to the analysis of other markers of ubiquitine-proteasome pathway (expression of MuRF-1 and atrogin-1) and autophagy lysosomal pathway (expression of Bnip3, Gabarapl1, LC-3B and Vps34) and to the analysis of SIRT1 function in this experimental model.

ACKNOWLEDGMENTS

Aurélia Defour was financially supported by a grant from the Caisse d'Epargne Rhone-Alpes. Etienne Lefai is gratefully acknowledged for his helpful discussion. Jean-Claude Barthélémy is acknowledged for the use of Luminex 200. Odile Sabido and Alain Guignandon are acknowledged for their help in using the videomicroscope. Philippe Courpron, Caisse d'Epargne Rhone-Alpes, is also gratefully acknowledged for his constant support.

REFERENCES

1. **Berthon P, Duguez S, Favier FB, Amirouche A, Feasson L, Vico L, Denis C, and Freyssenet D.** Regulation of ubiquitin-proteasome system, caspase enzyme activities, and extracellular proteinases in rat soleus muscle in response to unloading. *Pflugers Arch* 454: 625-633, 2007.
2. **Bodine SC, Latres E, Baumhueter S, Lai VK, Nunez L, Clarke BA, Poueymirou WT, Panaro FJ, Na E, Dharmarajan K, Pan ZQ, Valenzuela DM, DeChiara TM, Stitt TN, Yancopoulos GD, and Glass DJ.** Identification of ubiquitin ligases required for skeletal muscle atrophy. *Science* 294: 1704-1708, 2001.
3. **Cohen HY, Miller C, Bitterman KJ, Wall NR, Hekking B, Kessler B, Howitz KT, Gorospe M, de Cabo R, and Sinclair DA.** Calorie restriction promotes mammalian cell survival by inducing the SIRT1 deacetylase. *Science* 305: 390-392, 2004.
4. **Duguez S, Bihan MC, Gouttefangeas D, Feasson L, and Freyssenet D.** Myogenic and nonmyogenic cells differentially express proteinases, Hsc/Hsp70, and BAG-1 during skeletal muscle regeneration. *Am J Physiol Endocrinol Metab* 285: E206-215, 2003.
5. **Favier FB, Costes F, Defour A, Bonnefoy R, Lefai E, Bauge S, Peinnequin A, Benoit H, and Freyssenet D.** Downregulation of Akt/mammalian target of rapamycin pathway in skeletal muscle is associated with increased REDD1 expression in response to chronic hypoxia. *Am J Physiol Regul Integr Comp Physiol* 298: R1659-1666, 2010.
6. **Fujita S, Dreyer HC, Drummond MJ, Glynn EL, Cadenas JG, Yoshizawa F, Volpi E, and Rasmussen BB.** Nutrient Signalling in the Regulation of Human Muscle Protein Synthesis. *J Physiol*, 2007.
7. **Fulco M, Cen Y, Zhao P, Hoffman EP, McBurney MW, Sauve AA, and Sartorelli V.** Glucose restriction inhibits skeletal myoblast differentiation by activating SIRT1 through AMPK-mediated regulation of Nampt. *Dev Cell* 14: 661-673, 2008.
8. **Furuno K, Goodman MN, and Goldberg AL.** Role of different proteolytic systems in the degradation of muscle proteins during denervation atrophy. *J Biol Chem* 265: 8550-8557, 1990.
9. **Ghosh HS, McBurney M, and Robbins PD.** SIRT1 negatively regulates the mammalian target of rapamycin. *PLoS ONE* 5: e9199, 2010.
10. **Heilbronn LK, Civitarese AE, Bogacka I, Smith SR, Hulver M, and Ravussin E.** Glucose tolerance and skeletal muscle gene expression in response to alternate day fasting. *Obes Res* 13: 574-581, 2005.
11. **Jahnke VE, Sabido O, Defour A, Castells J, Lefai E, Roussel D, and Freyssenet D.** Evidence for mitochondrial respiratory deficiency in rat rhabdomyosarcoma cells. *PLoS ONE* 5: e8637, 2010.
12. **Kimball SR and Jefferson LS.** New functions for amino acids: effects on gene transcription and translation. *Am J Clin Nutr* 83: 500S-507S, 2006.
13. **Lecker SH, Jagoe RT, Gilbert A, Gomes M, Baracos V, Bailey J, Price SR, Mitch WE, and Goldberg AL.** Multiple types of skeletal muscle atrophy involve a common program of changes in gene expression. *Faseb J* 18: 39-51, 2004.
14. **Lee IH, Cao L, Mostoslavsky R, Lombard DB, Liu J, Bruns NE, Tsokos M, Alt FW, and Finkel T.** A role for the NAD-dependent deacetylase Sirt1 in the regulation of autophagy. *Proc Natl Acad Sci U S A* 105: 3374-3379, 2008.
15. **Mammucari C, Milan G, Romanello V, Masiero E, Rudolf R, Del Piccolo P, Burden SJ, Di Lisi R, Sandri C, Zhao J, Goldberg AL, Schiaffino S, and Sandri M.** FoxO3 Controls Autophagy in Skeletal Muscle In Vivo. *Cell Metab* 6: 458-471, 2007.
16. **Mordier S, Deval C, Bechet D, Tassa A, and Ferrara M.** Leucine limitation induces autophagy and activation of lysosome-dependent proteolysis in C2C12 myotubes through a

mammalian target of rapamycin-independent signaling pathway. *J Biol Chem* 275: 29900-29906, 2000.

17. **Morselli E, Maiuri MC, Markaki M, Megalou E, Pasparaki A, Palikaras K, Criollo A, Galluzzi L, Malik SA, Vitale I, Michaud M, Madeo F, Tavernarakis N, and Kroemer G.** Caloric restriction and resveratrol promote longevity through the Sirtuin-1-dependent induction of autophagy. *Cell Death and Disease* 1: e10, 2010.

18. **Nedachi T, Kadotani A, Ariga M, Katagiri H, and Kanzaki M.** Ambient glucose levels qualify the potency of insulin myogenic actions by regulating SIRT1 and FoxO3a in C2C12 myocytes. *Am J Physiol Endocrinol Metab* 294: E668-678, 2008.

19. **Nemoto S, Fergusson MM, and Finkel T.** Nutrient availability regulates SIRT1 through a forkhead-dependent pathway. *Science* 306: 2105-2108, 2004.

20. **Nisoli E, Tonello C, Cardile A, Cozzi V, Bracale R, Tedesco L, Falcone S, Valerio A, Cantoni O, Clementi E, Moncada S, and Carruba MO.** Calorie restriction promotes mitochondrial biogenesis by inducing the expression of eNOS. *Science* 310: 314-317, 2005.

21. **Rodgers JT, Lerin C, Haas W, Gygi SP, Spiegelman BM, and Puigserver P.** Nutrient control of glucose homeostasis through a complex of PGC-1alpha and SIRT1. *Nature* 434: 113-118, 2005.

22. **Sacheck JM, Hyatt JP, Raffaello A, Jagoe RT, Roy RR, Edgerton VR, Lecker SH, and Goldberg AL.** Rapid disuse and denervation atrophy involve transcriptional changes similar to those of muscle wasting during systemic diseases. *Faseb J* 21: 140-155, 2007.

23. **Sacheck JM, Ohtsuka A, McLary SC, and Goldberg AL.** IGF-I stimulates muscle growth by suppressing protein breakdown and expression of atrophy-related ubiquitin ligases, atrogin-1 and MuRF1. *Am J Physiol Endocrinol Metab* 287: E591-601, 2004.

24. **Sandri M, Sandri C, Gilbert A, Skurk C, Calabria E, Picard A, Walsh K, Schiaffino S, Lecker SH, and Goldberg AL.** Foxo transcription factors induce the atrophy-related ubiquitin ligase atrogin-1 and cause skeletal muscle atrophy. *Cell* 117: 399-412, 2004.

25. **Stitt TN, Drujan D, Clarke BA, Panaro F, Timofeyva Y, Kline WO, Gonzalez M, Yancopoulos GD, and Glass DJ.** The IGF-1/PI3K/Akt pathway prevents expression of muscle atrophy-induced ubiquitin ligases by inhibiting FOXO transcription factors. *Mol Cell* 14: 395-403, 2004.

26. **Taillandier D, Aurousseau E, Meynial-Denis D, Bechet D, Ferrara M, Cottin P, Ducastaing A, Bigard X, Guezennec CY, Schmid HP, and et al.** Coordinate activation of lysosomal, Ca 2+-activated and ATP-ubiquitin-dependent proteinases in the unweighted rat soleus muscle. *Biochem J* 316 (Pt 1): 65-72, 1996.

27. **Zhao J, Brault JJ, Schild A, Cao P, Sandri M, Schiaffino S, Lecker SH, and Goldberg AL.** FoxO3 Coordinately Activates Protein Degradation by the Autophagic/Lysosomal and Proteasomal Pathways in Atrophying Muscle Cells. *Cell Metab* 6: 472-483, 2007.

FIGURE LEGENDS

Figure 1. C2C12 myotube area during fasting and refeeding. C2C12 myotube area was determined by using AxioVision 4.7. Data are means ± SE from 10 myotubes. *** $P < 0.001$: significantly different from 0 min; † $P < 0.05$: significantly different from 240 min.

Figure 2. Glucose consumption and lactate production of C2C12 myotubes following fasting. *A)* Glucose consumption. *B)* Lactate production. Data are means ± SE from 8 independent experiments. Dotted lines indicate glucose consumption and lactate production of control myotubes. * $P < 0.05$, ** $P < 0.01$, and *** $P < 0.001$: significantly different from control myotubes.

Figure 3. Regulation of Akt/mTOR pathway during fasting and refeeding in C2C12 myotubes. Protein levels were determined by using Luminex technology and western blot. *A)*. Phospho-Akt S473 (♦) and total Akt (○) proteins. *B)* Phospho-GSK3 S21/S9 protein level. *C)* Phospho-p70S6K T412 (♦) and total p70S6K (○) proteins levels. *D)* A representative immunoblot of S6 S235/S236 phosphorylation level. *E)* Phospho-S6 S235/S236 protein level. Data are means ± SE from 4-7 independent experiments. * $P < 0.05$, ** < 0.01 and *** $P < 0.001$: significantly different from 0 min; ††† $P < 0.001$: significantly different from 240 min.

Figure 4. Chymotrypsin-like (○) and trypsin-like (♦) enzyme activities of 26S proteasome during fasting and refeeding in C2C12 myotubes. Data are means ± SE from 8 independent experiments.

Figure 5. Cathepsin B+L enzyme activity during fasting and refeeding in C2C12 myotubes. Data are means ± SE from 8 independent experiments. * $P < 0.05$, ** $P < 0.01$, and *** $P < 0.001$: significantly different from 0 min.

Figure 1

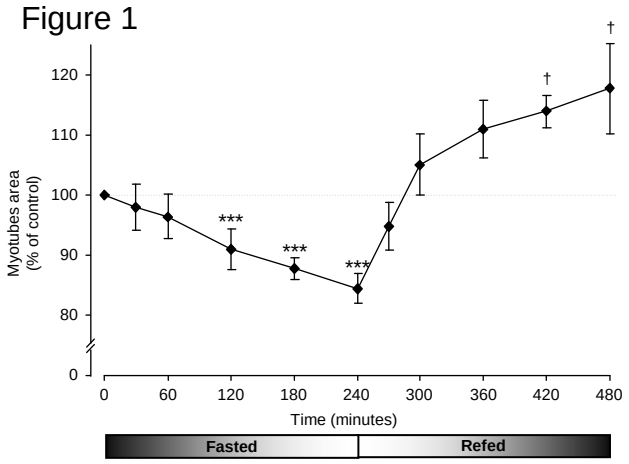
Myotubes area
(% of control)
120
110
100
90
80
0
***
***
***
†
†
0
60
120
180
240
300
360
420
480
Time (minutes)
Fasted
Refed

Figure 2

A

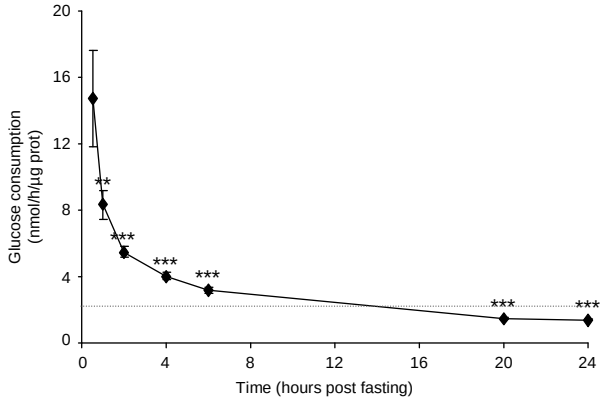
Glucose consumption
(nmol/h/µg prot)
20
16
12
8
4
0
0
4
8
12
16
20
24
Time (hours post fasting)
**
***
***
***
***
***

B

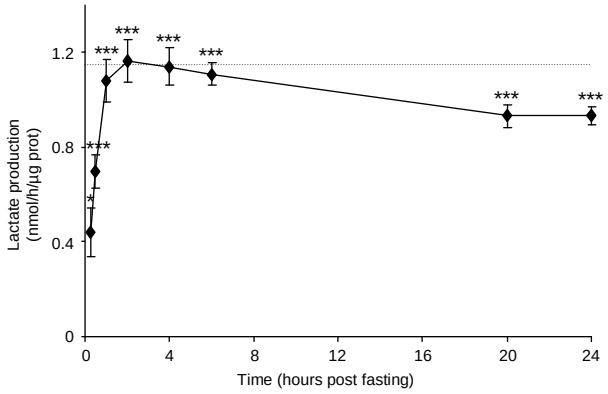
Lactate production
(nmol/h/µg prot)
1.2
0.8
0.4
0
0
4
8
12
16
20
24
Time (hours post fasting)
*
***
***
***
***
***
***
***

Figure 3

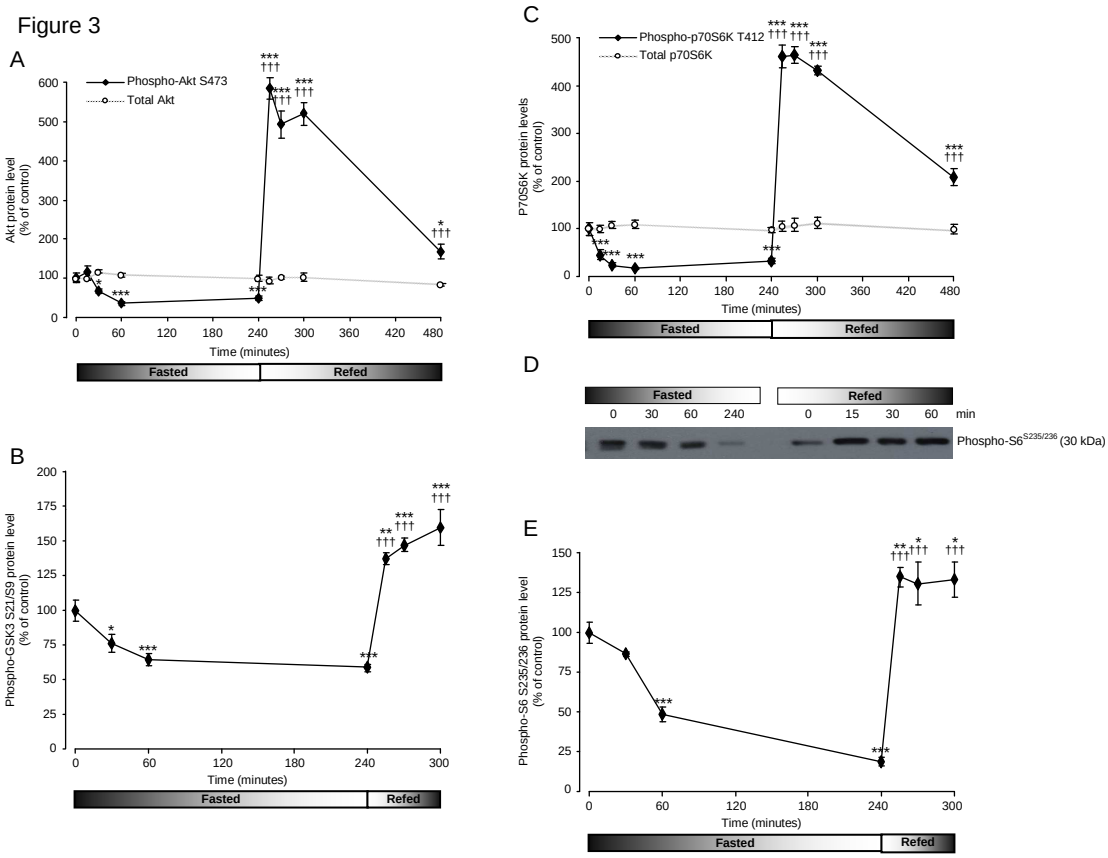
A
Phospho-Akt S473
Total Akt
Akt protein level (% of control)
Time (minutes)
Fasted
Refed
B
Phospho-GSK3 S21/S9 protein level (% of control)
Time (minutes)
Fasted
Refed
C
Phospho-p70S6K T412
Total p70S6K
P70S6K protein levels (% of control)
Time (minutes)
Fasted
Refed
D
Fasted
Refed
min
Phospho-S6S235/236 (30 kDa)
E
Phospho-S6 S235/236 protein level (% of control)
Time (minutes)
Fasted
Refed

Figure 4

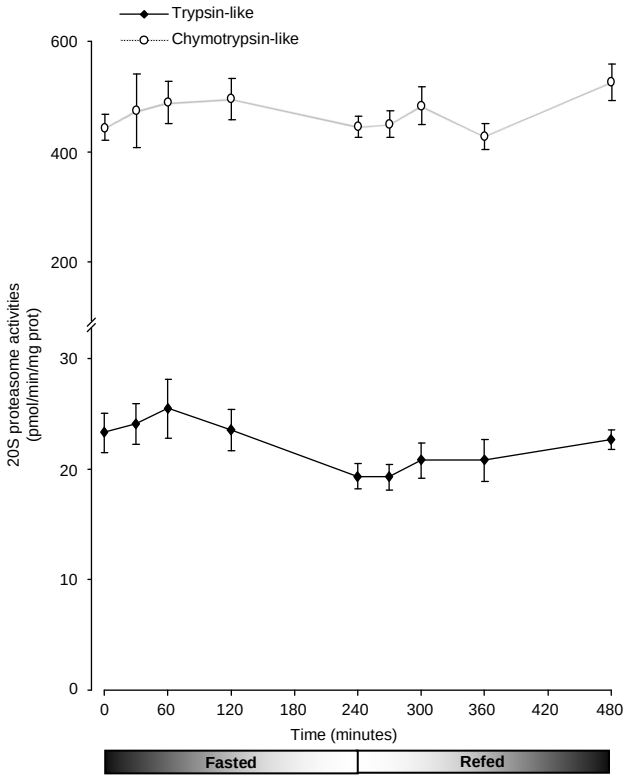
Trypsin-like
Chymotrypsin-like
600
400
200
30
20
10
0
20S proteasome activities
(pmol/min/mg prot)
0
60
120
180
240
300
360
420
480
Time (minutes)
Fasted
Refed

Figure 5

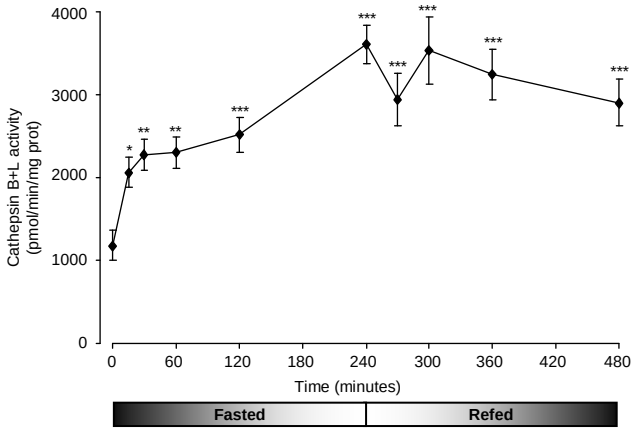
Cathepsin B+L activity
(pmol/min/mg prot)
4000
3000
2000
1000
0
0
60
120
180
240
300
360
420
480
Time (minutes)
Fasted
Refed

DISCUSSION

Lors de notre première étude, nous avons montré que :

- Sirt1 régulait l'expression génique de SREBP-1c de façon dépendante de LXR, et que ce mécanisme pourrait permettre de réguler l'expression de l'hexokinase II (Figure 24),
- l'EX527, un inhibiteur de Sirt1, permettrait de réduire d'environ 20 % la consommation de glucose de myotubes C2C12.

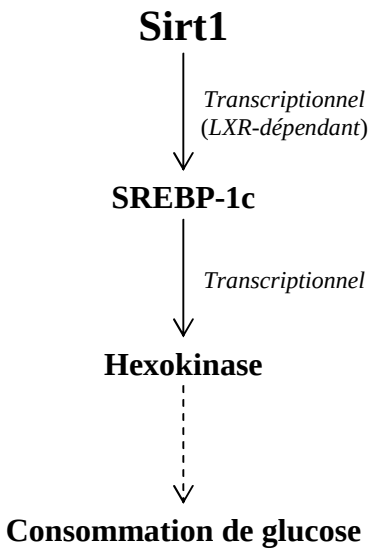

Figure 26. Schéma récapitulatif du mécanisme d'action potentiel de Sirt1 sur la régulation du métabolisme du glucose (LXR : liver X receptor ; Sirt1 : sirtuine 1 ; SREBP-1c : sterol regulatory element binding protein 1c).

Notre seconde étude *in vitro* sur des myotubes C2C12 a mis en évidence les évènements suivants :

- une inhibition marquée de la voie Akt/mTOR lors du jeûne qui précède l'amyotrophie des myotubes,
- une stimulation de la consommation de glucose lors de la renutrition des myotubes dénutrits,
- une augmentation de l'activité enzymatique cathepsine B + L lors du jeûne, augmentation se poursuivant lors de la renutrition.

Cette discussion n'a pas pour objet de reprendre les éléments déjà discutés dans les manuscrits, mais tentera plutôt d'apporter de nouveaux arguments de réflexion à travers la présentation de données préliminaires récemment acquises et le développement de plusieurs

perspectives. Nous présenterons d'abord dans une première partie les intérêts et les limites des modèles expérimentaux, puis dans une seconde partie l'implication de Sirt1 dans la régulation de l'expression de LXR et de SREBP-1c, puis dans une troisième partie l'implication de Sirt1 dans la régulation du métabolisme du glucose, et enfin dans une dernière partie le rôle éventuel de Sirt1 dans la régulation de la masse musculaire.

I. INTERETS ET LIMITES DES MODELES EXPERIMENTAUX

1. Intérêts des modèles expérimentaux

De nombreux travaux ont étudié les effets de Sirt1 sur la régulation du métabolisme énergétique dans le muscle strié squelettique (80, 134, 135). Contrairement aux études de la littérature qui utilisent largement des drogues pour stimuler l'activité de Sirt1, nous avons travaillé avec un modèle génétique de souris déficientes pour l'exon 4 de Sirt1 ($Sirt1^{\Delta ex4/\Delta ex4}$) ce qui nous permet de cibler directement et spécifiquement Sirt1. En effet, l'utilisation des activateurs de Sirt1 est largement controversée dans la littérature (paragraphe V.2.b de la seconde partie de la revue bibliographique). De plus, dans notre modèle de souris $Sirt1^{\Delta ex4/\Delta ex4}$, aucun challenge métabolique n'a été utilisé. En effet, la stimulation du métabolisme oxydatif par le resveratrol ou le SRT1720 n'a été observé que chez des souris soumises à un régime gras (80, 134). Nos données *in vivo* témoignent donc des effets à long terme d'une invalidation de Sirt1 indépendamment de tout régime. Nous avons par contre utilisé un inhibiteur de Sirt1, l'EX527, mais dont l'action spécifique a été clairement validée (92, 194).

2. Limites des modèles expérimentaux

La première limite de notre modèle de souris $Sirt1^{\Delta ex4/\Delta ex4}$ est l'effet éventuel compensatoire de l'invalidation de Sirt1 par une ou plusieurs autres sirtuines. Le taux de survie des souris KO Sirt1 à la naissance étant très faible (128, 202), on peut envisager que les souris qui ont survécu, ont compensé l'invalidation de Sirt1 par la surexpression d'une autre

sirtuine. Nous avons donc mesuré les niveaux en ARNm de Sirt6 et de Sirt2 (Figure 25). A l'exception de l'augmentation de Sirt6 dans le muscle *gastrocnemius* des souris Sirt1$^{\Delta ex4/\Delta ex4}$, aucune autre modification n'a été observée. Si effet compensatoire il y a, celui-ci ne serait probablement pas dû à la surexpression de Sirt2 ou Sirt6.

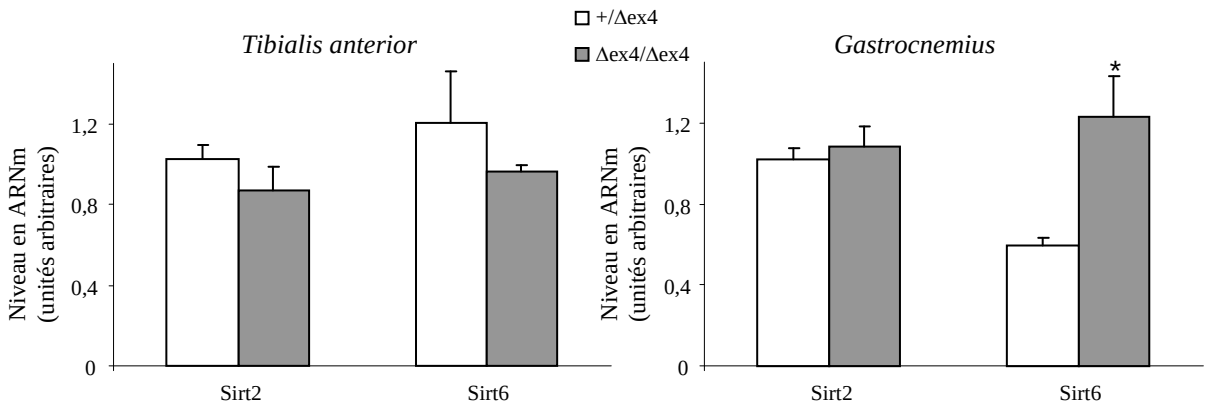

Figure 25. Niveau d'expression en ARNm de Sirt2 et Sirt6 dans le *tibialis anterior* et le *gastrocnemius* chez les souris Sirt1$^{\Delta ex4/\Delta ex4}$ et les souris contrôles Sirt1$^{+/\Delta ex4}$ (* $p < 0,05$: significativement différent de Sirt1$^{+/\Delta ex4}$; ARNm : acide ribonucléique messager ; ex4 : exon 4 ; Sirt : sirtuine).

Une autre limite à notre étude est l'utilisation de souris hétérozygotes (Sirt1$^{+/\Delta ex4}$) comme souris contrôles. Ainsi, il est possible que des modifications géniques soient aussi présentes chez les souris Sirt1$^{+/\Delta ex4}$, comme cela a été décrit pour la lypolyse (75). Cependant, ces modifications, si elles existent, ne pourraient que minimiser les effets observés dans notre étude.

Enfin, une limitation majeure à notre travail est le nombre restreint d'animaux avec lesquels nous avons travaillé. Comme il nous a été malheureusement impossible d'élever ces animaux à l'animalerie de Saint Etienne, nous avons uniquement pu recevoir les tissus musculaires prélevés sur quatre animaux.

En ce qui concerne le modèle *in vitro* de challenge métabolique, la principale limite est la privation totale en nutriments des myotubes C2C12, ce qui ne nous permet pas de différencier les effets respectifs de certaines molécules. Par exemple, nous ne pouvons pas différencier les effets de la restriction en glucose, qui augmentent le ratio NAD^+/NADH et donc qui active potentiellement Sirt1 (121), de ceux de la restriction en leucine, qui inhibent la voie Akt/mTOR (203).

II. SIRT1, SREBP-1c et LXR

L'invalidation de l'exon 4 chez les souris Sirt1$^{+/\Delta ex4}$ a permis de mettre en évidence que Sirt1 régulait l'expression génique de SREBP-1c de façon dépendante de LXR, ce mécanisme pouvant réguler l'expression de l'hexokinase II. Cependant, le mécanisme d'action de Sirt1 sur LXR reste à déterminer. Il a été montré, chez des cellules HEK293T, que Sirt1 déacétylait la lysine K432 de LXR-α du complexe LXR/RXR, ce qui permettrait d'activer la dégradation de LXR mais aussi son renouvellement et donc l'activité transcriptionnelle des promoteurs des gènes cibles (119) (Figure 19). Il serait donc intéressant de mesurer le niveau d'acétylation de LXR-α et –β. En collaboration avec l'équipe d'Etienne Lefai (UMR 870, Lyon), nous avons pu réaliser un profil d'acétylation par western blot des muscles prélevés chez les souris Sirt1$^{+/\Delta ex4}$ et Sirt1$^{\Delta ex4/\Delta ex4}$ (Figure 26).

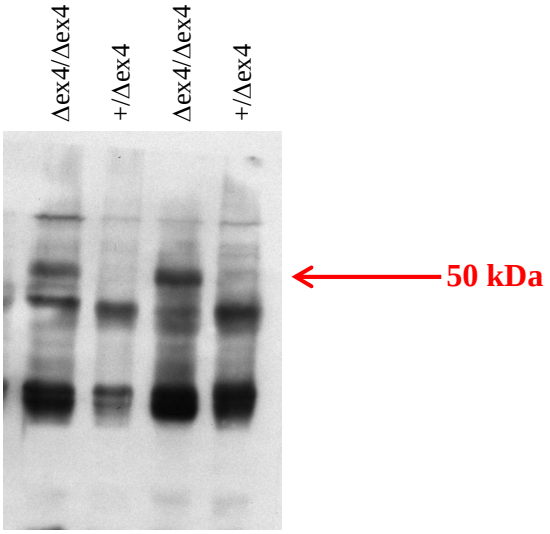

Figure 26. Niveau d'acétylation global du muscle *gastrocnemius* chez des souris Sirt1$^{\Delta ex4/\Delta ex4}$ et les souris contrôles Sirt1$^{+/\Delta ex4}$ (ex4 : exon 4 ; kDa : kilodaltons : Sirt1 : sirtuine 1).

Outre l'hyperacétylation globale des souris Sirt1$^{\Delta ex4/\Delta ex4}$, il apparaît systématiquement une bande hyperacétylée à environ 50 kDa, qui n'est pas présente chez les souris contrôles Sirt1$^{+/\Delta ex4}$. De façon intriguante, ce poids moléculaire est celui de LXR. Afin de valider l'origine de cette bande, nous envisageons donc de réaliser une immunoprécipitation LXR suivie d'une révélation western blot avec un anticorps lysine anti-acétylée. Ceci permettra de valider le mécanisme d'action de Sirt1 décrit dans le manuscrit 1.

III. SIRT1 ET METABOLISME DU GLUCOSE

Nos données permettent de mettre en lumière l'implication potentielle de Sirt1 dans la régulation de l'hexokinase II (Figure 24). Cependant, il est aussi possible d'envisager une action de Sirt1 sur la régulation de l'expression d'autres protéines associées au métabolisme du glucose. GLUT4 (glucose transporter type 4) pourrait être une cible. En effet, nos analyses du niveau d'expression de GLUT4 laissent penser qu'il pourrait être soumis à une régulation par Sirt1 (Figure 27). Toutefois, notre effectif de souris est beaucoup trop réduit pour que nous puissions valider cette hypothèse.

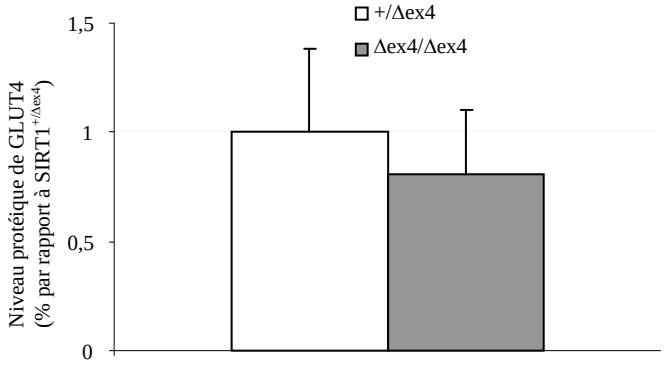

Figure 27. Niveau d'expression protéique de GLUT4 dans le muscle *gastrocnemius* chez les souris $Sirt1^{\Delta ex4/\Delta ex4}$ et les souris contrôles $Sirt1^{+/\Delta ex4}$ (ex4 : exon 4 ; GLUT4 : glucose transporter type 4 ; Sirt1 : sirtuine 1).

Au-delà de l'expression de GLUT4, ceci pose la question de l'action ciblée ou généralisée de Sirt1 sur l'expression des gènes associés au métabolisme du glucose. Puisque Sirt1 stimule la sécrétion de l'insuline par le pancréas (142, 143), il aurait été intéressant de mesurer la glycémie et la réponse de nos animaux à un test de tolérance au glucose. Afin d'apporter des éléments de réponse, nous avons montré *in vitro* que l'EX527, un inhibiteur de Sirt1, réduisait d'environ 20 % la consommation de glucose de myotubes C2C12, illustrant le rôle fonctionnel majeur de Sirt1 dans la régulation du métabolisme du glucose en situation normale, indépendemment de tout challenge métabolique. Mais cette expérience ne répond pas encore à la question énoncée ci-dessus. Pour déterminer si Sirt1 exerce un effet sur la capture du glucose, il faudrait mesurer l'entrée du 2-déoxy-glucose dans la cellule. Par ailleurs, une analyse plus complète du niveau d'expression des différentes enzymes de la glycolyse permettrait de savoir si l'effet de Sirt1 est ciblé ou au contraire général.

De façon indirecte, notre seconde étude montre que le niveau en ARNm Sirt1 est fortement stimulé lors de la renutrition chez les myotubes dénutrits (Figure 28), et ceci de façon concommitante à la stimulation de l'expression de l'hexokinase (Figure 29) et de la consommation de glucose. Bien qu'indirecte, ces données supportent l'importance de Sirt1 dans la régulation du métabolisme du glucose par la cellule musculaire.

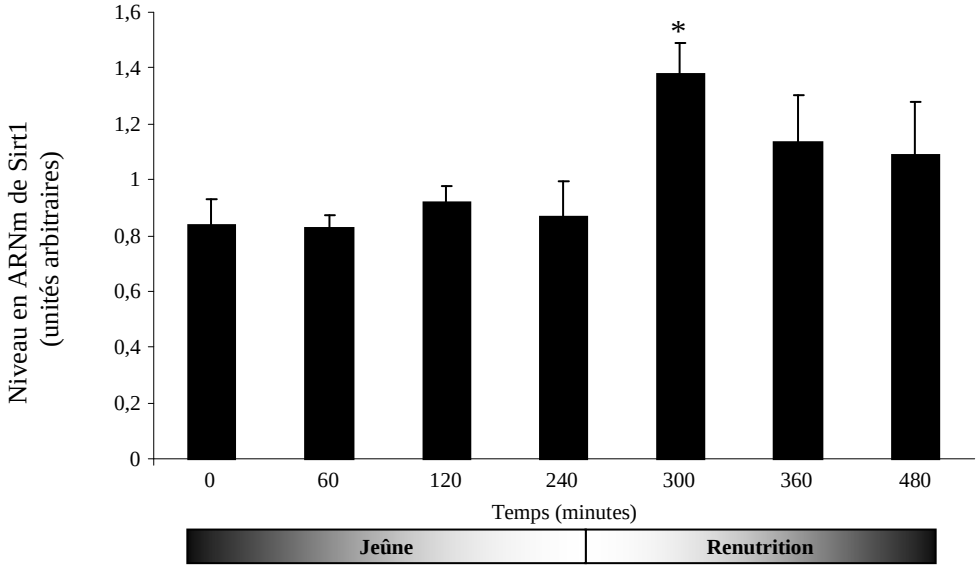

Figure 28. Niveau d'expression en ARNm de Sirt1 au cours d'un jeûne suivi d'une renutrition chez des myotubes C2C12 (* $p < 0,05$: significativement différent de 0 min ; ARNm : acide ribonucléique messager ; Sirt1 : sirtuine 1).

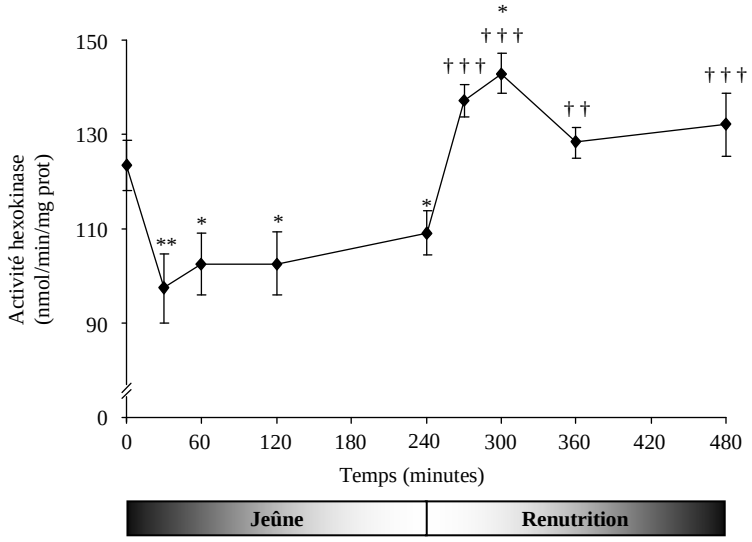

Figure 2. Niveau enzymatique de l'hexokinase au cours d'un jeûne suivi d'une renutrition chez des myotubes C2C12 (* $p < 0,05$, ** $p < 0,01$: significativement différent de 0 min et †† $p < 0,01$, ††† $p < 0,001$: significativement différent de 240 min ; mg : milligramme ; min : minute ; nmol : nanomole).

IV. SIRT1 ET MASSE MUSCULAIRE

Il a été démontré que Sirt1 était impliquée dans la régulation de la myogenèse chez des cellules musculaires C2C12 avec notamment une action de régulation négative sur les facteurs transcriptionnels muscle-spécifiques MyoD, myogénine et MEF2C (120). Or ces facteurs sont connus pour intervenir dans la régulation de l'expression des protéines muscle-spécifiques, cela pose donc la question de l'implication de Sirt1 dans la régulation de ces protéines dans le muscle strié adulte et de l'impact que cela pourrait avoir sur la masse musculaire. Nous avons observé dans notre première étude une diminution du poids des muscles des animaux Sirt1$^{\Delta ex4/\Delta ex4}$; toutefois cette différence n'était plus observée lorsque l'on ramenait le poids de muscle au poids de corps (voir tableau 1 manuscrit I). Ceci serait donc plutôt dû à un effet freinateur de Sirt1 sur la croissance (voir (32) pour une revue de la littérature).

Récemment, il a été montré que le niveau de phosphorylation de mTOR (mammalian target of rapamycin), S6K (ribosomal protein S6 kinase), S6 (ribosomal protein S6) et 4E-BP1 (eukaryotic initiation factor 4E-binding protein 1) était régulé positivement dans des MEFs issus de souris déficientes pour Sirt1 (204), ceci laissant supposer que la synthèse des protéines serait activée dans ces conditions. En accord avec ces données, nous avons également pu observer une tendance à l'augmentation de la phosphorylation des protéines AktP^{Ser473} et S6P$^{Ser235/236}$ dans le muscle *tibialis anterior* des souris Sirt1$^{\Delta ex4/\Delta ex4}$ (Figure 30). L'ensemble de ces résultats suggère que Sirt1 pourrait intervenir dans la régulation de la synthèse des protéines. Toutefois, ceci reste à démontrer.

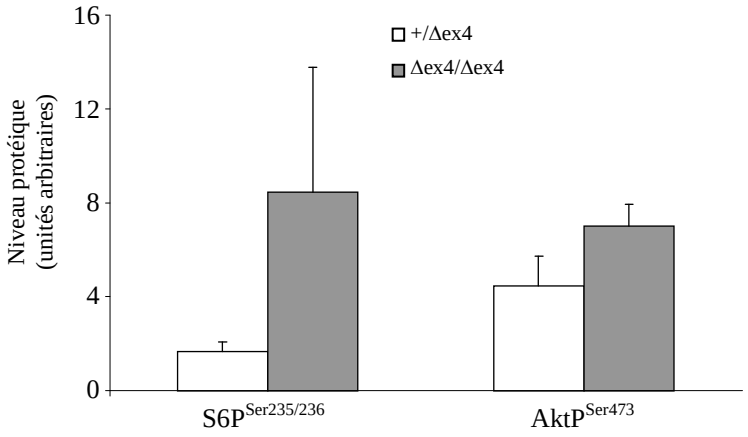

Figure 30. Niveau d'expression des protéines AktP^{Ser473} et S6P$^{Ser235/236}$ dans le muscle *tibialis anterior* chez les souris Sirt1$^{\Delta ex4/\Delta ex4}$ et les souris contrôles Sirt1$^{+/\Delta ex4}$ (ex4 : exon 4 ; S6P : ribosomal protein S6 ; Sirt1 : sirtuine 1).

Par ailleurs, des données récentes impliqueraient Sirt1 dans la stimulation de l'autophagie (100, 205) (voir discussion manuscrit II). Compte-tenu de l'importance de l'autophagie dans la régulation de la masse musculaire lors du jeûne (206, 207), l'implication fonctionnelle de Sirt1 dans ce mécanisme est à envisager dans la seconde étude. Nos données (Figure 28) montrent que le niveau en ARNm de Sirt1 n'est pas modifié durant le jeûne, alors que l'on peut observer une forte stimulation de ce niveau après 1 heure de renutrition. Fulco *et al*. ont montré que la restriction en glucose augmentait le ratio NAD^+/NADH, stimulant ainsi l'activité de Sirt1 (121). Il est donc tout à fait possible dans notre étude, que malgré l'absence d'augmentation du niveau en ARNm de Sirt1 lors du jeûne, l'activité de Sirt1 puisse être stimulée afin de réguler l'autophagie. De façon intéressante, l'augmentation transitoire du niveau en ARNm de Sirt1 au cours de la renutrition se produit dans une situation où le ratio NAD^+/NADH est diminué (121), réduisant ainsi l'activité de Sirt1. Il serait donc intéressant de déterminer :

- le niveau d'acétylation d'un substrat connu de Sirt1 comme p53 pour déterminer à quel moment (jeûne ou renutrition) l'activité de Sirt1 est modifiée,

- le niveau d'expression d'un certain nombre de marqueurs de l'autophagie tels que Binp3, Gabarapl1, LC3b et Vps34,

- si l'inhibiteur EX527 permet de modifier la régulation de l'expression des gènes de l'autophagie au cours du challenge métabolique.

CONCLUSION ET PERSPECTIVES

Les données de la première étude montrent clairement une implication fonctionnelle de Sirt1 dans la régulation du métabolisme du glucose dans le muscle strié squelettique. Au-delà des expérimentations qui permettront de renforcer nos résultats, il serait intéressant d'étudier le rôle de Sirt1 dans la régulation du métabolisme du glucose en situations pathologiques. Ainsi, il a été montré que l'expression de Sirt1 était réduite chez des sujets insulino-résistants (208). L'effet observé de l'EX527 mérite donc d'être validé *in vivo* dans un modèle de souris soumises à un régime gras.

Nous avons vu que les données de la seconde étude soulèvent plus de questions qu'elles n'apportent de réponses. Il est donc dans un premier temps important de mettre en place les expérimentations qui permettront d'apporter des éléments de réponse (voir discussion). Dans un second temps, si l'hypothèse de Sirt1 dans la régulation de l'autophagie s'avère exacte, il serait intéressant d'élargir notre étude à d'autres conditions physiologiques ou pathologiques dans lesquelles l'autophagie est stimulée comme l'hypoxie.

REFERENCES

1. Strahl B., D. Allis C. D. (2000) The language of covalent histone modifications. *Nature* 403:41-5.
2. Ito K., Barnes P. J., Adcock I. M. (2000) Glucocorticoid receptor recruitment of histone deacetylase 2 inhibits interleukin-1beta-induced histone H4 acetylation on lysines 8 and 12. *Mol Cell Biol* 20:6891-903.
3. Kornberg R. D., Lorch Y. (1999) Twenty-five years of the nucleosome, fundamental particle of the eukaryote chromosome. *Cell* 98:285-94.
4. de Ruijter A. J., van Gennip A. H., Caron H. N., Kemp S., van Kuilenburg A. B. (2003) Histone deacetylases (HDACs): characterization of the classical HDAC family. *Biochem J* 370:737-49.
5. Wade P. A. (2001) Transcriptional control at regulatory checkpoints by histone deacetylases: molecular connections between cancer and chromatin. *Hum Mol Genet* 10:693-8.
6. Forsberg E. C., Bresnick E. H. (2001) Histone acetylation beyond promoters: long-range acetylation patterns in the chromatin world. *Bioessays* 23:820-30.
7. Marmorstein R., Trievel R. C. (2009) Histone modifying enzymes: structures, mechanisms, and specificities. *Biochim Biophys Acta* 1789:58-68.
8. Marmorstein R., Roth S. Y. (2001) Histone acetyltransferases: function, structure, and catalysis. *Curr Opin Genet Dev* 11:155-61.
9. Mariadason J. M. (2008) HDACs and HDAC inhibitors in colon cancer. *Epigenetics* 3:28-37.
10. Kruszewski M., Szumiel I. (2005) Sirtuins (histone deacetylases III) in the cellular response to DNA damage-facts and hypotheses. *DNA Repair (Amst)* 4:1306-13.
11. Gao L., Cueto M. A., Asselbergs F., Atadja P. (2002) Cloning and functional characterization of HDAC11, a novel member of the human histone deacetylase family. *J Biol Chem* 277:25748-55.
12. Ivy J. M., Klar A. J., Hicks J. B. (1986) Cloning and characterization of four SIR genes of Saccharomyces cerevisiae. *Mol Cell Biol* 6:688-702.
13. Rine J., Strathern J. N., Hicks J. B., Herskowitz I. (1979) A suppressor of mating-type locus mutations in Saccharomyces cerevisiae: evidence for and identification of cryptic mating-type loci. *Genetics* 93:877-901.
14. Klar A. J., Fogel S., Macleod K. (1979) MAR1-a Regulator of the HMa and HMalpha Loci in SACCHAROMYCES CEREVISIAE. *Genetics* 93:37-50.
15. Frye R. A. (2000) Phylogenetic classification of prokaryotic and eukaryotic Sir2-like proteins. *Biochem Biophys Res Commun* 273:793-8.
16. Landry J., Sutton A., Tafrov S. T., Heller R. C., Stebbins J., Pillus L., Sternglanz R. (2000) The silencing protein SIR2 and its homologs are NAD-dependent protein deacetylases. *Proc Natl Acad Sci U S A* 97:5807-11.
17. Imai S., Armstrong C. M., Kaeberlein M., Guarente L. (2000) Transcriptional silencing and longevity protein Sir2 is an NAD-dependent histone deacetylase. *Nature* 403:795-800.
18. Smith J. S., Brachmann C. B., Celic I., Kenna M. A., Muhammad S., Starai V. J., Avalos J. L., Escalante-Semerena J. C., Grubmeyer C., Wolberger C., Boeke J. D. (2000) A phylogenetically conserved NAD+-dependent protein deacetylase activity in the Sir2 protein family. *Proc Natl Acad Sci U S A* 97:6658-63.
19. Kaeberlein M., McVey M., Guarente L. (1999) The SIR2/3/4 complex and SIR2 alone promote longevity in Saccharomyces cerevisiae by two different mechanisms. *Genes Dev* 13:2570-80.
20. Tissenbaum H. A., Guarente L. (2001) Increased dosage of a sir-2 gene extends lifespan in Caenorhabditis elegans. *Nature* 410:227-30.

21. Rogina B., Helfand S. L. (2004) Sir2 mediates longevity in the fly through a pathway related to calorie restriction. *Proc Natl Acad Sci U S A* 101:15998-6003.
22. Heilbronn L. K., Ravussin E. (2003) Calorie restriction and aging: review of the literature and implications for studies in humans. *Am J Clin Nutr* 78:361-9.
23. Lin S. J., Defossez P. A., Guarente L. (2000) Requirement of NAD and SIR2 for life-span extension by calorie restriction in Saccharomyces cerevisiae. *Science* 289:2126-8.
24. Frye R. A. (1999) Characterization of five human cDNAs with homology to the yeast SIR2 gene: Sir2-like proteins (sirtuins) metabolize NAD and may have protein ADP-ribosyltransferase activity. *Biochem Biophys Res Commun* 260:273-9.
25. Michishita E., Park J. Y., Burneskis J. M., Barrett J. C., Horikawa I. (2005) Evolutionarily conserved and nonconserved cellular localizations and functions of human SIRT proteins. *Mol Biol Cell* 16:4623-35.
26. Michan S., Sinclair D. (2007) Sirtuins in mammals: insights into their biological function. *Biochem J* 404:1-13.
27. Denu, J. M. (2003) Linking chromatin function with metabolic networks: Sir2 family of NAD(+)-dependent deacetylases. *Trends Biochem Sci* 28:41-8.
28. Denu J. M. (2005) The Sir 2 family of protein deacetylases. *Curr Opin Chem Biol* 9:431-40.
29. Tanny J. C., Moazed D. (2001) Coupling of histone deacetylation to NAD breakdown by the yeast silencing protein Sir2: Evidence for acetyl transfer from substrate to an NAD breakdown product. *Proc Natl Acad Sci U S A* 98:415-20.
30. Feige J. N., Auwerx J. (2008) Transcriptional targets of sirtuins in the coordination of mammalian physiology. *Curr Opin Cell Biol* 20:303-9.
31. Vinciguerra M., Fulco M., Ladurner A., Sartorelli V., Rosenthal N. (2010) SirT1 in muscle physiology and disease: lessons from mouse models. *Dis Model Mech* 3:298-303.
32. Finkel T., Deng C. X., Mostoslavsky R. (2009) Recent progress in the biology and physiology of sirtuins. *Nature* 460:587-91.
33. Voelter-Mahlknecht S., Mahlknecht U. (2006) Cloning, chromosomal characterization and mapping of the NAD-dependent histone deacetylases gene sirtuin 1. *Int J Mol Med* 17:59-67.
34. Huhtiniemi T., Wittekindt C., Laitinen T., Leppanen J., Salminen A., Poso A., Lahtela-Kakkonen M. (2006) Comparative and pharmacophore model for deacetylase SIRT1. *J Comput Aided Mol Des* 20:589-99.
35. Avalos J. L., Boeke J. D., Wolberger C. (2004) Structural basis for the mechanism and regulation of Sir2 enzymes. *Mol Cell* 13:639-48.
36. Autiero I., Costantini S., Colonna G. (2009) Human sirt-1: molecular modeling and structure-function relationships of an unordered protein. *PLoS One* 4:e7350.
37. Kwon H. S., Ott M. (2008) The ups and downs of SIRT1. *Trends Biochem Sci* 3:517-25.
38. Cohen H. Y., Miller C., Bitterman K. J., Wall N. R., Hekking B., Kessler B., Howitz K. T., Gorospe M., de Cabo R., Sinclair D. A. (2004) Calorie restriction promotes mammalian cell survival by inducing the SIRT1 deacetylase. *Science* 305:390-2.
39. Nisoli E., Tonello C., Cardile A., Cozzi V., Bracale R., Tedesco L., Falcone S., Valerio A., Cantoni O., Clementi E., Moncada S., Carruba M. O. (2005) Calorie restriction promotes mitochondrial biogenesis by inducing the expression of eNOS. *Science* 310:314-7.
40. Qin W., Yang T., Ho L., Zhao Z., Wang J., Chen L., Thiyagarajan M., Macgrogan D., Rodgers J. T., Puigserver P., Sadoshima J., Deng H. H., Pedrini S., Gandy S., Sauve

A., Pasinetti G. M. (2006) Neuronal SIRT1 activation as a novel mechanism underlying the prevention of Alzheimer's disease amyloid neuropathology by calorie restriction. *J Biol Chem* 281:21745-54.

41. Civitarese A. E., Carling S., Heilbronn L. K., Hulver M. H., Ukropcova B., Deutsch W. A., Smith S. R., Ravussin E. (2007) Calorie Restriction Increases Muscle Mitochondrial Biogenesis in Healthy Humans. *PLoS Med* 4:e76.
42. Firestein R., Blander G., Michan S., Oberdoerffer P., Ogino S., Campbell J., Bhimavarapu A., Luikenhuis S., de Cabo R., Fuchs C., Hahn W. C., Guarente L. P., Sinclair D. A. (2008) The SIRT1 deacetylase suppresses intestinal tumorigenesis and colon cancer growth. *PLoS ONE* 3:e2020.
43. Sun C., Zhang F., Ge X., Yan T., Chen X., Shi X., Zhai Q. (2007) SIRT1 Improves Insulin Sensitivity under Insulin-Resistant Conditions by Repressing PTP1B. *Cell Metab* 6:307-19.
44. Heilbronn L. K., Civitarese A. E., Bogacka I., Smith S. R., Hulver M., Ravussin E. (2005) Glucose tolerance and skeletal muscle gene expression in response to alternate day fasting. *Obes Res* 13:574-81.
45. Chen D., Bruno J., Easlon E., Lin S. J., Cheng H. L., Alt F. W., Guarente L. (2008) Tissue-specific regulation of SIRT1 by calorie restriction. *Genes Dev* 22:1753-7.
46. Kim D., Nguyen M. D., Dobbin M. M., Fischer A., Sananbenesi F., Rodgers J. T., Delalle I., Baur J. A., Sui G., Armour S. M., Puigserver P., Sinclair D. A., Tsai L. H. (2007) SIRT1 deacetylase protects against neurodegeneration in models for Alzheimer's disease and amyotrophic lateral sclerosis. *Embo J* 26:3169-79.
47. Prozorovski T., Schulze-Topphoff U., Glumm R., Baumgart J., Schroter F., Ninnemann O., Siegert E., Bendix I., Brustle O., Nitsch R., Zipp F., Aktas O. (2008) Sirt1 contributes critically to the redox-dependent fate of neural progenitors. *Nat Cell Biol* 10:385-94.
48. Sakamoto J., Miura T., Shimamoto K., Horio Y. (2004) Predominant expression of Sir2alpha, an NAD-dependent histone deacetylase, in the embryonic mouse heart and brain. *FEBS Lett* 556:281-6.
49. Sasaki T., Maier B., Bartke A., Scrable H. (2006) Progressive loss of SIRT1 with cell cycle withdrawal. *Aging Cell* 5:413-22.
50. Suwa M., Nakano H., Radak Z., Kumagai S. (2008) Endurance exercise increases the SIRT1 and peroxisome proliferator-activated receptor gamma coactivator-1alpha protein expressions in rat skeletal muscle. *Metabolism* 57:986-98.
51. Rathbone C. R., Booth F. W., Lees S. J. (2009) Sirt1 increases skeletal muscle precursor cell proliferation. *Eur J Cell Biol* 88:35-44.
52. Kume S., Uzu T., Horiike K., Chin-Kanasaki M., Isshiki K., Araki S., Sugimoto T., Haneda M., Kashiwagi A., Koya D. (2010) Calorie restriction enhances cell adaptation to hypoxia through Sirt1-dependent mitochondrial autophagy in mouse aged kidney. *J Clin Invest* 120:1043-55.
53. Nemoto S., Fergusson M. M., Finkel T. (2004) Nutrient availability regulates SIRT1 through a forkhead-dependent pathway. *Science* 306:2105-8.
54. Wang C., Chen L., Hou X., Li Z., Kabra N., Ma Y., Nemoto S., Finkel T., Gu W., Cress W. D., Chen J. (2006) Interactions between E2F1 and SirT1 regulate apoptotic response to DNA damage. *Nat Cell Biol* 8:1025-31.
55. Nahle Z., Polakoff J., Davuluri R. V., McCurrach M. E., Jacobson M. D., Narita M., Zhang M. Q., Lazebnik Y., Bar-Sagi D., Lowe S. W. (2002) Direct coupling of the cell cycle and cell death machinery by E2F. *Nat Cell Biol* 4:859-64.
56. Putzer B. M. (2007) E2F1 death pathways as targets for cancer therapy. *J Cell Mol Med* 11:239-51.

57. Chen W. Y., Wang D. H., Yen R. C., Luo J., Gu W., Baylin S. B. (2005) Tumor suppressor HIC1 directly regulates SIRT1 to modulate p53-dependent DNA-damage responses. *Cell* 123:437-48.
58. Wales M. M., Biel M. A., el Deiry W., Nelkin B. D., Issa J. P., Cavenee W. K., Kuerbitz S. J., Baylin S. B. (1995) p53 activates expression of HIC-1, a new candidate tumour suppressor gene on 17p13.3. *Nat Med* 1:570-7.
59. Guerardel C., Deltour S., Pinte S., Monte D., Begue A., Godwin A. K., Leprince D. (2001) Identification in the human candidate tumor suppressor gene HIC-1 of a new major alternative TATA-less promoter positively regulated by p53. *J Biol Chem* 276:3078-89.
60. Kim E. J., Kho J. H., Kang M. R., Um S. J. (2007) Active regulator of SIRT1 cooperates with SIRT1 and facilitates suppression of p53 activity. *Mol Cell* 28:277-90.
61. Kim J. E., Chen J., Lou Z. (2008) DBC1 is a negative regulator of SIRT1. *Nature* 451:583-6.
62. Zhao X., Sternsdorf T., Bolger T. A., Evans R., M. Yao T. P. (2005) Regulation of MEF2 by histone deacetylase 4- and SIRT1 deacetylase-mediated lysine modifications. *Mol Cell Biol* 25:8456-64.
63. Anantharaman V., Aravind L. (2008) Analysis of DBC1 and its homologs suggests a potential mechanism for regulation of Sirtuin domain deacetylases by NAD metabolites. *Cell Cycle* 7: 1467-72.
64. Sung J. Y., Kim R., Kim J. E., Lee J. (2010) Balance between SIRT1 and DBC1 expression is lost in breast cancer. *Cancer Sci* 101:1738-44.
65. Yeh, E. T., Gong, L. Kamitani, T. (2000) Ubiquitin-like proteins: new wines in new bottles. *Gene* 248:1-14.
66. Yang Y., Fu W., Chen J., Olashaw N., Zhang X., Nicosia S. V., Bhalla K., Bai W. (2007) SIRT1 sumoylation regulates its deacetylase activity and cellular response to genotoxic stress. *Nat Cell Biol* 9:1253-62.
67. Revollo J. R., Grimm A. A., Imai S. (2004) The NAD biosynthesis pathway mediated by nicotinamide phosphoribosyltransferase regulates Sir2 activity in mammalian cells. *J Biol Chem* 279:50754-63.
68. Milne J. C., Denu J. M. (2008) The Sirtuin family: therapeutic targets to treat diseases of aging. *Curr Opin Chem Biol* 12:11-7.
69. Howitz K. T., Bitterman K. J., Cohen H. Y., Lamming D. W., Lavu S., Wood J. G., Zipkin R. E., Chung P., Kisielewski A., Zhang L. L., Scherer B., Sinclair D. A. (2003) Small molecule activators of sirtuins extend Saccharomyces cerevisiae lifespan. *Nature* 425:191-6.
70. Wood J. G., Rogina B., Lavu S., Howitz K., Helfand S. L., Tatar M., Sinclair D. (2004) Sirtuin activators mimic caloric restriction and delay ageing in metazoans. *Nature* 430:686-9.
71. Viswanathan M., Kim S. K., Berdichevsky A., Guarente L. (2005) A role for SIR-2.1 regulation of ER stress response genes in determining C. elegans life span. *Dev Cell* 9:605-15.
72. Jarolim S., Millen J., Heeren G., Laun P., Goldfarb D. S., Breitenbach M. (2004) A novel assay for replicative lifespan in Saccharomyces cerevisiae. *FEMS Yeast Res* 5:169-77.
73. de Boer V. C., de Goffau M. C., Arts I. C., Hollman P. C., Keijer J. (2006) SIRT1 stimulation by polyphenols is affected by their stability and metabolism. *Mech Ageing Dev* 127:618-27.
74. Allard J. S., Perez E., Zou S., de Cabo R. (2008) Dietary activators of Sirt1. *Mol Cell Endocrinol* 299:58-63.

75. Picard F., Kurtev M., Chung N., Topark-Ngarm A., Senawong T., Machado De Oliveira R., Leid M., McBurney M. W., Guarente L. (2004) Sirt1 promotes fat mobilization in white adipocytes by repressing PPAR-gamma. *Nature* 429:771-6.
76. Chen J., Zhou Y., Mueller-Steiner S., Chen L. F., Kwon H., Yi S., Mucke L., Gan L. (2005) SIRT1 protects against microglia-dependent amyloid-beta toxicity through inhibiting NF-kappaB signaling. *J Biol Chem* 280:40364-74.
77. Kolthur-Seetharam U., Dantzer F., McBurney M. W., de Murcia G., Sassone-Corsi P. (2006) Control of AIF-mediated cell death by the functional interplay of SIRT1 and PARP-1 in response to DNA damage. *Cell Cycle* 5:873-7.
78. Frescas D., Valenti L., Accili D. (2005) Nuclear trapping of the forkhead transcription factor FoxO1 via Sirt-dependent deacetylation promotes expression of glucogenetic genes. *J Biol Chem* 280:20589-95.
79. Baur J. A., Pearson K. J., Price N. L., Jamieson H. A., Lerin C., Kalra A., Prabhu V. V., Allard J. S., Lopez-Lluch G., Lewis K., Pistell P. J., Poosala S., Becker K. G., Boss O., Gwinn D., Wang M., Ramaswamy S., Fishbein K. W., Spencer R. G., Lakatta E. G., Le Couteur D., Shaw R. J., Navas P., Puigserver P., Ingram D. K., de Cabo R., Sinclair D. A. (2006) Resveratrol improves health and survival of mice on a high-calorie diet. *Nature* 444:337-42.
80. Lagouge M., Argmann C., Gerhart-Hines Z., Meziane H., Lerin C., Daussin F., Messadeq N., Milne J., Lambert P., Elliott P., Geny B., Laakso M., Puigserver P., Auwerx J. (2006) Resveratrol Improves Mitochondrial Function and Protects against Metabolic Disease by Activating SIRT1 and PGC-1alpha. *Cell* 127:1109-22.
81. Saiko P., Szakmary A., Jaeger W., Szekeres T. (2008) Resveratrol and its analogs: defense against cancer, coronary disease and neurodegenerative maladies or just a fad? *Mutat Res* 658:68-94.
82. Orallo F. (2008) Trans-resveratrol: a magical elixir of eternal youth? *Curr Med Chem* 15:1887-98.
83. Pirola L., Frojdo S. (2008) Resveratrol: one molecule, many targets. *IUBMB Life* 60:323-32.
84. Canto C., Jiang L. Q., Deshmukh A. S., Mataki C., Coste A., Lagouge M., Zierath J. R., Auwerx J. (2010) Interdependence of AMPK and SIRT1 for Metabolic Adaptation to Fasting and Exercise in Skeletal Muscle. *Cell Metab* 11:213-219.
85. Canto C., Gerhart-Hines Z., Feige J. N., Lagouge M., Noriega L., Milne J. C., Elliott P. J., Puigserver P., Auwerx J. (2009) AMPK regulates energy expenditure by modulating NAD+ metabolism and SIRT1 activity. *Nature* 458:1056-60.
86. Fulco M., Sartorelli V. (2008) Comparing and contrasting the roles of AMPK and SIRT1 in metabolic tissues. *Cell Cycle* 7:3669-79.
87. Milne J. C., Lambert P. D., Schenk S., Carney D. P., Smith J. J., Gagne D. J., Jin L., Boss O., Perni R. B., Vu C. B., Bemis J. E., Xie R., Disch J. S., Ng P. Y., Nunes J. J., Lynch A. V., Yang H., Galonek H., Israelian K., Choy W., Iffland A., Lavu S., Medvedik O., Sinclair D. A., Olefsky J. M., Jirousek M. R., Elliott P. J., Westphal C. H. (2007) Small molecule activators of SIRT1 as therapeutics for the treatment of type 2 diabetes. *Nature* 450:712-6.
88. Grozinger C. M., Chao E. D., Blackwell H. E., Moazed D., Schreiber S. L. (2001) Identification of a class of small molecule inhibitors of the sirtuin family of NAD-dependent deacetylases by phenotypic screening. *J Biol Chem* 276:38837-43.
89. Bedalov A., Gatbonton T., Irvine W. P., Gottschling D. E., Simon J. A. (2001) Identification of a small molecule inhibitor of Sir2p. *Proc Natl Acad Sci U S A* 98:15113-8.

90. Mai A., Massa S., Lavu S., Pezzi R., Simeoni S., Ragno R., Mariotti F. R., Chiani F., Camilloni G., Sinclair D. A. (2005) Design, synthesis, and biological evaluation of sirtinol analogues as class III histone/protein deacetylase (Sirtuin) inhibitors. *J Med Chem* 48:7789-95.
91. Gey C., Kyrylenko S., Hennig L., Nguyen L. H., Buttner A., Pham H. D., Giannis A. (2007) Phloroglucinol Derivatives Guttiferone G, Aristoforin, and Hyperforin: Inhibitors of Human Sirtuins SIRT1 and SIRT2. *Angew Chem Int Ed Engl* 46:5219-22.
92. Napper A. D., Hixon J., McDonagh T., Keavey K., Pons J. F., Barker J., Yau W. T., Amouzegh P., Flegg A., Hamelin E., Thomas R. J., Kates M., Jones S., Navia M. A., Saunders J. O., DiStefano P. S., Curtis R. (2005) Discovery of indoles as potent and selective inhibitors of the deacetylase SIRT1. *J Med Chem* 48:8045-54.
93. Trapp J., Meier R., Hongwiset D., Kassack M. U., Sippl W., Jung M. (2007) Structure-Activity Studies on Suramin Analogues as Inhibitors of NAD(+)-Dependent Histone Deacetylases (Sirtuins). *ChemMedChem* 2:1419-31.
94. Bitterman K. J., Anderson R. M., Cohen H. Y., Latorre-Esteves M., Sinclair D. A. (2002) Inhibition of silencing and accelerated aging by nicotinamide, a putative negative regulator of yeast sir2 and human SIRT1. *J Biol Chem* 277:45099-107.
95. Lavu S., Boss O., Elliott P. J., Lambert P. D. (2008) Sirtuins--novel therapeutic targets to treat age-associated diseases. *Nat Rev Drug Discov* 7:841-53.
96. Hallows W. C., Lee S., Denu J. M. (2006) Sirtuins deacetylate and activate mammalian acetyl-CoA synthetases. *Proc Natl Acad Sci U S A* 103:10230-5.
97. Dey S., Bakthavatchalu V., Tseng M. T., Wu P., Florence R., Grulke E. A., Yokel R., Dhar S. K., Yang H. S., Chen Y., St Clair D. K. (2008) Interactions between SIRT1 and AP-1 reveal a Mechanistic Insight into the Growth Promoting Properties of Alumina (Al2O3) Nanoparticles in Mouse Skin Epithelial Cells. *Carcinogenesis* 29:1920-9.
98. Dai Y., Ngo D., Forman L. W., Qin D. C., Jacob J., Faller D. V. (2007) Sirt1 Is Required For Antagonist-Induced Transcriptional Repression Of Androgen-Responsive Genes By The Androgen Receptor. *Mol Endocrinol* 21:1807-21.
99. Fu M., Liu M., Sauve A. A., Jiao X., Zhang X., Powell M., Yang T., Gu W., Avantaggiati M. L., Pattabiraman N., Pestell T. G., Wang F., Quong A., Wang C., Pestell R. G. (2006) The Hormonal Control of Androgen Receptor Function through SIRT1. *Mol Cell Biol* 26:8122-35.
100. Lee I. H., Cao L., Mostoslavsky R., Lombard D. B., Liu J., Bruns N. E., Tsokos M., Alt F. W., Finkel T. (2008) A role for the NAD-dependent deacetylase Sirt1 in the regulation of autophagy. *Proc Natl Acad Sci U S A* 105:3374-9.
101. Gao Z., Ye J. (2008) Inhibition of transcriptional activity of c-JUN by SIRT1. *Biochem Biophys Res Commun* 376:793-6.
102. Asher G., Gatfield D., Stratmann M., Reinke H., Dibner C., Kreppel F., Mostoslavsky R., Alt F. W., Schibler U. (2008) SIRT1 regulates circadian clock gene expression through PER2 deacetylation. *Cell* 134:317-28.
103. Nakahata Y., Kaluzova M., Grimaldi B., Sahar S., Hirayama J., Chen D., Guarente L. P., Sassone-Corsi P. (2008) The NAD+-dependent deacetylase SIRT1 modulates CLOCK-mediated chromatin remodeling and circadian control. *Cell* 134:329-40.
104. Zhang Y., Zhang M., Dong H., Yong S., Li X., Olashaw N., Kruk P. A., Cheng J. Q., Bai W., Chen J., Nicosia S. V., Zhang X. (2008) Deacetylation of cortactin by SIRT1 promotes cell migration. *Oncogene* 28:445-60.
105. Mattagajasingh I., Kim C. S., Naqvi A., Yamamori T., Hoffman T. A., Jung S. B., Dericco J., Kasuno K., Irani K. (2007) SIRT1 promotes endothelium-dependent

vascular relaxation by activating endothelial nitric oxide synthase. *Proc Natl Acad Sci U S A* 104:14855-60.

106. Daitoku H., Hatta M., Matsuzaki H., Aratani S., Ohshima T., Miyagishi M., Nakajima T., Fukamizu A. (2004) Silent information regulator 2 potentiates Foxo1-mediated transcription through its deacetylase activity. *Proc Natl Acad Sci U S A* 101:10042-7.
107. Qiao L., Shao J. (2006) SIRT1 regulates adiponectin gene expression through Foxo1-C/EBPalpha transcriptional complex. *J Biol Chem* 281:39915-24.
108. Gan L., Han Y., Bastianetto S., Dumont Y., Unterman T. G., Quirion R. (2005) FoxO-dependent and -independent mechanisms mediate SirT1 effects on IGFBP-1 gene expression. *Biochem Biophys Res Commun* 337:1092-6.
109. Brunet A., Sweeney L. B., Sturgill J. F., Chua K. F., Greer P. L., Lin Y., Tran H., Ross S. E., Mostoslavsky R., Cohen H. Y., Hu L. S., Cheng H. L., Jedrychowski M. P., Gygi S. P., Sinclair D. A., Alt F. W., Greenberg M. E. (2004) Stress-dependent regulation of FOXO transcription factors by the SIRT1 deacetylase. *Science* 303:2011-5.
110. Motta M. C., Divecha N., Lemieux M., Kamel C., Chen D., Gu W., Bultsma Y., McBurney M., Guarente L. (2004) Mammalian SIRT1 represses forkhead transcription factors. *Cell* 116:551-63.
111. Kobayashi Y., Furukawa-Hibi Y., Chen C., Horio Y., Isobe K., Ikeda K., Motoyama N. (2005) SIRT1 is critical regulator of FOXO-mediated transcription in response to oxidative stress. *Int J Mol Med* 16:237-43.
112. van der Horst A., Tertoolen L. G., de Vries-Smits L. M., Frye R. A., Medema R. H., Burgering B. M. (2004) FOXO4 is acetylated upon peroxide stress and deacetylated by the longevity protein hSir2(SIRT1). *J Biol Chem* 279:28873-9.
113. Vaquero A., Scher M., Lee D., Erdjument-Bromage H., Tempst P., Reinberg D. (2004) Human SirT1 interacts with histone H1 and promotes formation of facultative heterochromatin. *Mol Cell* 16:93-105.
114. Takata T., Ishikawa F. (2003) Human Sir2-related protein SIRT1 associates with the bHLH repressors HES1 and HEY2 and is involved in HES1- and HEY2-mediated transcriptional repression. *Biochem Biophys Res Commun* 301:250-7.
115. Yang J., Kong X., Martins-Santos M. E., Aleman G., Chaco E., Liu G. E., Wu S. Y., Samols D., Hakimi P., Chiang C. M., Hanson R. W. (2009) Activation of SIRT1 by resveratrol represses transcription of the gene for the cytosolic form of phosphoenolpyruvate carboxykinase (GTP) by deacetylating hepatic nuclear factor 4alpha. *J Biol Chem* 284:27042-53.
116. Jeong J., Juhn K., Lee H., Kim S. H., Min B. H., Lee K. M., Cho M. H., Park G. H., Lee K. H. (2007) SIRT1 promotes DNA repair activity and deacetylation of Ku70. *Exp Mol Med* 39:8-13.
117. Hou X., Xu S., Maitland-Toolan K. A., Sato K., Jiang B., Ido Y., Lan F., Walsh K., Wierzbicki M., Verbeuren T. J., Cohen R. A. (2008) SIRT1 regulates hepatocyte lipid metabolism through activating AMP-activated protein kinase. *J Biol Chem* 283:20015-26.
118. Lan F., Cacicedo J. M., Ruderman N., Ido Y. (2008) SIRT1 modulation of the acetylation status, cytosolic localization and activity of LKB1; possible role in AMP-activated protein kinase activation. *J Biol Chem* 283:27628-35.
119. Li X., Zhang S., Blander G., Tse J. G., Krieger M., Guarente L. (2007) SIRT1 Deacetylates and Positively Regulates the Nuclear Receptor LXR. *Mol Cell* 28:91-106.

120. Fulco M., Schiltz R. L., Iezzi S., King M. T., Zhao P., Kashiwaya Y., Hoffman E., Veech R. L., Sartorelli V. (2003) Sir2 regulates skeletal muscle differentiation as a potential sensor of the redox state. *Mol Cell* 12:51-62.
121. Fulco M., Cen Y., Zhao P., Hoffman E. P., McBurney M. W., Sauve A. A., Sartorelli V. (2008) Glucose restriction inhibits skeletal myoblast differentiation by activating SIRT1 through AMPK-mediated regulation of Nampt. *Dev Cell* 14:661-73.
122. Yeung F., Hoberg J. E., Ramsey C. S., Keller M. D., Jones D. R., Frye R. A., Mayo M. W. (2004) Modulation of NF-kappaB-dependent transcription and cell survival by the SIRT1 deacetylase. *Embo J* 23:2369-80.
123. Bouras T., Fu M., Sauve A. A., Wang F., Quong A. A., Perkins N. D., Hay R. T., Gu W., Pestell R. G. (2005) SIRT1 deacetylation and repression of p300 involves lysine residues 1020/1024 within the cell cycle regulatory domain 1. *J Biol Chem* 280:10264-76.
124. Vaziri H., Dessain S. K., Ng Eaton E., Imai S. I., Frye R. A., Pandita T. K., Guarente L., Weinberg R. A. (2001) hSIR2(SIRT1) functions as an NAD-dependent p53 deacetylase. *Cell* 107:149-59.
125. Luo J., Nikolaev A. Y., Imai S., Chen D., Su F., Shiloh A., Guarente L., Gu W. (2001) Negative control of p53 by Sir2alpha promotes cell survival under stress. *Cell* 107:137-48.
126. Kume S., Haneda M., Kanasaki K., Sugimoto T., Araki S., Isono M., Isshiki K., Uzu T., Kashiwagi A., Koya D. (2006) Silent information regulator 2 (SIRT1) attenuates oxidative stress-induced mesangial cell apoptosis via p53 deacetylation. *Free Radic Biol Med* 40:2175-82.
127. Langley E., Pearson M., Faretta M., Bauer U. M., Frye R. A., Minucci S., Pelicci P. G., Kouzarides T. (2002) Human SIR2 deacetylates p53 and antagonizes PML/p53-induced cellular senescence. *Embo J* 21:2383-96.
128. Cheng H. L., Mostoslavsky R., Saito S., Manis J. P., Gu Y., Patel P., Bronson R., Appella E., Alt F. W., Chua K. F. (2003) Developmental defects and p53 hyperacetylation in Sir2 homolog (SIRT1)-deficient mice. *Proc Natl Acad Sci U S A* 100:10794-9.
129. Kamel C., Abrol M., Jardine K., He X., McBurney M. W. (2006) SirT1 fails to affect p53-mediated biological functions. *Aging Cell* 5:81-8.
130. Dai J. M., Wang Z. Y., Sun D. C., Lin R. X., Wang S. Q. (2006) SIRT1 interacts with p73 and suppresses p73-dependent transcriptional activity. *J Cell Physiol* 210:161-6.
131. Nemoto S., Fergusson M. M., Finkel T. (2005) SIRT1 functionally interacts with the metabolic regulator and transcriptional coactivator PGC-1{alpha}. *J Biol Chem* 280:16456-60.
132. Rodgers J. T., Lerin C., Haas W., Gygi S. P., Spiegelman B. M., Puigserver P. (2005) Nutrient control of glucose homeostasis through a complex of PGC-1alpha and SIRT1. *Nature* 434:113-8.
133. Rodgers J. T., Lerin C., Gerhart-Hines Z., Puigserver P. (2007) Metabolic adaptations through the PGC-1alpha and SIRT1 pathways. *FEBS Lett* 582:46-53.
134. Feige J. N., Lagouge M., Canto C., Strehle A., Houten S. M., Milne J. C., Lambert P. D., Mataki C., Elliott P. J., Auwerx J. (2008) Specific SIRT1 Activation Mimics Low Energy Levels and Protects against Diet-Induced Metabolic Disorders by Enhancing Fat Oxidation. *Cell Metab* 8:347-58.
135. Gerhart-Hines Z., Rodgers J. T., Bare O., Lerin C., Kim S. H., Mostoslavsky R., Alt F. W., Wu Z., Puigserver P. (2007) Metabolic control of muscle mitochondrial function and fatty acid oxidation through SIRT1/PGC-1alpha. *Embo J* 26:1913-23.

136. Amat R., Planavila A., Chen S. L., Iglesias R., Giralt M., Villarroya F. (2009) SIRT1 controls the transcription of the peroxisome proliferator-activated receptor-gamma Co-activator-1alpha (PGC-1alpha) gene in skeletal muscle through the PGC-1alpha autoregulatory loop and interaction with MyoD. *J Biol Chem* 284:21872-80.
137. Binda O., Nassif C., Branton P. E. (2008) SIRT1 negatively regulates HDAC1-dependent transcriptional repression by the RBP1 family of proteins. *Oncogene* 27:3384-92.
138. Kume S., Haneda M., Kanasaki K., Sugimoto T., Araki S. I., Isshiki K., Isono M., Uzu T., Guarente L., Kashiwagi A., Koya D. (2006) SIRT1 inhibits TGFbeta -induced apoptosis in glomerular mesangial cells via Smad7 deacetylation. *J Biol Chem* 282:151-8.
139. Dvir-Ginzberg M., Gagarina V., Lee E. J., Hall D. J. (2008) Regulation of cartilage-specific gene expression in human chondrocytes by SirT1 and NAMPT. *J Biol Chem* 283:36300-10.
140. Pagans S., Pedal A., North B. J., Kaehlcke K., Marshall B. L., Dorr A., Hetzer-Egger C., Henklein P., Frye R., McBurney M. W., Hruby H., Jung M., Verdin E., Ott M. (2005) SIRT1 regulates HIV transcription via Tat deacetylation. *PLoS Biol* 3:e41.
141. Ghosh H. S., Spencer J. V., Ng B., McBurney M. W., Robbins P. D. (2007) Sirt1 interacts with transducin-like enhancer of split-1 to inhibit NF-kappaB mediated transcription. *Biochem J* 408:105-11.
142. Bordone L., Motta M. C., Picard F., Robinson A., Jhala U. S., Apfeld J., McDonagh T., Lemieux M., McBurney M., Szilvasi A., Easlon E. J., Lin S. J., Guarente L. (2006) Sirt1 regulates insulin secretion by repressing UCP2 in pancreatic beta cells. *PLoS Biol* 4:e31.
143. Moynihan K. A., Grimm A. A., Plueger M. M., Bernal-Mizrachi E., Ford E., Cras-Meneur C., Permutt M. A., Imai S. (2005) Increased dosage of mammalian Sir2 in pancreatic beta cells enhances glucose-stimulated insulin secretion in mice. *Cell Metab* 2:105-17.
144. Amat R., Solanes G., Giralt M., Villarroya F. (2007) Sirt1 is involved in glucocorticoid-mediated control of uncoupling protein-3 gene transcription. *J Biol Chem* 282:34066-76.
145. Li K., Casta A., Wang R., Lozada E., Fan W., Kane S., Ge Q., Gu W., Orren D., Luo J. (2008) Regulation of WRN protein cellular localization and enzymatic activities by SIRT1 mediated deacetylation. *J Biol Chem* 283:7590-8.
146. Feige J. N., Auwerx J. (2007) DisSIRTing on LXR and cholesterol metabolism. *Cell Metab* 6:343-5.
147. Lehrke M., Lazar M. A. (2005) The many faces of PPARgamma. *Cell* 123:993-9.
148. Barak Y., Nelson M. C., Ong E. S., Jones Y. Z., Ruiz-Lozano P., Chien K. R., Koder A., Evans R. M. (1999) PPAR gamma is required for placental, cardiac, and adipose tissue development. *Mol Cell* 4:585-95.
149. Wang H., Qiang L., Farmer S. R. (2007) Identification of a domain within PPAR{gamma} regulating expression of a group of genes containing FGF21 that are selectively repressed by SIRT1 in adipocytes. *Mol Cell Biol* 28:188-200.
150. Jin Q., Zhang F., Yan T., Liu Z., Wang C., Ge X., Zhai Q. (2010) C/EBPalpha regulates SIRT1 expression during adipogenesis. *Cell Res* 20:470-9.
151. Banks A. S., Kon N., Knight C., Matsumoto M., Gutierrez-Juarez R., Rossetti L., Gu W., Accili D. (2008) SirT1 gain of function increases energy efficiency and prevents diabetes in mice. *Cell Metab* 8:333-41.
152. Qiang L., Wang H., Farmer S. R. (2007) Adiponectin Secretion is Regulated by SIRT1 and the ER oxidoreductase Ero1-L{alpha}. *Mol Cell Biol* 27:4698-707.

153. Zhang C. Y., Baffy G., Perret P., Krauss S., Peroni O., Grujic D., Hagen T., Vidal-Puig A. J., Boss O., Kim Y. B., Zheng X. X., Wheeler M. B., Shulman G. I., Chan C. B., Lowell B. B. (2001) Uncoupling protein-2 negatively regulates insulin secretion and is a major link between obesity, beta cell dysfunction, and type 2 diabetes. *Cell* 105:745-55.
154. Ramsey K. M., Mills K. F., Satoh A., Imai S. I. (2007) Age-associated loss of Sirt1-mediated enhancement of glucose-stimulated insulin secretion in BESTO mice. *Aging Cell* 7:78-88.
155. Puigserver P., Wu Z., Park C. W., Graves R., Wright M., Spiegelman B. M. (1998) A cold-inducible coactivator of nuclear receptors linked to adaptive thermogenesis. *Cell* 92:829-39.
156. Yoon J. C., Puigserver P., Chen G., Donovan J., Wu Z., Rhee J., Adelmant G., Stafford J., Kahn C. R., Granner D. K., Newgard C. B., Spiegelman B. M. (2001) Control of hepatic gluconeogenesis through the transcriptional coactivator PGC-1. *Nature* 413:131-8.
157. Herzig S., Long F., Jhala U. S., Hedrick S., Quinn R., Bauer A., Rudolph D., Schutz G., Yoon C., Puigserver P., Spiegelman B., Montminy M. (2001) CREB regulates hepatic gluconeogenesis through the coactivator PGC-1. *Nature* 413:179-83.
158. Puigserver P., Rhee J., Donovan J., Walkey C. J., Yoon J. C., Oriente F., Kitamura Y., Altomonte J., Dong H., Accili D., Spiegelman B. M. (2003) Insulin-regulated hepatic gluconeogenesis through FOXO1-PGC-1alpha interaction. *Nature* 423:550-5.
159. Rhee J., Inoue Y., Yoon J. C., Puigserver P., Fan M., Gonzalez F. J., Spiegelman B. M. (2003) Regulation of hepatic fasting response by PPARgamma coactivator-1alpha (PGC-1): requirement for hepatocyte nuclear factor 4alpha in gluconeogenesis. *Proc Natl Acad Sci U S A* 100:4012-7.
160. Lin J., Wu P. H., Tarr P. T., Lindenberg K. S., St-Pierre J., Zhang C. Y., Mootha V. K., Jager S., Vianna C. R., Reznick R. M., Cui L., Manieri M., Donovan M. X., Wu Z., Cooper M. P., Fan M. C., Rohas L. M., Zavacki A. M., Cinti S., Shulman G. I., Lowell B. B., Krainc D., Spiegelman B. M. (2004) Defects in adaptive energy metabolism with CNS-linked hyperactivity in PGC-1alpha null mice. *Cell* 119:121-35.
161. Ganjam G. K., Dimova E. Y., Unterman T. G., Kietzmann T. (2009) FoxO1 and HNF-4 are involved in regulation of hepatic glucokinase gene expression by resveratrol. *J Biol Chem* 284:30783-97.
162. Nakae J., Biggs W. H. 3rd, Kitamura T.,Cavenee W. K., Wright C. V., Arden K. C., Accili D. (2002) Regulation of insulin action and pancreatic beta-cell function by mutated alleles of the gene encoding forkhead transcription factor Foxo1. *Nat Genet* 32:245-53.
163. Nakae J., Kitamura T., Silver D. L., Accili D. (2001) The forkhead transcription factor Foxo1 (Fkhr) confers insulin sensitivity onto glucose-6-phosphatase expression. *J Clin Invest* 108:1359-67.
164. Erion D. M., Yonemitsu S., Nie Y., Nagai Y.,Gillum M. P., Hsiao J. J., Iwasaki T., Stark R., Weismann D., Yu X. X., Murray S. F., Bhanot S., Monia B. P., Horvath T. L., Gao Q., Samuel V. T., Shulman G. I. (2009) SirT1 knockdown in liver decreases basal hepatic glucose production and increases hepatic insulin responsiveness in diabetic rats. *Proc Natl Acad Sci U S A* 106:11288-93.
165. Rodgers J. T., Puigserver P. (2007) Fasting-dependent glucose and lipid metabolic response through hepatic sirtuin 1. *Proc Natl Acad Sci U S A* 104:12861-6.
166. Liu Y., Dentin R., Chen D., Hedrick S., Ravnskjaer K., Schenk S., Milne J., Meyers D. J., Cole P., Yates J. 3rd, Olefsky J., Guarente L., Montminy M. (2008) A fasting

inducible switch modulates gluconeogenesis via activator/coactivator exchange. *Nature* 456:269-73.

167. Willy P. J., Umesono K., Ong E. S., Evans R. M., Heyman R. A., Mangelsdorf D. J. (1995) LXR, a nuclear receptor that defines a distinct retinoid response pathway. *Genes Dev* 9:1033-45.
168. Janowski B. A., Grogan M. J., Jones S. A., Wisely G. B., Kliewer S. A., Corey E. J., Mangelsdorf D. J. (1999) Structural requirements of ligands for the oxysterol liver X receptors LXRalpha and LXRbeta. *Proc Natl Acad Sci U S A* 96:266-71.
169. Janowski B. A., Willy P. J., Devi T. R., Falck J. R., Mangelsdorf D. J. (1996) An oxysterol signalling pathway mediated by the nuclear receptor LXR alpha. *Nature* 383:728-31.
170. Meirhaeghe A., Crowley V., Lenaghan C., Lelliott C., Green K., Stewart A., Hart K., Schinner S., Sethi J. K., Yeo G., Brand M. D., Cortright R. N., O'Rahilly S., Montague C., Vidal-Puig A. J. (2003) Characterization of the human, mouse and rat PGC1 beta (peroxisome-proliferator-activated receptor-gamma co-activator 1 beta) gene in vitro and in vivo. *Biochem J* 373:155-65.
171. Brown M. S., Goldstein J. L. (1999) A proteolytic pathway that controls the cholesterol content of membranes, cells, and blood. *Proc Natl Acad Sci U S A* 96:11041-8.
172. Foufelle F., Ferre P. (2002) New perspectives in the regulation of hepatic glycolytic and lipogenic genes by insulin and glucose: a role for the transcription factor sterol regulatory element binding protein-1c. *Biochem J* 366:377-91.
173. Song C., Kokontis J. M., Hiipakka R. A., Liao S. (1994) Ubiquitous receptor: a receptor that modulates gene activation by retinoic acid and thyroid hormone receptors. *Proc Natl Acad Sci U S A* 91:10809-13.
174. Willy P. J., Mangelsdorf D. J. (1997) Unique requirements for retinoid-dependent transcriptional activation by the orphan receptor LXR. *Genes Dev* 11:289-98.
175. Chinetti G., Fruchart J. C., Staels B. (2006) Transcriptional regulation of macrophage cholesterol trafficking by PPARalpha and LXR. *Biochem Soc Trans* 34:1128-31.
176. Missero C., Calautti E., Eckner R., Chin J., Tsai L. H., Livingston D. M., Dotto G. P. (1995) Involvement of the cell-cycle inhibitor Cip1/WAF1 and the E1A-associated p300 protein in terminal differentiation. *Proc Natl Acad Sci U S A* 92:5451-5.
177. Yuan W., Condorelli G., Caruso M., Felsani A., Giordano A. (1996) Human p300 protein is a coactivator for the transcription factor MyoD. *J Biol Chem* 271:9009-13.
178. Puri P. L., Avantaggiati M. L., Balsano C., Sang N., Graessmann A., Giordano A., Levrero M. (1997) p300 is required for MyoD-dependent cell cycle arrest and muscle-specific gene transcription. *Embo J* 16:369-83.
179. Eckner R., Yao T. P., Oldread E., Livingston D. M. (1996) Interaction and functional collaboration of p300/CBP and bHLH proteins in muscle and B-cell differentiation. *Genes Dev* 10:2478-90.
180. Polesskaya A., Naguibneva I., Fritsch L., Duquet A., Ait-Si-Ali S., Robin P., Vervisch A., Pritchard L. L., Cole P., Harel-Bellan A. (2001) CBP/p300 and muscle differentiation: no HAT, no muscle. *Embo J* 20:6816-25.
181. Sartorelli V., Huang J., Hamamori Y., Kedes L. (1997) Molecular mechanisms of myogenic coactivation by p300: direct interaction with the activation domain of MyoD and with the MADS box of MEF2C. *Mol Cell Biol* 17:1010-26.
182. Puri P. L., Sartorelli V., Yang X. J., Hamamori Y., Ogryzko V. V., Howard B. H., Kedes L., Wang J. Y., Graessmann A., Nakatani Y., Levrero M. (1997) Differential roles of p300 and PCAF acetyltransferases in muscle differentiation. *Mol Cell* 1:35-45.

183. McKinsey T. A., Zhang C. L., Olson E. N. (2001) Control of muscle development by dueling HATs and HDACs. *Curr Opin Genet Dev* 11:497-504.
184. McKinsey T. A., Zhang C. L., Olson E. N. (2002) Signaling chromatin to make muscle. *Curr Opin Cell Biol* 14:763-72.
185. Sparrow D. B., Miska E. A., Langley E., Reynaud-Deonauth S., Kotecha S., Towers N., Spohr G., Kouzarides T., Mohun T. J. (1999) MEF-2 function is modified by a novel co-repressor, MITR. *Embo J* 18:5085-98.
186. Lu J., McKinsey T. A., Nicol R. L., Olson E. N. (2000) Signal-dependent activation of the MEF2 transcription factor by dissociation from histone deacetylases. *Proc Natl Acad Sci U S A* 97:4070-5.
187. Miska E. A., Karlsson C., Langley E., Nielsen S. J., Pines J., Kouzarides T. (1999) HDAC4 deacetylase associates with and represses the MEF2 transcription factor. *Embo J* 18:5099-107.
188. Wang Wang A. H., Bertos N. R., Vezmar M., Pelletier N., Crosato M., Heng H. H., Th'ng J., Han J., Yang X. J. (1999) HDAC4, a human histone deacetylase related to yeast HDA1, is a transcriptional corepressor. *Mol Cell Biol* 19:7816-27.
189. Lemercier C., Verdel A., Galloo B., Curtet S., Brocard M. P., Khochbin S. (2000) mHDA1/HDAC5 histone deacetylase interacts with and represses MEF2A transcriptional activity. *J Biol Chem* 275:15594-9.
190. Mal A., Sturniolo M., Schiltz R. L., Ghosh M. K., Harter M. L. (2001) A role for histone deacetylase HDAC1 in modulating the transcriptional activity of MyoD: inhibition of the myogenic program. *Embo J* 20:1739-53.
191. Nedachi T., Kadotani A., Ariga M., Katagiri H., Kanzaki M. (2008) Ambient Glucose Levels Qualify the Potency of Insulin Myogenic Actions by Regulating SIRT1 and FoxO3a in C2C12 myocytes. *Am J Physiol Endocrinol Metab* 294:E668-78.
192. Gurd B. J., Yoshida Y., Lally J., Holloway G. P., Bonen A. (2009) The deacetylase enzyme SIRT1 is not associated with oxidative capacity in rat heart and skeletal muscle and its overexpression reduces mitochondrial biogenesis. *J Physiol* 587:1817-28.
193. Chabi B., Adhihetty P. J., O'Leary M. F., Menzies K. J., Hood D. A. (2009) Relationship between Sirt1 expression and mitochondrial proteins during conditions of chronic muscle use and disuse. *J Appl Physiol* 107:1730-5.
194. Pacholec M., Bleasdale J. E., Chrunyk B., Cunningham D., Flynn D., Garofalo R. S., Griffith D., Griffor M., Loulakis P., Pabst B., Qiu X., Stockman B., Thanabal V., Varghese A., Ward J., Withka J., Ahn K. (2010) SRT1720, SRT2183, SRT1460, and resveratrol are not direct activators of SIRT1. *J Biol Chem* 285:8340-51.
195. Beher D., Wu J., Cumine S., Kim K. W., Lu S. C., Atangan L., Wang M. (2009) Resveratrol is not a direct activator of SIRT1 enzyme activity. *Chem Biol Drug Des* 74:619-24.
196. Dasgupta B., Milbrandt J. (2007) Resveratrol stimulates AMP kinase activity in neurons. *Proc Natl Acad Sci U S A* 104:7217-22.
197. Breen D. M., Sanli T., Giacca A., Tsiani E. (2008) Stimulation of muscle cell glucose uptake by resveratrol through sirtuins and AMPK. *Biochem Biophys Res Commun* 374:117-22.
198. Towler M. C., Hardie D. G. (2007) AMP-activated protein kinase in metabolic control and insulin signaling. *Circ Res* 100:328-41.
199. Um J. H., Park S. J., Kang H., Yang S., Foretz M., McBurney M. W., Kim M. K., Viollet B., Chung J. H. (2010) AMP-activated protein kinase-deficient mice are resistant to the metabolic effects of resveratrol. *Diabetes* 59:554-63.

200. Ruderman N. B., Julia Xu X., Nelson L., Cacicedo J. M., Saha A. K., Lan F., Ido Y. (2010) AMPK and SIRT1: a long-standing partnership? *Am J Physiol Endocrinol Metab* 298:E751-60.
201. Fullerton M. D., Steinberg G. R. (2010) SIRT1 takes a backseat to AMPK in the regulation of insulin sensitivity by resveratrol. *Diabetes* 59:551-3.
202. McBurney M. W., Yang X., Jardine K., Hixon M., Boekelheide K., Webb J. R., Lansdorp P. M., Lemieux M. (2003) The mammalian SIR2alpha protein has a role in embryogenesis and gametogenesis. *Mol Cell Biol* 23:38-54.
203. Kimball S. R., Jefferson L. S. (2006) Signaling pathways and molecular mechanisms through which branched-chain amino acids mediate translational control of protein synthesis. *J Nutr* 136:227S-31S.
204. Ghosh H. S., McBurney M., Robbins P. D. (2010) SIRT1 negatively regulates the mammalian target of rapamycin. *PLoS One* 5:e9199.
205. Morselli E., Maiuri MC., Markaki M., Megalou E., Pasparaki A., Palikaras K., Criollo A., Galluzzi L., Malik SA., Vitale I., Michaud M., Madeo F., Tavernarakis N. (2010) Caloric restriction and resveratrol prolong longevity via the Sirtuin-1-dependent induction of autophagy. *Cell Death Dis.* In press.
206. Mammucari C., Milan G., Romanello V., Masiero E., Rudolf R., Del Piccolo P., Burden S. J., Di Lisi R., Sandri C., Zhao J., Goldberg A. L., Schiaffino S., Sandri M. (2007) FoxO3 controls autophagy in skeletal muscle in vivo. *Cell Metab* 6:458-71.
207. Zhao J., Brault J. J., Schild A., Cao P., Sandri M., Schiaffino S., Lecker S. H., Goldberg A. L. (2007) FoxO3 coordinately activates protein degradation by the autophagic/lysosomal and proteasomal pathways in atrophying muscle cells. *Cell Metab* 6:472-83.
208. de Kreutzenberg S. V., Ceolotto G., Papparella I., Bortoluzzi A., Semplicini A., Man C. D., Cobelli C., Fadini G. P., Avogaro A. (2010) Downregulation of the longevity-associated protein sirtuin 1 in insulin resistance and metabolic syndrome: potential biochemical mechanisms. *Diabetes* 59:1006-15.

ANNEXES

I. ARTICLES DANS DES REVUES INTERNATIONALES

Downregulation of Akt/mammalian target of rapamycin pathway in skeletal muscle is associated with increased REDD1 expression in response to chronic hypoxia
Favier FB, Costes F, Defour A, Bonnefoy R, Lefai E, Bauge S, Peinnequin A, Benoit H and Freyssenet D.
American Journal of Physiology-Regulatory Integrative and Comparative Physiology, 2010 Jun 298(6):R1659-66.

Evidence for mitochondrial respiratory deficiency in rhaddomyosarcoma cells
Jahnke VE, Sabido O, Defour A, Castells J, Lefai E, Roussel D and Freyssenet D.
PLoS ONE, 2010 Jan 8;5(1):e8637.

Muscle-specific inactivation of mTOR causes metabolic defects leading to severe dystrophy
Risson V, Mazelin L, Roceri M, Sanchez H, Moncollin V, Corneloup C, Richard-Bulteau H, Vignaud A, Baas D, Defour A, Freyssenet D, Tanti JF, Le-Marchand-Brustel Y, Ferrier B, Conjard-Duplany A, Romanino K, Bauche S, Hantaï D, Mueller M, Kozma SC, Thomas G, Rüegg MA, Ferry A, Pende M, Bigard X, Koulmann N, Schaeffer L and Gangloff YG.
Journal of Cell Biolgy, 2009 Dec 14;187(6):859-74.

François B. Favier, Frédéric Costes, Aurélia Defour, Régis Bonnefoy, Etienne Lefai, Stéphane Baugé, André Peinnequin, Henri Benoit and Damien Freyssenet
Am J Physiol Regulatory Integrative Comp Physiol 298:1659-1666, 2010. First published Mar 17, 2010; doi:10.1152/ajpregu.00550.2009

You might find this additional information useful...

Supplemental material for this article can be found at:
http://ajpregu.physiology.org/cgi/content/full/00550.2009/DC1

This article cites 43 articles, 23 of which you can access free at:
http://ajpregu.physiology.org/cgi/content/full/298/6/R1659#BIBL

Updated information and services including high-resolution figures, can be found at:
http://ajpregu.physiology.org/cgi/content/full/298/6/R1659

Additional material and information about ***American Journal of Physiology - Regulatory, Integrative and Comparative Physiology*** can be found at:
http://www.the-aps.org/publications/ajpregu

This information is current as of May 28, 2010 .

The American Journal of Physiology - Regulatory, Integrative and Comparative Physiology publishes original investigations that illuminate normal or abnormal regulation and integration of physiological mechanisms at all levels of biological organization, ranging from molecules to humans, including clinical investigations. It is published 12 times a year (monthly) by the American Physiological Society, 9650 Rockville Pike, Bethesda MD 20814-3991. Copyright © 2005 by the American Physiological Society. ISSN: 0363-6119, ESSN: 1522-1490. Visit our website at http://www.the-aps.org/.

Downloaded from ajpregu.physiology.org on May 28, 2010

Am J Physiol Regul Integr Comp Physiol 298: R1659–R1666, 2010.
First published March 17, 2010; doi:10.1152/ajpregu.00550.2009.

Downregulation of Akt/mammalian target of rapamycin pathway in skeletal muscle is associated with increased REDD1 expression in response to chronic hypoxia

François B. Favier,[1,4] Frédéric Costes,[1] Aurélia Defour,[1] Régis Bonnefoy,[1] Etienne Lefai,[2] Stéphane Baugé,[3] André Peinnequin,[3] Henri Benoit,[1*] and Damien Freyssenet[1*]

[1]*Université de Lyon, Université Jean Monnet, Laboratoire de Physiologie de l'Exercice EA 4338, Saint Etienne, France;* [2]*Université de Lyon, Université Claude Bernard Lyon 1, INSERM U870 Régulations Métaboliques Nutrition et Diabètes, Oullins, France;* [3]*Département de Radiobiologie et Radiopathologie, Centre de Recherche du Service de Santé des Armées, La Tronche, France; and* [4]*Université de Montpellier 1, INRA UMR866 Différenciation Cellulaire et Croissance, Montpellier, France*

Submitted 31 August 2009; accepted in final form 10 March 2010

Favier FB, Costes F, Defour A, Bonnefoy R, Lefai E, Baugé S, Peinnequin A, Benoit H, Freyssenet D. Downregulation of Akt/mammalian target of rapamycin pathway in skeletal muscle is associated with increased REDD1 expression in response to chronic hypoxia. *Am J Physiol Regul Integr Comp Physiol* 298: R1659–R1666, 2010. First published March 17, 2010; doi:10.1152/ajpregu.00550.2009.—Although it is well established that chronic hypoxia leads to an inexorable loss of skeletal muscle mass in healthy subjects, the underlying molecular mechanisms involved in this process are currently unknown. Skeletal muscle atrophy is also an important systemic consequence of chronic obstructive pulmonary disease (COPD), but the role of hypoxemia in this regulation is still debated. Our general aim was to determine the molecular mechanisms involved in the regulation of skeletal muscle mass after exposure to chronic hypoxia and to test the biological relevance of our findings into the clinical context of COPD. Expression of positive and negative regulators of skeletal muscle mass were explored *1*) in the soleus muscle of rats exposed to severe hypoxia (6,300 m) for 3 wk and *2*) in vastus lateralis muscle of nonhypoxemic and hypoxemic COPD patients. In rodents, we observed a marked inhibition of the mammalian target of rapamycin (mTOR) pathway together with a strong increase in regulated in development and DNA damage response 1 (REDD1) expression and in its association with 14-3-3, a mechanism known to downregulate the mTOR pathway. Importantly, REDD1 overexpression in vivo was sufficient to cause skeletal muscle fiber atrophy in normoxia. Finally, the comparative analysis of skeletal muscle in hypoxemic vs. nonhypoxemic COPD patients confirms that hypoxia causes an inhibition of the mTOR signaling pathway. We thus identify REDD1 as a negative regulator of skeletal muscle mass during chronic hypoxia. Translation of this fundamental knowledge into the clinical investigation of COPD shows the interest to develop therapeutic strategies aimed at inhibiting REDD1.

14-3-3; proteasome; muscle atrophy; AMPK

SKELETAL MUSCLE ATROPHY CAN have a profound effect on overall health and viability. The consequences of a reduction in skeletal muscle mass are multiple and include a decrease in strength and power output, an increased fatigability, and an increase in insulin resistance. Identifying the mechanisms leading to muscle mass loss is therefore a fundamental question to develop therapeutic strategies. The maintenance of skeletal muscle mass results from the balance between protein synthesis and degradation, a disruption in this equilibrium promoting either muscle hypertrophy or muscle atrophy. Protein synthesis and degradation are coordinately regulated by Akt signaling pathways (reviewed in Refs. 14 and 34). When activated by phosphorylation, Akt can phosphorylate and inhibit forkhead transcription factors, thus repressing the expression of atrogenes (35, 39) and the subsequent degradation of targeted proteins by the ubiquitin/proteasome system (UPS). Furthermore, activation of the Akt/mammalian target of rapamycin (mTOR) pathway triggers skeletal muscle hypertrophy (6, 19). The Akt-mediated activation of mTOR is indirect and involves the phosphorylation and inhibition of tuberous sclerosis complex 2 (TSC2) by Akt (17). mTOR then stimulates protein translation notably through 4E-BP1 inhibition and ribosomal protein S6 kinase (S6K) activation (16, 21). The Akt/mTOR pathway is subjected to multiple regulatory influences. Particularly, regulated in development and DNA damage response 1 (REDD1) has been recently shown to inhibit mTOR signaling by releasing TSC2 from its inhibitory 14-3-3 partners (9) in response to cellular stress such as DNA damage (13), energy depletion (38), dexamethasone treatment (42), alcohol intoxication (22), or low O_2 concentration (7).

In healthy subjects exposed to high altitude, chronic hypoxia leads to an inexorable loss of skeletal muscle mass, which has been mainly attributed to hypophagia. However, chronic hypoxia also downregulates skeletal muscle mass regardless of the nutritional status (4). Importantly, hypoxia has been shown to trigger hypophosphorylation of mTOR and its downstream effectors 4E-BP1 and S6K in HEK-293 cells (2), indicating that the Akt/mTOR pathway is sensitive to oxygen deprivation. Furthermore, REDD1 is strongly upregulated in response to hypoxia (7, 37), and REDD1 is essential for mTOR signaling inhibition by low O_2 concentration in mouse embryonic fibroblasts (7). Altogether, these observations suggest that REDD1 could contribute to skeletal muscle atrophy during prolonged hypoxia via the inhibition of mTOR and the subsequent reduction of protein translation. In addition, inhibition of mTOR by REDD1 may also activate the UPS through the mTOR complex 2-Akt-Foxo pathway (15).

Chronic hypoxia is a common feature of chronic obstructive pulmonary disease (COPD), and loss of skeletal muscle mass has been identified as a major determinant of disability in COPD and an independent predictor of mortality (36). Multiple

* H. Benoit and D. Freyssenet were equally contributing senior authors.
Address for reprint requests and other correspondence: H. Benoit, Laboratoire de Physiologie de l'Exercice EA 4338, Faculté de Médecine, 15 rue Ambroise Paré, 42023 Saint Etienne Cedex 2, France (e-mail: henri.benoit@univ-st-etienne.fr).

 0363-6119/10 Copyright © 2010 the American Physiological Society

Downloaded from ajpregu.physiology.org on May 28, 2010

factors have been evoked to explain the atrophy of skeletal muscle in COPD patients, including chronic inflammation, oxidative stress, sedentarity, altered hormonal status, and hypoxia (41, 43). Although hypoxemia is generally less severe in COPD patients than the one observed in subjects exposed to high altitude, the regulation of Akt/mTOR pathway by REDD1 could be one factor contributing to skeletal muscle atrophy in COPD patients.

In the present study, we demonstrated that the Akt/mTOR pathway is downregulated in rat skeletal muscle in response to chronic hypoxia and in skeletal muscle of hypoxemic COPD patients. Furthermore, while REDD1 has not been shown to be required for muscle atrophy, our data show that REDD1 per se is sufficient to trigger skeletal muscle atrophy in the rodent model. Our study provides molecular insights into the mechanisms involved in the regulation of skeletal muscle mass in response to chronic hypoxia and their potential relevance in COPD.

Table 1. *Primer sequences used for PCR analysis*

Gene	Primer Sequence
ACTB	F: 5'-TCACGTCATCACTATCGGCAATG-3'
(GenBank NM_031144)	R: 5'-TTTCATGGATGCCACAGGATTC-3'
ARBP	F: 5'-CCTGCAGACTCGGTTCCTAGAG-3'
(GenBank NM_022402)	R: 5'-CAACAGTCGGCTAGCCAATCTG-3'
Atrogin-1	F: 5'-GCTTGTGCGATGTTAGCCAAGAA-3'
(GenBank NM_133521)	R: 5'-GAAAGTGAGAGCGAGCAGCTCT-3'
CycA	F: 5'-TATCTGCACTGCCAAGACTGAGTG-3'
(GenBank NM_017101)	R: 5'-CTTCTTGCTGGTCTTGCCATTCC-3'
HPRT	F: 5'-CTCATGGACTGATTATGGACAGGAC-3'
(GenBank NM_012583)	R: 5'-GCAGGTCAGCAAAGAACTTATAGCC-3'
MuRF1	F: 5'-GCGAACGACGGAGTTCAGACTATG-3'
(GenBank NM_080903)	R: 5'-CCTTCACCTGCTGGCTGTTTTC-3'
REDD1	F: 5'-TCCCTGGACAGCAGCAACAC-3'
(GenBank NM_080906)	R: 5'-CTTGGCACACAGGTGCTCATC-3'

ACTB, β-actin; ARBP, acidic ribosomal phosphoprotein P0; CycA, cyclophilin A; HPRT, hypoxanthine guanine phosphoribosyl transferase; MuRF1, muscle-specific RING finger protein 1; REDD1, regulated in development and DNA damage response 1.

METHODS

Animals and tissue collection. The protocol was approved by the Comité d'Ethique de la Plate-Forme d'Expérimentation Animale de la Faculté de Médecine (Université Jean Monnet, Saint Etienne). Animals were kept in the Plate-Forme d'Expérimentation Animale (Université Jean Monnet) in accordance with the Helsinki Accords for Human Treatment of animals during experimentation.

Fourteen-week-old male Wistar rats (Charles River Laboratories, L'Arbresles, France; $n = 30$) were randomly assigned into three groups. Hypoxic animals (H group, $n = 10$) were housed in a hypobaric chamber to a simulated altitude of 6,300 m (45.2 kPa, 340 mmHg) for 16 days after 5 days of progressive acclimatization. H rats were fed ad libitum. Two other groups of rats ($n = 10$/group) were maintained in normoxia: control animals (C group) were fed ad libitum, whereas pair-fed animals (PF group) were restricted to have the same food intake as the H group. At the end of the experimental period, soleus (SOL) and extensor digitorum longus (EDL) muscles were removed under general anesthesia (injection of 90 mg/kg ketamine and 10 mg/kg xylazine ip). Animals were then euthanized by pentobarbital sodium overdose.

Histochemical analysis. SOL and EDL muscles were cut transversely at the widest point. Serial transverse sections (12 μm) were cut in a cryostat at −20°C. The tissue slices were then processed by the myosin adenosine triphosphatase method after acid preincubation at pH 4.35 (3). Fiber cross-sectional areas (FCSA) of ~ 180 SOL and 300 EDL fibers per muscle were measured by using a light microscope connected to a computerized image analysis system (UTHSCSA Image Tool 3.00).

mRNA analysis. mRNA isolation, reverse transcriptase reaction, and real-time quantitative PCR were conducted as previously described (1). Data were normalized to cyclophilin A, hypoxanthine guanine phosphoribosyl transferase, acidic ribosomal phosphoprotein P0, and β-actin mRNA levels. Primer sequences are presented in Table 1.

Enzyme activities. Proteins were extracted in a buffer consisting of 75 mM Na_2HPO_4, 25 mM KH_2PO_4, and 2 mM EDTA. Protein concentration was spectrophotometrically measured at 750 nm using a protein assay (Bio-Rad Laboratories, Hercules, CA). Chymotrypsin-like (EC 3.4.21.1), trypsin-like (EC 3.4.21.4), and caspase-like (EC 3.4.13.17) activities of 20S proteasome and cathepsin B+L (EC 3.4.22.1 and EC 3.4.22.15) activities were fluorometrically measured ($\lambda exc = 380$ nm and $\lambda exc = 460$ nm) on a SFM25 fluorimeter (Kontron Instruments, Eching, Germany) (3, 11).

Western blot analysis. Experiments were conducted as previously described (1). Briefly, tissue was homogenized in lysis buffer (in mM: 50 Tris-HCl, 100 NaCl, 2 EDTA, 2 EGTA, 50 β-glycerophosphate, 50 NaF, 1 sodium orthovanadate, 3 benzamidine, 1 PMSF, and 120 nM okadaic acid, 10 μg/ml aprotinin, 10 μg/ml leupeptin, and 1% Triton X-100), and centrifuged at 12,000 *g* for 20 min (4°C). Protein concentration of the supernatant was spectrophotometrically measured at 750 nm using Bio-Rad protein assay. Equal amounts of protein were separated on SDS-PAGE and transferred to nitrocellulose membranes. Gel loading was systematically checked by Coomassie and Ponceau staining (data not shown). With the exception of calpain-2 (1:1,600, cat. no. 39168; Abcam, Cambridge, MA) and -3 (1:100, cat. no. CALP-21A2; Novocastra, Newcastle upon Tyne, UK), glycogen synthase kinase (GSK)3β (1:1,000, cat. no. PA1–26168; Affinity BioReagents, Rockford, IL), REDD1 (1:750, cat. no. 10638–1-AP; Protein Tech Group, Chicago, IL), S6K (1:2,000, cat. nos. A300, 510A; Bethyl Lab, Montgomery, TX), TSC2 (1:200, cat. no. sc-893; Santa Cruz Biotechnology, Santa Cruz, CA), ubiquitin (1:400, cat. no. PW8810; Biomol International, Plymouth Meeting, PA) and 14-3-3 β (1:200, cat. no. sc-1657; Santa Cruz Biotechnology), primary antibodies against Akt (cat. no. 9272), Akt T308 (cat. no. 2965), Akt S473 (cat. no. 9271), AMP-activated protein kinase (AMPK) T172 (cat. no. 2531), GSK3β S9 (cat. no. 9336), 4E-BP1 (cat. no. 9452), 4E-BP1 T37/46 (cat. no. 9459), mTOR (cat. no. 2972), mTOR S2448 (cat. no. 2971), S6 ribosomal protein (S6) (cat. no. 2217), S6 S235/236 (cat. no. 4856), and TSC2 T1462 (cat. no. 3611) were all 1:1,000 and from Cell Signaling Technology, Danvers, MA). Incubation with horseradish peroxidase-conjugated rabbit anti-mouse (1:3,000; Dako, Carpinteria, CA), or goat anti-rabbit (1:2,000; Dako) antibodies was used for chemiluminescent detection of proteins. Films were scanned and quantified using the NIH Image 1.63 program.

REDD1 immunoprecipitation. Lysates containing 150 μg of total protein were incubated with pan-14-3-3 mouse monoclonal antibody (cat. no. MS-1504; LabVision, Fremont, CA) overnight at 4°C. Complexes were immunoprecipitated using protein G Sepharose (Sigma Aldrich, St Louis, MO) for 2 h at 4°C and then washed twice with lysis buffer prior to analysis by 12.5% SDS-PAGE and immunoblotting with REDD1 and 14-3-3 antibodies.

Gene electrotransfer experiments. REDD1 expression plasmid (pCMV-REDD1, GeneService, Cambridge, UK), β-galactosidase expression plasmid (pCMV-β-gal, Clontech, Palo Alto, CA) and pcDNA 3.1-Zeo empty vector (Invitrogen, Carlsbad, CA) were purified (EndoFree Plasmid Mega kit, Qiagen, Valencia, CA) and dissolved in sterile endotoxin-free 0.9% saline solution. Male Wistar rats ($n = 5$) were anesthetized as described above. The SOL muscle was then surgically exposed and injected with 75 μg of pCMV-REDD1 and 75 μg of pCMV-β-gal. Contralateral SOL muscle was similarly injected, but pcDNA3.1-Zeo was used instead of pCMV-REDD1. Electric pulses were delivered by using GET42 electroporator as

Downloaded from ajpregu.physiology.org on May 28, 2010

Table 2. *Hematocrit, body weight, soleus muscle weight, and muscle fiber cross-sectional area in control (C), hypoxic (H), and pair fed (PF) rats*

	C	H	PF
Hematocrit, %	43.1 ± 3.8	67 ± 7.2[c,f]	44.3 ± 4
Body weight, g	425 ± 13.9	331.4 ± 16.3[c,e]	353.5 ± 12.8[c]
SOL weight, mg	163.1 ± 12.3	134.9 ± 13.5[c,e]	151.7 ± 13.5
Protein content, mg/muscle	17,1 ± 1.53	12.91 ± 2,34[c,d]	14,7 ± 1,8[b]
Type I FCSA, μm²	4114 ± 668	3621 ± 409[a]	3854 ± 281
Type II FCSA, μm²	3638 ± 558	2383 ± 728[b,d]	3203 ± 704

SOL, soleus muscle; FCSA, fiber cross-sectional area. Type I fibers represent ~ 90% of total fibers. [a]$P < 0.05$, [b]$P < 0.01$ and [c]$P < 0.001$: different from C; [d]$P < 0.05$, [e]$P < 0.01$, and [f]$P < 0.001$: different from PF.

previously described (12). The fascia and skin were then closed with sutures. Seven days after gene electrotransfer, SOL muscles were removed under general anesthesia. Serial transverse sections (12-μm) were stained for β-galactosidase activity and counterstained with hematoxylin-eosin-saffron (12). FCSA was measured in transfected blue fibers and nontransfected fibers (100 fibers/condition).

COPD subjects and Western blot analysis. Nine patients with mild-to-severe COPD were separated according to the absence or presence of resting hypoxemia (Pa_{O_2} < 60 mmHg). They had been free of exacerbation of their disease for at least 2 mo and did not receive oral corticosteroids. Hypoxemic patients were treated with long-term oxygen therapy for 15 h/day but breathed ambient air for at least 3 h at the time of the biopsy. Muscle biopsies were taken from the vastus lateralis using Weil-Blakesley forceps.

Written consent in accordance with the policy statement regarding the use of human subjects was obtained from all the subjects. This investigation was approved by the Rhône-Alpes-Loire Regional Consultant Committee on Human Protection from Medical Research (DGS No. 2005/023) in accordance with the Declaration of Helsinki.

Protein extraction from muscle samples was performed as described above. Immunolabeling against Akt, Akt T308, GSK3β, GSK3β S9, S6K, S6K T389 (cat. no. 9205, Cell Signaling Technology) and REDD1 were performed as described above.

Statistical analysis. Data are presented as means ± SE on graphs and means ± SD in tables. Statistical comparisons were performed using two-way or one-way ANOVA. Fisher's post hoc test or unpaired *t*-test was then used to determine specific mean difference. All of the statistical analyses were performed using StatView (SAS Institute). The significance level was set at 0.05.

RESULTS

Hypophagia-independent effect of chronic hypoxia on skeletal muscle loss. To test whether hypoxia causes skeletal muscle atrophy regardless of nutritional status, 10 rats were exposed to 6,300 m for 21 days (H group) and compared with

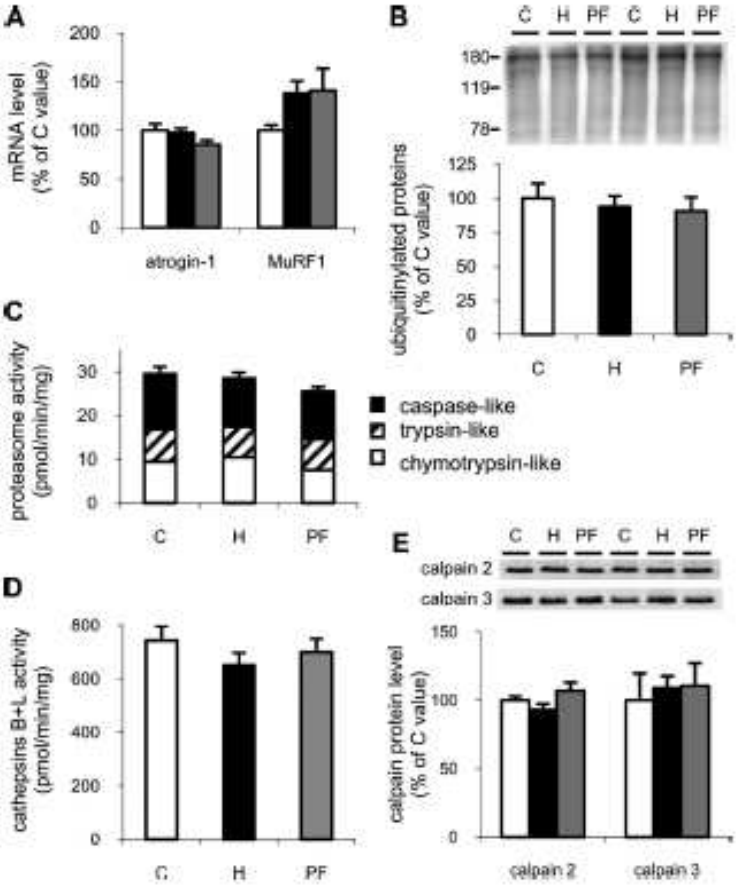

Fig. 1. Ubiquitin/proteasome system is not altered in soleus muscles of hypoxic rats. *A*: mRNA expression of atrogin-1 and muscle-specific RING finger 1 (MuRF1) ubiquitin ligases. *B*: representative immunoblots of total ubiquitin-conjugated proteins (result from 2 different animals per group are shown) and Western blot quantification. *C*: caspase-, trypsin-, and chymotrypsin-like activities of the proteasome 20S. *D*: cathepsins B+L activities. *E*: representative immunoblots of calpain-2 and -3 protein content and corresponding quantification. C, control group; H, hypoxic group; PF, pair-fed group (n = 10 per group).

Downloaded from ajpregu.physiology.org on May 28, 2010

a normoxic control group fed ad libitum (C group) and a normoxic pair-fed group (PF group). Although Pa_{O_2} was not assessed here, previous data show that Pa_{O_2} is ~ 40 mmHg after 21 days at 5,500 m (31), supporting the existence of marked hypoxemia. Consistently, the adaptation to hypoxic stress was illustrated by the increase in hematocrit in H vs. C and PF animals (Table 2). As expected, body weight of H rats was smaller than their normoxic C and PF counterparts (Table 2). Skeletal muscle mass was also affected by severe hypoxia as muscle weight, total protein content, and FCSA of SOL muscle were lower for the H group compared with C and PF groups (Table 2). The ratio of the difference in muscle mass (C − PF)/(C − H) indicates that ~ 60% of muscle mass loss in hypoxia was independent of hypophagia. It is noteworthy that similar results were obtained in EDL muscle (data not shown). Thus, in agreement with previous studies (4, 33), these data show that hypoxia also exerts a hypophagia-independent effect on skeletal muscle mass loss.

Chronic hypoxia and the UPS. The UPS is a main component of the cellular proteolytic machinery, and its activation is associated with muscle mass loss (29). However, the UPS did not seem to be profoundly altered in response to 3 wk of hypoxia. Indeed, mRNA level of MuRF1 and atrogin-1 (Fig. 1*A*), the amount of ubiquitinylated proteins (Fig. 1*B*), and the sum of the three activities of the 20S proteasome (Fig. 1*C*) were not significantly different between H and PF/C groups. It should be noted that the contribution of a transient increase in proteolysis earlier during hypoxia exposure has not been investigated in this study. Similarly, activity of cathepsin B+L (Fig. 1*D*) and expression of calpain-2 and -3 (Fig. 1*E*) were not altered by oxygen reduction, suggesting that lysosomal and Ca^{2+}-dependent systems were not stimulated by hypoxia. Also noteworthy is that the C and PF groups did not differ for any of these parameters.

Chronic hypoxia downregulates the Akt/mTOR pathway. Bodine et al. (6) characterized the Akt/mTOR pathway as a key regulator of skeletal muscle mass and observed that both phosphorylated and total protein contents are altered during skeletal muscle atrophy. Hypoxia-induced atrophy of SOL muscle was associated with significant decreases in the protein content of Akt (23%), mTOR (50%), S6K (25%), and S6 (33%) compared with the PF group (Fig. 2, *A* and *B*). Moreover, hypoxia strongly reduced the phosphorylation of Akt on T308 (36%) and S473 (46%) (Fig. 2, *C* and *D*). Consistently, the phosphorylation of GSK3β S9 and TSC2 T1462 by Akt was also significantly reduced by ~ 30%. mTOR phosphorylation on S2448 and S6 phosphorylation on S235/236 were also significantly reduced. (it should be noted that we did not succeed in detecting S6K phosphorylation on T389 in rodent muscles). However, 4E-BP1 phosphorylation on T37/46 was unaffected. Phosphorylated AMPK can directly activate TSC2 (18) and thus indirectly inhibit mTOR (8). Nevertheless, and in agreement with previous studies (2, 7), AMPK did not seem to participate to mTOR signaling inhibition during hypoxia as phosphorylation of AMPKα on T172 was reduced by ~ 50% ($P < 0.01$) in H group (Fig. 3). Overall, these data showed that severe hypoxia caused a marked inhibition of the Akt/mTOR pathway.

REDD1 associates with 14-3-3 during chronic hypoxia and causes muscle fiber atrophy in vivo. REDD1 has been shown to be a negative regulator of mTOR signaling in mouse embryonic fibroblasts during hypoxia (7). Here, hypoxic animals exhibited a 370% (H vs. C, $P < 0.001$) and 210% (H vs. PF, $P < 0.001$) increase in REDD1 protein level (Fig. 4, *A* and *B*). Importantly, no variation was observed at the mRNA level (Fig. 4*C*), suggesting a posttranscriptional regulation of REDD1 expression by hypoxia. Recently, REDD1 was shown to bind to 14-3-3 family proteins in vitro, thus leading to the dissociation of the TSC2/14-3-3 complex and ultimately to the inhibition of mTOR signaling (9). We therefore investigated the biological relevance of such a mechanism in hypoxia-induced muscle mass loss. Immunoprecipitation of 14-3-3 revealed an increase in

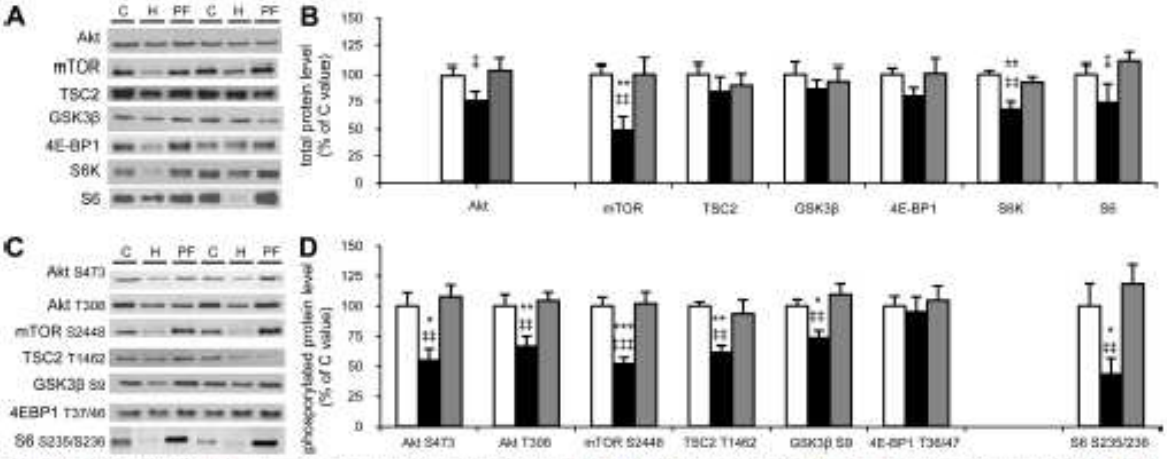

Fig. 2. Chronic hypoxia downregulates the Akt, mammalian target of rapamycin (mTOR) pathway in rat soleus muscle. *A*: representative immunoblots of Akt, mTOR, tuberous sclerosis complex 2 (TSC2), glycogen synthase kinase (GSK)3β, 4E-BP1, S6 kinase (S6K), and S6 ribosomal protein (S6) total protein content in C , H, and PF groups (columns same as in Fig. 1). *B*: corresponding quantification. *C*: representative immunoblots of Akt S473, Akt T308, mTOR S2448, TSC2 T1462, GSK3β S9, 4E-BP1 T37/46, and S6 S235/236 protein content in C, H, and PF groups (columns identified in Fig. 1). *D*: corresponding quantification. *$P < 0.05$, **$P < 0.01$ and ***$P < 0.001$: different from C group; ‡$P < 0.05$, ‡‡$P < 0.01$ and ‡‡‡$P < 0.001$: different from PF ($n = 10$ per group).

Downloaded from ajpregu.physiology.org on May 28, 2010

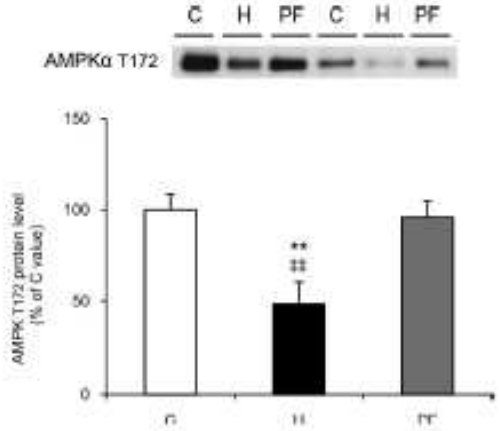

Fig. 3. AMPKα phosphorylation is reduced during chronic hypoxia. Representative immunoblots and corresponding quantification of AMPKα T172 in the soleus muscle of C, H, and PF rats. $^{**}P < 0.01$, different from C group; $‡‡P < 0.01$, different from PF group ($n = 10$ per group).

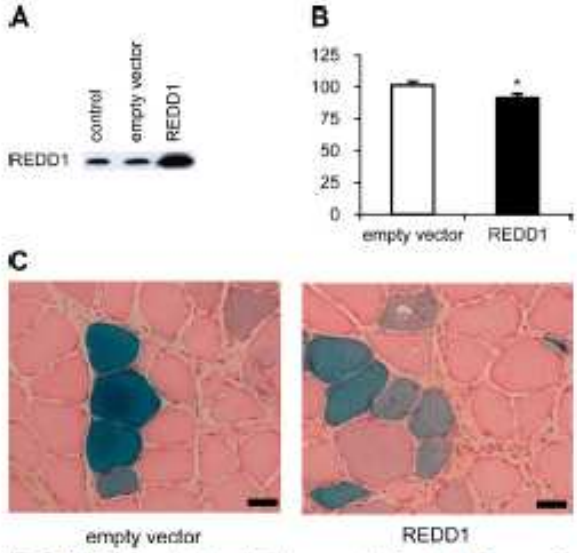

Fig. 5. REDD1 gene electrotransfer induces muscle fiber atrophy in normoxia. *A*: immunoblots of REDD1 protein expression in HEK-293 cells nontransfected (control) or transfected with 1 μg of an empty vector or a REDD1 expression vector. Cells were harvested 48 h after transfection. *B*: mean fiber cross-sectional area (FCSA) of β-galactosidase positive fibers normalized to negative fibers in muscles electroporated with empty vector and REDD1 expression vector. Absolute values are 3,780 ± 114 and 3,417 ± 116 μm² in fibers electroporated with empty and REDD1 expression vectors, respectively. Note that β-galactosidase expression per se has no effect on muscle fibers size. *C*: representative images of hematoxylin-eosin-saffron-stained muscles electroporated with empty vector (blue) or REDD1 expression vector (blue) (scale bar = 50 μm). $^{*}P < 0.05$, different from fibers electroporated with empty vector.

REDD1/14-3-3 association in H vs. C ($P < 0.05$) and PF ($P = 0.06$) muscles (Fig. 4, *A* and *B*), suggesting that TSC2 dissociation from 14-3-3 may contribute to inhibit mTOR signaling during chronic hypoxia. These data suggest that REDD1 could negatively regulate skeletal muscle mass. Thus, we determined whether ectopic expression of REDD1 was sufficient to cause skeletal muscle fiber atrophy in normoxia. After ensuring that our expression vector was sufficient to induce a large increase in REDD1 protein level in HEK-293 cells (Fig. 5*A*), SOL muscles were electroporated with the REDD1 expression vector. Histomorphometric analysis evidenced that REDD1 overexpression caused a 10% reduction in muscle FCSA compared with fibers electroporated with the empty vector ($P < 0.05$; Fig. 5, *B* and *C*). Therefore, REDD1 overexpression is sufficient to cause muscle fiber atrophy in normoxia.

Akt/mTOR signaling and REDD1/14-3-3 association in hypoxemic COPD patients. The biological relevance of these findings was explored in a human model of chronic hypoxemia. COPD patients were divided into two groups, depending on the presence or the absence of resting hypoxemia. With the exception of the arterial O_2 pressure, nonhypoxemic and hypoxemic patients did not differ for any anthropometric and ventilatory parameters (Table 3). While total protein content of Akt, GSK3β, and S6 remained unchanged (data not shown), hypoxemia significantly reduced the phosphorylation of Akt T308, GSK3β S9, and S6K T389 (Fig. 6, *A* and *B*). In agreement with these observations, 14-3-3/REDD1 association was nonsignificantly increased (38%) in hypoxemic vs. nonhypoxemic patients (Fig. 6, *A* and *C*). These results suggest

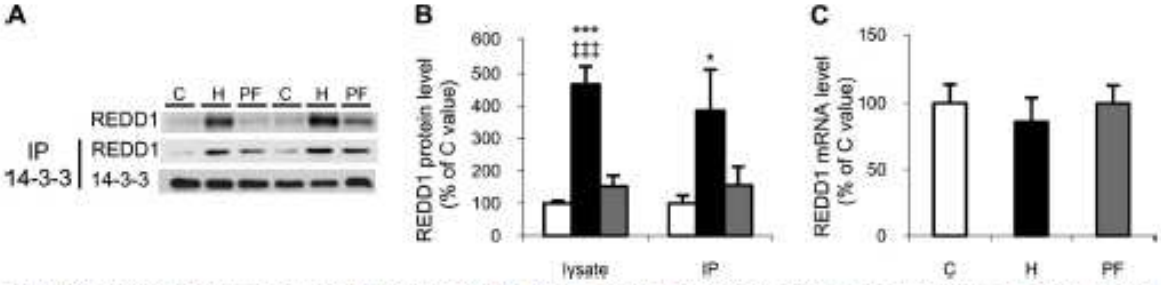

Fig. 4. Chronic hypoxia increases regulated in development and DNA damage response 1 (REDD1) protein expression and promotes its binding to 14-3-3 in soleus muscle. *A*: representative immunoblots of REDD1 protein level in lysate. Representative immunoblots of REDD1 and 14-3-3 protein level after 14-3-3 immunoprecipitation (IP 14-3-3). Note that 14-3-3 expression remained unchanged. *B*: quantification of REDD1 protein content and REDD1/14-3-3 association in the soleus muscle of C, H, and PF groups (columns identified in *C*). *C*: REDD1 mRNA expression. $^{*}P < 0.05$ and $^{***}P < 0.001$, different from C group; $‡‡‡P < 0.001$, different from PF ($n = 6$ per group).

Downloaded from ajpregu.physiology.org on May 28, 2010

Table 3. *Characteristics of nonhypoxemic (n = 4) and hypoxemic (n = 5) chronic obstructive pulmonary disease (COPD) patients*

Characteristic	Nonhypoxemic	Hypoxemic
Age, y	62 ± 9.5	64.2 ± 7.6
Height, cm	165 ± 7	168.4 ± 5.5
Weight, kg	74 ± 9.4	67.2 ± 16.1
BMI, kg/m^2	27.2 ± 3.1	23.8 ± 6.1
FEV_1, liter/s	1.08 ± 0.32	0.88 ± 0.22
FEV_1, % predicted	42.5 ± 8.6	32.8 ± 11.2
Pa_{O_2}, mmHg	72.6 ± 5.2	54.3 ± 5.6*

BMI, body mass index; FEV_1, forced expiratory volume in liters/s; Pa_{O_2}, arterial oxygen pressure. *$P < 0.01$, different from nonhypoxemic.

that REDD1 may contribute to skeletal muscle atrophy in hypoxemic COPD patients.

DISCUSSION

In this study, we show that severe hypoxia causes hypophagia-independent muscle mass loss and downregulates the Akt/mTOR pathway, together with an increase in REDD1/14-3-3 association. A similar inhibition of Akt/mTOR pathway was observed in skeletal muscle of hypoxemic COPD patients. Finally, we also demonstrated that REDD1 overexpression was sufficient to induce skeletal muscle fiber atrophy in normoxia. The present findings are compatible with a mechanism according to which REDD1 reduces muscle mass in hypoxia by releasing the inhibitory action of 14-3-3 on TSC2, thus promoting mTOR inhibition.

Three weeks of severe hypoxia led to a reduction in skeletal muscle mass. However, it is questionable whether the reported decrease in skeletal muscle mass is due to atrophy per se, or inhibition of postnatal muscle growth. In other words, did the animals lose muscle mass or did they simply not gain muscle mass at the same rate as they would under normoxic conditions? Analysis of muscle growth curve according to muscle weight (See supplemental Fig. 1 available online at the *American Journal of Physiology–Regulatory, Integrative and Comparative Physiology* website.) indicates that muscle growth was not completely achieved at the beginning of the experiment (animal weight was 350 g), suggesting that inhibition of muscle growth and atrophy per se are contributing mechanisms to hypoxia-induced muscle mass loss.

The lower muscle mass was associated with a sharp decrease in Akt/mTOR signaling, while the UPS was not altered after 3 wk of severe hypoxia. However, we cannot rule out the contribution of a transient increase in proteolysis earlier during hypoxia exposure. Indeed, some transitory adaptations may be back to baseline values after 3 wk. This could be particularly relevant for the ubiquitin proteasome system, as a transitory activation of this proteolytic pathway has been frequently reported at the onset of skeletal muscle atrophy (5, 23). Our observations are consistent with previous in vitro studies showing that acute hypoxia inhibits Akt/mTOR pathway in HEK-293 cells (2, 25). Moreover, we recorded a diminution in Akt, mTOR, S6K, and S6 protein expression, corroborating the decrease in mTOR expression reported in subjects exposed to 4,559 m for 7–9 days (40). Altogether, these data show that hypoxia triggers molecular events that result in the inhibition of major regulators of the translational machinery.

The TSC1/2 complex is an important crossroad of mTOR signaling that integrates multiple regulatory influences (14). Akt prevents TSC1/2 dimerization by phosphorylating TSC2 on S939 and T1462 (17, 28). In the present study, TSC2 phosphorylation at T1462 was reduced in hypoxia, indicating a decrease in Akt activity. Consistently, Akt phosphorylation at T308 was reduced by hypoxia, suggesting a decrease in Akt activation by the phosphoinositide-dependent protein kinase-1. Full activation of Akt also requires to the phosphorylation of S473 by the mTOR complex 2 (15). The decrease in Akt phosphorylation at S473 thus indicates that mTOR complex 2 activity is also affected by hypoxia (see below). This reinforces the hypothesis that Foxo-induced proteolysis may have been stimulated during hypoxic exposure.

Akt-mediated inhibition of TSC1/2 complex involves the sequestration of TSC2 by 14-3-3 (26) when TSC2 is phosphorylated by Akt on S939 and T1462 (9). Moreover, Deyoung et al. (9) showed in HEK-293T cells that REDD1 binds to 14-3-3, leading to the release of TSC2 (9). A similar mechanism involving REDD2 has recently been demonstrated (30), but REDD2 is not sensitive to hypoxia (32, 37). Here, REDD1 expression was dramatically increased, further supporting that REDD1 is highly responsive to hypoxia (20, 24, 37). In

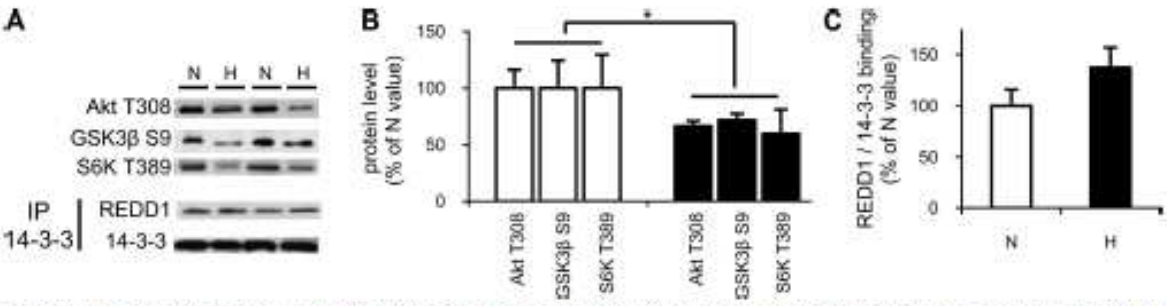

Fig. 6. Regulation of Akt/mTOR pathway and REDD1/14-3-3 binding in nonhypoxemic (N) and hypoxemic (H) chronic obstructive pulmonary disease (COPD) patients. *A*: representative immunoblots of Akt T308, GSK3β S9, and S6K T389 protein level in lysate. Representative immunoblots of REDD1 and 14-3-3 protein level after 14-3-3 immunoprecipitation (IP 14-3-3) in vastus lateralis of COPD patients. Note that 14-3-3 expression remained unchanged. *B*: quantification of Akt T308, GSK3β S9, and S6K T389 protein level in N and H COPD subjects. *C*: quantification of REDD1/14-3-3 association. *$P < 0.05$, different from N patients (n = 4–5 per group).

Downloaded from ajpregu.physiology.org on May 28, 2010

addition, chronic hypoxia induced a strong increase in REDD1/14-3-3 association. Together with the decrease in TSC2 phosphorylation on T1462, this mechanism likely contributes to release TSC2 from 14-3-3 in muscles from hypoxic rats. In turn, this regulation probably results in a greater TSC1/TSC2 association, therefore contributing to the strong reduction in the phosphorylation of mTOR on S2448 and S6 on S235/236 in H group. Regarding mTOR phosphorylation, one should note that mTOR activity is also regulated by protein interactions (15). Therefore, and although mTOR phosphorylation at Ser2448 was statistically decreased, supporting a response of this site-specific phosphorylation of Ser2448 to hypoxia, we cannot also exclude the possibility that mTOR could be also specifically regulated by protein interaction in response to chronic hypoxia. It is noteworthy that it has been shown that REDD1 overexpression caused Akt inhibition by decreasing T308 and S473 phosphorylation in neurons (27). Therefore, the decrease in Akt phosphorylation in SOL muscles from hypoxic animals may also result from an inhibition of mTOR complex 2 by REDD1. Altogether, these data identify REDD1 as a critical regulator of the Akt/mTOR pathway during hypoxia in vivo and point to the potential role of REDD1 as an atrophic factor. To test this hypothesis, we determined the effect of REDD1 overexpression in normoxia on skeletal muscle fiber area. This experiment demonstrates that ectopic REDD1 expression decreases skeletal muscle fiber area. Additional information regarding the role of REDD1 would be provided by the use of dominant-negative models aimed at determining whether REDD1 is required for muscle atrophy.

Loss of skeletal muscle mass has been identified as a major determinant of disability in COPD patients (36). Many causes have been proposed to explain muscle atrophy in COPD patients (41, 43), but the knowledge of the biochemical pathways involved is limited. One possibility would be a reduction in Akt/mTOR pathway activation. However, Doucet et al. (10) showed that nonhypoxemic COPD patients (Pa_{O_2} = 76 mmHg) with low muscle mass exhibited an increase in Akt/mTOR activation compared with COPD patients with preserved muscle mass. In the present study, we hypothesized that the severity of hypoxemia could be a factor contributing to downregulate Akt/mTOR signaling pathway. We observed that skeletal muscle of hypoxemic COPD patients (Pa_{O_2} = 54 mmHg) displayed a significant reduction in Akt/mTOR signaling compared with nonhypoxemic COPD patients (Pa_{O_2} = 73 mmHg). In agreement with our observations in rodents, REDD1 protein was detectable in human skeletal muscle and its binding to 14-3-3 was nonsignificantly increased in skeletal muscles of hypoxemic COPD patients (38%). One should note that this observation was obtained with a limited number of subjects (n = 4/group). Additional subjects must be included to definitely conclude on the regulation of REDD1 by 14-3-3 in skeletal muscle of COPD patients.

Perspectives and Significance

This work represents a significant advance in the understanding of the mechanisms leading to skeletal muscle atrophy in response to chronic hypoxia. The present data reveal the existence of a mechanism by which hypoxia-induced expression of REDD1 actively contributes to the inhibition of mTOR pathway in rat skeletal muscle. Our preliminary data also suggests that this mechanism could be relevant in skeletal muscle of hypoxemic COPD patients. Importantly, REDD1 expression is also stimulated by glucocorticoid administration (42) and nutritional deprivation (38), two common features of COPD. Defining strategies aimed at disrupting REDD1/14-3-3 association may thus represent a promising way to counteract skeletal muscle loss in COPD patients. Future research should be aimed at delineating the potential mechanism(s) responsible for the increase in REDD1 expression, as well as examine the importance of REDD1 in mediating skeletal muscle adaptations in response to other forms of stress.

ACKNOWLEDGMENTS

The authors are grateful to Thierry Busso (EA 4338, Saint Etienne, France) and Laurent Schaeffer (UMR 5239, Lyon, France) for helpful discussions. Maurice Hayot and Jacques Mercier (INSERM, ERI 25, Montpellier, France) are gratefully acknowledged for help in COPD study.

GRANTS

This work was supported by the Ministère de la Santé (Programme Hospitalier de Recherche Clinique 2004, Grant 0408079 to F. Costes). F. Favier was supported by an Allocation Doctorale de Recherche from the Ministère de l'Enseignement Supérieur et de la Recherche.

DISCLOSURES

No conflicts of interest, financial, or otherwise, are declared by the author(s).

REFERENCES

1. **Amirouche A, Durieux AC, Banzet S, Koulmann N, Bonnefoy R, Mouret C, Bigard X, Peinnequin A, Freyssenet D.** Down-regulation of Akt/mTOR signaling pathway in response to myostatin overexpression in skeletal muscle. *Endocrinology* 150: 286–294, 2009.
2. **Arsham AM, Howell JJ, Simon MC.** A novel hypoxia-inducible factor-independent hypoxic response regulating mammalian target of rapamycin and its targets. *J Biol Chem* 278: 29655–29660, 2003.
3. **Berthon P, Duguez S, Favier FB, Amirouche A, Feasson L, Vico L, Denis C, Freyssenet D.** Regulation of ubiquitin-proteasome system, caspase enzyme activities, and extracellular proteinases in rat soleus muscle in response to unloading. *Pflügers Arch* 454: 625–633, 2007.
4. **Bigard AX, Douce P, Merino D, Lienhard F, Guezennec CY.** Changes in dietary protein intake fail to prevent decrease in muscle growth induced by severe hypoxia in rats. *J Appl Physiol* 80: 208–215, 1996.
5. **Bodine SC, Latres E, Baumhueter S, Lai VK, Nunez L, Clarke BA, Poueymirou WT, Panaro FJ, Na E, Dharmarajan K, Pan ZQ, Valenzuela DM, DeChiara TM, Stitt TN, Yancopoulos GD, Glass DJ.** Identification of ubiquitin ligases required for skeletal muscle atrophy. *Science* 294: 1704–1708, 2001.
6. **Bodine SC, Stitt TN, Gonzalez M, Kline WO, Stover GL, Bauerlein R, Zlotchenko E, Scrimgeour A, Lawrence JC, Glass DJ, Yancopoulos GD.** Akt/mTOR pathway is a crucial regulator of skeletal muscle hypertrophy and can prevent muscle atrophy in vivo. *Nat Cell Biol* 3: 1014–1019, 2001.
7. **Brugarolas J, Lei K, Hurley RL, Manning BD, Reiling JH, Hafen E, Witters LA, Ellisen LW, Kaelin WG Jr.** Regulation of mTOR function in response to hypoxia by REDD1 and the TSC1/TSC2 tumor suppressor complex. *Genes Dev* 18: 2893–2904, 2004.
8. **Cheng SW, Fryer LG, Carling D, Shepherd PR.** Thr2446 is a novel mammalian target of rapamycin (mTOR) phosphorylation site regulated by nutrient status. *J Biol Chem* 279: 15719–15722, 2004.
9. **Deyoung MP, Horak P, Sofer A, Sgroi D, Ellisen LW.** Hypoxia regulates TSC1/2 mTOR signaling and tumor suppression through REDD1-mediated 14-3-3 shuttling. *Genes Dev* 22: 239–251, 2008.
10. **Doucet M, Russell AP, Leger B, Debigare R, Joanisse DR, Caron MA, LeBlanc P, Maltais F.** Muscle atrophy and hypertrophy signaling in patients with chronic obstructive pulmonary disease. *Am J Respir Crit Care Med* 176: 261–269, 2007.
11. **Duguez S, Bihan MC, Gouttefangeas D, Feasson L, Freyssenet D.** Myogenic and nonmyogenic cells differentially express proteinases, Hsc/

Downloaded from ajpregu.physiology.org on May 28, 2010

Hsp70, and BAG-1 during skeletal muscle regeneration. *Am J Physiol Endocrinol Metab* 285: E206–E215, 2003.
12. **Durieux AC, Bonnefoy R, Manissolle C, Freyssenet D.** High-efficiency gene electrotransfer into skeletal muscle: description and physiological applicability of a new pulse generator. *Biochem Biophys Res Commun* 296: 443–450, 2002.
13. **Ellisen LW, Ramsayer KD, Johannessen CM, Yang A, Beppu H, Minda K, Oliner JD, McKeon F, Haber DA.** REDD1, a developmentally regulated transcriptional target of p63 and p53, links p63 to regulation of reactive oxygen species. *Mol Cell* 10: 995–1005, 2002.
14. **Favier FB, Benoit H, Freyssenet D.** Cellular and molecular events controlling skeletal muscle mass in response to altered use. *Pflügers Arch* 456: 587–600, 2008.
15. **Guertin DA, Stevens DM, Thoreen CC, Burds AA, Kalaany NY, Moffat J, Brown M, Fitzgerald KJ, Sabatini DM.** Ablation in mice of the mTORC components raptor, rictor, or mLST8 reveals that mTORC2 is required for signaling to Akt-FOXO and PKCα, but not S6K1. *Dev Cell* 11: 859–871, 2006.
16. **Hornberger TA, Stuppard R, Conley KE, Fedele MJ, Fiorotto ML, Chin ER, Esser KA.** Mechanical stimuli regulate rapamycin-sensitive signalling by a phosphoinositide 3-kinase-, protein kinase B- and growth factor-independent mechanism. *Biochem J* 380: 795–804, 2004.
17. **Inoki K, Li Y, Zhu T, Wu J, Guan KL.** TSC2 is phosphorylated and inhibited by Akt and suppresses mTOR signalling. *Nat Cell Biol* 4: 648–657, 2002.
18. **Inoki K, Zhu T, Guan KL.** TSC2 mediates cellular energy response to control cell growth and survival. *Cell* 115: 577–590, 2003.
19. **Izumiya Y, Hopkins T, Morris C, Sato K, Zeng L, Viereck J, Hamilton JA, Ouchi N, Lebrasseur NK, Walsh K.** Fast/glycolytic muscle fiber growth reduces fat mass and improves metabolic parameters in obese mice. *Cell Metab* 7: 159–172, 2008.
20. **Jin HO, An S, Lee HC, Woo SH, Seo SK, Choe TB, Yoo DH, Lee SB, Um HD, Lee SJ, Park MJ, Kim JI, Hong SI, Rhee CH, Park IC.** Hypoxic condition- and high cell density-induced expression of Redd1 is regulated by activation of hypoxia-inducible factor-1α and Sp1 through the phosphatidylinositol 3-kinase/Akt signaling pathway. *Cell Signal* 19: 1393–1403, 2007.
21. **Kubica N, Bolster DR, Farrell PA, Kimball SR, Jefferson LS.** Resistance exercise increases muscle protein synthesis and translation of eukaryotic initiation factor 2Bε mRNA in a mammalian target of rapamycin-dependent manner. *J Biol Chem* 280: 7570–7580, 2005.
22. **Lang CH, Frost RA, Vary TC.** Acute alcohol intoxication increases REDD1 in skeletal muscle. *Alcohol Clin Exp Res* 32: 796–805, 2008.
23. **Lecker SH, Jagoe RT, Gilbert A, Gomes M, Baracos V, Bailey J, Price SR, Mitch WE, Goldberg AL.** Multiple types of skeletal muscle atrophy involve a common program of changes in gene expression. *FASEB J* 18: 39–51, 2004.
24. **Lee M, Ilikrum M, Oh S, Bull DA, Kim SW.** Sp1-dependent regulation of the RTP801 promoter and its application to hypoxia-inducible VEGF plasmid for ischemic disease. *Pharm Res* 21: 736–741, 2004.
25. **Liu L, Cash TP, Jones RG, Keith B, Thompson CB, Simon MC.** Hypoxia-induced energy stress regulates mRNA translation and cell growth. *Mol Cell* 21: 521–531, 2006.
26. **Liu MY, Cai S, Espejo A, Bedford MT, Walker CL.** 14-3-3 interacts with the tumor suppressor tuberin at Akt phosphorylation site(s). *Cancer Res* 62: 6475–6480, 2002.
27. **Malagelada C, Jin ZH, Greene LA.** RTP801 is induced in Parkinson's disease and mediates neuron death by inhibiting Akt phosphorylation/activation. *J Neurosci* 28: 14363–14371, 2008.
28. **Manning BD, Tee AR, Logsdon MN, Blenis J, Cantley LC.** Identification of the tuberous sclerosis complex-2 tumor suppressor gene product tuberin as a target of the phosphoinositide 3-kinase/akt pathway. *Mol Cell* 10: 151–162, 2002.
29. **Mitch WE, Goldberg AL.** Mechanisms of muscle wasting. The role of the ubiquitin-proteasome pathway. *N Engl J Med* 335: 1897–1905, 1996.
30. **Miyazaki M, Esser KA.** REDD2 is enriched in skeletal muscle and inhibits mTOR signaling in response to leucine and stretch. *Am J Physiol Cell Physiol* 296: C583–C592, 2009.
31. **Ou LC, Chen J, Fiore E, Leiter JC, Brinck-Johnsen T, Birchard GF, Clemons G, Smith RP.** Ventilatory and hematopoietic responses to chronic hypoxia in two rat strains. *J Appl Physiol* 72: 2354–2363, 1992.
32. **Pisani DF, Leclerc L, Jarretou G, Marini JF, Dechesne CA.** SMHS1 is involved in oxidative/glycolytic-energy metabolism balance of muscle fibers. *Biochem Biophys Res Commun* 326: 788–793, 2005.
33. **Rose MS, Houston CS, Fulco CS, Coates G, Sutton JR, Cymerman A.** Operation Everest II: Nutrition and body composition. *J Appl Physiol* 65: 2545–2551, 1988.
34. **Sandri M.** Signaling in muscle atrophy and hypertrophy. *Physiology (Bethesda)* 23: 160–170, 2008.
35. **Sandri M, Sandri C, Gilbert A, Skurk C, Calabria E, Picard A, Walsh K, Schiaffino S, Lecker SH, Goldberg AL.** Foxo transcription factors induce the atrophy-related ubiquitin ligase atrogin-1 and cause skeletal muscle atrophy. *Cell* 117: 399–412, 2004.
36. **Schols AM, Broekhuizen R, Weling-Scheepers CA, Wouters EF.** Body composition and mortality in chronic obstructive pulmonary disease. *Am J Clin Nutr* 82: 53–59, 2005.
37. **Shoshani T, Faerman A, Mett I, Zelin E, Tenne T, Gorodin S, Moshel Y, Elbaz S, Budanov A, Chajut A, Kalinski H, Kamer I, Rozen A, Mor O, Keshet E, Leshkowitz D, Einat P, Skaliter R, Feinstein E.** Identification of a novel hypoxia-inducible factor 1-responsive gene, RTP801, involved in apoptosis. *Mol Cell Biol* 22: 2283–2293, 2002.
38. **Sofer A, Lei K, Johannessen CM, Ellisen LW.** Regulation of mTOR and cell growth in response to energy stress by REDD1. *Mol Cell Biol* 25: 5834–5845, 2005.
39. **Stitt TN, Drujan D, Clarke BA, Panaro F, Timofeyva Y, Kline WO, Gonzalez M, Yancopoulos GD, Glass DJ.** The IGF-1/PI3K/Akt pathway prevents expression of muscle atrophy-induced ubiquitin ligases by inhibiting FOXO transcription factors. *Mol Cell* 14: 395–403, 2004.
40. **Vigano A, Ripamonti M, De Palma S, Capitanio D, Vasso M, Wait R, Lundby C, Cerretelli P, Gelfi C.** Proteins modulation in human skeletal muscle in the early phase of adaptation to hypobaric hypoxia. *Proteomics* 8: 4668–4679, 2008.
41. **Wagner PD.** Possible mechanisms underlying the development of cachexia in COPD. *Eur Respir J* 31: 492–501, 2008.
42. **Wang H, Kubica N, Ellisen LW, Jefferson LS, Kimball SR.** Dexamethasone represses signaling through the mammalian target of rapamycin in muscle cells by enhancing expression of REDD1. *J Biol Chem* 281: 39128–39134, 2006.
43. **Wust RC, Degens H.** Factors contributing to muscle wasting and dysfunction in COPD patients. *Int J Chron Obstruct Pulmon Dis* 2: 289–300, 2007.

Downloaded from ajpregu.physiology.org on May 28, 2010

OPEN ACCESS Freely available online

PLoS one

Evidence for Mitochondrial Respiratory Deficiency in Rat Rhabdomyosarcoma Cells

Vanessa E. Jahnke[1], Odile Sabido[1,2], Aurélia Defour[1], Josiane Castells[1], Etienne Lefai[3], Damien Roussel[4], Damien Freyssenet[1]*

1 Université de Lyon, Université Jean Monnet, Laboratoire de Physiologie de l'Exercice EA4338, Saint Etienne, France, 2 Université de Lyon, Université Jean Monnet, Centre Commun de Cytométrie en Flux, Saint Etienne, France, 3 Université de Lyon, Université Claude Bernard Lyon 1, Régulations Métaboliques Nutrition et Diabètes INSERM U870, Oullins, France, 4 Université de Lyon, Université Claude Bernard Lyon 1, Laboratoire de Physiologie Intégrative Cellulaire et Moléculaire CNRS U5123, Villeurbanne, France

Abstract

Background: Mitochondria can sense signals linked to variations in energy demand to regulate nuclear gene expression. This retrograde signaling pathway is presumed to be involved in the regulation of myoblast proliferation and differentiation. Rhabdomyosarcoma cells are characterized by their failure to both irreversibly exit the cell cycle and complete myogenic differentiation. However, it is currently unknown whether mitochondria are involved in the failure of rhabdomyosarcoma cells to differentiate.

Methodology/Principal Findings: Mitochondrial biogenesis and metabolism were studied in rat L6E9 myoblasts and R1H rhabdomyosarcoma cells during the cell cycle and after 36 hours of differentiation. Using a combination of flow cytometry, polarographic and molecular analyses, we evidenced a marked decrease in the cardiolipin content of R1H cells cultured in growth and differentiation media, together with a significant increase in the content of mitochondrial biogenesis factors and mitochondrial respiratory chain proteins. Altogether, these data indicate that the mitochondrial inner membrane composition and the overall process of mitochondrial biogenesis are markedly altered in R1H cells. Importantly, the dysregulation of protein-to-cardiolipin ratio was associated with major deficiencies in both basal and maximal mitochondrial respiration rates. This deficiency in mitochondrial respiration probably contributes to the inability of R1H cells to decrease mitochondrial H_2O_2 level at the onset of differentiation.

Conclusion/Significance: A defect in the regulation of mitochondrial biogenesis and mitochondrial metabolism may thus be an epigenetic mechanism that may contribute to the tumoral behavior of R1H cells. Our data underline the importance of mitochondria in the regulation of myogenic differentiation.

Citation: Jahnke VE, Sabido O, Defour A, Castells J, Lefai E, et al. (2010) Evidence for Mitochondrial Respiratory Deficiency in Rat Rhabdomyosarcoma Cells. PLoS ONE 5(1): e8637. doi:10.1371/journal.pone.0008637

Editor: Alejandro Lucia, Universidad Europea de Madrid, Spain

Received July 6, 2009; **Accepted** December 11, 2009; **Published** January 8, 2010

Copyright: © 2010 Jahnke et al. This is an open-access article distributed under the terms of the Creative Commons Attribution License, which permits unrestricted use, distribution, and reproduction in any medium, provided the original author and source are credited.

Funding: This work was supported by the Ligue Contre le Cancer Comité de la Loire (grant to D. Freyssenet). V.E. Jahnke was supported by an Allocation Doctorale de Recherche from the Ligue Contre le Cancer. The funders had no role in study design, data collection and analysis, decision to publish, or preparation of the manuscript.

Competing Interests: The authors have declared that no competing interests exist.

* E-mail: damien.freyssenet@univ-st-etienne.fr

Introduction

Adult skeletal muscle fibers are formed via the fusion of individual myoblasts during development. Although multinucleated muscle fibers are considered to be permanently differentiated and therefore incapable of mitotic activity, skeletal muscle retains the capacity to repair and regenerate, mainly due to the presence of satellite cells. During muscle regeneration after injury, satellite cells are activated, proliferate by multiple rounds of cell division, fuse together and with existing damaged muscle fibers to form differentiated muscle fibers. Myoblasts can also return to quiescence and contribute to the self-renewal of satellite cell population (reviewed in [1]). Recapitulation of the myogenic program requires energy production for the execution of a number of regulatory biosynthesis events such as DNA synthesis, mitosis but also protein and lipid synthesis. As the major energy source in most of cells, mitochondrial oxidative phosphorylation may therefore play important regulatory roles during myogenesis.

Rhabdomyosarcoma, the most common soft tissue sarcoma in children and adolescents, arises from immature cells that are destined to form striated skeletal muscle [2]. Although rhabdomyosarcoma cells express a number of myogenic-dependent proteins [3,4,5], these cells are characterized by their failure to both irreversibly exit the cell cycle and complete skeletal muscle differentiation program [4]. Therefore, rhabdomyosarcoma cells constitute an interesting model to study the mechanisms that control myogenic differentiation.

The incapacity of rhabdomyosarcoma cells to differentiate has been assigned to different chromosomal abnormalities. For example, two chromosomal translocations, t(2;13)(q35;q14) and t(1;13)(p36;q14), are associated with numerous alveolar rhabdomyosarcomas, the resulting fusion proteins (PAX3-FKHR and PAX7-FKHR) acquiring the capacity to inhibit MyoD and the subsequent differentiation of rhabdomyosarcoma cells [6,7,8]. Besides the genetic characterization of rhabdomyosarcoma,

epigenetic mechanisms may also contribute to the failure of rhabdomyosarcomas cells to differentiate. In 1956, Otto Warburg described that experimentally-induced tumour cells exhibited a reduced oxidative phosphorylation and an increased glycolysis [9], raising the possibility that the original non-carcinogenic phenotype of these mammalian cells was regulated by mitochondrial oxidative phosphorylation. This hypothesis is supported by a number of studies showing that experimental inhibition or activation of mitochondrial biogenesis and mitochondrial metabolism strongly modulates *in vitro* and *in vivo* oncogenic phenotype [10,11,12,13,14,15]. Importantly, this regulatory function of mitochondria seems to be particularly relevant for the regulation of myogenic differentiation. *In vitro* and *in vivo* myogenesis is accompanied by a tight regulation of mitochondrial biogenesis [16,17,18]. Furthermore, the disruption of mitochondrial membrane potential in C2C12 myoblasts is responsible for an invasive behaviour [10,19]. Conversely, the stimulation of mitochondrial oxidative metabolism by pyruvate blocks the proliferation of L6E9 muscle cells [20], and the stimulation of mitochondrial biogenesis induces the expression of myogenin and muscle-specific genes [21,22]. A defect in mitochondrial biogenesis and/or mitochondrial metabolism may thus contribute to the failure of rhabdomyosarcoma cells to exit the cell cycle and differentiate.

Here, we report that the expression of mitochondrial proteins and mitochondrial biogenesis factors is markedly increased in rhabdomyosarcoma cells, together with a large decrease in cardiolipin content. The differential regulation of mitochondrial protein expression and cardiolipin content was associated with major deficiencies in both basal and maximal mitochondrial respiration rates. These findings indicate that a defect in the regulation of mitochondrial biogenesis and mitochondrial metabolism is an epigenetic mechanism that may contribute to the tumoral behavior of R1H cells. Furthermore, they establish functional links between the regulation of mitochondrial biogenesis and the regulation of myogenic differentiation.

Results

Cell Cycle Analysis of L6E9 and R1H Rhabdomyosarcoma Cells

Figure 1 indicates the relative distribution of L6E9 and R1H cells in G1, S and G2M phases when cultured with growth medium (Figure 1A) and differentiation medium (Figure 1B). In agreement with the tumoral behavior of rhabdomyosarcoma cells, R1H cells cultured with differentiation medium for 36 hours failed to exit the cell cycle and were still cycling, as evidenced by the presence of cells in S (11.6%) and G2M (20.8%) phases. For comparison purpose, 0.5% and 8.9% of L6E9 cells were in S and G2M phases, respectively. In agreement with these observations, PCNA, a cofactor of DNA polymerase δ during S phase, whose expression was reduced by 50% at the onset of differentiation in L6E9 cells, was even significantly increased in R1H cells cultured with differentiation medium, further illustrating the failure of R1H cells to exit the cell cycle (Figure 1C).

Regulation of Mitochondrial Biogenesis

We first determined the content of cardiolipin, the phospholipid signature of the mitochondrial inner membrane that accounts for 20% of mitochondrial phospholipids [23]. When observed under fluorescence microscopy, L6E9 mitochondria stained with NAO, a fluorophore which binds to cardiolipin [24], appeared bright, which contrasted with the faint intensity of NAO staining in R1H cells (Figure 2A). Quantitative analysis of NAO fluorescence by flow cytometry corroborated this observation (Figure 2B). Furthermore, R1H cells poorly increased their cardiolipin content during the cell cycle (37%), whereas a two-fold increase was observed in L6E9 cells. To quantitate directly the regulation of mitochondrial content, we next used a fluorochrome (MitoTracker Deep Red) that yields a fluorescence signal proportional to the density of mitochondria. As shown in Figure 2C, the mitochondrial content was increased by about 2-fold in G2M phases compared to G1 phases in L6E9 and R1H cells. In agreement with these observations, the ratio of mitochondrial DNA to nuclear DNA was similar in L6E9 and R1H cells (Figure 2D). Overall, these data suggest that a progressive depletion of the cardiolipin content occurs as R1H cells divide, while mitochondrial content is preserved.

We next investigated the expression of mitochondrial biogenesis factors and respiratory chain proteins (Table 1). As previously observed [25], expression of mitochondrial proteins and mitochondrial biogenesis factors in L6E9 myoblasts was decreased at the onset of differentiation. One reminiscent feature of this analysis was the higher amount of mitochondrial respiratory chain proteins in R1H cells when compared to L6E9 cells. This pattern was particularly marked for cells cultured in differentiation medium. In agreement with these data, the protein content of mitochondrial biogenesis factors was also higher in R1H cells compared to L6E9 cells. Most importantly, the decrease in the expression of mitochondrial biogenesis factors and respiratory chain proteins observed in L6E9 cells cultured with differentiation medium for 36 hours did not occur in R1H cells. Altogether these data indicate that the mitochondrial inner membrane composition and the overall process of mitochondrial biogenesis are markedly altered in R1H cells.

Cellular Metabolism

To test the bioenergetic relevance of these observations, mitochondrial respiration was determined. The rate of basal respiration was dramatically lower in R1H cells than in L6E9 cells both in growth and differentiation media (Table 2). Similarly, oligomycin-insensitive respiration was lower in R1H cells compared to L6E9 cells. The rate of FCCP-stimulated maximal respiration was even more markedly reduced. When expressed as a percent of basal respiration, oxygen consumption dedicated to mitochondrial ATP synthesis accounted for about 70%, whereas proton leak across the mitochondrial inner accounted for the remaining 30% (Figure 3A). This was consistently observed in L6E9 and R1H cells both in growth medium and differentiation medium. Despite lower rates of oxygen consumption, mitochondria of R1H cells thus allocated the same proportion of energy to produce ATP or to counteract proton leakage when compared to L6E9 cells, indicating that mitochondrial inner membrane permeability was similar between L6E9 and R1H cells. By contrast, the mitochondrial respiratory reserve (FCCP-induced maximal respiration rate minus basal endogenous respiration rate) was dramatically reduced in R1H cells. Therefore, the endogenous respiration of R1H cells was almost maximally stimulated in the basal state, with mitochondria operating at 80% and 60% of maximal respiration under growth and differentiation conditions, respectively. For comparison purposes, L6E9 cells retained a large mitochondrial respiratory reserve, leading mitochondria to operate at 37% and 30% of maximal respiration under growth and differentiation conditions, respectively. Reduced mitochondrial respiration suggests that R1H cells should have switch to a glycolytic energy production to sustain the rate of proliferation. Accordingly, lactate production by R1H cells was about 3-fold higher than the one reported for L6E9 cells (Figure 3B).

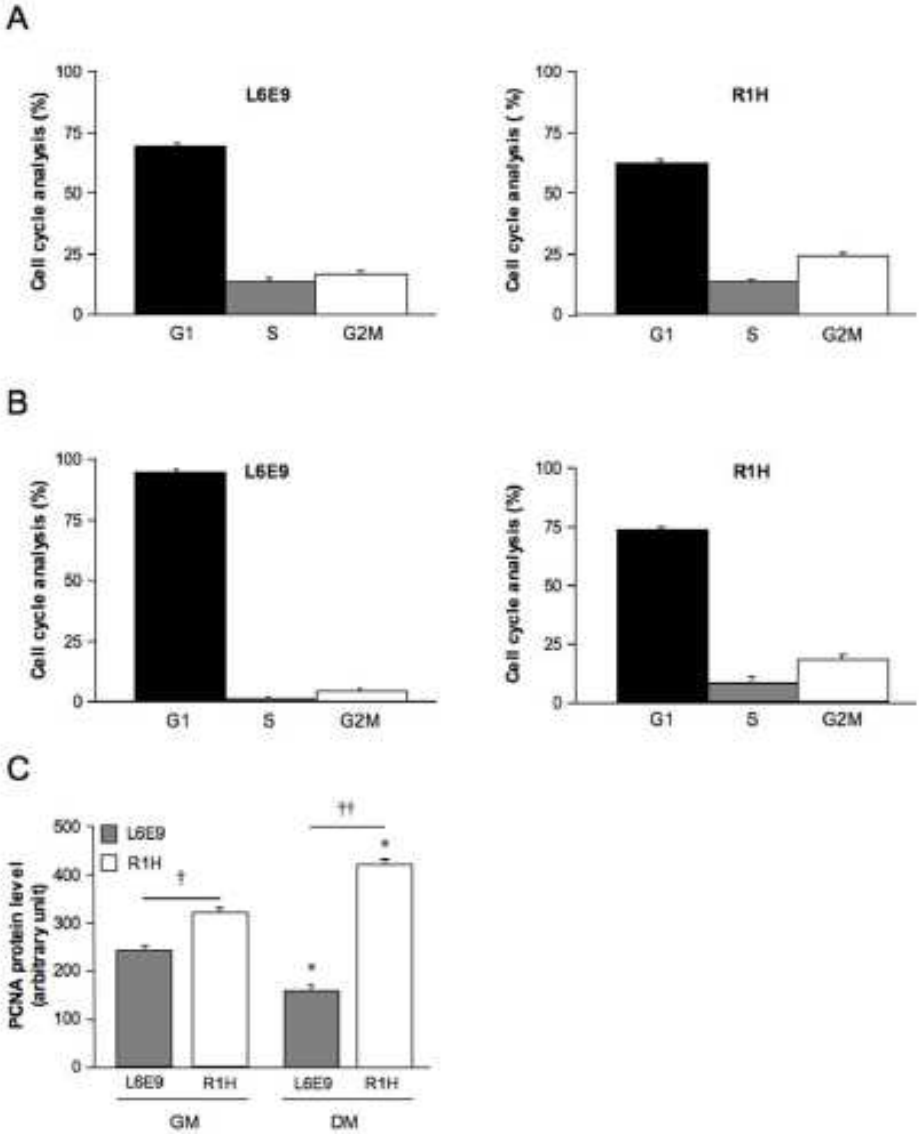

Figure 1. Cell cycle analysis and proliferating cell nuclear antigen (PCNA) protein content in L6E9 and R1H cells. Cell cycle analysis of L6E9 myoblasts and R1H cells cultured in growth medium (A) and differentiation medium for 36 hours (B). Cell cycle analysis was performed after doublet exclusion on morphologically normal living cells. (C) PCNA protein level in L6E9 myoblasts and R1H cells cultured in growth medium (GM) and differentiation medium (DM). PCNA immunolabeling was performed after doublet exclusion on morphologically normal fixed cells. Data are means ± SE from 6 culture dishes. * $P<0.05$: significantly different from corresponding cells in GM; † $P<0.05$ and †† $P<0.01$: significantly different from L6E9 myoblasts.
doi:10.1371/journal.pone.0008637.g001

Limited Import of Mitochondrial Protein Does Not Account for the Decrease in Mitochondrial Respiration in R1H Cells

With the exception of 13 proteins encoded by the mitochondrial genome, all others mitochondrial proteins are encoded by the nuclear genome and thus need to be imported in mitochondria [26]. A defect in mitochondrial import leading to a cytosolic accumulation of mitochondrial proteins could therefore explain the paradoxical observation that mitochondrial protein content was increased in R1H cells, together with a marked decrease in mitochondrial respiration. To examine this hypothesis, cytosolic and mitochondrial fractions were prepared and analyzed for the

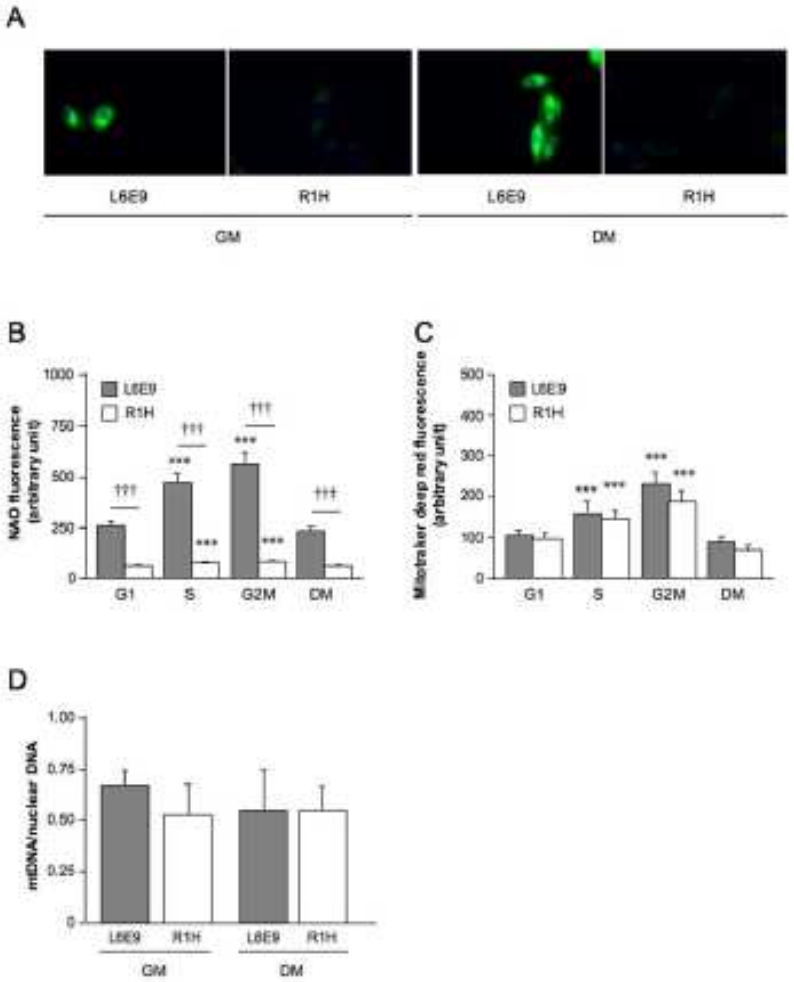

Figure 2. Cardiolipin content, mitochondrial content and mtDNA content. (A) Representative image of mitochondrial staining by nonyl acridine orange (NAO) in L6E9 myoblasts and R1H cells cultured in growth medium (GM) and in differentiation medium (DM) for 36 hours. Nuclei were stained with Hoechst 33342. Cells were visualized by fluorescence microscopy (Olympus inverse microscope IX81 system). (B) Cardiolipin content was determined from the geometric means of height NAO fluorescence signal. (C) Mitochondrial content was assessed from the geometric means of Mitotracker deep red fluorescence signal. Flow cytometry analysis was performed on living cells after doublet exclusion as a function of L6E9 and R1H cells position in the cell cycle (G1, S and G2M). Cells were cultured in GM and DM. (D) mtDNA quantity calculated as the ratio of mitochondrial subunit II of cytochrome oxidase to peptidylprolyl isomerase A DNA levels determined by real-time PCR in L6E9 and R1H cultured in GM and DM. Data are means ± SE from 6 culture dishes. *** $P<0.001$: significantly different from corresponding cells in G1 phase; ††† $P<0.001$: significantly different from L6E9 myoblasts.
doi:10.1371/journal.pone.0008637.g002

expression of Core 2 subunit of complex III and ATP synthase α protein content. Purity of the mitochondrial fraction was clearly indicated by the level of lactate dehydrogenase activity, which represented less than 5% of total lactate dehydrogenase activity (Figure 4A). As illustrated in Figure 4B, Core 2 and ATP synthase α proteins were detected in the mitochondrial fraction, whereas only traces were present in the cytosolic fraction. Similar observations were done for the 13.4 kDa subunit of complex III (data not shown) and citrate synthase (Figure 4C). Altogether, these data indicate that the reported increased in mitochondrial protein expression was not associated with a defect in mitochondrial protein import and that the decrease in mitochondrial respiration observed in R1H cells was rather due to a functional deficit in one or several complexes of the respiratory chain.

Mitochondrial H_2O_2 Level

We next addressed the biological relevance of the reported deficiency in mitochondrial respiratory capacity of R1H cells. As an organelle participating in cell signaling [27], we hypothesized that the mitochondrial deficiency reported herein could alter the

Table 1. Protein content of mitochondrial proteins and mitochondrial biogenesis factors.

	Growth medium		Differentiation medium	
	L6E9	R1H	L6E9	R1H
Core 2	101.2±6.0	228.1±21.2†††	67.5±3.4***	460.6±53.8**, †††
13.4	130.8±7.0	462.0±34.7†††	66.6±4.3***	456.6±19†††
2006	93.4±3.1	121.8±19.5	76.3±4.9*	166.8±27††
PGC-1α	87.9±4.5	117.4±9.0†	9.2±0.6**	120.0±2.7†††
PPARα	74.8±4.3	58.1±14.4†	5.7±0.3***	95.4±42**, †††
PPARδ	85.6±3.5	128.0±23.0	12.2±0.7***	125.5±10.4†
NOS1	56.8±2.6	81.7±8.9†	5.5±0.4***	105.3±8.3†††

Analyses were performed on cells cultured in growth medium and differentiation medium. Geometric means of the fluorescence intensity peaks were used to determine the protein content. Data are means ± SE from 6 culture dishes. * $P<0.05$, ** $P<0.01$ and *** $P<0.001$: significantly different from corresponding cells in GM; † $P<0.05$, †† $P<0.01$ and ††† $P<0.001$: significantly different from L6E9 cells.

doi:10.1371/journal.pone.0008637.t001

production of signaling agents involved in the regulation of myogenic differentiation. We particularly investigated H_2O_2 production as mitochondria are a major site of free radical production in the cell and this production is frequently altered in tumor tissues [28]. Furthermore, an increase in H_2O_2 concentration has been shown to completely abolish the differentiation of myoblasts into myotubes [29] and the stimulation of mitochondrial ROS production induced a rhabdomyosarcoma-like phenotype in human fibroblasts [14]. In the present study, mitochondria were identified as a major source of H_2O_2 as illustrated by a marked reduction in fluorescence of H_2DCFDA, a marker of mitochondrial H_2O_2 level [30], after the addition of the mitochondrial uncoupler CCCP (Figure 5A). Striking differences were observed in the regulation of mitochondrial H_2O_2 production. The two-fold increase in H_2DCFDA fluorescence during the transition from G1 to S phases in L6E9 cells was not observed in R1H cells (Figure 5B). Most importantly, the strong reduction in mitochondrial H_2O_2 level that occurred when cells were switched to a differentiation medium did not occur in R1H cells. We therefore tested the possibility that an antioxidant supplementation would force R1H cells to exit the

Table 2. Oxygen consumption rates of L6E9 and R1H cells.

	Growth medium		Differentiation medium	
	L6E9	R1H	L6E9	R1H
Basal	33.6±3.7	13.8±1.2†††	27.5±1.6	18.2±1.0*, †††
Oligomycin-insensitive	8.7±1.0	4.7±0.8††	9.2±1.6	5.9±1.4
FCCP-stimulated	91.1±16.6	18.2±3.0†††	93.0±14.3	31.7±3.7*, ††
RCR	10.4±3.0	3.9±0.9†	10.1±3.4	5.4±1.0

Oxygen consumption rates were measured in L6E9 myoblasts and R1H cells cultured in growth medium or in differentiation medium at 37°C by polarography in DMEM serum free (basal), in the presence of oligomycin, and after the addition of FCCP. Respiration rates are expressed in nmol $O_2.min^{-1}.cell^{-1}$. Respiratory control ratio (RCR) was calculated as the ratio between FCCP-stimulated and oligomycin insensitive respiration rates. For more details see Materials and Methods. Data are means ± SE from 12 independent culture dishes. * $P<0.05$, significantly different from corresponding cells in GM. † $P<0.05$, †† $P<0.01$ and ††† $P<0.001$: significantly different from L6E9 cells.

doi:10.1371/journal.pone.0008637.t002

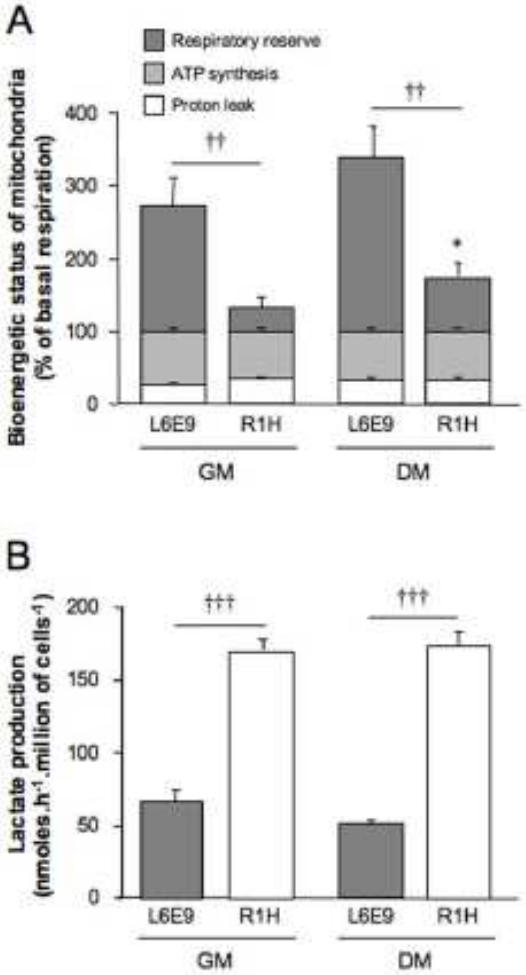

Figure 3. Bioenergetic status of L6E9 and R1H cells. (A) Mitochondrial proton leak (oligomycin insensitive respiration), mitochondrial ATP synthesis (basal respiration minus oligomycin-insensitive respiration) and mitochondrial respiratory reserve (FCCP-stimulated respiration minus basal respiration) are expressed as a percent of corresponding basal mitochondrial respiration reported in Table 2. Data are means ± SE from 12 independent culture dishes cultured in growth medium (GM) and differentiation medium (DM). (B) Lactate production of L6E9 and R1H cells cultured in GM and DM. Data are means ± SE from 6 independent culture dishes. * $P<0.05$: significantly different from corresponding cells in GM; †† $P<0.01$: significantly different from L6E9 myoblasts.

doi:10.1371/journal.pone.0008637.g003

cell cycle. Preincubation of the cells with 20 mM N-acetyl cysteine, which was effective in reducing basal H_2O_2 production, did not induce cell cycle arrest of R1H cells (data not shown).

Discussion

Rhabdomyosarcoma arises as a consequence of an unbalance between proliferation and differentiation of myoblasts that maintains myoblasts in replicative state. Rhabdomyosarcoma cells

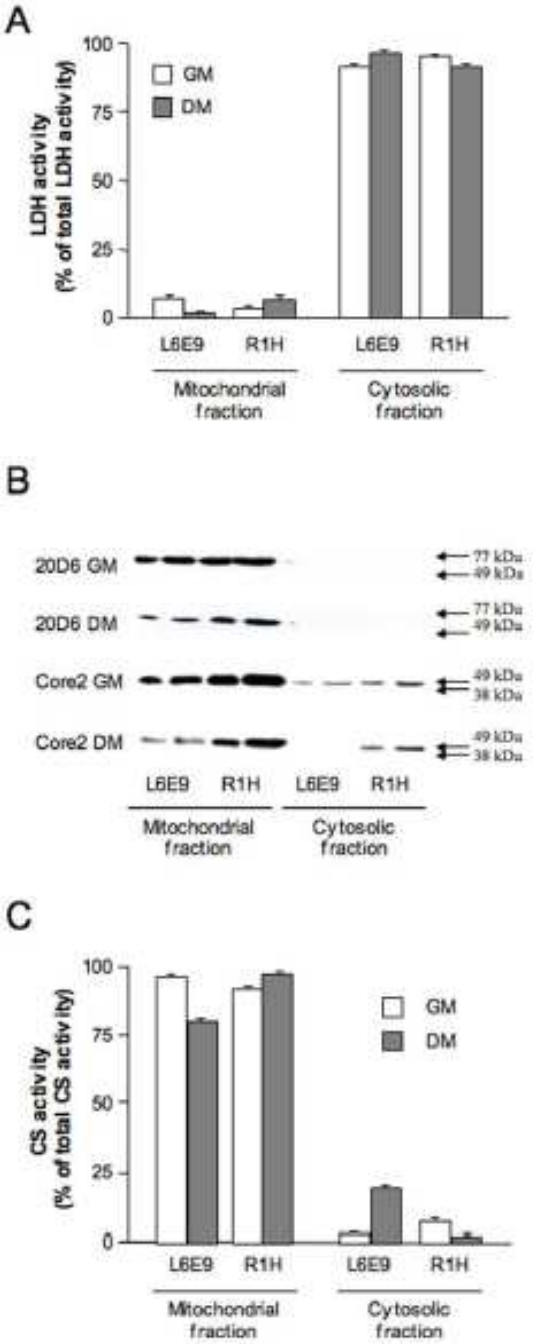

Figure 4. Mitochondrial import of Core 2 subunit of complex III, ATP synthase α (20D6) and citrate synthase. Lactate dehydrogenase (LDH) activity (A), Core 2 subunit of complex III and 20D6 protein content (B) and citrate synthase (CS) activity (C) were determined in mitochondrial and cytosolic fractions of L6E9 and R1H cells cultured in growth medium (GM) and differentiation medium (DM) for 36 hours. Data are means ± SE from 3 culture flasks.
doi:10.1371/journal.pone.0008637.g004

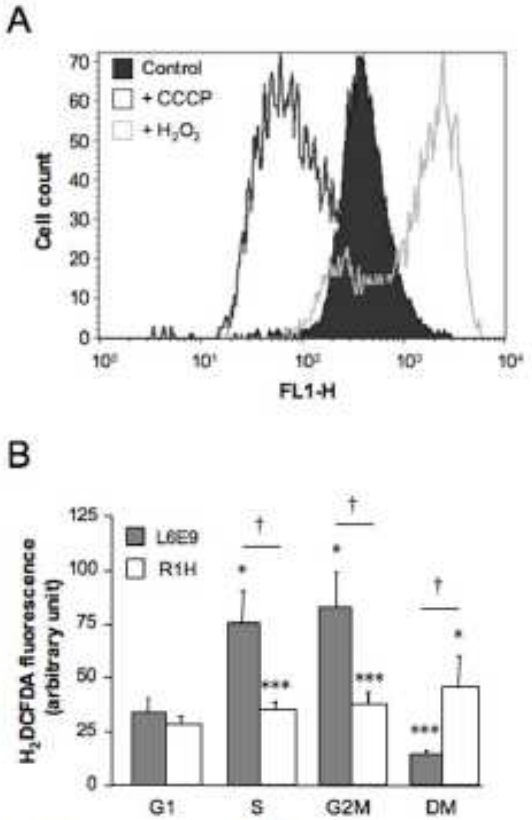

Figure 5. Mitochondrial H_2O_2 level. (A) Representative frequency histogram of 2′,7′-dichlorodihydrofluorescein diacetate (H_2DCFDA) fluorescence (FL1-H) obtained in L6E9 myoblasts cultured in growth medium. Positive and negative controls were obtained by incubating cells with 100 μM H_2O_2 (right displacement) and 1 mM CCCP (left displacement), respectively. (B) H_2DCFDA fluorescence was determined from the geometric means of fluorescence intensity peaks. Analyses were performed on morphologically normal living cells cultured in growth medium (G1, S and G2M phases) and differentiation medium (DM) for 36 hours. Data are means ± SE from 6 culture dishes. * $P<0.05$ and *** $P<0.001$: significantly different from corresponding cells in G1 phase; † $P<0.05$: significantly different from L6E9 myoblasts.
doi:10.1371/journal.pone.0008637.g005

thus constitute an interesting model to study the cellular mechanisms that control the myogenic differentiation program. The present study supports the hypothesis that a deficiency in mitochondrial metabolism is an epigenetic mechanism that contributes to the failure of rhabdomyosarcoma cells to differentiate. Corollary, it also supports the notion that a tight regulation of mitochondrial biogenesis and mitochondrial metabolism is necessary for the proper engagement of myoblasts towards the myogenic fate.

The composition of proteins and phospholipids of the mitochondrial inner membrane is crucial for mitochondrial function. Here, we show that a progressive depletion of the cardiolipin content occurs as R1H cells divide, while mitochondrial content is preserved. The biogenesis of cardiolipin and the relative distribution of the major lipid components of mitochondria (cardiolipin,

phosphatidylcholine, phosphatidylethanolamine) are therefore profoundly modified in R1H cells. Alteration in organelle biogenesis was also observed at the protein level, since expression of mitochondrial respiratory chain proteins (core II, 13.4 and 20D6) and mitochondrial biogenesis factors (PGC-1α, PPARα, PPARδ and NOS1) was significantly increased. Specifically, the repression of mitochondrial proteins and mitochondrial biogenesis factors expression that occurs in L6E9 cells at the onset of differentiation (present study, [25]), did not occur in R1H cells. Taken together, these data clearly illustrate that the regulation of mitochondrial biogenesis is strongly altered in R1H cells.

The dysregulation of mitochondrial biogenesis observed in R1H cells was associated with a major alteration in mitochondrial metabolism. Oxygen consumption dedicated to drive ATP synthesis and mitochondrial respiratory reserve were dramatically reduced in R1H cells, leading mitochondria of R1H cells to be almost maximally stimulated under basal respiration. R1H cells seem to compensate the decrease in mitochondrial metabolism by increasing ATP production through lactate production. However, this metabolic pathway may not be sufficient to produce enough ATP when a large energy demand is required [15], as occurring during myoblast proliferation and differentiation. Therefore, such bioenergetic features suggest that R1H cells have a drastically lower capacity to face a metabolic aerobic challenge, despite the higher rate of lactate production. From a teleological point of view, the marked increase in mitochondrial protein expression and mitochondrial biogenesis factors reported therein may be interpreted as a vain attempt of R1H cells to counteract the decrease in mitochondrial respiratory capacity, as previously observed in mitochondrial myopathies [31] and in response to mitochondrial DNA depletion [32]. To explain the paradoxical observation that an increased mitochondrial protein content was not translated into functional respiratory capacity in R1H cells, we hypothesized that a defect in mitochondrial protein import could lead to a cytosolic accumulation of mitochondrial proteins. However, this was not the case as our cellular fractionation analysis clearly indicates that mitochondrial respiratory proteins encoded by the nuclear genome (Core 2 and 13.4 kDa subunits of complex III, ATP synthase subunit α and citrate synthase) are effectively imported inside the mitochondria. Another possibility would be that the observed changes in the protein-to-cardiolipin ratio alter the functionality of the respiratory chain and/or the assembly of respiratory complexes in R1H cells. In agreement with this hypothesis, previous studies have demonstrated that experimental (mutant deficient in cardiolipin) and physiological (aging) conditions leading to cardiolipin depletion, markedly decrease the respiratory capacity of mitochondria [33,34]. Importantly, of the mitochondrial respiratory chain complexes, complex I was the most severely impaired [34]. Together with the observation that complex I activity is reduced in R1H cells [35], our report that cardiolipin content is strongly decreased in R1H cells may thus contribute to explain the decrease in the respiratory capacity of R1H cells. Overall, these data suggest that a tight regulation between protein and phospholipid syntheses is necessary to produce functional mitochondria.

H_2O_2, the intermediate detoxification product of superoxide ion by superoxide dismutase, is involved in the regulation of myogenic differentiation. It has been notably reported that exposure of differentiating myoblasts to H_2O_2 almost totally abolished muscle-specific protein expression and myogenic differentiation, whereas this effect was reversed by the addition of a reactive oxygen species scavenger [29]. A decrease in H_2O_2 level at the onset of differentiation would be therefore a permissive event necessary for the continuation of the myogenic program. Importantly, ion superoxide production and the subsequent production of H_2O_2 are tightly coupled to the activity of complexes I and III of the respiratory chain [36,37], and the cardiolipin content of the inner mitochondrial membrane [33]. Therefore, the reported deficiency in mitochondrial respiration and the decrease in cardiolipin content of R1H cells may profoundly impact the regulation of mitochondrial H_2O_2 production and ultimately contribute to the failure of R1H cells to differentiate. In agreement with this hypothesis, H2O2 production was fairly constant in R1H cells induced to differentiate, which contrasted with the decrease in H2O2 level occurring at the onset of differentiation in L6E9 myoblasts. However, supplementation of R1H cells with N-acetyl cysteine, a powerful antioxidant molecule, did not rescue the failure of R1H cells to differentiate, suggesting that other factors must contribute to the failure of R1H cells to differentiate.

In summary, we identified a mitochondrial respiratory deficiency in R1H rhabdomyosarcoma cells that may result from an unbalance between mitochondrial protein expression and cardiolipin biosynthesis. A defect in the regulation of mitochondrial biogenesis and mitochondrial metabolism may thus be an epigenetic mechanism that may contribute to the tumoral behavior of R1H cells. Furthermore, our data further establish functional links between the regulation of mitochondrial biogenesis and the regulation of myogenic differentiation.

Materials and Methods

Cell Culture

Experiments were performed on rat L6E9 muscle cells (gift from Dr D.A. Hood, York University, Canada) and rat rhabdomyosarcoma tumor cells (gift from Dr A. Raabe, University Medical Center Hamburg-Eppendorf, Germany). The tumor was derived from the rhabdomyosarcoma R1H [38], which was originally derived from the BA1112 tumor [39]. Cells were cultured in Dulbecco's modified Eagle's medium (DMEM) supplemented with 20% fetal bovine serum and 1% penicillin-streptomycin (P/S) at 37°C and 5% CO_2 in air, in 100 mm plastic dishes. At 80% confluence, cells were either trypsinized or allowed to differentiate for 36 hours in DMEM supplemented with 2% horse serum and 1% P/S.

Flow Cytometry Analyses

Cells (10^6 cells/ml) were analyzed on a FACSDiva (BD Biosciences, San Jose, CA, USA). Before analyses, cells were gated to perform measurements on morphologically normal single living cells (doublet exclusion and propidium iodide staining) as a function of the position of cells in G1, S, and G2M phases of the cell cycle (9 µM Hoechst 33342) [25]. Cell cycle was analyzed with ModFit™ 3.1 software. Data were analyzed using BD Diva™ 5.0.3 or BD Cell Quest Pro™4.0.2.

Cardiolipin content, mitochondrial content, and mitochondrial H_2O_2 level. Nonyl acridine orange (NAO, Sigma), Mitotracker® Deep Red FM (Invitrogen) and 2',7'-dichlorodihydrofluorescein diacetate (H_2DCFDA, Invitrogen) were used to determine cardiolipin content [24], mitochondrial content [40] and mitochondrial H_2O_2 level [30], respectively. NAO and H_2DCFDA stainings were performed according to [25] with some modifications. NAO and H_2DCFDA concentrations were 2 µM for R1H cells. For Mitotracker® Deep Red FM staining, cells (10^6/ml) were successively incubated at 37°C with Hoechst 33342 (9 µM, 90 min) and Mitotracker® Deep Red FM (1 µM, 15 min).

Immunolabelling experiments. Cell immunoreactivity against complex III (Core II and 13.4 subunits) and ATP synthase α (20D6) of the respiratory chain, proliferating cell nuclear antigen

(PCNA, PC10, NeoMarkers), peroxysome proliferator activated receptor (PPAR) γ co-activator-1α (PGC-1α, sc-13067, Santa Cruz Biotechnology), PPARα (sc-9000, Santa Cruz Biotechnology), PPARδ (sc-7197, Santa Cruz Biotechnology) and neuronal nitric oxide synthase (NOS1, sc-648, Santa Cruz Biotechnology) were performed as previously described [25].

Fluorescence Microscopy

Myoblasts and rhabdomyosarcoma cells were cultured on coverslips in DMEM supplemented with 20% fetal bovine serum and 1% P/S. Cells were stained with NAO as described [25]. Fluorescence was visualized with an Olympus inverse fluorescent microscope IX81 system.

Mitochondrial DNA Analysis

Total DNA was extracted from muscle cells using phenol/chloroform/isoamyl alcohol (25:24:1) followed by ethanol precipitation. The content of mtDNA was calculated using real-time quantitative PCR by measuring the threshold cycle ratio (ΔCt) of a mitochondrial-encoded gene (subunit II of cytochrome oxidase, forward 5'-CTTACAAGACGCCACATCAC-3', reverse 5'-GAATTCGTAGGGAGGGAAGG-3') versus a nuclear-encoded gene (peptidylprolyl isomerase A, forward 52-ACACGCCA-TAATGGCACTGG-32, reverse 52-CAGTCTTGGCAGTG-CAGAT-32). mtDNA-to-nuclear DNA ratio were normalized to the protein content.

Cell Respiration

L6E9 and R1H cells were trypsinized, washed and finally suspended at a final concentration of 2×10^6 cells per ml in serum-free DMEM. Cell respiration was measured as previously described [15]. Briefly, the cell suspension (500 µl) was immediately transferred to a 1 ml chamber of a Clarke-type oxygen electrode (Hansatech, UK) maintained at 37°C using a recirculating water bath. Basal cell respiration is the sum of the oxygen consumed for mitochondrial ATP synthesis, mitochondrial proton leak and non-mitochondrial reactions. Myxothiazol (8 µM) was used to check potential non-mitochondrial sources of oxygen consumption. Non-mitochondrial respiration rates were considered insignificant as myxothiazol-inhibited respiration was not detectable. Basal endogenous coupled respiration rate of cells was determined by measuring the linear rate of oxygen consumption. Oligomycin (10 µg/ml) was then added to inhibit ATP synthase (non-phosphorylating respiration). Carbonyl cyanide-p-trifluoromethoxyphenylhydrazone (FCCP) was sequentially added at different concentrations ranging from 500 nM to 900 nM. This titration was systematically performed in order to determine the optimal FCCP concentration that gives maximal uncoupled respiration rate. Using this approach, mitochondrial proton leak (oligomycin-insensitive respiration rate), mitochondrial ATP synthesis (basal respiration rate minus oligomycin-insensitive respiration rate) and mitochondrial respiratory reserve (FCCP-induced maximal respiration rate minus basal respiration rate) were determined. Oxygen calibration was performed by adding $Na_2S_2O_4$.

Lactate Measurement

L6E9 and R1H cells were cultured as described above in 100 mm plastic dishes. At the end of the culture period (72 hours for cells in proliferation and 36 hours for cells in differentiation medium), cells were rinsed, trypsined and numbered. Lactate concentrations were determined on culture media obtained at the beginning and the end of the culture period by using an electrochemical analyser YSI 2300 STAT PLUS (Yellow Springs Instruments, Yellow Springs, Ohio, USA). Calibration was done by using a 5 mM standard lactate solution.

Core 2 Subunit of Complex III and ATP Synthase α Protein Content in Cytosolic and Mitochondrial Fractions

Mitochondrial and cytosolic fractions from L6E9 and R1H cells were prepared using the MITOISO2 kit (Sigma) following the manufacturer's instructions. Purity of mitochondrial and cytosolic fractions was systematically assessed by the measurement of lactate dehydrogenase enzyme activities according to [41]. Equal amount of cells (100,000 and 200,000 cells) were then separated on a 12.5% SDS-PAGE. After electrotransfer, the membranes were saturated with 5% (w:v) non-fat dry milk in Tris-buffered saline (1 hour at room temperature) and then incubated overnight with the primary antibody either directed against the Core 2 subunit of complex III (13.4) (1:10,000 dilution v:v) or the ATP synthase α (20D6) (1:40,000 v:v). Corresponding secondary antibodies (1:3,000 dilution v:v) were incubated for 90 min. Protein immunoreactivity was determined by chemiluminescence. Quantification of the signal intensity was determined on scanned films by using NIH image 1.63. Finally, citrate synthase activity was also determined on cytosolic and mitochondrial fractions [41].

Supplementation with N-Acetyl Cysteine

R1H cells were supplemented with 20 mM N-acetyl cysteine (Sigma) in the culture medium over the entire differentiation period (36 hours). Cells were then trypsinized and stained with 9 µM Hoescht 33342 for a cell cycle analysis [25].

Statistics

Data are means ± SE from 6 independent culture dishes. Mean difference between myoblasts and rhabdomyosarcoma cells in G1, S and G2M was determined by using a two-way analysis of variance. Scheffe post-hoc test was used to identify specific mean difference. Unpaired *t* test was used to determine specific mean differences between myoblasts cultured in growth and in differentiation media. Unpaired *t* test was also used to determine mean difference between myoblasts in G1 and at the onset of differentiation. The α level of significance was set at 0.05.

Acknowledgments

We thank Catherine Godinot, Delphine Boudard and Denis Gispetas for their advices during the preparation of the project. Catherine Godinot is also acknowledged for the kind provision of complex III and ATP synthase antibodies.

Author Contributions

Conceived and designed the experiments: VEJ DF. Performed the experiments: VEJ or AD JC EL DF. Analyzed the data: VEJ or DF. Contributed reagents/materials/analysis tools: or DR DF. Wrote the paper: VEJ DF.

References

1. Charge SB, Rudnicki MA (2004) Cellular and molecular regulation of muscle regeneration. Physiol Rev 84: 209-238.
2. Merino G, Helman LJ (1998) Rhabdomyosarcoma-working out the pathways. Oncogene 18: 5340-5348.

3. Dias P, Parham DM, Shapiro DN, Tapscott SJ, Houghton PJ (1992) Monoclonal antibodies to the myogenic regulatory protein MyoD1: epitope mapping and diagnostic utility. Cancer Res 52: 6431–6439.
4. Tapscott SJ, Thayer MJ, Weintraub H (1993) Deficiency in rhabdomyosarcomas of a factor required for MyoD activity and myogenesis. Science 259: 1450–1453.
5. Tonin PN, Scrable H, Shimada H, Cavenee WK (1991) Muscle-specific gene expression in rhabdomyosarcomas and stages of human fetal skeletal muscle development. Cancer Res 51: 5100–5106.
6. Epstein JA, Shapiro DN, Cheng J, Lam PY, Maas RL (1996) Pax3 modulates expression of the c-Met receptor during limb muscle development. Proc Natl Acad Sci U S A 93: 4213–4218.
7. Galili N, Davis RJ, Fredericks WJ, Mukhopadhyay S, Rauscher FJ 3rd, et al. (1993) Fusion of a fork head domain gene to PAX3 in the solid tumour alveolar rhabdomyosarcoma. Nat Genet 5: 230–235.
8. Shapiro DN, Sublett JE, Li B, Downing JR, Naeve CW (1993) Fusion of PAX3 to a member of the forkhead family of transcription factors in human alveolar rhabdomyosarcoma. Cancer Res 53: 5108–5112.
9. Warburg O (1956) On the origin of cancer cells. Science 123: 309–314.
10. Amuthan G, Biswas G, Annadathottathuvareth HK, Vijayasarathy C, Shephard HM, et al. (2002) Mitochondrial stress-induced calcium signaling, phenotypic changes and invasive behavior in human lung carcinoma A549 cells. Oncogene 21: 7830–7840.
11. Biswas G, Guha M, Avadhani NG (2005) Mitochondria-to-nucleus stress signaling in mammalian cells: nature of nuclear gene targets, transcription regulation, and induced resistance to apoptosis. Gene 354: 132–139.
12. Cavalli LR, Varella-Garcia M, Liang BC (1997) Diminished tumorigenic phenotype after depletion of mitochondrial DNA. Cell Growth Differ 8: 1189–1198.
13. Chen Y, Cairns R, Papandreou I, Koong A, Denko NC (2009) Oxygen consumption can regulate the growth of tumors, a new perspective on the warburg effect. PLoS ONE 4: e7033.
14. Goondemange S, Seyer P, Carraro A, Bernaw P, Pessemesse L, et al. (2008) Stimulation of mitochondrial activity by p43 overexpression induces human dermal fibroblast transformation. Cancer Res 68: 4285–4291.
15. Desquiret V, Loiseau D, Jacques C, Douay O, Malthiery Y, et al. (2006) Dinitrophenol-induced mitochondrial uncoupling in vivo triggers respiratory adaptation in HepG2 cells. Biochim Biophys Acta 1757: 21–30.
16. Duguez S, Feasson L, Denis C, Freyssenet D (2002) Mitochondrial biogenesis during skeletal muscle regeneration. Am J Physiol Endocrinol Metab 282: E802–809.
17. Moyes CD, Mathieu-Costello OA, Tsuchiya N, Filburn C, Hansford RG (1997) Mitochondrial biogenesis during cellular differentiation. Am J Physiol 272: C1345–1351.
18. Rasmussen AH, Langen RC, Schrauwen P, Schaart G, Schols AM, et al. (2009) Regulation of mitochondrial biogenesis during myogenesis. Mol Cell Endocrinol (2009) Oct 3: [Epub ahead of print].
19. Amuthan G, Biswas G, Zhang SY, Klein-Szanto A, Vijayasarathy C, et al. (2001) Mitochondria-to-nucleus stress signaling induces phenotypic changes, tumor progression and cell invasion. Embo J 20: 1910–1920.
20. Duguez S, Sabido O, Freyssenet D (2004) Mitochondrial-dependent regulation of myoblast proliferation. Exp Cell Res 299: 27–33.
21. Rochard P, Rodier A, Casas F, Cassar-Malek I, Marchal-Victorion S, et al. (2000) Mitochondrial activity is involved in the regulation of myoblast differentiation through myogenin expression and activity of myogenic factors. J Biol Chem 275: 2733–2744.
22. Seyer P, Grandemange S, Busso M, Carraro A, Gamelin F, et al. (2006) Mitochondrial activity regulates myoblast differentiation by control of c-Myc expression. J Cell Physiol 207: 75–86.
23. Fleischer S, Rouser G, Fleischer B, Casu A, Kritchevsky G (1967) Lipid composition of mitochondria from bovine heart, liver, and kidney. J Lipid Res 8: 170–180.
24. Petit JM, Maftah A, Ratinaud MH, Julien R (1992) 10N-nonyl acridine orange interacts with cardiolipin and allows the quantification of this phospholipid in isolated mitochondria. Eur J Biochem 209: 267–273.
25. Jahnke VE, Sabido O, Freyssenet D (2009) Control of mitochondrial biogenesis, ROS level, and cytosolic Ca2+ concentration during the cell cycle and the onset of differentiation in L6E9 myoblasts. Am J Physiol Cell Physiol 296: C1185–1194.
26. Freyssenet D, Berthon P, Denis C (1996) Mitochondrial biogenesis in skeletal muscle in response to endurance exercises. Arch Physiol Biochem 104: 129–141.
27. Freyssenet D (2007) Energy sensing and regulation of gene expression in skeletal muscle. J Appl Physiol 102: 529–540.
28. Szatrowski TP, Nathan CF (1991) Production of large amounts of hydrogen peroxide by human tumor cells. Cancer Res 51: 794–798.
29. Langen RC, Schols AM, Kelders MC, Van Der Velden JL, Wouters EF, et al. (2002) Tumor necrosis factor-alpha inhibits myogenesis through redox-dependent and -independent pathways. Am J Physiol Cell Physiol 283: C714–721.
30. Beebacher JL, Bois NC (2001) Chemically de-acetylated 2',7'-dichlorodihydrofluorescein diacetate as a probe of respiratory burst activity in mononuclear phagocytes. J Immunol Methods 251: 81–91.
31. Heddi A, Lestienne P, Wallace DC, Stepien G (1993) Mitochondrial DNA expression in mitochondrial myopathies and coordinated expression of nuclear genes involved in ATP production. J Biol Chem 268: 12156–12163.
32. Li K, Neufer PD, Williams RS (1998) Nuclear responses to depletion of mitochondrial DNA in human cells. Am J Physiol 269: C1265–1270.
33. Petrosillo G, Matera M, Moro N, Ruggiero FM, Paradies G (2009) Mitochondrial complex I dysfunction in rat heart with aging: critical role of reactive oxygen species and cardiolipin. Free Radic Biol Med 46: 88–94.
34. Ohtsuka T, Nishijima M, Suzuki K, Akamatsu Y (1993) Mitochondrial dysfunction of a cultured Chinese hamster ovary cell mutant deficient in cardiolipin. J Biol Chem 268: 22914–22919.
35. Kuhn T, Pelz T, Qu X, Hunegen G, Dunst J, et al. (2007) Mitochondrial OXPHOS Functions in RH Rhabdomyosarcoma and Skeletal Muscles of the Rat. Neurochem Res 32: 973–980.
36. Balaban RS, Nemoto S, Finkel T (2005) Mitochondria, oxidants, and aging. Cell 120: 483–495.
37. Nicholls DG (2004) Mitochondrial membrane potential and aging. Aging Cell 3: 35–40.
38. Barendsen GW, Broome JJ (1969) Experimental radiotherapy of a rat rhabdomyosarcoma with 15 MeV neutrons and 300 kV x-rays. I. Effects of single exposures. Eur J Cancer 5: 373–391.
39. Reinhold HS. (1965) A cell dispersion technique for use in quantitative transplantation studies with solid tumours. Eur J Cancer 1: 67–71.
40. Light E, Tessato L, Fernandes R, Rosa E, Prada N, et al. (2005) Characterization of cells with different mitochondrial membrane potential during apoptosis. Cytometry A 68: 28–35.
41. Bazzi AE, Sabido O, Freyssenet D (2003) Mitotic activity of rat muscle satellite cells in response to serum stimulation: relation with cellular metabolism. Exp Cell Res 283: 196–205.

THE JOURNAL OF CELL BIOLOGY

Published December 14, 2009

This article has original data in the JCB DataViewer
http://jcb-dataviewer.rupress.org/jcb/browse/1904

JCB: Article

Muscle inactivation of mTOR causes metabolic and dystrophin defects leading to severe myopathy

Valérie Risson,[1] Laetitia Mazelin,[1] Mila Roceri,[2] Hervé Sanchez,[3] Vincent Moncollin,[1] Claudine Corneloup,[1] Hélène Richard-Bulteau,[3] Alban Vignaud,[4] Dominique Baas,[1] Aurélia Defour,[5] Damien Freyssenet,[5] Jean-François Tanti,[6,7] Yannick Le-Marchand-Brustel,[6,7] Bernard Ferrier,[8] Agnès Conjard-Duplany,[8] Klaas Romanino,[9] Stéphanie Bauché,[10] Daniel Hantaï,[10] Matthias Mueller,[11] Sara C. Kozma,[12] George Thomas,[12] Markus A. Rüegg,[9] Arnaud Ferry,[4] Mario Pende,[2] Xavier Bigard,[3] Nathalie Koulmann,[3] Laurent Schaeffer,[1] and Yann-Gaël Gangloff[1]

[1]Laboratoire de Biologie Moléculaire de la Cellule, Centre National de la Recherche Scientifique, Unité Mixte de Recherche 5239, FR128, Université de Lyon, Equipe Différenciation Neuromusculaire, Ecole Normale Supérieure, 69364 Lyon Cedex 07, France
[2]Institut National de la Santé et de la Recherche Médicale, Unité 845, Faculté de Médecine Necker, Université Paris Descartes, 75730 Paris Cedex 15, France
[3]Department of Human Factors, Research Center of the Health of the Military, La Tronche 38702, France
[4]Unité Mixte de Recherche 787, Université Pierre et Marie Curie, Paris F-75013, France
[5]Laboratoire de Physiologie de l'Exercice, Equipe d'Accueil 4338, Université Jean Monnet, Pôle de Recherche et d'Enseignement Supérieur, Université de Lyon, F-42023 Saint-Etienne, France
[6]Institut National de la Santé et de la Recherche Médicale, Unité 895, Centre Méditerranéen de Médecine Moléculaire, F-06204 Nice, France
[7]Faculty of Medicine, University of Nice Sophia Antipolis, F-06204 Nice, France
[8]Métabolomique et Maladies Métaboliques, Institut National de la Santé et de la Recherche Médicale, Unité 820, Faculté de Médecine R.T.H. Laennec, Université Claude Bernard Lyon 1, 69372 Lyon Cedex 08, France
[9]Biozentrum, University of Basel, CH-4056 Basel, Switzerland
[10]Institut National de la Santé et de la Recherche Médicale, Université Pierre et Marie Curie, Unité Mixte de Recherche 975, Hôpital de la Salpêtrière, 75651 Paris Cedex 13, France
[11]Department of Development and Molecular Pathways, Novartis Institute for Biomedical Research, Novartis Pharma AG, 4057 Basel, Switzerland
[12]Department of Genome Science, Genome Research Institute, University of Cincinnati, Cincinnati, OH 45237

Downloaded from jcb.rupress.org on March 26, 2010

Mammalian target of rapamycin (mTOR) is a key regulator of cell growth that associates with raptor and rictor to form the mTOR complex 1 (mTORC1) and mTORC2, respectively. Raptor is required for oxidative muscle integrity, whereas rictor is dispensable. In this study, we show that muscle-specific inactivation of mTOR leads to severe myopathy, resulting in premature death. mTOR-deficient muscles display metabolic changes similar to those observed in muscles lacking raptor, including impaired oxidative metabolism, altered mitochondrial regulation, and glycogen accumulation associated with protein kinase B/Akt hyperactivation. In addition, mTOR-deficient muscles exhibit increased basal glucose uptake, whereas whole body glucose homeostasis is essentially maintained. Importantly, loss of mTOR exacerbates the myopathic features in both slow oxidative and fast glycolytic muscles. Moreover, mTOR but not raptor and rictor deficiency leads to reduced muscle dystrophin content. We provide evidence that mTOR controls dystrophin transcription in a cell-autonomous, rapamycin-resistant, and kinase-independent manner. Collectively, our results demonstrate that mTOR acts mainly via mTORC1, whereas regulation of dystrophin is raptor and rictor independent.

V. Risson, M. Roceri, and L. Mazelin contributed equally to this paper.

Correspondence to Laurent Schaeffer: laurent.Schaeffer@ens-lyon.fr; or Yann-Gaël Gangloff: Yann-Gael.Gangloff@ens-lyon.fr

Y.-G. Gangloff and L. Schaeffer contributed equally to this paper.

Abbreviations used in this paper: ChIP, chromatin immunoprecipitation; CMV, cytomegalovirus; CSA, cross-sectional area; DGC, dystrophin-glycoprotein complex; DMD, Duchenne MD; DmKO, raptor/rictor muscle double knockout; ES, embryonic stem; GC, gastrocnemius; GP, glycogen phosphorylase; HSA, human skeletal muscle α-actin; LDH, lactate dehydrogenase; MD, muscular dystrophy; MHC, myosin heavy chain; mTOR, mammalian target of rapamycin; mTORC, mTOR complex; PFK, phosphofructokinase; PK, pyruvate kinase; PLA, plantaris; RAmKO, raptor muscle knockout; RImKO, rictor muscle knockout; TA, tibialis anterior; TTP, time to peak twitch tension.

Introduction

Muscle structure, mass, and composition are critical for motility, whole body metabolism, and viability. Skeletal muscle is composed of heterogeneous myofibers with distinct metabolic properties, rates of contraction, and susceptibility to fatigue

© 2009 Risson et al. This article is distributed under the terms of an Attribution–Noncommercial–Share Alike–No Mirror Sites license for the first six months after the publication date (see http://www.jcb.org/misc/terms.shtml). After six months it is available under a Creative Commons License (Attribution–Noncommercial–Share Alike 3.0 Unported license, as described at http://creativecommons.org/licenses/by-nc-sa/3.0/).

The Rockefeller University Press $30.00
J. Cell Biol. Vol. 187 No. 6 859–874
www.jcb.org/cgi/doi/10.1083/jcb.200903131

Supplemental Material can be found at:
http://jcb.rupress.org/cgi/content/full/jcb.200903131/DC1
Original image data can be found at:
http://jcb-dataviewer.rupress.org/jcb/browse/1904

Published December 14, 2009

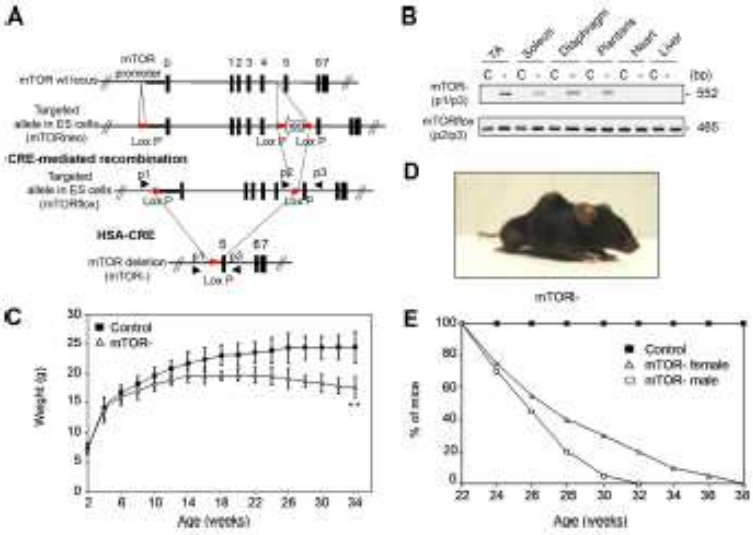

Figure 1. **Muscle-specific inactivation of mTOR.** (A) mTOR^{flox} and mTOR$^-$ mice were generated as described in Materials and methods. (B) PCR analysis of Cre-mediated recombination of the mTOR^{flox} allele (p2/p3) showing that the deleted mTOR allele (p1/p3) was exclusively detected in skeletal muscles of mTOR$^-$ mice. C, control; −, mTOR$^-$. (C) Growth curves of mTOR$^-$ and control female mice (n = 15 mice). (D) Morphology of 22-wk-old female mTOR$^-$ mice. (E) Survival curve of mTOR$^-$ and control mice (n = 20). **, $P < 0.01$. Data indicate mean ± SD.

(Bassel-Duby and Olson, 2006; Schiaffino et al., 2007) but exhibits remarkable metabolic and morphological adaptive capabilities in response to several physiological (e.g., exercise) and pathological (systemic diseases, myopathy, and aging) conditions. These adaptive processes include hypertrophy, atrophy, regeneration, fiber type conversion, or mitochondrial biogenesis.

As a conserved Ser/Thr kinase, the mammalian target of rapamycin (mTOR) is a central regulator of cell growth by integrating signals from nutrients, growth factors, energy status, and environmental stress. mTOR resides in two structurally and functionally distinct signaling complexes: mTOR complex 1 (mTORC1) and mTORC2. The raptor-containing complex mTORC1 regulates a vast range of cellular activities, including transcription, translation, ribosome biogenesis, and autophagy (Wullschleger et al., 2006). A key cellular substrate for mTORC1 is the ribosomal S6 kinase (S6K1), which is phosphorylated at its hydrophobic motif residue, Thr389. The rictor-containing complex mTORC2 is proposed to regulate actin organization. Moreover, mTORC2 is one of the kinases able to phosphorylate PKB/Akt on Ser473 (Jacinto et al., 2004; Sarbassov et al., 2004; Bentzinger et al., 2008).

Under acute treatment, rapamycin is thought to selectively inhibit mTORC1. Conversely, mTORC2 is considered rapamycin insensitive, although prolonged treatment disrupts mTORC2 assembly in certain cell lines (Sarbassov et al., 2006). In addition, the recent development of the ATP-competitive inhibitor Torin1, which suppresses both mTORC1 and mTORC2, allowed the identification of rapamycin-resistant mTORC1-dependent functions required for cap-dependent translation and suppression of autophagy (Thoreen et al., 2009).

Rapamycin-sensitive mTORC1 functions have been shown to be required for muscle growth (Bodine et al., 2001; Rommel et al., 2001; Ohanna et al., 2005) as well as for the maintenance of mitochondrial oxidative function by directly regulating mitochondrial gene expression through the control of a YY1 (Yin Yang 1)–PGC1α transcriptional complex (Cunningham et al., 2007). Consistent with this, muscle-specific inactivation of the mTORC1 component raptor in raptor muscle knockout (RAmKO) mice leads to muscle atrophy, impaired oxidative capacity, and increased glycogen stores, resulting in dystrophic features that were most prominent in oxidative muscles (Bentzinger et al., 2008). In contrast, the muscle-specific loss of the mTORC2 component rictor in rictor muscle knockout (RImKO) mice has minimal impact on muscle physiology (Bentzinger et al., 2008; Kumar et al., 2008), and raptor/rictor muscle double knockout (DmKO) show similar pathological changes as RAmKO mice. These studies suggested that mTOR functions in adult skeletal muscle require only mTORC1 (Bentzinger et al., 2008). However, there is evidence that some functions of mTOR, such as the activation of terminal oligopyrimidine mRNA translation, could be independent of mTORC1 and mTORC2 (Patursky-Polischuk et al., 2009).

The aim of this study was to determine the physiological functions of mTOR in differentiated mouse skeletal muscle. Because conventional mTOR knockout mice die during early embryogenesis (Gangloff et al., 2004; Murakami et al., 2004), we generated muscle-specific mTOR knockout (mTOR$^-$) mice. In this study, we show that these animals develop a severe myopathy, displaying features of muscular dystrophy (MD) and metabolic myopathy, leading to premature death between 22 and 38 wk of age. Although the metabolic alterations are similar between mTOR$^-$ and RAmKO/DmKO mice, mTOR deficiency more severely affects muscle contractile properties. In addition, mTOR$^-$ muscles, in contrast to RAmKO and RImKO muscles, display reduced content of components of the dystrophin–glycoprotein complex (DGC). Finally, we demonstrate that mTOR controls dystrophin transcription in a cell-autonomous, rapamycin-resistant, and kinase-independent manner.

Downloaded from jcb.rupress.org on March 26, 2010

Published December 14, 2009

Table I. **mTOR⁻ mice exhibit reduced body weight associated with a strong reduction in the mass of fast-twitch glycolytic muscles**

Variable	Control	mTOR⁻	% Control
Body weight (g)	17.41 ± 1.05	15.85 ± 1.37[a]	91.0
Soleus weight (mg)	4.93 ± 0.64	5.00 ± 0.61	101.4
Soleus/body weight (mg/g)	0.28 ± 0.03	0.32 ± 0.03[b]	114.3
TA weight (mg)	30.93 ± 3.56	24.54 ± 2.29[a]	79.3
TA/body weight (mg/g)	1.78 ± 0.22	1.55 ± 0.04[a]	87.1
GC weight (mg)	71.13 ± 5.23	56.27 ± 4.79[a]	79.1
GC/body weight (mg/g)	4.09 ± 0.26	3.55 ± 0.07[a]	86.8
PLA weight (mg)	10.81 ± 0.53	8.37 ± 0.85[a]	77.4
PLA/body weight (mg/g)	0.62 ± 0.03	0.53 ± 0.06[a]	85.5
Liver (mg)	868.26 ± 53.77	851.84 ± 102.75	98.1
Liver/body weight (mg/g)	50.05 ± 4.50	53.69 ± 3.40	107.3
Fat pad weight (mg)	295.78 ± 40.15	286.73 ± 30.12	96.9
Fat pad/body weight (mg/g)	16.98 ± 1.90	18.08 ± 1.15	106.9
Heart weight (mg)	120.62 ± 9.49	114.17 ± 9.07	94.7
Heart/body weight (mg/g)	6.95 ± 0.68	7.22 ± 0.50	103.9

Values are for 6-wk-old control and mTOR⁻ female mice. Fat data includes ovarian, uterine, and retroperitoneal fat pads. Data indicate mean ± SD ($n > 5$ mice/group).
[a]$P < 0.01$.
[b]$P < 0.05$.

Results

Muscle-specific inactivation of mTOR leads to premature death

To investigate the role of mTOR in skeletal muscle development and function, we developed a conditional *mTOR* gene inactivation strategy based on the Cre-*loxP* system (Fig. 1 A). mTOR$^{flox/flox}$ mice were crossed with human skeletal muscle α-actin (HSA)–Cre mice in which Cre-mediated recombination occurs in postmitotic myofibers but not in satellite cells (Nicole et al., 2003). At birth, Cre-positive mTOR$^{flox/flox}$ (mTOR⁻) pups were viable, born at expected Mendelian ratios, and indistinguishable from their control littermates. PCR analysis confirmed the efficient deletion of the *mTOR* allele specifically in skeletal muscle (Fig. 1 B). At ~4 wk of age, the growth rate of mutant animals started to decrease (Fig. 1 C). By the age of 13 wk, mutant mice started to develop spinal deformity, which increased with age in the form of kyphosis, a sign of muscle weakness, accompanied by breathing difficulties and abnormal posture of the hindlimbs (Fig. 1 D). mTOR⁻ mice eventually died between 22 and 38 wk of age (Fig. 1 E).

mTOR⁻ mice develop a progressive MD

We next characterized muscles from mTOR⁻ mice by morphometric and histological examinations. By the age of 6 wk, the body weight of mTOR⁻ mice was reduced by ~10% compared with controls. This reduction could be attributed to a strong decrease in the mass of fast-twitch glycolytic muscles such as tibialis anterior (TA), gastrocnemius (GC), and plantaris (PLA; Table I). In contrast, the mass of the slow-twitch oxidative soleus muscle was not significantly affected by mTOR deficiency and was even increased after normalization to body weight. Of note, the weight of other organs remained unaffected in mTOR⁻ mice. At this age, fiber number was not significantly different between mTOR⁻ and control muscles (unpublished data), excluding hypoplasia as the cause of reduced mass in fast-twitch muscles. However, the reduction in mTOR-TA muscle mass was associated with a 24% decrease of the mean cross-sectional area (CSA), whereas mTOR⁻ soleus muscle displayed a 6% increase of the mean CSA (Fig. 2 A). In addition, mTOR⁻ muscles showed characteristic dystrophic features that were exacerbated in oxidative muscles (Fig. 2 B). These included degeneration with phagocytosis and mononuclear cell infiltration (Fig. 2 B, green arrows), variation in fiber size with small atrophic fibers (Fig. 2 B, yellow arrows), interfiber connective tissue (Fig. 2 B, thin arrows), and a marked number of regenerated muscle fibers with centrally located nuclei (Fig. 2 B, black arrows) that increased with age (Fig. 2 C). Ongoing muscle regeneration was further confirmed at the molecular level by the activation of the expression of perinatal muscle myosin heavy chain (MHC) MyH8, IGF-II, and myogenin (Fig. 2 D). Dystrophic hallmarks were prominent in the diaphragm, which additionally showed fibrosis (Fig. 2 B, asterisk) and fatty infiltration (Fig. 2 B, red arrows), suggesting that respiratory failure might be the cause of premature death.

To examine a potential relationship between the prominent dystrophic features in oxidative muscles and fiber types, we analyzed the composition of MHC isoforms in whole muscles from 6-wk-old mice. In soleus the shift was from MHC-2X toward MHC-1 (Fig. 2 E and Fig. S1), in TA from MHC-2B toward MHC-2X and -2A (Fig. 2 F), and in PLA from MHC-2B toward MHC-2X and MHC-1 (Fig. 2 G). Therefore, loss of mTOR induces a significant shift toward the expression of slower MHC isoforms, indicating contractile dysfunctions in all types of muscles.

mTOR deficiency more severely affects muscle functional properties than loss of raptor

To assess the functional consequences of mTOR inactivation in skeletal muscle, the muscle contractile performance was analyzed in response to nerve and/or muscle stimulation in 9-wk-old mice (Table II). Both absolute maximum tetanic (Po)

Downloaded from jcb.rupress.org on March 28, 2010

Published December 14, 2009

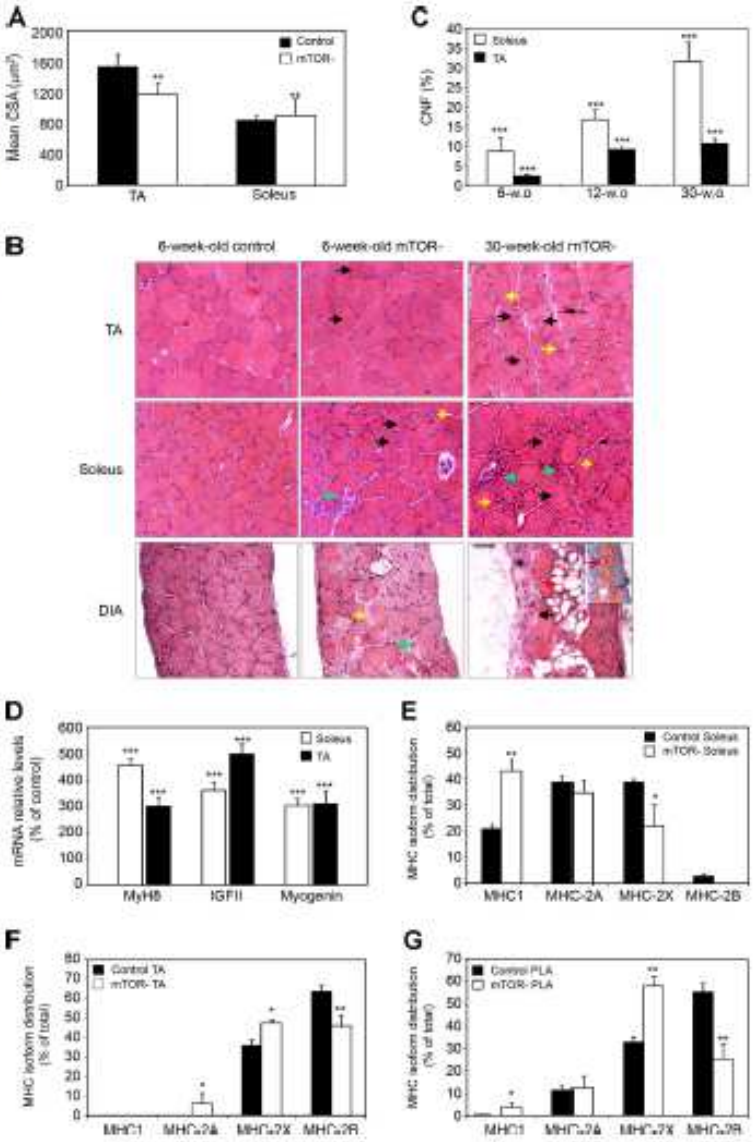

Figure 2. **mTOR⁻ mice develop a progressive MD.** (A) Analysis of the mean fiber CSA in TA and soleus muscles from 6-wk-old mice ($n = 4$). (B) H&E-stained transverse sections of TA, soleus, and diaphragm (DIA) muscles from control and mTOR⁻ mice. Degeneration with phagocytosis and mononuclear cell infiltration (green arrows), variation in fiber size with small atrophic fibers (yellow arrows), interfiber connective tissue (thin arrows), regenerated muscle fibers with centrally located nuclei (black arrows), fibrosis (asterisk), and fatty infiltration (red arrows) are shown. Adipogenic differentiation was confirmed by oil red O staining as shown in the inset. Bar, 50 μm. (C) Percentage of centrally nucleated fibers (CNF) increases with age in mTOR⁻ muscles. (D) Relative mRNA levels of MyHB, IGF-II, and myogenin in mTOR⁻ muscles from 6-wk-old mice. (E–G) Graphs show the percentage distribution of MHC isoforms I, 2B, 2X, and 2A in soleus (E), TA (F), and PLA (G) muscles from 6-wk-old control and mTOR⁻ mice. (C–G) $n = 5$ sample sets. *, $P < 0.05$; **, $P < 0.01$; ***, $P < 0.001$. Data indicate mean ± SEM.

Downloaded from jcb.rupress.org on March 28, 2010

and twitch (Pt) forces were significantly decreased in mTOR⁻ soleus and TA muscles compared with control muscles. Stimulation of mTOR⁻ TA directly or via its nerve gave rise to a similar reduction in absolute Po, indicating that neurotransmission was not altered in mTOR⁻ mice. The reduction in force production was more pronounced in mTOR⁻ TA because of the large decrease in muscle mass observed in fast-twitch muscles. Indeed, when Po was normalized for TA muscle mass or for soleus muscle CSA, the specific maximum tetanic force (sPo) was reduced to the same extent (by ~30%) in both mTOR⁻ TA and soleus muscles, further indicating that muscle weakness of mTOR⁻ mice is not only caused by a loss of contractile muscle mass. In contrast, loss of raptor in muscles from age-matched RAmKO mice did not significantly alter sPo.

Moreover, mTOR⁻ muscles contracted and relaxed slowly as shown by the increased time to peak twitch tension (TTP) and one-half relaxation time (RT50%), which is consistent with the MHC distribution toward slower isoforms. Furthermore, mTOR⁻ soleus muscle was twofold less resistant to fatigue (F20%) than control muscle, whereas RAmKO muscles were more resistant to fatigue (Bentzinger et al., 2008).

We next tested whether mTOR or raptor deficiency impacts resistance to contraction-induced injury in situ by subjecting

Published December 14, 2009

Table II. **Comparison of muscle contractile properties between mTOR⁻ and RAmKO mice**

Mice	Control	mTOR⁻/RAmKO	% Control
Soleus muscle			
mTOR			
Mass (mg)	7.6 ± 0.4	7.5 ± 0.3	98.7
Po (mN)[a]	141.6 ± 33.2	104.3 ± 24.0[c]	73.6
sPo (mN/mm²)[a]	187.9 ± 42.0	134.5 ± 37.1[c]	71.6
Pt (mN)[a]	26.4 ± 3.7	16.2 ± 4.1[d]	61.4
TTP (ms)[a]	82.7 ± 11.1	171.5 ± 73.8[d]	207.4
RT50% (ms)[a]	131.7 ± 45.3	375.4 ± 228.2[c]	285.0
F20% (ms)[a]	85.1 ± 14.5	41.1 ± 18.9[d]	48.3
Raptor			
Mass (mg)	7.1 ± 0.9	6.5 ± 0.9	90.9
Po (mN)[a]	155.6 ± 24.6	141.7 ± 11.0	91.0
sPo (mN/mm²)[a]	211.5 ± 38.7	212.4 ± 19.3	100.4
TA muscle			
mTOR			
Mass (mg)	37.5 ± 1.2	32.7 ± 2.2[d]	87.2
Po (mN)[a]	536.3 ± 100.7	332.0 ± 55.4[d]	61.9
Po (mN)[b]	567.1 ± 79.1	359.7 ± 34.8[d]	63.4
sPo (mN/mg)[b]	15.1 ± 2.2	11.0 ± 1.4[c]	73.0
Pt (mN)[b]	106.4 ± 25.8	60.5 ± 9.5[d]	56.7
TTP (ms)[b]	31.5 ± 2.4	42.4 ± 9.3	134.6
RT50% (ms)[b]	33.2 ± 3.8	58.0 ± 10.9[d]	174.7
Deficit (%)[b]	−12.7 ± 5.0	−56.0 ± 12.9[d]	−340.9
Raptor			
Mass (mg)	41.0 ± 2.4	36.2 ± 1.7[d]	88.5
Po (mN)[b]	607.1 ± 35.7	497.0 ± 55.2[d]	81.9
sPo (mN/mg)[b]	14.9 ± 1.4	13.8 ± 1.8	92.5
Deficit (%)[b]	−12.0 ± 3.5	−12.2 ± 7.3	1.5

Muscle contractile properties of 9-wk-old mTOR and raptor mice were assessed by recording isometric forces in response to electrical stimulation. The following data were measured: muscle mass, Po, sPo, Pt, TTP, RT50%, time taken for maximal twitch tension to fall by 20% (F20%), and the percentage of force deficit following repetitive eccentric contractions (deficit). The data indicate mean ± SD ($n > 4$ mice/group).

[a]Muscle electrical stimulation.

[b]Nerve electrical stimulation.

[c]$P < 0.05$.

[d]$P < 0.01$.

TA muscles to a series of high stress muscle-eccentric contractions. Importantly, loss of mTOR but not of raptor resulted in increased force deficit, indicating a higher susceptibility to injury of mTOR⁻ muscle. Collectively, these data show that mTOR deficiency more severely affects muscle contractile properties than loss of raptor.

mTOR⁻ muscles display reduced levels of DGC components and induction of utrophin

Most forms of MD arise from mutations in the DGC, which provides a physical link between the extracellular matrix and the intracellular cytoskeleton (Durbeej and Campbell, 2002). Force deficits after eccentric contractions are a functional hallmark of dystrophin-deficient muscle (Watchko et al., 2002). This observation prompted us to examine dystrophin levels in mTOR⁻ muscles. Western blot analysis revealed a strong reduction in muscle dystrophin content in 6-wk-old mTOR⁻ mice (Fig. 3 A and Table S1). In Duchenne MD (DMD) and the *mdx* mouse model for DMD, loss of dystrophin is associated with the concurrent down-regulation of other DGC members (Ohlendieck and Campbell, 1991) and with a compensatory up-regulation of its autosomal homologue utrophin (Tinsley et al., 1998). mTOR⁻ muscles also showed decreased expression of several DGC components, including β-sarcoglycan and β-dystroglycan, and induction of utrophin (Fig. 3 A and Table S1). Dystrophin content was further reduced in mutant soleus and TA muscles from 11-wk-old mice, reaching 13 and 17% of the levels in control muscles (Fig. S2 and Table S2). In contrast, expression of caveolin-3 and calpain 3, whose deficiency leads to additional forms of MD (Watchko et al., 2002), was significantly up-regulated.

The DGC plays a major role in regulating membrane integrity, and its loss leads to sarcolemmal fragility and permeability (Straub et al., 1997). However, the overall sarcolemmal integrity of quiescent mTOR⁻ muscle fibers was maintained because rare muscle fibers exhibited Evans blue dye uptake (Fig. 3 B), and elevated creatine kinase serum levels were not detected in mTOR⁻ mice (not depicted). Importantly, immunofluorescence analysis showed that residual dystrophin was still present along the sarcolemma of the noncentronucleated fibers (Fig. 3 C). Thus, it is likely that residual DGC may modulate membrane damage in mTOR⁻ muscles.

Downloaded from jcb.rupress.org on March 28, 2010

Published December 14, 2009

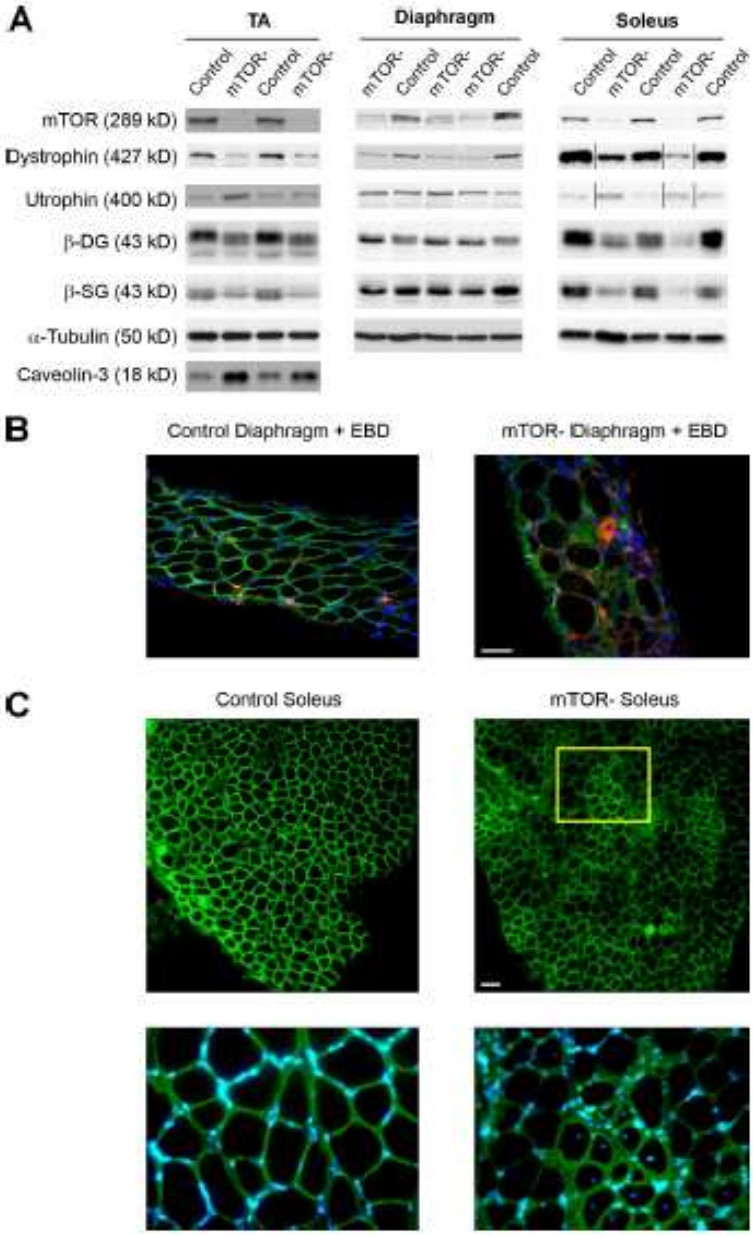

Figure 3. **Reduced DGC amount and utrophin induction in mTOR⁻ muscles.** (A) Soleus, diaphragm, and TA muscle extracts from 6-wk-old mice were immunoblotted with the indicated antibodies to examine dystrophy-related protein levels. Black lines indicate that intervening lanes have been spliced out. (B) Rare Evans blue–positive fibers can be detected in mTOR⁻ diaphragms from 30-wk-old mice. (C) Dystrophin immunostaining (green) and Hoechst staining (blue) on soleus muscle sections from 11-wk-old control and mTOR⁻ mice showing sarcolemmal localization of residual dystrophin. A higher magnification view (inset) shows that dystrophin expression is reduced in noncentronucleated fibers, whereas it is normal in regenerating centronucleated fibers. Bars, 50 µm.

Downloaded from jcb.rupress.org on March 26, 2010

mTOR controls dystrophin expression in a cell-autonomous, rapamycin-resistant, and kinase-independent manner

To gain better insight into the regulation of dystrophin by mTOR, we performed mTOR knockdown in primary myotubes derived from mTOR^{flox} mice infected with Cre-expressing adenovirus (Fig. 4 A). Although mTOR inactivation in cultured myotubes did not prevent terminal differentiation as shown by the induction of the late myogenic differentiation markers α-skeletal actin and troponin T, it led to a rapid and strong down-regulation of the dystrophin protein. These results demonstrate that the mTOR cell autonomously regulates dystrophin levels.

We next assessed whether reduced dystrophin content reflects changes at the mRNA levels. In cultured mTOR⁻ myotubes and muscles, mRNA levels for several DGC components were significantly reduced as compared with control levels, indicating possible transcriptional defects (Fig. 4, B and C).

Published December 14, 2009

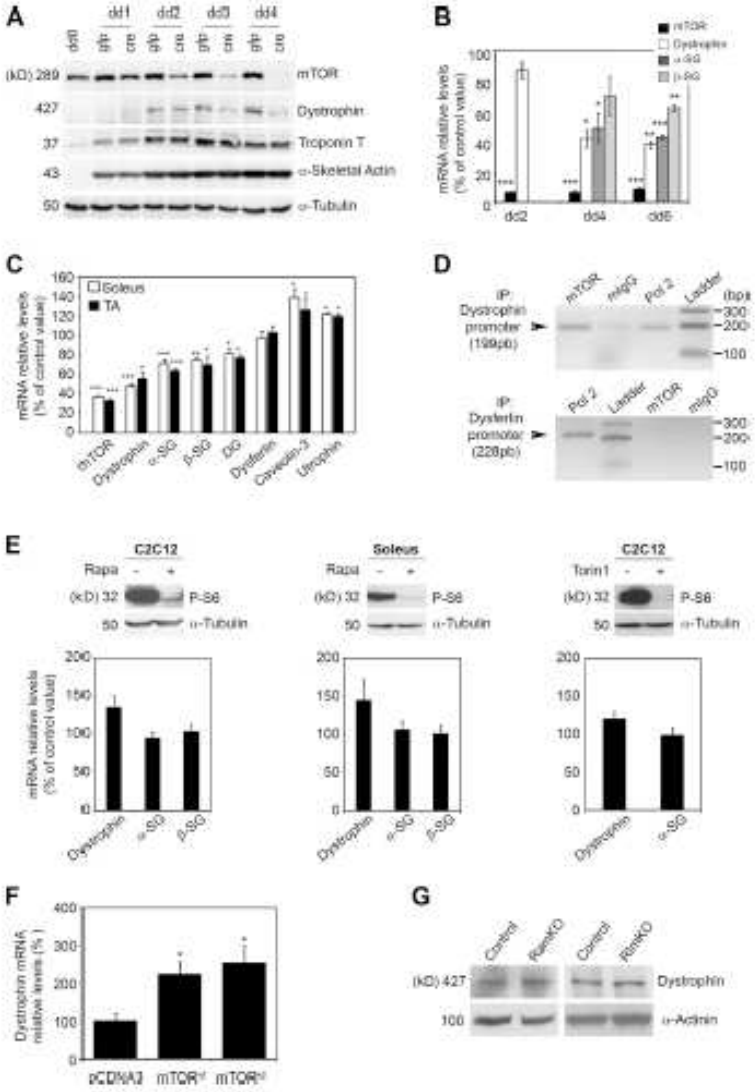

Figure 4. **mTOR controls dystrophin expression.** (A) Time course for mTOR inactivation, dystrophin down-regulation, and induction of terminal differentiation markers in cultured mTOR^{flox} myotubes. The myotubes were transduced by CMV-GFP or CMV-Cre adenovirus on differentiation day 1 (dd1), harvested at a different time point after differentiation, and immunoblotted with the indicated antibodies. (B) Relative mRNA levels of mTOR and the indicated DGC components in mTOR^{flox} myotubes transduced by Ad-Cre ($n = 3$). (C) Relative mRNA levels of mTOR and the indicated dystrophy-related genes in muscles from 6-wk-old mice ($n = 5$). (D) Detection of mTOR on the dystrophin promoter by ChIP assay. Antibodies against mTOR (lane 1), normal mouse IgG (lane 2), or RNA polymerase 2 (lane 3) were used to immunoprecipitate (IP) a mouse TA chromatin extract. The precipitated DNA was analyzed by PCR using primers for the dystrophin (top) or dysferlin (bottom) promoter. (E, top) Western blot analysis showing the phosphorylation status of S6 protein in C2C12 myotubes in the absence (−) or presence (+) of 20 nM rapamycin or 250 nM Torin1 for 48 h from differentiation day 4. For soleus muscle, C57BL/6 mice were daily injected intraperitoneally with 2.5 mg/kg rapamycin or vehicle for 8 d. (bottom) mRNA levels for the indicated DGC components in C2C12 myotubes and soleus muscle in absence or presence of the indicated mTOR inhibitors. (F) Relative mRNA levels of dystrophin in the TA muscle fibers of mTOR$^{-/-}$ mice 12 d after in vivo coelectroporation of rat wild-type (wt) or kinase-dead (kd) mTOR and pRNAT-GFP vector. Graphs show means versus pcDNA3-electroporated control ($n = 5$ mice/group). (G) Western blot analysis showing dystrophin protein levels in soleus muscle from 14-wk-old RAmKO and RImKO mice. *, $P < 0.05$; **, $P < 0.01$; ***, $P < 0.001$. Data indicate mean ± SEM.

Downloaded from jcb.rupress.org on March 28, 2010

In contrast, no change was detected for dysferlin, whereas caveolin-3 and utrophin were up-regulated.

Because mTOR was shown to interact and positively regulate the activity of the transcription factor YY1 in myotubes (Cunningham et al., 2007) and YY1 was shown to bind the dystrophin promoter (Galvagni et al., 1998), we hypothesized that mTOR should bind to the dystrophin promoter. To test our hypothesis, we performed chromatin immunoprecipitation (ChIP) analysis on TA muscle from control mice (Fig. 4 D). We found that mTOR is bound to the promoter of the dystrophin gene at the same extent as RNA polymerase II, whereas it was not bound to the dysferlin promoter. These results strongly suggest that mTOR directly regulates the dystrophin promoter.

We next determined whether dystrophin regulation involved rapamycin-sensitive mTOR functions and mTOR kinase activity. In cultured C2C12 myotubes and mouse soleus muscle, neither rapamycin nor Torin1 treatment reduced dystrophin mRNA levels, although both mTOR inhibitors efficiently inhibited mTORC1 signaling (Fig. 4 E). Consistently, overexpression of a rat mTOR wild type or mTOR kinase dead into the TA muscle of mTOR$^{-/-}$ mice by in vivo DNA electroporation significantly increased dystrophin mRNA levels by 2.1 and 2.5 times, respectively, as compared with control (Fig. 4 F). In agreement with these observations, dystrophin levels were not reduced in muscles lacking raptor and rictor (Fig. 4 G). Collectively, these findings demonstrate that mTOR controls dystrophin expression in a

Published December 14, 2009

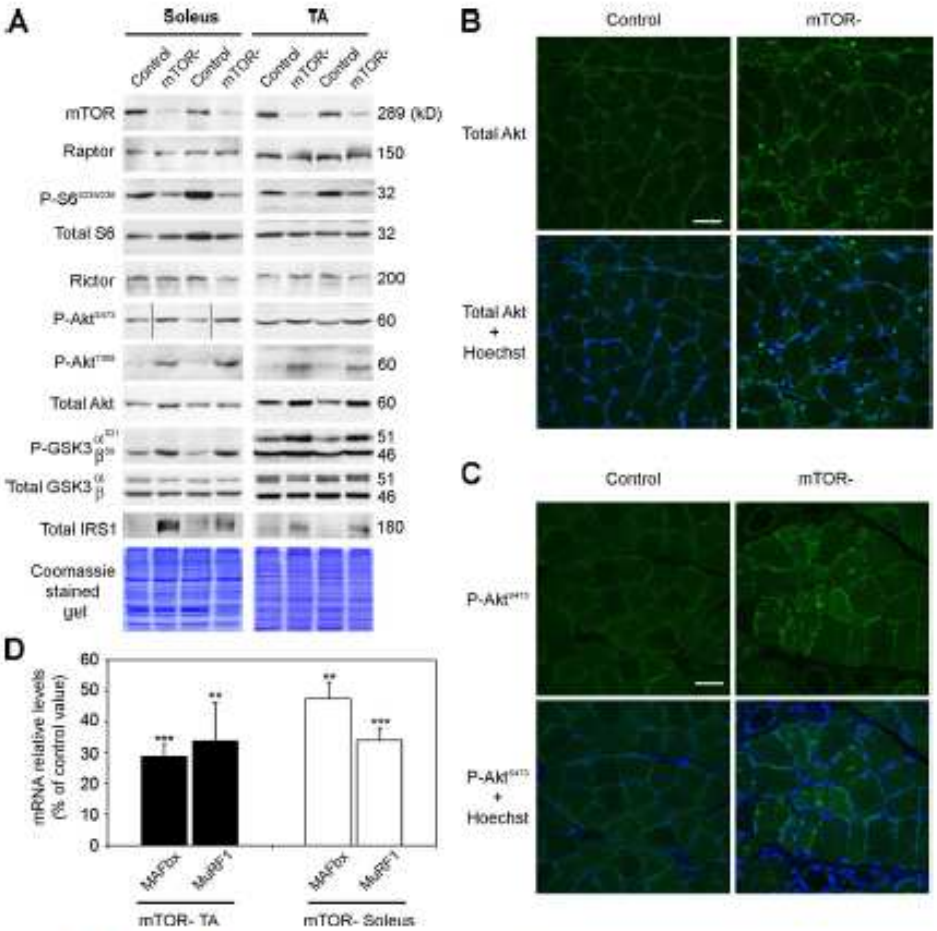

Figure 5. **Signal transduction in mTOR⁻ muscles.** (A) Muscle extracts from 6-wk-old mice were immunoblotted with the indicated antibodies to examine mTORC1 and mTORC2 signaling in soleus and TA muscles. Black lines indicate that intervening lanes have been spliced out. (B and C) Immunofluorescence staining for total PKB/Akt (B) and P-PKB/Akt (C; green) and Hoechst staining (blue) on control and mTOR⁻ soleus muscle sections. Bars, 50 µm. (D) Relative mRNA levels of MuRF1 and MAFbx in mTOR⁻ soleus and TA muscles. **, $P < 0.01$; ***, $P < 0.001$. Data indicate means versus control ± SEM ($n = 5$ sample sets).

rapamycin-resistant and kinase-independent manner independently of raptor and rictor.

MD in mTOR⁻ mice is associated with a down-regulation of mTORC1 signaling and hyperactivation of PKB/Akt

We next investigated the consequences of mTOR depletion on signal transduction in mutant muscles. Western blot analysis revealed that mTOR protein level was strongly decreased in mutant muscles (Fig. 5 A and Table S3). Residual mTOR expression likely arose from nonmuscle cells as well as from cells in which the mTOR allele was not recombined, including newly repaired muscle fibers and satellite cells. In contrast, expression of the specific mTORC1 and mTORC2 components, raptor and rictor, respectively, remained unchanged. mTORC1 and mTORC2 activity in mutant muscles was next assessed by monitoring phosphorylation of S6 and PKB/Akt, respectively. Decreased phosphorylation of S6 was consistent with down-regulation of mTORC1. Surprisingly, phosphorylation of the mTORC2 downstream target PKB/Akt was strongly increased on Ser473. This observation implies the existence of a distinct kinase from mTOR able to phosphorylate PKB/Akt at this residue as previously suggested (Bentzinger et al., 2008). In addition, PDK1-dependent phosphorylation of PKB/Akt on Thr308 was also increased. Increased PKB/Akt activation in mTOR⁻ muscle could result from the suppression of the inhibitory feedback from S6K on insulin signaling. The negative feedback involves S6K phosphorylation of IRS-1 leading to its degradation, thereby suppressing insulin signaling (Um et al., 2006). Consistent with the loss of negative feedback, IRS-1 protein levels were strongly increased in mTOR⁻ muscles (Fig. 5 A). Interestingly, hyperactivation of PKB/Akt was accompanied by an up-regulation of its protein

Downloaded from jcb.rupress.org on March 26, 2010

Published December 14, 2009

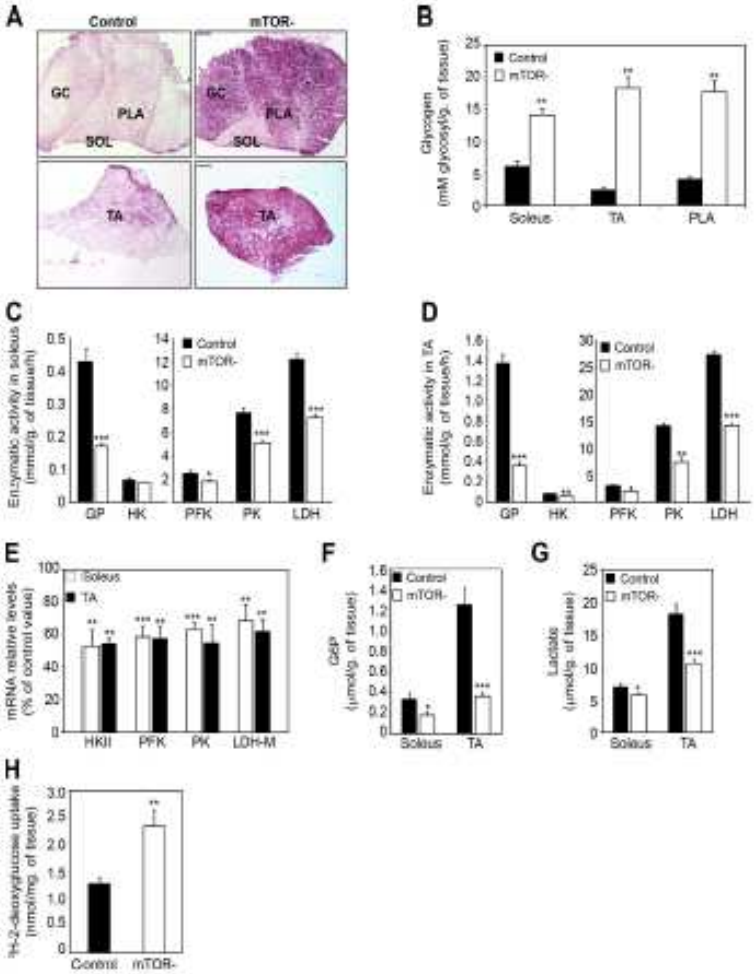

Figure 6. **Altered glucose usage and glycogen accumulation in mTOR⁻ muscle.** (A) Representative periodic acid Schiff staining of soleus (SOL), PLA, GC, and TA muscle sections from 6-wk-old mice showing glycogen accumulation in mTOR⁻ muscles. Bar, 400 µm. (B) Quantification of muscle glycogen content ($n = 5$ sample sets). (C and D) GP and glycolytic enzyme activity in soleus (C) and TA (D) muscles (control, $n = 5$; mTOR⁻, $n = 4$). (E) Relative mRNA levels of the indicated glycolytic enzymes in mTOR⁻ muscles ($n = 5$ sample sets). (F) Quantification of intramuscular glucose-6-phosphate (G6P) in control and mTOR⁻ mice. (G) Quantification of intramuscular lactate in control and mTOR⁻ mice. (H) Enhanced basal glucose uptake in isolated soleus muscle from 5-wk-old control and mTOR⁻ mice ($n = 5$–6 mice). (F and G) $n = 8$ sample sets. HK, hexokinase. *, $P < 0.05$; **, $P < 0.01$; ***, $P < 0.001$. Data indicate mean ± SEM.

Downloaded from jcb.rupress.org on March 26, 2010

level, a feature that has been previously reported in both DMD and *mdx* muscles, irrespective of the muscle pathogenic state (Dogra et al., 2006). Consistently, immunostaining for PKB/Akt (Fig. 5 B) and P-PKB/Akt^{S473} (Fig. 5 C) was stronger in regenerating centronucleated and nonregenerating mTOR⁻ muscle fibers compared with control fibers.

PKB/Akt has been shown to phosphorylate and inactivate the forkhead box transcription factors FoxO1 and FoxO3, thereby blocking the transcriptional up-regulation of the atrophy-related genes MAFbX and MuRF1 (Stitt et al., 2004). Consistent with PKB/Akt hyperactivation, both MaFbX and MuRF1 mRNA were down-regulated in mTOR⁻ muscles (Fig. 5 D), indicating that the atrophy observed in mutant muscle is not associated with activation of the ubiquitin proteasome pathway. In addition, PKB/Akt phosphorylates and inactivates GSK3, an inhibitory kinase of glycogen synthase (Cross et al., 1997). Accordingly, phosphorylation of the regulatory residues Ser9 in GSK3β and/or Ser21 in GSK3α was increased in mTOR⁻ muscles (Fig. 5 A).

Loss of mTOR leads to increased muscle glucose uptake and glycogen accumulation

Inactivation of GSK3 by PKB/Akt was shown to promote glycogen synthesis (Cross et al., 1997), suggesting that glycogen synthesis might be increased in mTOR⁻ muscles. Consistent with this, periodic acid Schiff staining demonstrated that glycogen content was strongly increased in mTOR⁻ muscles (Fig. 6 A). Quantification of glycogen levels showed a 2.3-, 7.5-, and 4.3-fold increase in mTOR⁻ soleus, TA, and PLA muscles, respectively, as compared with control muscles (Fig. 6 B). We next assessed whether increased glycogen content in mTOR⁻ muscles could also result from diminished glycogenolysis and glycolytic capacity. Indeed, the activity of glycogen phosphorylase (GP), hexokinase, phosphofructokinase (PFK), pyruvate kinase (PK), and lactate dehydrogenase (LDH) was consistently reduced in mTOR⁻ soleus (Fig. 6 C) and TA muscles (Fig. 6 D). In addition, reduced activity of glycolytic enzymes in mTOR⁻ muscles was associated with a significant reduction in their expression (Fig. 6 E).

Published December 14, 2009

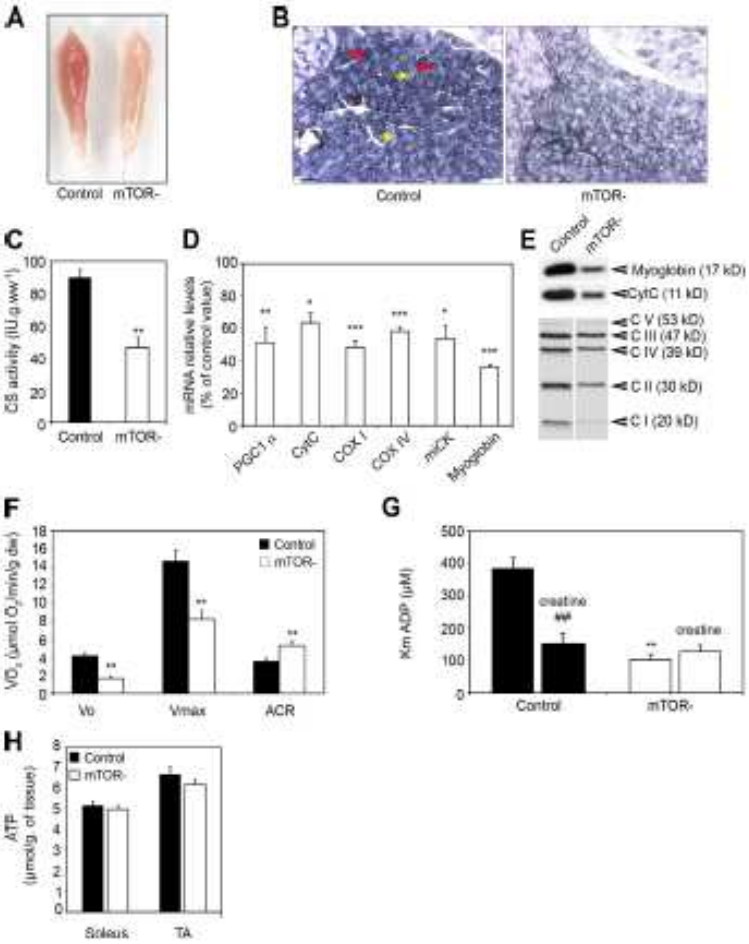

Figure 7. **Impaired oxidative metabolism in mTOR⁻ soleus muscle.** (A) mTOR⁻ soleus muscle is paler than control muscle. (B) Succinate dehydrogenase histochemical staining demonstrating alterations of oxidative metabolism in mTOR⁻ soleus muscle from 6-wk-old mice. Oxidative and glycolytic fibers are indicated by red and yellow arrows, respectively. Bar, 100 μm. (C) Decreased citrate synthase (CS) activity in mTOR⁻ soleus muscle ($n = 5$ sample sets). (D) Relative mRNA levels of genes involved in oxidative energy production in mTOR⁻ soleus muscle ($n = 5$ sample sets). (E) Western blot analysis showing reduced protein levels for myoglobin, cytochrome c (cytc), and respiratory chain components (CI–CV) in mTOR⁻ soleus muscle. Equal protein loading was controlled by measuring total protein content and Coomassie blue staining. (F) Effect of mTOR depletion on mitochondrial respiration in saponin-skinned fibers from soleus muscles from 6-wk-old mice with glutamate and malate as substrates. The following data were measured: basal rate of mitochondrial oxygen consumption in the absence of ADP (Vo), maximal rate of oxygen consumption in the presence of 2 mM ADP (Vmax), and acceptor control ratio (ACR; control, $n = 15$; mTOR⁻, $n = 8$). (G) Effect of mTOR depletion on mitochondria sensitivity for ADP in saponin-skinned fibers from soleus muscles. The apparent Km for ADP was measured in the absence and presence of 20 mM creatine (control, $n = 8$; mTOR⁻, $n = 5$). (H) Intramuscular ATP levels in muscles from control and mTOR⁻ mice ($n = 8$ sample sets). **, $P < 0.01$ (for control with creatine versus control without creatine); **, $P < 0.01$ (for mTOR⁻ without creatine versus control without creatine). Data indicate mean ± SEM.

Downloaded from jcb.rupress.org on March 26, 2010

Consistent with diminished glycolytic flow, reduced levels of glucose-6-phosphate (Fig. 6 F) and lactate (Fig. 6 G) were measured in mTOR⁻ muscles. Importantly, this decrease was not caused by defects in glucose uptake because basal 2-deoxyglucose uptake was even increased 1.8-fold into isolated mTOR⁻ soleus muscle compared with controls (Fig. 6 H).

mTOR deficiency in muscle alters mitochondrial regulation and oxidative capacity

At the macroscopic level, mTOR⁻ muscles appeared paler than control muscles. This was particularly striking in mTOR⁻ soleus muscles, which lacked the red color characteristic of oxidative muscles (Fig. 7 A). Moreover, staining for succinate dehydrogenase, a marker of mitochondrial complex II, was weak in mTOR⁻ soleus fibers to the extent that the difference in oxidative activity classically observed between fiber types was barely detectable (Fig. 7 B). These observations suggested changes to have taken place in the metabolic properties of mTOR⁻ soleus muscle. Recent evidence indicates that mTORC1 controls mitochondrial biogenesis and respiration, notably via YY1 and PGC1α (Cunningham et al., 2007; Bentzinger et al., 2008). In agreement, measurement of citrate synthase activity indicated a twofold reduction in mitochondrial content (Fig. 7 C), and the expression of several genes involved in oxidative metabolism was markedly reduced in mTOR⁻ soleus muscle (Fig. 7, D and E).

To investigate the consequences of mTOR inactivation on intrinsic oxidative capacities in soleus muscles, we analyzed mitochondrial respiration and function in saponin-skinned fibers with nonlimiting amounts of substrate and oxygen. Consistent with decreased mitochondrial content in mTOR⁻ soleus, the rate of oxygen consumption in muscle was diminished both in the absence (basal) or presence (maximal) of ADP, whereas the ratio of maximal to basal respiration (acceptor control ratio) was increased (Fig. 7 F). These results indicate that the lack of mTOR in soleus muscles reduced the maximal capacity of oxidative phosphorylation, whereas the

Published December 14, 2009

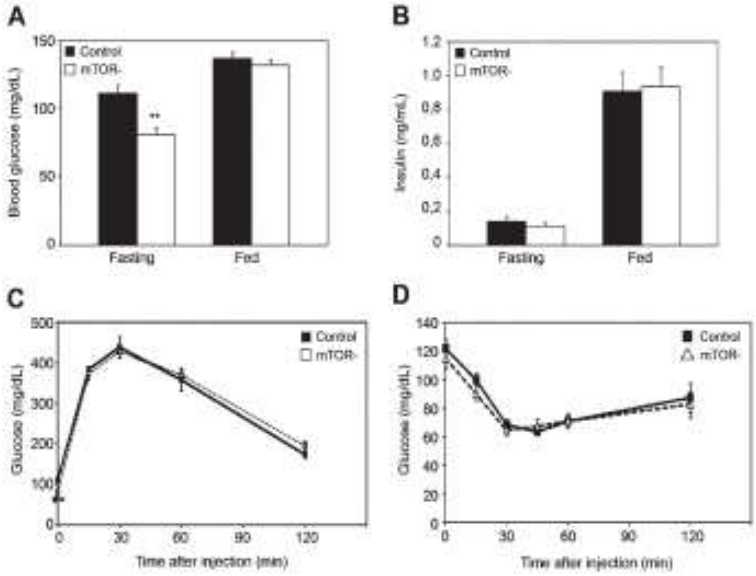

Figure 8. **Glucose homeostasis and insulin sensitivity in mTOR⁻ mice.** (A) Fasting and fed blood glucose concentrations in mTOR⁻ and control male mice. (B) Fasting and fed serum insulin concentrations in mTOR⁻ and control male mice ($n = 7$ mice/group). (C) Glucose tolerance test on male mice ($n = 15$ mice/group). (D) Insulin tolerance test on mTOR⁻ and control mice ($n = 8$ mice/group). **, $P < 0.01$. Data indicate mean ± SEM.

coupling efficiency between oxidation and phosphorylation was improved. Mitochondrial function depends on its sensitivity to ADP and creatine, which differs in oxidative and glycolytic muscle fibers (Kuznetsov et al., 1996). In oxidative fibers, the apparent Km (Michaelis–Menten constant) for ADP is high and is decreased by creatine as a consequence of the functional coupling of mitochondrial creatine kinase to ATP production and energy transfer (Fig. 7 G). Surprisingly, in mTOR⁻ soleus muscle fibers, the apparent Km for ADP was unusually low and remained unaffected by creatine. Altogether, our findings demonstrate that loss of mTOR not only affects mitochondrial biogenesis and oxygen consumption, but additionally leads to profound changes into the mitochondria metabolic properties of oxidative fibers, which share characteristics with those of glycolytic fibers. However, intramuscular ATP concentrations were not significantly reduced in mTOR⁻ muscles (Fig. 7 H).

mTOR deficiency in muscle does not impair whole body glucose homeostasis

We next investigated the effect of mTOR deficiency in skeletal muscle on whole body glucose homeostasis. In the fasting state, mTOR⁻ mice had significantly lower glucose levels (Fig. 8 A), which is possibly the result of increased basal glucose uptake in skeletal muscle (Fig. 6 H). However, the glucose and insulin concentrations in the fed state and the insulin level in fasting mice were not statistically different between mTOR⁻ and control mice (Fig. 8, A and B), suggesting that glucose tolerance and insulin sensitivity were not affected. Consistent with this, mTOR⁻ and control mice showed similar responses during the glucose tolerance test (Fig. 8 C) and the insulin tolerance test (Fig. 8 D). Collectively, these results indicate that mTOR functions in skeletal muscle are not crucial in controlling whole body glucose homeostasis.

Discussion

To determine the physiological role of mTOR in postnatal skeletal muscle, we generated muscle-specific mTOR knockout mice (mTOR⁻) using *HSA*-Cre mice expressing Cre in postmitotic myofibers but not in satellite cells (Nicole et al., 2003). Our study reveals that mTOR deficiency in skeletal muscle leads to metabolic changes resulting in glycogen accumulation. Specifically, these changes include an increase in glucose uptake and glycogen synthesis associated with reduced glycogen breakdown through glycogenolysis and glycolytic and oxidative pathways. Our in vivo data support and extend findings of previous in vitro studies (Hardwick et al., 1999; Peng et al., 2002; Edinger et al., 2003; Schieke et al., 2006; Cunningham et al., 2007). Indeed, mammalian cells transfected with mTOR or raptor short hairpin RNAs or treated with rapamycin demonstrate altered glycolysis and oxidative metabolism associated with a parallel change in gene expression. In addition, mTOR inhibition by rapamycin abrogated the PKB/Akt-mediated induction of glycolytic enzymes in a constitutive PKB/Akt murine model of prostate intraepithelial neoplasia (Majumder et al., 2004). Finally, mTOR and raptor have been shown to directly regulate mitochondrial biogenesis and oxidative functions through the control of a YY1–PGC1α transcriptional complex (Cunningham et al., 2007). Our study further reveals that deficiency in intracellular energy transfer could be an additional mechanistic basis for the mitochondrial alterations in mTOR⁻ muscle.

However, intramuscular ATP levels were preserved in mTOR⁻ mice. Similarly, ATP concentration was not changed in cells treated with rapamycin, despite lower rates of oxygen consumption and glycolysis (Cunningham et al., 2007). Although glucose metabolism was altered, basal glucose uptake and glycogen synthesis were increased in mTOR⁻ muscle. These effects

Downloaded from jcb.rupress.org on March 26, 2010

Published December 14, 2009

are probably mediated by the hyperactivation of PKB/Akt in mutant muscles. Increased basal glucose uptake in muscle could possibly contribute to the lower basal glucose levels in mTOR⁻ mice. However, glucose tolerance and insulin sensitivity were not affected in mTOR⁻ mice, indicating that muscle mTOR does not play a crucial role in controlling whole body glucose homeostasis.

Decreased oxidative capacity, altered mitochondrial regulation, glycogen accumulation, and hyperactivation of PKB/Akt were also reported in RAmKO but not in RImKO muscles (Bentzinger et al., 2008), indicating that mTORC1 disruption likely accounts for these changes in mTOR⁻ muscles. Although glycolytic pathways were not investigated in RAmKO mice, our observations strongly suggest that glycolytic capacity is also reduced in this model. Hyperactivation of PKB/Akt in mTOR⁻ muscle is associated with reduced mTORC1 signaling and increased IRS-1 levels, indicating that this feature results from the loss of the well-documented S6K-mediated inhibitory feedback on IRS-1 (Um et al., 2006) as observed in RAmKO muscle (Bentzinger et al., 2008). In addition, the persistence of PKB/Akt phosphorylation on Ser473 in mTOR⁻ muscle is reminiscent of muscle lacking both raptor and rictor but still containing mTOR. Thus, our observations confirm and extend the findings by Bentzinger et al. (2008) that skeletal muscles express a kinase distinct from mTOR that is able to phosphorylate PKB/Akt on this site. In line with this, additional kinases, designated as PDK2 kinases, have been proposed to phosphorylate Akt on Ser473 (Bayascas and Alessi, 2005). Despite the hyperactivation of PKB/Akt in raptor-deficient muscles, RAmKO mice exhibited altered glucose tolerance (Bentzinger et al., 2008). It is not clear at present how raptor and rictor (Kumar et al., 2008) but not mTOR inactivation in muscle generates glucose intolerance.

In addition, we show that loss of mTOR in muscle results in a progressive muscle myopathy similar to that observed in RAmKO mice (Bentzinger et al., 2008). However, muscle pathology is exacerbated and extended to all types of muscles in mTOR⁻ mice. For example, mTOR⁻ muscles contain up to 35% of regenerating fibers, whereas the proportion of regenerating fibers remained very low in RAmKO mice. Moreover, mTOR deficiency severely affects the functional properties of slow- and fast-twitch skeletal muscles, whereas the contractile properties of the fast glycolytic extensor digitorum longus muscle were mainly spared in RAmKO mice. Finally, the sPo remained unaltered in muscles from RAmKO mice, whereas it is reduced by almost 30% in mTOR⁻ muscles, thus demonstrating that muscle weakness of mTOR⁻ mice is not only caused by a loss of muscle mass.

A possible explanation for the more severe myopathy in mTOR⁻ muscle is our finding that these muscles additionally exhibit reduced levels of both dystrophin and the entire DGC, a feature that is observed neither in RAmKO nor RImKO muscles. Consistently with this finding, mTOR⁻ muscles display several features reminiscent of *mdx* and DMD muscles. At the molecular level, these include the up-regulation of utrophin (Tinsley et al., 1998), caveolin-3 (Repetto et al., 1999), and PKB/Akt protein levels (Acharyya et al., 2005; Dogra et al., 2006; Peter and Crosbie, 2006). Finally, the functional characteristics of mTOR⁻ muscles are similar to *mdx* muscle, as they also exhibit a contraction-induced force deficit (Watchko et al., 2002). In addition, skeletal muscle from *mdx* mice generally shows increased mass attributed to the ongoing cycle of degeneration and regeneration, producing larger but weaker muscle fibers (Watchko et al., 2002).

However, mTOR⁻ muscles do not display increased sarcolemmal permeability, one of the most characteristic and early features of muscles lacking dystrophin (Straub et al., 1997), although sarcolemmal fragility of mTOR⁻ muscle is demonstrated by the great force deficits associated with eccentric contractions. Importantly, dystrophin levels in mTOR⁻ muscles reach ~10–20% of those in control muscles, and levels of DGC components are only mildly decreased, whereas the entire protein complex is lost in DMD and *mdx* muscle (Ohlendieck and Campbell, 1991). Therefore, it is likely that residual sarcolemmal DGC or utrophin–glycoprotein complex modulate membrane damage of mTOR⁻ muscles (Peter et al., 2009). In line with this, studies on *mdx* mice treated with gentamicin have demonstrated that 10–20% of dystrophin levels are sufficient to restore the assembly of DGC and can afford significant but not complete protection against injury (Barton-Davis et al., 1999).

We also provide evidence that the reduction of dystrophin is based on a reduction of transcripts. Moreover, we show that mTOR binds the dystrophin promoter, strongly suggesting that this reduction is controlled at the transcriptional level. mTOR controls the transcription of many genes (Peng et al., 2002). In particular, mTOR interacts with and positively regulates YY1 transcriptional activity to activate mitochondrial gene expression in myotubes (Cunningham et al., 2007). Interestingly, YY1 has also been shown to bind and regulate the dystrophin promoter (Galvagni et al., 1998). Therefore, it is tempting to speculate that mTOR may positively modulate YY1 function in myotubes to drive dystrophin expression. In addition, our findings that mTOR regulatory function on dystrophin transcription is insensitive to rapamycin are consistent with the observation that mTOR interacts with YY1 independently of rapamycin and that dystrophin is not down-regulated in RAmKO muscles. Interestingly, using rapamycin, Akt activation was shown to prevent the force deficit induced in *mdx* muscles by eccentric contractions independently of mTOR (Blaauw et al., 2008). Our finding that mTOR regulates dystrophin expression in a rapamycin-resistant manner may provide an explanation for this discrepancy.

We also provided evidence that mTOR kinase activity is not required to regulate dystrophin, thus further extending the list of catalytic independent mTOR functions. Indeed, mTOR was shown to regulate IGF-II expression and myogenesis via a kinase-independent mechanism (Erbay and Chen, 2001; Erbay et al., 2003).

Collectively, our data point toward a new and specific role of mTOR in the regulation of dystrophin expression in a way that is not strictly dependent on mTORC1 and mTORC2. Of note, down-regulation of dystrophin in mTOR⁻ muscle cannot be attributed to the loss of both mTORC1 and mTORC2 functions because DmKO mice neither display a more severe phenotype than RAmKO nor the characteristic Akt protein

Downloaded from jcb.rupress.org on March 26, 2010

Published December 14, 2009

up-regulation observed in dystrophin-deficient muscles (Dogra et al., 2006). Evidence for mTOR functions that do not involve the contribution of these mTORCs is supported by a recent study showing that mTOR regulates terminal oligopyrimidine mRNA translation in a raptor- and rictor-independent manner (Patursky-Polischuk et al., 2009).

In conclusion, we demonstrate that the loss of mTOR in skeletal muscle leads to a severe myopathy, thereby further extending the list of disorders related to mTOR dysfunction. Our findings underscore the critical role of mTOR in regulating the genetic repertoire required for the appropriate maintenance of skeletal muscle integrity. About 40% of all myopathies have not yet been genetically characterized, whereas mTOR$^-$ muscles recapitulate many of the features of a broad range of these disorders, suggesting that alterations of mTOR-mediated processes could contribute to these disorders. Therefore, the importance of the mTOR pathway in maintaining muscle integrity provides new avenues of investigation in the diagnosis and therapy of skeletal muscle pathologies.

Materials and methods

Animals

The generation of the mTOR^{neo} embryonic stem (ES) clones used to functionally inactivate the mTOR gene was described previously (Gangloff et al., 2004). In brief, a targeting vector was produced by introducing a loxP site upstream of the mTOR promoter region and a neo cassette flanked by two loxP sites in the intron preceding exon 6. To generate mTOR^{neo} ES cells, the construct was electroporated into 129SV/ae ES cells, and G418-resistant clones were screened for homologous recombination by Southern blotting. For excision of the floxed PGK^{neo} cassette, the mTOR^{neo} ES cells were transfected with 0.8 µg pEGFP-N1 (Takara Bio Inc.) and 0.2 µg pMC-Cre using transfection reagent (Effectene; QIAGEN). ES cells expressing EGFP were cultured in the presence and absence of G418. G418-sensitive colonies were analyzed by PCR. ES cells showing the selective deletion of the neomycin resistance cassette and containing the mTOR floxed allele were injected into C57BL/6J blastocysts to generate chimeric mice. Chimeric mice were mated with C57BL/6J mice to generate the heterozygous floxed mutant (mTOR$^{+/flox}$) through germline transmission. Positive F1 offspring were identified by PCR and further backcrossed with C57BL/6J mice during five generations (F5 offspring). mTOR$^{+/flox}$ mice were interbred to obtain a homozygous mutant (mTOR$^{flox/flox}$). mTOR$^{flox/flox}$ (control) mice were bred with HSA-Cre mice to generate Cre-positive mTOR$^{flox/flox}$ (mTOR$^-$) mice. ES cells and mice were genotyped by PCR.

The primers used to identify the mTOR flox allele were p2 (5'-GCTCTTGAGGCAAATGCCACTATCACC-3') and p3 (5'-TCATTACCTTCTCATCAGCCAGCAGTT-3'), and the primers to identify the recombined mTOR$^-$ allele were p1 (5'-TTCATTCCCTTGAAAGCCAGTCTCACC-3') and p3. The animals were provided with mouse chow and water ad libitum in a restricted-access, specific pathogen-free animal care facility at the Ecole Normale Superieure of Lyon (Plateau de Biologie Experimentale de la Souris). All procedures were performed in accordance with national and European legislation on animal experimentation.

In vivo electroporation of mTOR mutants

Expression vectors were injected into TA muscles (7 µg total DNA in 30 µl 0.9% NaCl) of 6-wk-old mTOR$^-$ female mice. Injected muscles were electroporated with 1-cm^2 plaque electrodes as described previously (Méjat et al., 2005). The electroporated DNA mixtures contained 5 µg of the rat mTOR expression vectors (wild type or kinase dead) and 2 µg pRNAT-GFP, allowing the visualization and microdissection of electroporated fibers for further gene expression analysis by quantitative real-time PCR. pcDNA3/mTOR eukaryotic expression plasmids encoding wild-type or kinase-dead (D2338A) rat mTOR were generated previously (Brunn et al., 1997).

ChIP assay

Mouse TA muscles were incubated for 15 min on ice in buffer RBI (100 mM KCl, 5 mM $MgCl_2$, 5 mM EDTA, 5 mM Na pyrophosphate, pH 6.8, and protease inhibitors) then transferred to a 2% formaldehyde solution for 15 min at 37°C. Reactions were stopped by addition of glycine at 0.125 M final and incubation at 25°C for 5 min. After a PBS wash, muscles were crushed in lysis buffer A (10 mM Tris-HCl, pH 7.9, 85 mM KCl, 0.5% NP-40, and protease inhibitors). The mixture was homogenized by 20 strokes of Dounce followed by a 5-min spin at 5,000 rpm at 4°C. The pellet was resuspended in lysis buffer B (50 mM Tris-HCl, pH 8, 10 mM EDTA, 1% SDS, and protease inhibitors) incubated on ice for 10 min followed by a 5-min centrifugation at 5,000 rpm at 4°C. The supernatant was sonicated in a Bioruptor (Diagenode) for 15 min (medium; 30 s/30 s cycles). The size of chromatin fragment was checked to be in the range of 300–500-bp length on an agarose gel after de–cross-linking. ChIP was performed using the EZ Magna ChIP kit (Millipore) with 200 µg chromatin and 20 µg antibody.

The antibodies used were mTOR (Cell Signaling Technology), normal mouse IgG (12–371; Millipore), and anti-RNA Pol2 CTD4H8 (05-623B; Millipore). PCR conditions were optimized for each couple of primers. The primers used were 5'-AGTTGAACATTATTTGAACT-3' and 5'-ACTGAGTGAGTCAACATAGT-3' for the dystrophin promoter and 5'-ACAGTCAGGGAAGGAAGCAA-3' and 5'-CCTTCCACCTCTGTTCAGGA-3' for the dysferlin promoter.

Muscle histology, immunohistochemistry, morphometric measurements, and imaging

Skeletal muscles were collected, embedded in tragacanth gum, and quickly frozen in isopentane cooled in liquid nitrogen. 10-µm-thick sections were obtained from the middle portion of frozen muscles and processed for histological and immunohistochemical analysis according to standard protocols. The fiber CSA and the number of centrally nucleated fibers were determined for three consecutive H&E-stained sections from at least four animals using Metamorph software (version 6.3; MDS Analytical Technologies). For immunostaining, cross sections were fixed in acetone at −20°C permeabilized with 0.1% Triton X-100/PBS, and incubated with specific primary antibody followed by Alexa Fluor 488–labeled secondary antibodies (Invitrogen).

The following primary antibodies were used: dystrophin (Dys2; Novocastra), Akt (Cell Signaling Technology), and P-Akt (Cell Signaling Technology). For vital staining with Evans blue dye, the dye was resuspended in PBS at 1 mg/0.1 ml/10 g body wt and injected intraperitoneally. Muscles were collected after 24 h, and frozen sections were rinsed in PBS and examined by fluorescence microscopy.

Confocal microscopy was performed using a spectral confocal laser-scanning microscope (TCS SP5; Leica) on an upright microscope (DM6000 B; Leica). Confocal software (LAS AF; Leica) was used for acquisition with a Plan Apo 63× NA 1.4 oil objective (HCX; Leica). Fluorescence and light microscopy were performed using an upright microscope (Axioplan2; Carl Zeiss, Inc.) and 10× NA 0.3 (Ph1), 20× NA 0.5, or 40× NA 0.75 Plan NeoFluar objectives (Carl Zeiss, Inc.). Images were captured using a charge-coupled device monochrome camera (Coolsnap HQ; Photometrics) and MetaMorph software. For all imaging, exposure settings were identical between compared samples. All samples for microscopy were viewed at room temperature.

Quantitative real-time PCR and immunoblot analysis

Total RNA was isolated from cultured cells or muscle tissues using Trizol (Invitrogen). RNA was analyzed by quantitative real-time PCR using SYBR Green (Roche). The data were normalized to cyclophilin B, β2-microglobulin, and hypoxanthine–guanine phosphoribosyltransferase mRNA levels, which gave similar results. Western blots were performed as described previously (Ohanna et al., 2005). Primary antibodies used to study mTOR signaling were obtained from Cell Signaling Technology. Primary antibodies against dystrophy-related proteins were obtained from Novocastra, and antibodies against troponin T were obtained from Sigma-Aldrich. Antibodies against respiratory chain components, myoglobin, and cytochrome c were obtained from Mitosciences, Santa Cruz Biotechnolgoy, Inc., and BD, respectively.

Cell cultures

Primary cultures were derived from GC and TA muscles of 4-wk-old mTOR^{flox} mice as described previously (Ohanna et al., 2005). mTOR^{flox} myoblasts were differentiated in DME/Ham F12 containing 2% horse serum. The myotubes were transduced by cytomegalovirus (CMV)-GFP or CMV-Cre adenovirus (Genethon) at 100 MOI on differentiation day 1 and harvested at different time points for gene expression analysis by quantitative real-time PCR or Western blotting. C2C12 myoblasts were differentiated in DME with 2% horse serum and treated at differentiation day 4 with vehicle (DMSO),

Downloaded from jcb.rupress.org on March 26, 2010

Published December 14, 2009

20 nM rapamycin, or 250 nM Torin1 for 48 h and harvested for gene expression analysis by quantitative real-time PCR or Western blotting.

Enzyme analysis

Frozen muscle samples were homogenized in a stabilizing medium containing 50% glycerol, 20 mM phosphate buffer, pH 7.4, 5 mM β-mercaptoethanol, 0.5 mM EDTA, and 0.02% BSA at a dilution of 1:50 based on wet weight. All of the enzyme activities were measured at 22°C as described previously (Passonneau and Lowry, 1993). Hexokinase activity was determined in a two-step assay. The glucose-6-phosphate accumulated for 60 min in the first step and reacted with NADP and glucose-6-phosphate dehydrogenase in a second step. The NADPH generated was detected by fluorescence spectroscopy with excitation/emission wavelengths of 350/460 nm. GP, PFK, PK, and LDH activities were measured in a one-step spectrophotometer assay by directly measuring the rate of appearance or disappearance of NADPH/NADH at 340 nm for 10 min. For GP activity measurement, glucose-1-phosphate formation was coupled to phosphoglucomutase and glucose-6-phosphate dehydrogenase reactions. For PFK activity measurement, fructose-1,6-bisphosphate formation was coupled to aldolase, triosephosphate isomerase, and glycerol-3-phosphate dehydrogenase reactions. For PK activity measurement, pyruvate formation was coupled to LDH reaction. LDH activity was measured in the direction of lactate formation. Citrate synthase activity was determined by using Ellman's reagent with acetyl-CoA and oxaloacetate (Leek et al., 2001). Standards were carried out through the entire procedure.

Determination of intramuscular glucose-6-phosphate, lactate, and ATP concentrations

Muscles were quickly removed from anesthesized animals, weighted, and directly frozen in liquid nitrogen. Muscles were homogenized in 0.65 M perchloric acid (1:40 wt/vol) and incubated for 15 min at 4°C. Muscle homogenates were centrifuged at 5,000 *g* for 10 min at 4°C. Resulting acid supernatants were neutralized with 2 N KOH in 0.4 M TEA/KCl and used for the fluorometric determination of lactate, ATP, and glucose-6-phosphate contents by coupled enzyme assays (Passonneau and Lowry, 1993).

Glucose and insulin tolerance tests

For glucose tolerance tests, 12-wk-old male mice were fasted overnight and injected intraperitoneally with 3 mg glucose/g body wt. For the insulin tolerance test, 4-h-fasted male mice were injected intraperitoneally with insulin (0.75 mIU/g body wt; Sigma-Aldrich). Blood glucose levels were determined from tail venous blood using an automatic glucose monitor (Roche). Serum levels of insulin were determined with murine ELISA kit (Linco Research).

Glucose uptake assays

After cervical dislocation of the mice, the soleus muscle was rapidly isolated and tied to stainless steel clips by the tendons. All incubations were performed at 37°C under an atmosphere of 95% O_2/5% CO_2 in 1 ml Krebs-Ringer bicarbonate buffer, pH 7.3, supplemented with 1% BSA (fraction V; pH 7; Intergen) and 2 mM sodium pyruvate. Glucose transport was measured as follows: after a preincubation period of 15 min, muscles were incubated for 10 min in the same medium supplemented with 2-[^{3}H]deoxyglucose (0.1 mM and 0.5 μCi/ml). Afterward, muscles were washed for 30 min in ice-cold saline buffer and dissolved in 1 N NaOH before scintillation counting for ^{3}H-labeled radioactivity was performed. Sample aliquots were used for protein determination.

Functional properties of mitochondria

Respiratory parameters of the total mitochondrial population were studied in situ in fresh saponin-skinned fibers (50 μg/ml saponin for 30 min) and determined with a Clark electrode (Hansatech Instruments) in an oxygraphic cell at 22°C as described previously (Kuznetsov et al., 2008). Respiration rates were expressed as μmol O_2/min/g dry weight. Respiration solution, pH 7.1, contained 10 mM EGTA-CaEGTA buffer (free Ca^{2+} concentration 100 nM), 1 mM free Mg^{2+}, 20 mM taurine, 0.5 mM dithiothreitol, 20 mM imidazole, ionic strength 160 (potassium methane sulfonate), 5 mM glutamate, 2 mM malate, 3 mM phosphate, and 2 mg/ml BSA. Basal oxygen consumption without ADP (V_0) was recorded in the presence or absence of 20 mM creatine, and increasing amounts of ADP were added until maximal respiration was reached. After measurements, fibers were carefully removed, dried, and weighed. The ADP-stimulated respiration (V_{ADP}) above basal oxygen consumption (V_0) was plotted as a function of ADP with and without creatine. The apparent Km values for ADP in the presence or absence of creatine and V_{ADP} were calculated with a nonlinear fit of the Michaelis–Menten equation. The maximal respiration rate (Vmax) = V_{ADP} + V_0. The acceptor control ratio = Vmax/V_0. Three determinations were made for each muscle sample.

Measurements of muscle contractile properties and lengthening contractions

Mice were anesthetised with 60 mg/kg pentobarbital. The knee and foot were fixed using clamps and pins. The isometric contractile properties of TA muscles were studied in situ as previously described (Moulsol et al., 2006). The distal tendon of the TA muscle was attached to a lever arm of a servomotor system (305B Dual-Mode Lever; Aurora Scientific). All data provided by the servomotor system were recorded and analyzed on a microcomputer using the Powerlab system (4SP; ADInstruments) and software (Chart 4; ADInstruments). The sciatic nerve (proximally crushed) was stimulated by a bipolar silver electrode using a supramaximal (10 V) square wave pulse of 0.1-ms duration. In some instances, muscles were directly stimulated (80 V). All isometric contraction measurements were made at an initial muscle length of L0 (length at which maximal tension, Pt, was obtained during the twitch). Po was measured during isometric contractions in response to electrical stimulation (frequency of 25–150 Hz; train of stimulation of 500 ms). sPo was calculated by dividing Po by muscle weight. Pt, TTP, and RT50% were also measured in response to a single stimulation. The in situ contraction–induced injury protocol for the TA muscle used in this study was similar to that described previously (Dellorusso et al., 2001). The sciatic nerve was stimulated for 300 ms (frequency of 125 Hz). An isometric contraction of the TA muscle was initiated during the first 100 ms. Then, muscle lengthening (3 mm; ~45% fiber length [Lf]) at a velocity of 15 mm/s (~2 Lf/s) was imposed during the last 200 ms. Two lengthening contractions of the TA muscle were performed, each separated by a 60-s rest period. The force deficit after contraction-induced damage was determined by calculating the difference between the Po measured 1 min after the lengthening contractions and the Po determined before lengthening contractions and was expressed as a percentage of Po determined before lengthening contractions.

The isometric contractile properties of soleus muscles were studied in vitro as previously described (Agbulut et al., 2009). Soleus muscles were soaked in an oxygenated Krebs solution (95% O_2 and 5% CO_2) containing 58.5 mM NaCl, 24 mM $NaHCO_3$, 5.4 mM KCl, 1.2 mM KH_2PO_4, 1.8 mM $CaCl_2$, 1 mM $MgSO_4$, and 10 mM glucose, pH 7.4, and maintained at a temperature of 22°C. One of the muscle tendons was attached to a lever arm of a servomotor system (300B Dual-Mode Lever; Aurora Scientific). After equilibration (30 min), electrical stimulation was delivered through electrodes running parallel to the muscle. 1-ms pulses were generated by a high power stimulator (701B; Aurora Scientific). Po was measured during isometric contractions in response to electrical stimulation (frequency of 50–125 Hz; train of stimulation of 1,500 ms). sPo was calculated by dividing the force by the estimated CSA of the muscle. Assuming muscles have a cylindrical shape and a density of 1.06 mg mm^{-3}, the CSA corresponds to the volume of the muscle divided by Lf. The Lf to L0 ratio of 0.70 was used to calculate Lf. Fatigue resistance was determined after a 5-min rest period. The muscles were stimulated at 50 Hz during 500 ms every second for 1 min. The time taken for initial force to fall by 20% (F20%) was calculated.

Myosin isoform identification

Muscles were subjected to the analysis of MHC isoforms as described previously (Talmadge and Roy, 1993). Myosin was extracted from small sections of muscles in 7 vol of buffer solution (0.3 M NaCl, 0.1 M NaH_2PO_4, 0.05 M Na_2HPO_4, 0.01 M $Na_4P_2O_7$, 1 mM $MgCl_2$-$6H_2O$, 10 mM EDTA, and 1.4 mM 2β-mercaptoethanol, pH 6.5). Myosin was separated in acrylamide gel solution containing 30% glycerol, 8% acrylamide-bis (50:1), 0.2 M Tris, 0.1 M glycine, and 0.4% SDS using a Mini Protean II system (Bio-Rad Laboratories). Gels were run at 72 V for 31 h and silver stained. The bands were scanned and quantified using a densitometer equipped with an integrator (GS-800; Bio-Rad Laboratories).

Statistical analysis

A two-tailed Student's *t* test was used for statistical analysis. All data are expressed as means ± SEM or SD, and significance was established at the $P < 0.05$ level.

Online supplemental material

Fig. S1 shows the distribution of the different fiber types on soleus muscle transverse sections from control and mTOR$^-$ mice. Fig. S2 shows Western blot analysis for dystrophy-related proteins in 11-wk-old mTOR$^-$ muscles.

Downloaded from jcb.rupress.org on March 26, 2010

Published December 14, 2009

Table S1 presents the quantification of Western blot analysis for DGC components in muscles from 6-wk-old control and mTOR⁻ mice. Table S2 presents the quantification of Western blot analysis for dystrophy-related proteins in muscles from 11-wk-old control and mTOR⁻ mice. Table S3 presents the quantification of Western blot analysis for signal transduction in mTOR⁻ muscles. Online supplemental material is available at http://www.jcb.org/cgi/content/full/jcb.200903131/DC1.

We thank R.D. Roy and C. Scott for critical reading of the manuscript and helpful discussions, J. Melki for providing the HSA-Cre line, and B. Sonnular and A. Tran-Van-Minh for technical assistance. We thank the Novartis Foundation and the animal (Le Plateau de Biologie Expérimental de la Souris) and microscopy (Plateau Technique Imagerie/Microscopie) facilities of the IFR128 Biosciences. We also thank the Whitehead Institute and Dana-Farber Cancer Institute for supplying Torin1 inhibitor and Dr. G. Chiang from the Brockhouse Institute for Materials Research for supplying the rat mTOR plasmids.

This work was supported by an EMBO fellowship (to Y.-G. Gangloff), the Association Française contre les Myopathies (to L. Mazelin, L. Schaeffer, and Y.-G. Gangloff), the Agence Nationale de la Recherche (to M. Panda and Y.-G. Gangloff), the Association pour la Recherche contre le Cancer (to Y.-G. Gangloff), and the Ministère de la Recherche et de la Technologie (ACI BDPI to L. Schaeffer).

Submitted: 24 March 2009
Accepted: 13 November 2009

References

Acharyya, S., M.E. Butchbach, Z. Sahenk, H. Wang, M. Saji, M. Carathers, M.D. Ringel, R.J. Skipworth, K.C. Pearon, M.A. Hollingsworth, et al. 2005. Dystrophin glycoprotein complex dysfunction: a regulatory link between muscular dystrophy and cancer cachexia. *Cancer Cell.* 8:421–432. doi:10.1016/j.ccr.2005.10.004

Aghulut, O., A. Vignaud, C. Hourde, E. Mouisel, F. Fougerousse, G.S. Butler-Browne, and A. Ferry. 2009. Slow myosin heavy chain expression in the absence of muscle activity. *Am. J. Physiol. Cell Physiol.* 296:C205–C214. doi:10.1152/ajpcell.00408.2008

Barton-Davis, E.R., L. Cordier, D.I. Shoturma, S.E. Leland, and H.L. Sweeney. 1999. Aminoglycoside antibiotics restore dystrophin function to skeletal muscles of mdx mice. *J. Clin. Invest.* 104:375–381 . doi:10.1172/JCI7866

Bassel-Duby, R., and E.N. Olson. 2006. Signaling pathways in skeletal muscle remodeling. *Annu. Rev. Biochem.* 75:19–37. doi:10.1146/annurev.biochem.75.103004.142622

Bayascas, J.R., and D.R. Alessi. 2005. Regulation of Akt/PKB Ser473 phosphorylation. *Mol. Cell.* 18:143–145. doi:10.1016/j.molcel.2005.03.020

Bentzinger, C.F., K. Romanino, D. Cloetta, S. Lin, J.H. Mascarenhas, F. Oliveri, J. Xia, E. Casanova, C.F. Costa, M. Brink, et al. 2008. Skeletal muscle-specific ablation of raptor, but not of rictor, causes metabolic changes and results in muscle dystrophy. *Cell Metab.* 8:411–424. doi:10.1016/j.cmet.2008.10.002

Blaauw, B., C. Mammucari, L. Toniolo, L. Agatea, R. Abraham, M. Sandri, C. Reggiani, and S. Schiaffino. 2008. Akt activation prevents the force drop induced by eccentric contractions in dystrophin-deficient skeletal muscle. *Hum. Mol. Genet.* 17:3686–3696. doi:10.1093/hmg/ddn264

Bodine, S.C., T.N. Stitt, M. Gonzalez, W.O. Kline, G.L. Stover, R. Bauerlein, E. Zlotchenko, A. Scrimgeour, J.C. Lawrence, D.J. Glass, and G.D. Yancopoulos. 2001. Akt/mTOR pathway is a crucial regulator of skeletal muscle hypertrophy and can prevent muscle atrophy in vivo. *Nat. Cell Biol.* 3:1014–1019. doi:10.1038/ncb1101-1014

Brunn, G.J., C.C. Hudson, A. Sekulić, J.M. Williams, H. Hosoi, P.J. Houghton, J.C. Lawrence Jr., and R.T. Abraham. 1997. Phosphorylation of the translational repressor PHAS-I by the mammalian target of rapamycin. *Science.* 277:99–101. doi:10.1126/science.277.5322.99

Cross, D.A., P.W. Watt, M. Shaw, J. van der Kaay, C.P. Downes, J.C. Holder, and P. Cohen. 1997. Insulin activates protein kinase B, inhibits glycogen synthase kinase-3 and activates glycogen synthase by rapamycin-insensitive pathways in skeletal muscle and adipose tissue. *FEBS Lett.* 406:211–215. doi:10.1016/S0014-5793(97)00240-8

Cunningham, J.T., J.T. Rodgers, D.H. Arlow, F. Vazquez, V.K. Mootha, and P. Puigserver. 2007. mTOR controls mitochondrial oxidative function through a YY1-PGC-1alpha transcriptional complex. *Nature.* 450:736–740. doi:10.1038/nature06322

Dellorusso, C., R.W. Crawford, J.S. Chamberlain, and S.V. Brooks. 2001. Tibialis anterior muscles in mdx mice are highly susceptible to contraction-induced injury. *J. Muscle Res. Cell Motil.* 22:467–475. doi:10.1023/A:1014587918367

Dogra, C., H. Changotra, J.E. Wergedal, and A. Kumar. 2006. Regulation of phosphatidylinositol 3-kinase (PI3K)/Akt and nuclear factor-kappa B signaling pathways in dystrophin-deficient skeletal muscle in response to mechanical stretch. *J. Cell. Physiol.* 208:575–585. doi:10.1002/jcp.20696

Durbeej, M., and K.P. Campbell. 2002. Muscular dystrophies involving the dystrophin-glycoprotein complex: an overview of current mouse models. *Curr. Opin. Genet. Dev.* 12:349–361. doi:10.1016/S0959-437X(02)00309-X

Edinger, A.L., C.M. Linardic, G.G. Chiang, C.B. Thompson, and R.T. Abraham. 2003. Differential effects of rapamycin on mammalian target of rapamycin signaling functions in mammalian cells. *Cancer Res.* 63:8451–8460.

Erbay, E., and J. Chen. 2001. The mammalian target of rapamycin regulates C2C12 myogenesis via a kinase-independent mechanism. *J. Biol. Chem.* 276:36079–36082. doi:10.1074/jbc.C100406200

Erbay, E., I.H. Park, P.D. Nuzzi, C.J. Schoenherr, and J. Chen. 2003. IGF-II transcription in skeletal myogenesis is controlled by mTOR and nutrients. *J. Cell Biol.* 163:931–936. doi:10.1083/jcb.200307158

Galvagni, F., E. Cartocci, and S. Oliviero. 1998. The dystrophin promoter is negatively regulated by YY1 in undifferentiated muscle cells. *J. Biol. Chem.* 273:33708–33713. doi:10.1074/jbc.273.50.33708

Gangloff, Y.G., M. Mueller, S.G. Dann, P. Svoboda, M. Sticker, J.F. Spetz, S.H. Um, E.J. Brown, S. Cereghini, G. Thomas, and S.C. Kozma. 2004. Disruption of the mouse mTOR gene leads to early postimplantation lethality and prohibits embryonic stem cell development. *Mol. Cell. Biol.* 24:9508–9516. doi:10.1128/MCB.24.21.9508-9516.2004

Hardwick, J.S., F.G. Kuruvilla, J.K. Tong, A.F. Shamji, and S.L. Schreiber. 1999. Rapamycin-modulated transcription defines the subset of nutrient-sensitive signaling pathways directly controlled by the Tor proteins. *Proc. Natl. Acad. Sci. USA.* 96:14866–14870. doi:10.1073/pnas.96.26.14866

Jacinto, E., R. Loewith, A. Schmidt, S. Lin, M.A. Rüegg, A. Hall, and M.N. Hall. 2004. Mammalian TOR complex 2 controls the actin cytoskeleton and is rapamycin insensitive. *Nat. Cell Biol.* 6:1122–1128. doi:10.1038/ncb1183

Kumar, A., T.E. Harris, S.R. Keller, K.M. Choi, M.A. Magnuson, and J.C. Lawrence. 2008. Muscle-specific deletion of rictor impairs insulin-stimulated glucose transport and enhances basal glycogen synthase activity. *Mol. Cell. Biol.* 28:61–70.

Kuznetsov, A.V., T. Tiivel, P. Sikk, T. Kaambre, L. Kay, Z. Daneshrad, A. Rossi, L. Kadaja, N. Peet, E. Seppet, and V.A. Saks. 1996. Striking differences between the kinetics of regulation of respiration by ADP in slow-twitch and fast-twitch muscles in vivo. *Eur. J. Biochem.* 241:909–915. doi:10.1111/j.1432-1033.1996.00909.x

Kuznetsov, A.V., V. Veksler, F.N. Gellerich, V. Saks, R. Margreiter, and W.S. Kunz. 2008. Analysis of mitochondrial function in situ in permeabilized muscle fibers, tissues and cells. *Nat. Protoc.* 3:965–976. doi:10.1038/nprot.2008.61

Leek, B.T., S.R. Mudaliar, R. Henry, O. Mathieu-Costello, and R.S. Richardson. 2001. Effect of acute exercise on citrate synthase activity in untrained and trained human skeletal muscle. *Am. J. Physiol. Regul. Integr. Comp. Physiol.* 280:R441–R447.

Majumder, P.K., P.G. Febbo, R. Bikoff, R. Berger, Q. Xue, L.M. McMahon, J. Manola, J. Brugarolas, T.J. McDonnell, T.R. Golub, et al. 2004. mTOR inhibition reverses Akt-dependent prostate intraepithelial neoplasia through regulation of apoptotic and HIF-1-dependent pathways. *Nat. Med.* 10:594–601. doi:10.1038/nm1052

Méjat, A., F. Ramond, R. Bassel-Duby, S. Khochbin, E.N. Olson, and L. Schaeffer. 2005. Histone deacetylase 9 couples neuronal activity to muscle chromatin acetylation and gene expression. *Nat. Neurosci.* 8:313–321. doi:10.1038/nn1408

Mouisel, E., B. Blondet, P. Escourrou, A. Chatonnet, J. Molgó, and A. Ferry. 2006. Outcome of acetylcholinesterase deficiency for neuromuscular functioning. *Neurosci. Res.* 55:389–396. doi:10.1016/j.neures.2006.05.002

Murakami, M., T. Ichisaka, M. Maeda, N. Oshiro, K. Hara, F. Edenhofer, H. Kiyama, K. Yonezawa, and S. Yamanaka. 2004. mTOR is essential for growth and proliferation in early mouse embryos and embryonic stem cells. *Mol. Cell. Biol.* 24:6710–6718. doi:10.1128/MCB.24.15.6710-6718.2004

Nicole, S., B. Desforges, G. Millet, J. Lesbordes, C. Cifuentes-Diaz, D. Vertes, M.L. Cao, F. De Backer, L. Languille, N. Roblot, et al. 2003. Intact satellite cells lead to remarkable protection against *Smn* gene defect in differentiated skeletal muscle. *J. Cell Biol.* 161:571–582. doi:10.1083/jcb.200210117

Ohanna, M., A.K. Sobering, T. Lapointe, L. Lorenzo, C. Praud, E. Petroulakis, N. Sonenberg, P.A. Kelly, A. Sotiropoulos, and M. Pende. 2005. Atrophy of S6K1(-/-) skeletal muscle cells reveals distinct mTOR effectors for cell cycle and size control. *Nat. Cell Biol.* 7:286–294. doi:10.1038/ncb1231

Ohlendieck, K., and K.P. Campbell. 1991. Dystrophin-associated proteins are greatly reduced in skeletal muscle from mdx mice. *J. Cell Biol.* 115:1685–1694. doi:10.1083/jcb.115.6.1685

Passonneau, J.V., and O.H. Lowry. 1993. Enzymatic Analysis: A Practical Guide. Humana Press, Inc., Totowa, NJ. 403 pp.

Downloaded from jcb.rupress.org on March 26, 2010

Published December 14, 2009

Patursky-Polischuk, I., M. Stolovich-Rain, M. Hausner-Hanochi, J. Kasir, N. Cybulski, J. Avruch, M.A. Rüegg, M.N. Hall, and O. Meyuhas. 2009. The TSC-mTOR pathway mediates translational activation of TOP mRNAs by insulin largely in a raptor- or rictor-independent manner. *Mol. Cell. Biol.* 29:640–649. doi:10.1128/MCB.00980-08

Peng, T., T.R. Golub, and D.M. Sabatini. 2002. The immunosuppressant rapamycin mimics a starvation-like signal distinct from amino acid and glucose deprivation. *Mol. Cell. Biol.* 22:5575–5584. doi:10.1128/MCB.22.15.5575-5584.2002

Peter, A.K., and R.H. Crosbie. 2006. Hypertrophic response of Duchenne and limb-girdle muscular dystrophies is associated with activation of Akt pathway. *Exp. Cell Res.* 312:2580–2591. doi:10.1016/j.yexcr.2006.04.024

Peter, A.K., C.Y. Ko, M.H. Kim, N. Hsu, N. Ouchi, S. Rhie, Y. Izumiya, L. Zeng, K. Walsh, and R.H. Crosbie. 2009. Myogenic Akt signaling upregulates the utrophin-glycoprotein complex and promotes sarcolemma stability in muscular dystrophy. *Hum. Mol. Genet.* 18:318–327. doi:10.1093/hmg/ddn358

Repetto, S., M. Bado, P. Broda, G. Lucania, E. Masetti, F. Sotgia, I. Carbone, A. Pavan, E. Bonilla, G. Cordone, et al. 1999. Increased number of caveolae and caveolin-3 overexpression in Duchenne muscular dystrophy. *Biochem. Biophys. Res. Commun.* 261:547–550. doi:10.1006/bbrc.1999.1055

Rommel, C., S.C. Bodine, B.A. Clarke, R. Rossman, L. Nunez, T.N. Stitt, G.D. Yancopoulos, and D.J. Glass. 2001. Mediation of IGF-1-induced skeletal myotube hypertrophy by PI(3)K/Akt/mTOR and PI(3)K/Akt/GSK3 pathways. *Nat. Cell Biol.* 3:1009–1013. doi:10.1038/ncb1101-1009

Sarbassov, D.D., S.M. Ali, D.H. Kim, D.A. Guertin, R.R. Latek, H. Erdjument-Bromage, P. Tempst, and D.M. Sabatini. 2004. Rictor, a novel binding partner of mTOR, defines a rapamycin-insensitive and raptor-independent pathway that regulates the cytoskeleton. *Curr. Biol.* 14:1296–1302. doi:10.1016/j.cub.2004.06.054

Sarbassov, D.D., S.M. Ali, S. Sengupta, J.H. Sheen, P.P. Hsu, A.F. Bagley, A.L. Markhard, and D.M. Sabatini. 2006. Prolonged rapamycin treatment inhibits mTORC2 assembly and Akt/PKB. *Mol. Cell.* 22:159–168. doi:10.1016/j.molcel.2006.03.029

Schiaffino, S., M. Sandri, and M. Murgia. 2007. Activity-dependent signaling pathways controlling muscle diversity and plasticity. *Physiology (Bethesda).* 22:269–278.

Schieke, S.M., D. Phillips, J.P. McCoy Jr., A.M. Aponte, R.F. Shen, R.S. Balaban, and T. Finkel. 2006. The mammalian target of rapamycin (mTOR) pathway regulates mitochondrial oxygen consumption and oxidative capacity. *J. Biol. Chem.* 281:27643–27652. doi:10.1074/jbc.M603536200

Stitt, T.N., D. Drujan, B.A. Clarke, F. Panaro, Y. Timoleyva, W.O. Kline, M. Gonzalez, G.D. Yancopoulos, and D.J. Glass. 2004. The IGF-1/PI3K/Akt pathway prevents expression of muscle atrophy-induced ubiquitin ligases by inhibiting FOXO transcription factors. *Mol. Cell.* 14:395–403. doi:10.1016/S1097-2765(04)00211-4

Straub, V., J.A. Rafael, J.S. Chamberlain, and K.P. Campbell. 1997. Animal models for muscular dystrophy show different patterns of sarcolemmal disruption. *J. Cell Biol.* 139:375–385. doi:10.1083/jcb.139.2.375

Talmadge, R.J., and R.R. Roy. 1993. Electrophoretic separation of rat skeletal muscle myosin heavy-chain isoforms. *J. Appl. Physiol.* 75:2337–2340.

Thoreen, C.C., S.A. Kang, J.W. Chang, Q. Liu, J. Zhang, Y. Gao, L.J. Reichling, T. Sim, D.M. Sabatini, and N.S. Gray. 2009. An ATP-competitive mammalian target of rapamycin inhibitor reveals rapamycin-resistant functions of mTORC1. *J. Biol. Chem.* 284:8023–8032. doi:10.1074/jbc.M900301200

Tinsley, J., N. Deconinck, R. Fisher, D. Kahn, S. Phelps, J.M. Gillis, and K. Davies. 1998. Expression of full-length utrophin prevents muscular dystrophy in mdx mice. *Nat. Med.* 4:1441–1444. doi:10.1038/4033

Um, S.H., D. D'Alessio, and G. Thomas. 2006. Nutrient overload, insulin resistance, and ribosomal protein S6 kinase 1, S6K1. *Cell Metab.* 3:393–402. doi:10.1016/j.cmet.2006.05.003

Watchko, J.F., T.L. O'Day, and E.P. Hoffman. 2002. Functional characteristics of dystrophic skeletal muscle: insights from animal models. *J. Appl. Physiol.* 93:407–417.

Wullschleger, S., R. Loewith, and M.N. Hall. 2006. TOR signaling in growth and metabolism. *Cell.* 124:471–484. doi:10.1016/j.cell.2006.01.016

Downloaded from jcb.rupress.org on March 26, 2010

II. COMMUNICATIONS AFFICHEES LORS DE CONGRES NATIONAUX ET INTERNATIONAUX

Western blot et luminex : des techniques différentes, des résultats similaires
Joassard O, Defour A, Barthelemy JC, Sabido O, Bechet D, Berthon P, Freyssenet D.
11ème colloque Rhône-Alpes de Quantimétrie cellulaire, Juin 2010, Saint Etienne.

Sirtuin1 regulates SREBP-1c gene expression through LXR dependent mechanism
Defour A, de Castro Perez A, Lefai E, Gu Y, Peinnequin A, Bechet D, Freyssenet D.
1st International Congress of Translational Research in Human Nutrition, Mars 2010, Clermont Ferrand.

Morphological and metabolic responses of C2C12 myotubes following food deprivation and refeeding
Defour A, Castells J, Sabido O, Lefai E, Bechet E, Freyssenet D.
5th Cachexia Conference, Décembre 2009, Barcelone.

A role for sirtuin 1 in the regulation of skeletal muscle metabolism : a preliminary study
Defour A, de Castro Perez A, Castells J, Sabido O, Peinnequin A, Lefai E, Bechet D, Freyssenet D.
38th European Muscle Conference, Septembre 2009, Lille. Publié dans le Journal of Muscle Research and Cell Motility : 2010 Jan 9; 30(7):307-338.

Sirtuine 1, une protéine impliquée dans le contrôle du métabolisme du glucose dans le muscle strié squelettique
Defour A, de Castro Perez A, Lefai E, Peinnequin A, Bechet D, Freyssenet D.
Journée de l'école doctorale EDSIS, Avril 2009, Saint Etienne. Prix du meilleur poster.

Ce travail a fait l'objet d'un poster au

11ème colloque Rhône-Alpes de Quantimétrie cellulaire

Saint Etienne, Juin 2010

WESTERN BLOT ET LUMINEX : DES TECHNIQUES DIFFERENTES, DES RESULTATS SIMILAIRES

JOASSARD Olivier, DEFOUR Aurélia, BARTHELEMY Jean-Claude, SABIDO Odile, BECHET Daniel, BERTHON Phanélie, FREYSSENET Damien

WESTERN BLOT ET LUMINEX : DES TECHNIQUES DIFFERENTES DES RESULTATS SIMILAIRES

[1]JOASSARD O., [1]DEFOUR A., [2]BARTHELEMY J.C., [1]SABIDO O., [3]BECHET D., [1]BERTHON P., [1]FREYSSENET D.

[1] Laboratoire de Physiologie de l'Exercice, EA 4338, Université Jean Monnet, 42023 Saint Etienne, France.
[2] CHU Saint-Etienne, France.
[3] INRA UMR 1019, Unité Nutrition Humaine, St Genès Champanelle, France.

INTRODUCTION

Le WESTERN BLOT est une technique couramment utilisée en biologie moléculaire pour l'analyse de l'expression de protéines. Technologie récente, le LUMINEX possède de nombreuses applications en immunologie, infectiologie, génétique, cancérologie ou en biochimie. Le but de cette étude a été d'analyser la voie de signalisation intracellulaire Pi3K/Akt/mTOR par Western blot et par Luminex.

PRINCIPE

WESTERN BLOT

Méthode d'identification de protéines :
-séparation électrophorétique sur gel
-transfert sur membrane
-marquage à l'aide d'un anticorps spécifique
-révélation de l'anticorps fixé.

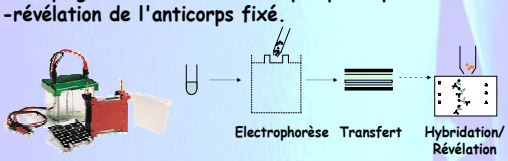

LUMINEX

Fondée sur le principe de la cytométrie en flux, cette technique allie l'utilisation de microsphères fluorescentes à une double lecture après excitation par 2 lasers.

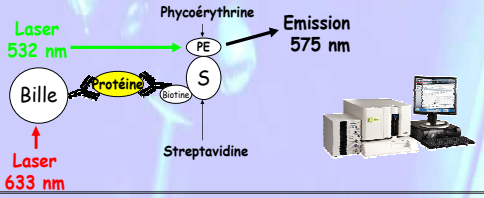

RESULTATS

PROTOCOLE DE DENUTRITION – RENUTRITION SUR MYOTUBES C2C12

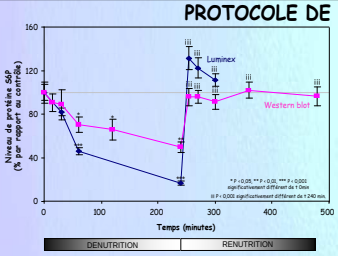

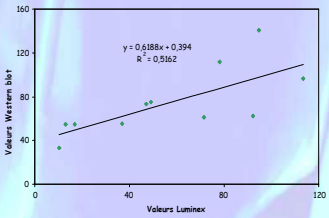

Corrélation Luminex/Western blot en dénutrition

PROTOCOLE D'INJECTION DE FORMOTEROL SUR TISSU MUSCULAIRE DE RATS

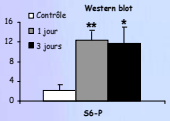

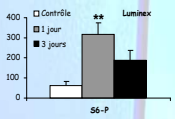

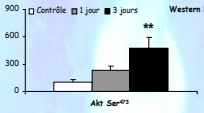

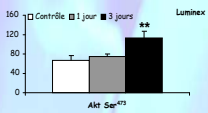

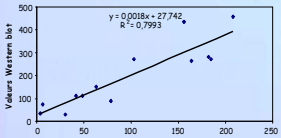

Corrélation Luminex/Western blot S6-P

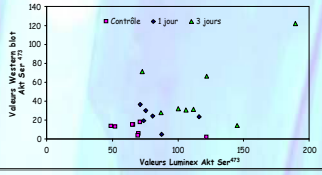

TABLEAU COMPARATIF

		Western blot	Luminex
Nombre d'échantillons		18 ou 28	94
Nombre de protéines lues simultanément		1	5
Temps de travail	Temps de manip avec incubation (h)	36	20
	Temps traitement des données approximatif (min)	90	60
Coût des réactifs par analyte et par échantillon (€)		2.5	5

DISCUSSION

La technique Luminex est utilisée en routine pour mesurer le niveau d'expression de cytokines. Le Western blot, quant à lui, reste la technique de référence pour l'analyse semi-quantitative des protéines. La comparaison des résultats de ces 2 techniques, sur des protocoles différents (cellules, tissus musculaires), montre l'intérêt de la technique du Luminex à des fins de recherche dans l'exploration des voies de signalisation intracellulaire. Le Luminex apparaît donc, comme étant une technique de substitution du Western blot.

Ce travail a fait l'objet d'un poster au congrès

International Congress of Translational Research in Human Nutrition

Clermont Ferrand, Mars 2010

SIRTUIN1 REGULATES SREBP-1c GENE EXPRESSION THROUGH LXR DEPENDENT MECHANISM

DEFOUR Aurélia, CASTRO PEREZ Andréa, LEFAI Etienne, GU Yansong, PEINNEQUIN André, BECHET Daniel, FREYSSENET Damien

Sirtuin1 regulates SREBP-1c gene expression through LXR-dependent mechanism

DEFOUR A[1], CASTRO PEREZ A[1], LEFAI E[2], GU Y[3], PEINNEQUIN A[4], BECHET D[5], FREYSSENET D[1]

[1]Université de Lyon, Université Jean Monnet, Laboratoire de Physiologie de l'Exercice EA 4338, Saint Etienne, France ; [2]Université de Lyon, Université Claude Bernard Lyon 1, INSERM U870, Régulations Métaboliques Nutrition et Diabètes, Oullins, France ; [3]Department of Immunolgy, University of Washington School of Medicine, Seattle, WA 98 195, USA ; [4]Département de Radiologie et Radiopathologie, Centre de Recherche du Service de Santé des Armées, La Tronche, France ; [5]INRA UMR 1019, Unité Nutrition Humaine, St Genès Champanelle, France

Sirtuin 1 (Sirt1) is a NAD^+-dependent histone deacetylase that has been identified as a key enzyme involved in the regulation of neoglucogenesis in liver and mitochondrial biogenesis in skeletal muscle. Furthermore, pharmacological stimulation of Sirt1 has been shown to improve glucose homeostasis by enhancing insulin sensitivity in mice submitted to a high-fat diet, suggesting that Sirt1 could be involved in the regulation of glucose metabolism in skeletal muscle.

We first determined whether Sirt1 regulates the expression of genes involved in glucose transport. Expression of glucose transporter 4, hexokinase and sterol response element binding protein 1 (SREBP-1c), a transcription factor regulating hexokinase expression in skeletal muscle, was significantly decreased respectively, in *Tibialis Anterior* and *Gastrocnemius* muscles in knock out mice lacking exon 4 of Sirt1 gene (16.4 ± 1.8 months; n = 4) when compared to heterozygote mice (14.8 ± 2.0 months; n = 4).

Importantly, Sirt1 deacetylates and positively regulates liver X receptor (LXR) which has been shown to strongly activate SREBP-1c gene expression through LXR-response elements. We then determined whether Sirt1 stimulates SREBP-1c through a LXR-dependent mechanism. Electrotransfer of a Sirt1 expression vector in mice *Tibialis Anterior* muscles (1.5 months; n = 8) showed that Sirt1 overexpression increased by 2-fold SREBP-1c promoter transactivation. This increase was abolished when two LXR-response elements were deleted in SREBP-1c promoter.

We conclude that Sirt1 stimulates the expression of SREBP-1c through a LXR dependent manner, suggesting that Sirt1 could regulate the expression of genes involved in glucose transport.

SIRTUIN1 REGULATES SREBP1C GENE EXPRESSION THROUGH A LXR-DEPENDENT MECHANISM IN SKELETAL MUSCLE

[1]DEFOUR A, [1]CASTRO PEREZ A, [2]LEFAI E, [3]GU Y, [4]PEINNEQUIN A, [5]BECHET D and [1]FREYSSENET D

[1] Université de Lyon, Université Jean Monnet, Laboratoire de Physiologie de l'Exercice, EA 4338, Saint Etienne, France, [2] Université de Lyon, Université Claude Bernard 1, INSERM U870, Régulations Métaboliques, Nutrition, et Diabètes, Oullins, France, [3] University of Washington, School of Medicine, Department of Immunology, Seattle, USA, [4] Département de Radiologie et de Radiothérapie, Centre de Recherche du Service de Santé des Armées, La Tronche, France, [5] INRA UMR 1019, Unité Nutrition Humaine, St Genès Champanelle, France.

INTRODUCTION

Sirtuin 1 (Sirt1) is a NAD+-dependent histone deacetylase which stimulates mitochondrial biogenesis in skeletal muscle and gluconeogenesis in liver. Furthermore, pharmacological stimulation of Sirt1 partially protects from high fat diet-induced hyperglycemia in mice and stimulates cell glucose uptake in L6 myotubes, suggesting that Sirt1 regulates the expression of genes involved in the regulation of glucose homeostasis in skeletal muscle.

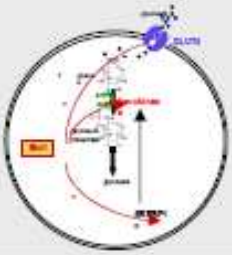

SREBP1c (sterol regulatory element binding protein 1c) has an important role in the regulation of hexokinase expression [Guillemin et al. J Lipid Res (2006)]. In skeletal muscle, SREBP1c gene expression is strongly activated by the liver X receptor (LXR) [Chen et al. PNAS (2004) ; Dif et al. Biochem J (2006)]. Moreover, Sirt1 deacetylates and positively regulates LXR in HEK293T cells [Li et al. Molecular Cell (2007)]. These data suggest that Sirt1 could regulate SREBP1c gene expression through a LXR-dependent mechanism.

MATERIALS & METHODS

Does Sirt1 regulate the expression of genes involved in the regulation of glucose homeostasis in skeletal muscle ?

SIRT1 KNOCK-OUT MICE

ctrl	heterozygotes	n = 4	14.8 months
ko	ko Sirt1 exon 4	n = 4	16.4 months

- Gastrocnemius (GAS) and Tibialis Anterior (TA) muscles

Does Sirt1 regulate SREBP1c gene expression through a LXR-dependent mechanism?

GENE ELECTROTRANSFER IN TA MICE MUSCLES

SREBP1c reporter plasmids (wild type or mutated on two LXR-response elements) were electrotransfected together with an empty vector or a Sirt1 expression plasmid or a LXRα expression plasmid

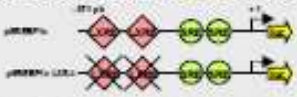

RESULTS

Glucose transporter 4 (GLUT4) protein level decreased in Sirt1 ko mice.

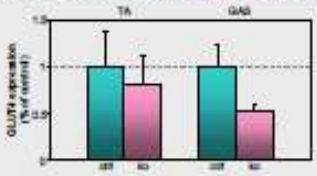

Hexokinase activity decreased in Sirt1 ko mice.

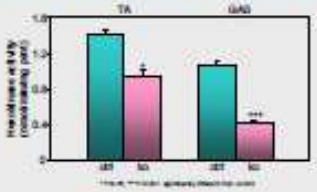

mRNA level of SREBP1c decreased in Sirt1 ko mice.

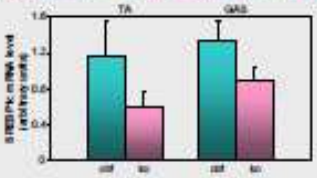

Sirt1 protein expression increased by 2-fold after gene electrotransfer.

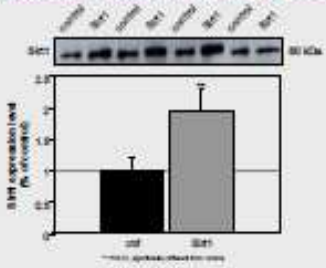

Sirt1 overexpression increased SREBP1c promoter transactivation.

Sirt1-induced increase in SREBP1c promoter transactivation was abolished when the two LXRE were deleted.

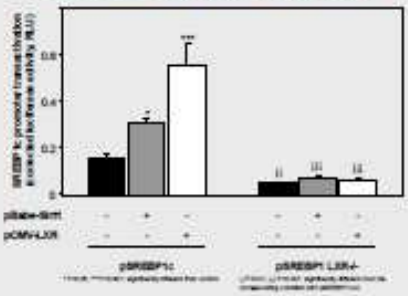

CONCLUSION

We propose this model to explain the regulation of glucose homeostasis by Sirt1 in skeletal muscle.

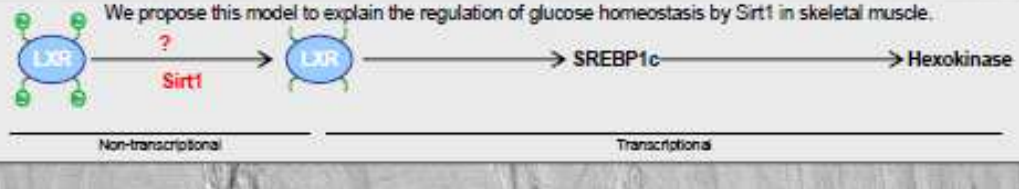

Ce travail a fait l'objet d'un poster au congrès

5th Cachexia Conference

Barcelone, Décembre 2009

MORPHOLOGICAL AND METABOLIC RESPONSES OF C2C12 MYOTUBES FOLLOWING FOOD DEPRIVATION AND REFEEDING

DEFOUR Aurélia, CASTELLS Josiane, SABIDO Odile, LEFAI Etienne, BECHET Daniel, FREYSSENET Damien

Morphological and metabolic responses of C2C12 myotubes following food deprivation and refeeding

DEFOUR A[1], CASTELLS J[1], SABIDO O[1], LEFAI E[2], BECHET D[3], FREYSSENET D[1]

[1]Laboratoire de Physiologie de l'Exercice, EA 4338, Université Jean Monnet, Saint Etienne, PRES Université de Lyon, France ; [2]INSERM U870, INRA UMR1235, Régulations Métaboliques, Nutrition, et Diabètes, Université Lyon 1, Oullins, PRES Université de Lyon, France ; [3]INRA UMR 1019, Unité Nutrition Humaine, Centre Clermont-Ferrand-Theix, St Genès Champanelle, France

Skeletal muscle is a prominent tissue involved in the regulation of metabolic homeostasis by its capacity to oxidize fatty acids and glucose. To test the adaptations of skeletal muscle cells following food deprivation, we developed an *in vitro* experimental model of C2C12 myotubes submitted to a metabolic challenge consisting in 4 hours of food deprivation followed by 20 hours of refeeding. During the time course of this metabolic challenge, we determined the morphological and metabolic responses of C2C12 myotubes. Myotube area decreased progressively (~20% at 4 hours) during food deprivation and increased progressively to reach control values 18 hours after refeeding. Accordingly, the phosphorylation of ribosomal protein S6, which is involved in the regulation of protein synthesis, decreased and increased in a time-dependant manner during food deprivation (~75% at 4 hours) and refeeding (~500% at 4 hours), respectively. Refeeding was accompanied by a strong increase in glucose consumption (~400% at 15 minutes), which progressively decreased to control level 20 hours after refeeding. During this period, glucose metabolism, which was initially oxidative, progressively switched to a glycolytic metabolism (~35%). Furthermore, food deprivation was accompanied by a transient decrease (~20% at 15 minutes) in hexokinase and citrate synthase activities, which recovered progressively during food deprivation and refeeding. The expression of sirtuin 1, a NAD^+-dependent histone deacetylase, potentially involved in the regulation of hexokinase expression, decreased during food deprivation (~40% at 4 hours). We are currently assessing the contribution of sirtuin 1 in these morphological and metabolic adaptations.

MORPHOLOGICAL AND METABOLIC RESPONSES OF C2C12 MYOTUBES FOLLOWING FOOD DEPRIVATION AND REFEEDING

[1]DEFOUR A, [1]CASTELLS J, [1]SABIDO O, [2]LEFAI E, [3]BECHET D and [1]FREYSSENET D

[1] Laboratoire de Physiologie de l'Exercice, EA 4338, Université Jean Monnet, Saint Etienne, PRES Université de Lyon, France, [2] INSERM U870, INRA UMR 1235, Régulations Métaboliques, Nutrition, et Diabètes, Université Lyon 1, Oullins, PRES Université de Lyon, France, [3] INRA UMR 1019, Unité Nutrition Humaine, Centre Clermont-Ferrand-Theix, St Genès Champanelle, France.

INTRODUCTION

Skeletal muscle is quantitavely the largest organ in the body and is the major tissue involved in the regulation of metabolic homeostasis by its capacity to oxidize fatty acids and glucose. To test the adaptations of skeletal muscle following food deprivation, we developed an in vitro experimental model of C2C12 myotubes submitted to a metabolic challenge (food deprivation followed by refeeding). Markers of muscle atrophy (myotube area, phosphorylation of ribosomal protein S6) and markers of glycolytic and oxidative metabolisms were measured.

MATERIALS & METHODS

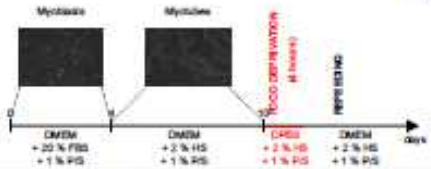

- C2C12 myotubes
- FOOD DEPRIVATION AND REFEEDING :
  - Lactate production and glucose consumption by YSI 2300 STAT PLUS (n = 8)
  - Myotubes area by Carl Zeiss, Cell Observer Z1 and Axiovision 4.7 (n = 10)
  - Protein expression by enzymatic assays and Western blot (n = 8)
- Statistics (Anova 1) : * P<0.05, ** P<0.01, *** P<0.001 significantly different from 0 min
  ! P<0.05, !! P<0.01, !!! P<0.001 significantly different from 240 min

Food deprivation-induced myotube atrophy was associated with the dephosphorylation of ribosomal S6 protein on Ser235/236.

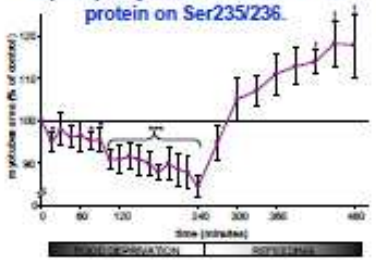

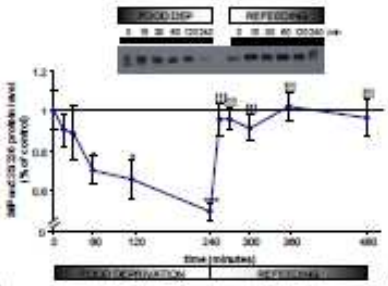

Lactate production from glucose, which represented less than 5% of total glucose consumption, increased to 35% during refeeding.

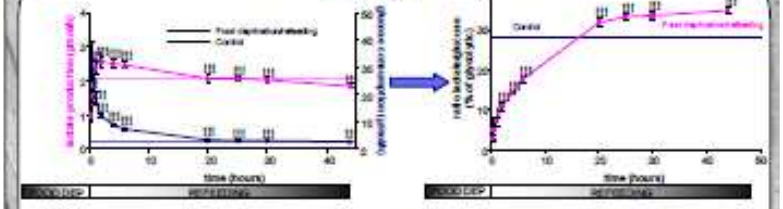

Hexokinase activity increased during refeeding.

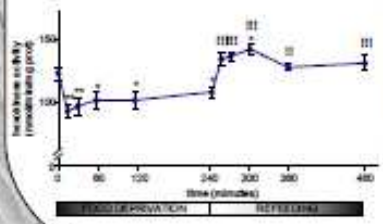

The expression of Sirtuin1, a histone deacetylase involved in the regulation of glucose homeostasis, remained unchanged.

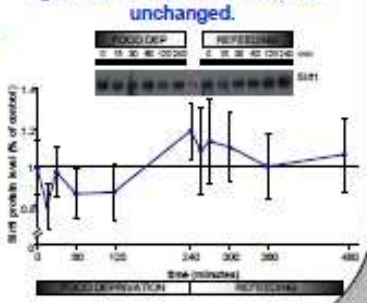

DISCUSSSION

This study shows that food deprivation is associated with mytotube atrophy that could be partly explained by inactivation of the Akt/mTOR pathway.

The increase in glucose consumption at the beginning of refeeding was associated with the increase in hexokinase expression. However, regulation of Sirt1 expression did not seem to be involved in these adaptations.

Ce travail a fait l'objet d'un poster au congrès

38th European Muscle Conference

Lille, Septembre 2009

A ROLE FOR SIRTUIN1 IN THE REGULATION OF SKELETAL MUSCLE METABOLISM : A PRELIMINARY STUDY

DEFOUR Aurélia, CASTRO PERZ Andréa, CASTELLS Josiane, SABIDO Odile, PEINNEQUIN André, LEFAI Etienne, BECHET Daniel, FREYSSENET Damien

Résumé publié dans

Journal of Muscle Research and Cell Motility, 2010 Jan 9; 30(7):307-338.

A possible role for sirtuin1 in the regulation of glucose metabolism in skeletal muscle

DEFOUR A[1], CASTRO PEREZ A[1], CASTELLS J[1], LEFAI E[2], PEINNEQUIN A[3], BECHET D[4], FREYSSENET D[1]

[1]Laboratoire de Physiologie de l'Exercice, EA 4338, Université Jean Monnet, Saint Etienne, PRES Université de Lyon, France ; [2]INSERM U870, INRA UMR1235, Régulations Métaboliques, Nutrition, et Diabètes, Université Lyon 1, Oullins, PRES Université de Lyon, France ; [3]Département de Radiologie et Radiopathologie, Centre de Recherche du Service de Santé des Armées, La Tronche, France ; [4]INRA UMR 1019, Unité Nutrition Humaine, Centre Clermont-Ferrand-Theix, St Genès Champanelle, France

Sirtuin 1 (Sirt1) is a NAD^+-dependent histone deacetylase that has been identified as a key enzyme involved in the regulation of neoglucogenesis in liver and mitochondrial biogenesis in skeletal muscle. Furthermore, pharmacological stimulation of Sirt1 has been shown to improve glucose homeostasis by enhancing insulin sensitivity in mice submitted to a high-fat diet. As proper skeletal muscle function is important for glucose homeostasis, these data suggest that Sirt1 could be involved in the regulation of glucose metabolism in skeletal muscle. We determined whether Sirt1 regulates the expression of glucose transporter 4 (GLUT4), hexokinase and sterol response element binding protein 1 (SREBP-1c), a transcription factor regulating hexokinase expression in skeletal muscle. We used knock out (KO) mice lacking exon 4 of Sirt1 gene (16.4 months ± 1.8 ; n = 4) and heterozygote mice as controls (14.8 months ± 2.0 ; n = 4). We showed that GLUT4 protein expression was decreased by 20 % in *tibialis anterior* (TA) and 50 % in *gastrocnemius* (GAS) of Sirt1 KO mice. Similarly, hexokinase activity was diminished by 30 % in TA and 60 % in GAS. Finally, SREBP-1c mRNA expression was decreased by 50 % in TA and 30 % in GAS. Additional experiments will be performed to determine the molecular mechanisms involved in the regulation of glucose metabolism by Sirt1.

A ROLE FOR SIRTUIN1 IN THE REGULATION OF SKELETAL MUSCLE METABOLISM : A PRELIMINARY STUDY

[1]DEFOUR A, [1]CASTRO PEREZ A, [1]CASTELLS J, [1]SABIDO O, [2]PEINNEQUIN, [3]LEFAI E, [4]BECHET D and [1]FREYSSENET D

[1] Laboratoire de Physiologie de l'Exercice, EA 4338, Université Jean Monnet, Saint Etienne, PRES Université de Lyon, France, [2] Département de Radiologie et Radiopathologie, Centre de Recherche du Service de Santé des Armées, La Tronche, France, [3] INSERM U870, Régulations Métaboliques, Nutrition, et Diabètes, Université Lyon 1, Oullins, PRES Université de Lyon, France, [4] INRA UMR 1019, Unité Nutrition Humaine, Centre Clermont-Ferrand-Theix, St Genès Champanelle, France.

INTRODUCTION

Sirtuin1 (Sirt1) is a NAD+-dependent histone deacetylase involved in liver neoglucogenesis and mitochondrial biogenesis in skeletal muscle. Furthermore, stimulation of Sirt1 activity improves glucose homeostasis in mice. As skeletal muscle plays an important role in glucose homeostasis, we hypothesized that Sirt1 may be involved in the regulation of glucose metabolism in skeletal muscle. To test this hypothesis, Sirt1 knock-out (ko) mice were investigated for the expression of proteins involved in the regulation of glucose transport. An *in vitro* experimental model of C2C12 myotubes submitted to a metabolic challenge (fasting and refeeding) was also developped.

MATERIALS & METHODS

- Mice :

ctrl	heterozygotes	n = 4	14.8 months
ko	ko Sirt1 exon 4	n = 4	16.4 months

- *Gastrocnemius* (GAS) and *Tibialis Anterior* (TA) muscles
- Enzymatic assays, RT-qPCR and immunoblotting
- Statistics : * P<0.05, *** P<0.001 significantly different from control

- C2C12 myotubes
- Fasting and refeeding kinetic

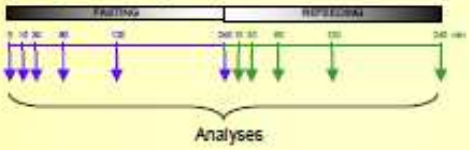

- Measurement of myotubes area (Carl Zeiss, Cell Observer Z1)
- Immunoblotting (Sirt1 n = 4 ; S6P n = 3)
- Enzymatic assays (n = 8)
- Statistics : * P<0.05, ** P<0.01, *** P<0.001 significantly different from 0 min

RESULTS

mRNA level of SREBP1c (a transcription factor regulating hexokinase expression) decreases in ko Sirt1 mice.

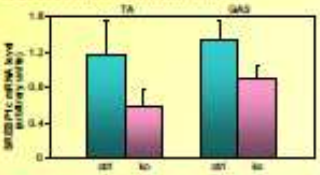

Hexokinase activity decreases in ko Sirt1 mice.

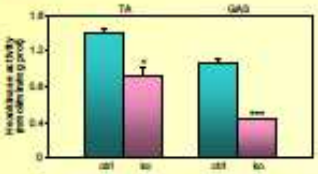

Glucose transporter 4 (GLUT4) protein level decreases in ko Sirt1 mice.

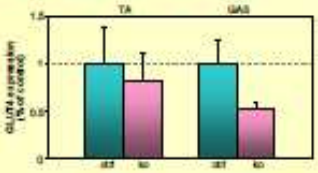

Sirt1 protein level tends to decrease during fasting.

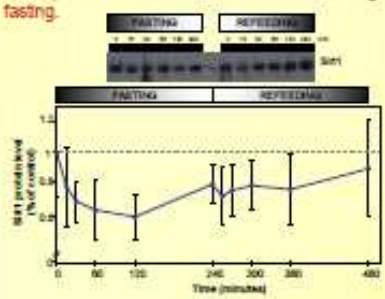

Hexokinase activity decreases quickly during fasting (15 min) and recovers early during refeeding.

Citrate synthase activity decreases during fasting (60 min) and recovers progressively during fasting and refeeding.

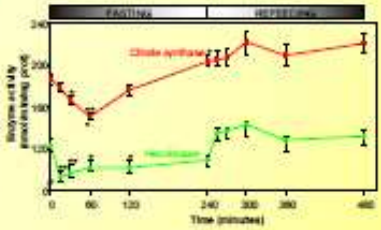

Myotubes area decreases progressively during fasting and increases during refeeding to reach values that are above controls (0 min).

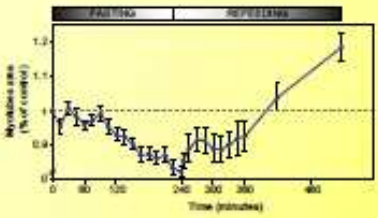

Phosphorylation of ribosomal protein S6 on Ser235/236 decreases progressively during fasting and increases sharply during refeeding (255 min).

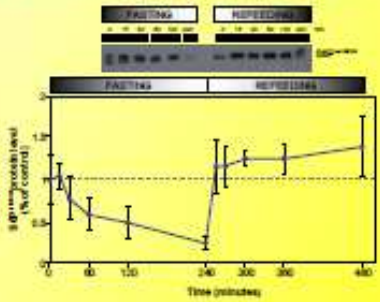

DISCUSSSION

The study on Sirt1 ko mice shows that Sirt1 may regulate the expression of key proteins involved in glucose metabolism. The role of LXRα in the regulation of SREBP1c expression by Sirt1 will be studied.

The *in vitro* study shows that a metabolic adaptation precedes the atrophy (fasting) and hypertrophy (refeeding) of myotubes. Additonal experiments will be performed to determine the role of Sirt1 in this regulation.

Ce travail a fait l'objet d'un poster à la

Journée de l'Ecole Doctorale de Saint Etienne

Saint Etienne, Avril 2009

SIRTUINE1, UNE PROTEINE IMPLIQUEE DANS LE CONTROLE DU METABOLISME DU GLUCOSE DANS LE MUSCLE STRIE SQUELETTIQUE

DEFOUR Aurélia, CASTRO PERZ Andréa, LEFAI Etienne, PEINNEQUIN André, BECHET Daniel, FREYSSENET Damien

Prix du meilleur poster.

Sirtuine 1, une protéine impliquée dans le contrôle du métabolisme du glucose dans le muscle strié squelettique

Aurélia DEFOUR[1], Andréa de CASTRO PEREZ[1], Etienne LEFAI[2], André PEINNEQUIN[3], Daniel BECHET[4] et Damien FREYSSENET[1]

[1] Laboratoire de Physiologie de l'Exercice, EA 4338, Université Jean Monnet, Saint Etienne, PRES Université de Lyon, France.
[2] INSERM U870, INRA UMR1235, Régulations Métaboliques, Nutrition, et Diabètes, Université Lyon 1, Oullins, PRES Université de Lyon, France.
[3] Département de Radiologie et Radiopathologie, Centre de Recherche du Service de Santé des Armées, La Tronche, France.
[4] INRA UMR 1019, Unité Nutrition Humaine, Centre Clermont-Ferrand-Theix, St Genès Champanelle, France.

CONTEXTE

Sirtuine 1 (Sirt1) :

-histone déacétylase

-Sirt1 stimule la biogénèse mitochondriale dans le muscle strié squelettique

-Sirt1 prévient l'hyperglycémie induite par un régime gras

Muscle strié squelettique :

-représente 40 % du poids corporel

-tissu principal de l'oxydation du glucose

HYPOTHÈSE : Quel est le rôle de Sirt1 dans la régulation du métabolisme du glucose dans le muscle strié squelettique ?

MATERIEL ET METHODES

- 2 populations de souris :

ctrl	hétérozygotes	n = 4	14,8 mois
KO	KO Sirt1 exon 4	n = 4	16,4 mois

- prélèvements des muscles *Gastrocnemius* (GAS) et *Tibialis Anterior* (TA)
- dosage enzymatique, RT-qPCR et Western blot
- test-t apparié * P<0,05, *** P<0,001

OBJECTIF : Sirt1 régule l'entrée du glucose dans la fibre musculaire

1.Sirt1 régule-t-elle l'expression du transporteur GLUT4 ?

2.Sirt1 régule-t-elle l'expression de l'enzyme hexokinase (phosphorylant irréversiblement le glucose en glucose-6-phosphate) ?

3.Sirt1 contrôle-t-elle l'expression de SREBP1c, qui lui-même régule l'expression de l'hexokinase ?

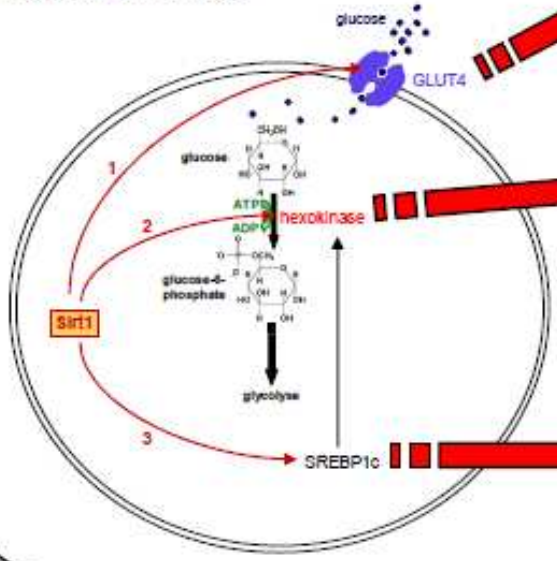

RESULTATS

Diminution du niveau d'expression de la protéine GLUT4 chez les souris KO Sirt1

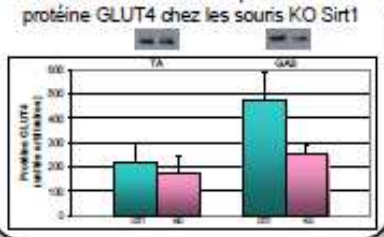

Diminution du niveau d'activité de l'enzyme hexokinase chez les souris KO Sirt1

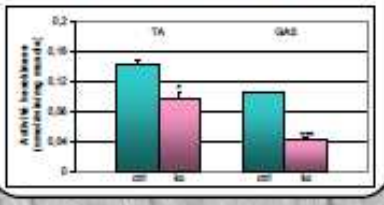

Diminution du niveau d'expression de l'ARNm SREBP1c chez les souris KO Sirt1

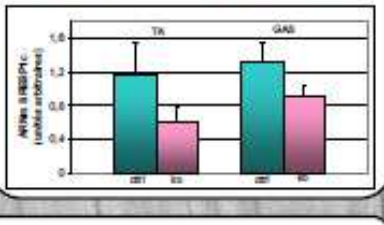

CONCLUSION ET PERSPECTIVES

La diminution des régulateurs clés du métabolisme du glucose (GLUT4, hexokinase et SREBP1c) par l'invalidation du gène Sirt1 chez la souris montre que Sirt1 a un rôle majeur dans la régulation de l'entrée du glucose dans la fibre musculaire. Des études complémentaires seront menées pour déterminer :
- le rôle de Sirt1 sur la régulation de l'entrée du glucose dans la fibre musculaire (*in vitro*)
- la régulation transcriptionnelle de SREBP1c, hexokinase et GLUT4 par Sirt1 (*in vivo*).

Fonctions métaboliques de Sirtuine 1 dans le muscle strié squelettique : contribution à l'étude de la régulation de l'expression de SREBP-1c et rôle potentiel lors d'un jeûne chez des myotubes C2C12

Sirt1 (Sirtuine 1) est une protéine histone déacétylase dépendante de NAD^+ qui stimule la néoglucogénèse et inhibe la glycolyse dans le foie, et qui augmente l'oxydation des acides gras dans le muscle strié squelettique. Le but de ce travail de thèse à été de définir les fonctions métaboliques de Sirt1 dans le muscle strié squelettique. Nous avons tout d'abord montré, à l'aide d'un modèle de souris déficientes pour le gène Sirt1, que Sirt1 régulait l'expression de l'hexokinase II et de SREBP-1c, protéine régulatrice de l'expression de l'hexokinase. De plus, un modèle d'électrotransfert de gènes permettait de mettre en évidence que Sirt1 régulait l'expression de SREBP-1c de façon LXR-dépendante. Enfin, l'inhibition de Sirt1 par l'EX527 aboutissait à une diminution de la consommation de glucose chez des myotubes C2C12. Prises ensemble, ces données suggèrent un rôle important de Sirt1 dans la régulation du métabolisme du glucose dans le muscle strié squelettique. Dans un second temps, nous avons déterminé le rôle potentiel de Sirt1 lors d'un jeûne chez des myotubes C2C12. Un jeûne entraînait une augmentation de l'activité cathepsine B + L et une déphosphorylation des protéines Akt^{S473}, $GSK3^{S21/S9}$, $p70S6K^{T412}$ et $S6^{S235/S236}$ qui précèdait une amyotrophie des myotubes. La renutrition aboutissait à une rephosphorylation de ces protéines et à un retour à la normale de la taille des myotubes. L'activité cathepsine B + L restait cependant élevée. Enfin, le niveau en ARNm de Sirt1 était augmenté de façon transitoire lors de la renutrition. D'autres mesures de marqueurs des voies protéolytiques et de l'activité de Sirt1 sont à envisager. Nos données ainsi que celles de la littérature suggèrent que Sirt1 pourrait avoir un rôle dans la régulation de l'autophagie lors du jeûne. Pour conclure, ce travail de thèse met en évidence un rôle pour Sirt1 dans la régulation du métabolisme du glucose dans le muscle strié squelettique et apporte de nouvelles perspectives dans l'étude de la régulation de ce métabolisme en conditions pathologiques.

Mots clés : jeûne, LXR, masse musculaire, métabolisme du glucose, muscle strié squelettique, Sirt1 et SREBP-1c.

Metabolic functions of sirtuin 1 in skeletal muscle: contribution to the study of regulation of the SREBP-1c expression and potential role during fasting in C2C12 myotubes

Sirt1 (Sirtuin 1) is a NAD^+-dependent histone deacetylase, which stimulates gluconeogenesis and inhibits glycolysis in the liver, and which increases fatty acid oxidation in skeletal muscle. The aim of this thesis was to define the metabolic functions of Sirt1 in skeletal muscle. We first showed, using a mouse model lacking the Sirt1 gene, that Sirt1 regulated expression of hexokinase II and SREBP-1c, a protein that regulates hexokinase expression. In addition, a model of gene electrotransfer allowed us to show that Sirt1 regulated expression of SREBP-1c in a LXR-dependent manner. Finally, inhibition of Sirt1 by EX527 resulted in a decrease of glucose consumption in C2C12 myotubes. Taken together, these data suggest an important role of Sirt1 in the regulation of glucose metabolism in skeletal muscle. Secondly, we determined the potential role of Sirt1 during fasting in C2C12 myotubes. Fasting resulted in an increase in cathepsin B + L activity and a dephosphorylation of Akt^{S473}, $GSK3^{S21/S9}$, $p70S6K^{T412}$ and $S6^{S235/S236}$ preceding a myotubes atrophy. Refeeding led to a rephosphorylation of these proteins and a return to normal size of myotubes. However, cathepsin B + L activity remained elevated. Finally, the level of Sirt1 mRNA was transiently increased during refeeding. Other measures of proteolytic pathways and Sirt1 activity markers will de determined. Our data and those of the literature suggest that Sirt1 could play a role in autophagy regulation during fasting. To conclude, this thesis highlights a role for Sirt1 in the regulation of glucose metabolism in skeletal muscle and provides new perspectives in the study of regulation of this metabolism in pathological conditions.

Keywords: fasting, glucose metabolism, LXR, muscle mass, Sirt1, skeletal muscle and SREBP-1c.